MIR-744 MODULATION BY DISTURBED FLOW AND ITS ROLE IN ENDOTHELIAL INFLAMMATION AND ATHEROSCLEROSIS

A Dissertation

Presented to

The Academic Faculty

by

Rachel Simmons

In Partial Fulfillment

of the Requirements for the Degree

Doctor of Philosophy in the

Wallace H. Coulter Department of Biomedical Engineering

Georgia Institute of Technology

December 2017

MIR-744 MODULATION BY DISTURBED FLOW AND ITS ROLE IN ENDOTHELIAL INFLAMMATION AND ATHEROSCLEROSIS

Approved by:

Dr. Hanjoong Jo, Advisor
School of Biomedical Engineering
Georgia Institute of Technology

Dr. Loren Williams
School of Chemistry & Biochemistry
Georgia Institute of Technology

Dr. Michael Davis
School of Biomedical Engineering
Georgia Institute of Technology

Dr. Charles Searles
School of Medicine, Division of Cardiology
Emory University

Dr. Younan Xia
School of Biomedical Engineering
Georgia Institute of Technology

Date Approved: October 3, 2017

ACKNOWLEDGEMENTS

First of all, I would like to thank everyone on my thesis committee for reading this document! Thank you Dr. Xia for collaborating with us in the past, as well as writing all the reference letters and providing insight into all my projects as a whole! Thank you Dr. Williams for asking very insightful questions and sparking discussion during committee meetings. Furthermore, thank you for your suggestions on how to best present my work! Thank you Dr. Searles for providing an expertise in miRNAs and a clinical perspective to better this work. Thank you Dr. Davis for providing your expertise in cardiovascular biology, as well as helpful tips for how to best quantify the data. Furthermore, I would like to especially thank my advisor, Dr. Jo, for providing his insight into all aspects of the project, including data acquisition, analysis, and how best to present the data at the end. The combined expertise of my thesis committee allowed me to identify the most critical experiments and interpret their findings in the broader scheme of cardiovascular disease.

Thank you to my former lab mates Inhwan, Chanwoo, Jessie, and Jack for the excellent conversations and help with experiments. Also thank you Dong won and Sunkum for help with the mouse studies and general lab support. Thank you to all of my current lab mates as well, including Marwa, Joan, Sanjoli, Cat, Darian, and Nico. I would also like to thank our "neighbors" the Davis Lab, especially Srishti for reagents and the wonderful chats!

Finally, I would especially like to thank my family Pam, Crystal, Alyssa, and Jacob for everything as well as friends such as Layla and Aras, Farnaz, and Subin for all of their support and with which this project wouldn't be possible!

TABLE OF CONTENTS

LIST OF FIGURES

LIST OF TABLES

LIST OF ABBREVIATIONS

d-flow	Disturbed flow
OS	Oscillatory shear stress
miRNA	MicroRNA
HUVECs	Human Umbilical Vein ECs
HAECs	Human Aortic ECs
iMAECs	immortalized Mouse Aortic ECs
TGFβ1	Transforming Growth Factor
ECs	Endothelial Cells
PCL	Partial Carotid Ligation
ApoE	Apolipoprotein E
LNA	Locked Nucleic Acid
LDL	Low Density Lipoprotein
LS	Laminar shear stress
LCA	Left Carotid Artery
RCA	Right Carotid Artery
S-flow	stable, unidirectional flow
KLF2	Kruppel Like Factor
VCAM1	Vascular Cell Adhesion Molecule
eNOS	endothelial Nitric Oxide Synthase
MMP	Matrix Metalloproteinase
NFkB	Nuclear Factor k B
UTR	Untranslatable Region
Ago2	Argonaute 2
RISC	RNA-Induced Silencing Complex
TA	Thoracic Aorta
GC	Greater Curvature
TSB	Target Site Blocker
PCL	Partial Carotid Ligation
LC	Lesser Curvature
S.C.	subcutaneous injection

SUMMARY

Atherosclerosis is a disease of chronic inflammation affecting the vascular wall of larger arteries. Atherogenesis is the main cause of myocardial infarction, ischemic stroke and peripheral arterial disease, however, the underlying molecular mechanisms are still incompletely understood. D-flow is known to regulate endothelial cell function via a process known as mechanotransduction. The mechanisms by which d-flow induces pro-atherogenic responses predominantly involve endothelial gene expression, including differential microRNA (miRNA) expression.

miRNAs are a large class of evolutionarily conserved, noncoding RNAs which function as post-transcriptional regulators by interacting with the 3' untranslated region (3' UTR) of specific target mRNAs in a sequence-specific manner [1]. It is thought that a single miRNA can target hundreds of mRNAs. These miRNAs negatively regulate gene expression through translational repression or mRNA cleavage, depending on the degree of complementarity. The majority of flow sensitive miRNAs have been characterized *in vitro*. Therefore, only a limited number of direct links to atherosclerosis have been established [2].

In previous studies by our group, the primate-specific miRNA, miR-663, was identified as a shear-sensitive miRNA involved in endothelial inflammation [3]. Despite these findings, as it is not conserved in mice, animal studies could not be conducted. However, we found that miR-744 is conserved across mammalian species and shares a seed sequence with miR-663. Finally, miR-744 is highly expressed in patients with heart failure, thus implicating the relevance of this miRNA to cardiovascular pathologies. Therefore, our overall hypothesis is that overexpression of the miR-744 in disturbed flow regions causes suppression of key target genes that promote endothelial homeostasis, thus tipping the balance towards endothelial inflammation and atherosclerosis.

The goal of this project was to elucidate the effects of d-flow-induced miR-744 on endothelial gene expression and the mechanisms initiating endothelial inflammation and atherosclerosis. To test the hypothesis, miR-744 modulation of OS-induced endothelial inflammation was assessed *in vitro*, direct targets of miR-744 were established *in vitro*, and the therapeutic effect of miR-744 inhibition on atherosclerosis development was assessed *in vivo*.

In Aim 1, we found that miR-744 is upregulated by OS in both human and murine endothelial cells, the acutely flow disturbed LCA, and the chronically flow disturbed lesser curvature (LC). Furthermore, we found that supplementation of miR-744 by mimics increases monocyte adhesion as well as multiple inflammatory cell adhesion molecules such as VCAM1, ICAM1, MCP-1, and p65. Finally, inhibition of miR-744 by an LNA-based antimiRNA (antimiR) can reduce OS-induced expression of these same inflammatory markers.

In Aim 2, we discovered by sequencing mRNAs directly bound to Ago2 in RISC specific targets of miR-744 in ECs. We filtered these targets based on conservation between species and through multiple validation steps, we found that LIMS2 is a conserved target of miR-744. Furthermore, we studied LIMS2 and found that LIMS2 silencing itself promotes endothelial inflammation via siRNA.

Finally, in Aim 3, we found that although global inhibition of miR-744 did not significantly inhibit atherosclerosis progression, inhibition of the specific interaction of mIR-744 and LIMS2 by TSBs showed a reduction in plaque. The work presented here has resulted in the discovery of a novel, shear-sensitive miRNA, a novel, shear-sensitive gene, and underscores the importance of the specificity of the miRNA-gene interaction. Finally, we found that LIMS2 binds to the well-known integrin-linked kinase (ILK), which may explain its role in inflammation. This work also provides a foundation for future studies to develop more targeted therapeutic strategies for CVD.

CHAPTER 1 INTRODUCTION

1.1 Vascular Fluid Mechanics and Hemodynamics in the Arteries

The basic arterial wall structure consists of three layers: the innermost intimal layer comprised of the endothelium, the middle medial layer mainly comprised of smooth muscle cells, and the outermost adventitial layer, comprised of fibroblastic cells. The endothelium is a monolayer of cells which function as the barrier between the blood and the rest of the vessel wall, as well as a surface to resist blood clotting. Smooth muscle cells mainly act as the mechanical strength needed to support blood pressure-induced stretch. The forces experienced by the arterial wall include the normal stress of blood pressure induced by blood flow, the circumferential stretch induced by cyclic strain driven by the pressure pulse, and the wall shear stress exerted by the blood flowing tangential to the surface of the blood vessel. Wall shear stress (WSS), the frictional force between the blood and the endothelium, has emerged as a major determinant of endothelial function and gene expression. **Thus, the focus of this thesis is the effect of wall shear stress on the endothelium and its role in pathophysiology of atherosclerosis.**

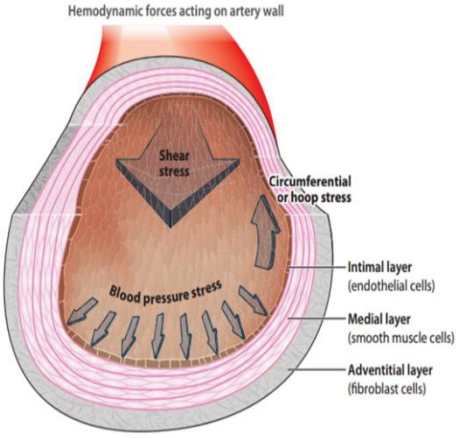

Figure 1.1 Hemodynamic Forces on the Artery Wall.

The blood vessel wall is comprised of the intimal, medial, and adventitial layers. The forces experienced by the arterial wall include the normal stress of blood pressure induced by blood flow, the circumferential stretch induced by cyclic strain driven by the pressure pulse, and the wall shear stress exerted by the blood flowing tangential to the surface of the blood vessel. Adapted from Tarbell et al. (2014)

1.2 Atherosclerosis and Localization of Plaques

Although atherosclerosis is the most common cause of death in the world [1] and thus is widely studied, it is a complex disease and the mechanisms by which it occurs are still being elucidated. What is known is that atherosclerosis is an inflammatory disease occurring in the arterial wall. Atherosclerosis is initiated by inflammation in the endothelial layer, which allows the endothelium to become more permeable. After the barrier of the endothelium is compromised, bloodborne lipids such as those associated with low density lipoproteins (LDL), accumulate under in the intima. Once these lipids are present, immune cells, particularly monocytes, transmigrate into the intima as well with the aid of the endothelium and upon contact with the LDL, become foam cells to create lesions. These initial lesions then become progressively larger with age. The lesions, or plaques, are what characterizes atherosclerosis [2].

It is generally regarded that there are distinct stages of plaque progression. In brief, these include LDL accumulation in the intima, oxidation by resident macrophages and smooth muscle cells, recruitment of circulating monocytes by cytokines and transmigration by binding to endothelial cell adhesion molecules, foam cell formation, smooth muscle migration to the intimal layer, smooth muscle proliferation, and finally the formation of a necrotic core. Although plaques can be heterogeneous in nature, the consequences of plaque formation end in occlusion of the artery and a loss of blood flow and oxygen to downstream regions and organs. This can occur by either the development of a large, occlusive plaque, or a smaller, vulnerable plaque which erodes so that the endothelium is denuded and an occlusive thrombus forms [3-5].

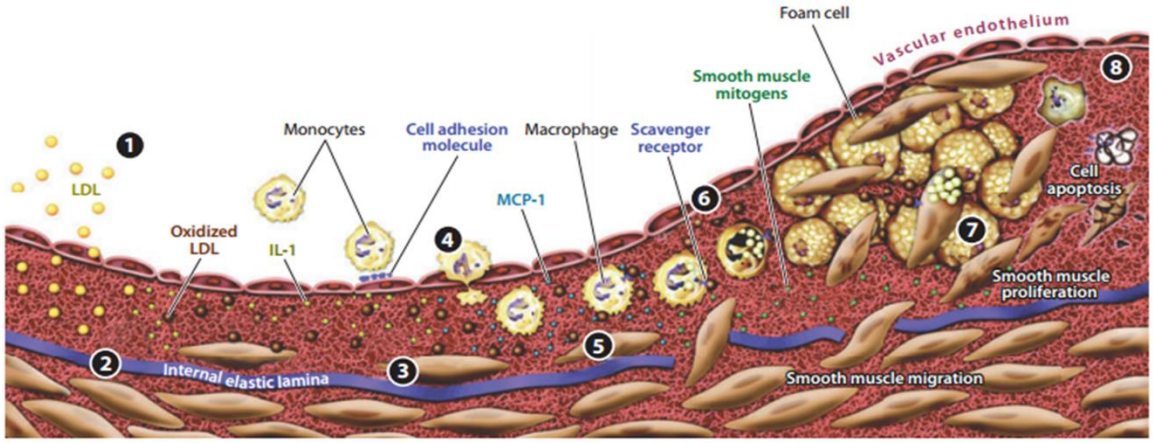

Figure 1.2 Stages of Atherosclerosis. The development of an atherosclerotic plaque initiates with LDL infiltration into the subendothelium, where it is oxidized by macrophages and smooth muscle cells, resulting in the conversion of macrophages to foam cells (1 and 2). The release of growth factors and cytokines by the resultant dysfunctional endothelium attracts additional monocytes (3 and 4). Foam cell accumulation and smooth muscle cell proliferation result in the growth of the plaque (6-8). Adapted from Faxon et al. (2004)

Interestingly, it has been observed that atherosclerotic plaques develop in specific regions of the vasculature. Specifically, as early as the 1960s, it was observed that plaques develop at sites of curvature, branching, or cross-sectional expansion and these sites experience flow separation [6]. At these regions, the flow departs from pulsatile, unidirectional flow to create flow-separation zones including flow reversal, oscillatory flow, and turbulence [7-10]. These sites include the abdominal aorta, the carotid bifurcation, and the lesser curvature of the aorta [6]. However, Caro and colleagues were the first to show that lesions develop directly upstream of these flow dividers in regions of low wall shear stress [11, 12]. Following this initial study, Caro and Nerem perfused the common carotid arteries of dogs and studied cholesterol uptake, which is one of the initiating steps of atherosclerosis [13]. They found that the uptake of lipids in arteries could not be correlated with fluid phase mass transport rates, which lead the investigators to conclude that the blood flow directly on the arterial wall affected the cholesterol transport. In conjunction with Caro's initial study, the hypothesis that atherosclerosis is localized to

areas of low wall shear stress due to its effect on the arterial wall was validated by many other investigators [14-20]. Particularly, Ku and colleagues noted that not only is low wall shear stress an indicator of a site of plaque development, but also in these regions there is a reversal of the flow during the pulsatile flow cycle. **Taken together, the flow pattern associated with atherosclerotic plaques corresponds to low, oscillating, shear stress known as disturbed flow (d-flow or OS).**

1.3 Endothelial Regulation by Flow

Although Caro and Nerem found that the direct flow of fluid on the arterial wall affected cholesterol transport, it was not shown until later that the endothelium was involved. The direct effect of fluid flow on endothelial cells (ECs) was first demonstrated by Nerem and Dewey independently [21, 22]. In these studies, these investigators found that ECs align in the direction of flow. Later, Frangos et al. and Grabowski et al. observed that application of shear stress to static cells rapidly induced the antithrombotic prostacyclin [23, 24]. Furthermore, Mo et al. and Shen et al. independently found that shear transiently induces release of intracellular Ca^{2+}, which acts as a signaling molecule [25, 26]. Finally, Kuchan et al. and Korenaga et al. found that shear induces sustained release of the vasodilator nitric oxide (NO) [27-29]. Taken together, these studies on cultured ECs suggested that fluid shear stress directly affects the phenotype of ECs.

The main functions of the endothelium are to maintain a barrier between the blood and underlying tissues, regulation of vascular tone, recruitment of immune cells to sites of injury, and to form new blood vessels. Numerous studies have shown that each of these endothelial functions is greatly impacted by shear stress. One of the earliest functions to be studied was endothelial permeability as described above (Caro and Nerem), as well as further studies into the effects on individual transport pathways (tight junctions, adherens junctions, vesicles, and leaky junctions[13]. Specifically, endothelial permeability increases after the onset of shear stress, but decreases after prolonged exposure [30, 31].

Furthermore, it was found that the biphasic response of endothelial permeability is due to increases in NO production from shear stress, which decrease permeability [32-34]. Taken together, these studies suggest that the acute increase in permeability is most relevant to the microcirculation, which responds to needs of specific organs, whereas the chronic response, which is downregulation of permeability due to sustained shear, are protective against the formation of atherosclerosis in that LDL is not allowed to penetrate the wall [35]. Furthermore, it has been shown in a mouse model of atherosclerosis that endothelial permeability is increased in atheroprone regions due to the degradation of the endothelial extracellular matrix (ECM) by matrix metalloproteinases (MMPs) [36]. Additionally, alterations in the endothelial ECM lead to stiffening of the intimal layer, which also affects endothelial permeability [37]. Not only does d-flow negatively impact endothelial permeability and ECM integrity and stiffness, it has also been shown to increase migration and angiogenesis [38, 39].

Due to the effects of flow on the endothelium, it is unsurprising that several studies have found that there are site-specific changes in the endothelium at plaque-prone regions, particularly at curves, branches, and bifurcations. Numerous studies have shown that monocyte adhesion to the endothelium has been enhanced in these regions due to the presence of increased chemoattractants and adhesion molecules [40-42]. Furthermore, endothelial transcription profiles taken in these d-flow regions from mice [43] and pigs [44] indicate that in general, ECs exhibit a pro-inflammatory phenotype when exposed to d-flow. Hajra et al. found that the subunits of the pro-inflammatory nuclear transcription factor NFκB (p65, IκBα, IκBβ) were upregulated in areas of the proximal aortas of mice which were prone to lesion formation [43]. NFκB was only activated in a minority of the cells basally, but was highly activated when stimulated with LPS or hypercholesterolemia. Later, Passerini et al. found that in ECs isolated from either the inner aortic arch of pigs, which experiences d-flow, vs. the descending thoracic aorta, which experiences unidirectional laminar flow/laminar shear stress (LS), there was a general upregulation of

several inflammatory cytokines and NFκB elements [44]. Furthermore, in cells isolated from the thoracic aorta expressed more antioxidative genes, which are generally less inflammatory. Taken together, these studies indicated that the endothelium in these regions has a pro-inflammatory phenotype. **Overall, disturbed blood on endothelium induces pro-inflammatory changes that impact endothelial leakiness, stiffness, and the ability to form new vessels.**

1.4 Models of Flow and Shear Stress to Study Endothelial Function and Atherosclerosis

1.4.1 *In vitro* Models of Shear Stress

There are a variety of *in vitro* and *in vivo* models to study the effects of d-flow on the endothelium specifically, as well as atherosclerosis (summarized in **Figure 1.3**). One of the first and most characterized *in vitro* models of shear stress is the cone-and-plate viscometer [22, 45]. In this system, shear stress is applied to cultured cells in a stationary plate by a rotating cone. A modified version was later introduced [46], which included a speed-controlled motor with variable rotational velocities. More recently, our lab has developed a modified cone-and-plate which is housed in a standard incubator and programmed shear stress profiles can be controlled by computer [47, 48]. Another *in vitro* model is the parallel-plate flow chamber, developed originally by Frangos, McIntire, and colleagues [23, 49]. In this system, a flow chamber consisting of a polycarbonate plate, a rectangular Silastic gasket, and a glass slide (or cover slip) with the attached EC monolayer were held together by a vacuum maintained at the periphery of the slide. Although the cone-and-plate and the parallel-plate flow chamber systems are the most commonly used *in vitro* shear systems, microfluidic chambers have become more recently used as they allow for high throughput experiments. This method was pioneered and commercialized by Schaff et al. [50-52].

1.4.2 *In vivo* Models of Shear Stress and Atherosclerosis

Although *in vitro* models provide insight into the role of shear stress in endothelial biology, *in vivo* models allow for the study of shear stress on disease development. These models are available in a variety of animals, including pigs, rats, and mice [53]. However, due to ease of genetic and physical manipulation, mice are the most popular animal model. One of the first models of atherosclerosis was the hypercholesterolemia model developed by Paigen et al. [54-57]. It was found that only the C57BL/6J strain could develop atherosclerosis if hypercholesterolemia was induced by genetic mutation and high-fat diet. The two most widely used mutations are the apolipoprotein E (ApoE) disruption [58-60] and the LDL receptor deletion [61]. The most common diets are Paigen's diet, which includes cholate [55], and the Western diet, which does not include cholate and is less inflammatory [59, 62]. Other models of atherosclerosis use surgical intervention to the arteries to induce atherosclerosis. Specifically, models such as injection of foreign proteins [63, 64] in rabbits, drying models in rats [65], and the more established wire [66] and later balloon injury models [67, 68] in mice directly injured the artery. However, the constrictive perivascular cuff model in mice [69-71] and the ligation models in mice are the most popular methods to rapidly induce atherosclerosis by alterations in flow, and thus shear stress (in conjunction with hypercholesterolemia). In the perivascular cuff model, the constricted region experiences higher shear stress, whereas the proximal section is exposed to d-flow and thus develops atherosclerotic plaques. Both complete ligations and incomplete ligations are also commonly used. In the complete ligations, the carotid artery is ligated, which induces vascular remodeling, neointimal hyperplasia, and atheroma formation [17, 71-81]. However, in this model, there is no shear stress. Finally, among the incomplete ligations, first studied in pigs [82], we have robustly developed a partial carotid ligation model [83]. In this model, 3 of the 4 branches of the left carotid artery is ligated while the right artery serves as an internal control (**Figure 1.3-E**).

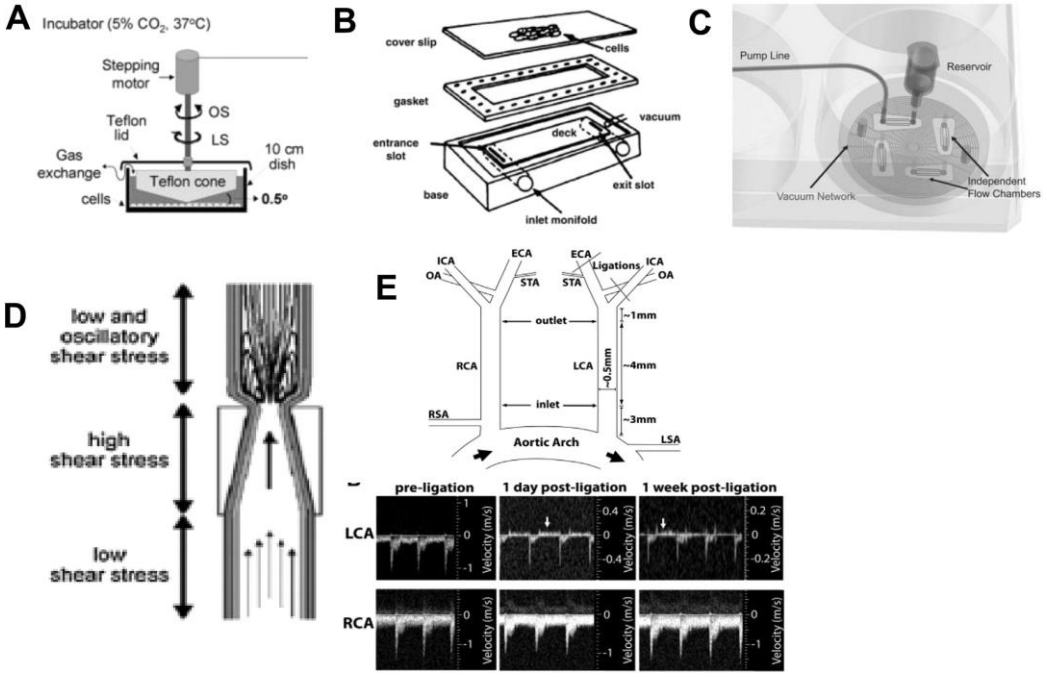

Figure 1.3 Models of flow and shear stress. Cone-and-plate viscometer. Adapted from Jo et al. (1991) (A). Parallel plate flow chamber. Adapted from Lawrence et al. (1987) (B). Microfluidic flow chamber. Adapted from Schaff et al. (2007) (C). Carotid cuff model Adapted from Cheng et al. (2005) (D). Partial carotid ligation model. Adapted from Nam et al. (2010). (E).

1.5 Mechanosensing and Mechanotransduction in Atherosclerosis

1.5.1 Mechanosensors

On the luminal, junctional, and basal surfaces of ECs, there are numerous mechanoreceptors capable of detecting and responding to shear stress stimuli. After activation of any one of these mechanoreceptors, a complex network of several intracellular pathways is triggered in a process known as mechanotransduction (summarized in **Figure 1.4)**. These pathways are activated simultaneously and/or cross-talk with each other. These pathways lead to regulation of several transcription factors, which bind positive or negative shear stress responsive elements (SSREs) in the promoters of mechanosensitive genes, thus inducing or suppressing gene expression respectively. Furthermore, a shear stress stimulus could trigger a change in conformation of a membrane protein in order to expose previously

hidden sites. Thus, a new binding site would be available to downstream biochemical substrates, which would initiate a cell signaling cascade. Below, we discuss the role of major mechanical sensors, including platelet endothelial cell adhesion molecule 1 (PECAM1), the glycocalyx, caveolins, cytoskeletal structures, integrins, angiotensin type 1 (AT1) receptor (AT1R), and the nucleus in the regulation of endothelial function.

PECAM1 is an important molecule that is present on the endothelial surface and is primarily localized to junctions between ECs. PECAM1 becomes phosphorylated at tyrosine residues in response to mechanical stimuli. Osawa et al. report that this phosphorylation causes association of PECAM1 with SHP-2, a phosphatase that activates extracellular signal-regulated kinase (ERK) [84]. ERK activation, which has been previously implicated in mechanotransduction, depends on PECAM1 phosphorylation. Therefore, it can be speculated that in response to mechanical disturbance of the plasma membrane, PECAM1 becomes phosphorylated by an unknown kinase, and subsequently recruits SHP-2, thereby activating ERK. In turn, SHP-2 can dephosphorylate PECAM1, however, persistent flow-shear stress could re-initiate the phosphorylation cycle, thus maintaining the cellular response [85]. Furthermore, PECAM1 (in complex with vascular endothelial growth factor receptor (VEGFR2) and VE-cadherin) activates phosphatidylinositol-3-OH kinase (PI3K), which is another mechanosensitive signaling kinase. After PI3K is activated, another mechanosensitve kinase which is involved in the same signaling pathway as PI3K, Akt, is also activated. Akt activation leads to cytoskeletal arrangement so that ECs exposed to anti-atherogenic LS align in the direction of flow, whereas in ECs exposed to pro-atherogenic OS, have Rac1 activation, which in turn leads to increased reactive oxygen species (ROS) and NFκB activation. Thus, in OS, the same mechanosensors lead to the expression of pro-inflammatory genes by activating NFκB. [86, 87]

The glycocalyx is also present on the surface of ECs. The glycocalyx is comprised of various macromolecules. Some of these include glycoproteins bearing oligosaccharides and terminal sialic acids, proteoglycans, and glycosaminoglycans (GAGs) [88]. The glycocalyx constantly senses the shear stress on the endothelium. The glycocalyx also interacts with other plasma proteins, enzymes, enzyme inhibitors, growth factors and cytokines through structural cationic sites, as well as cationic amino acids, in order to make a matrix of biopolyelectrolytes [88-92]. It is frequently observed that the glycocalyx undergoes structural and functional modifications when interacting with these molecules [93-96]. These properties allow the glycocalyx to function as a selectively permeable barrier for macromolecules by filtering molecules based on size and charge. Given its role as a selectively permeable barrier, its ability to sense the mechanical forces imposed by blood flow, and sequentially transduce these signals into intracellular biochemical responses with vasoregulatory properties [97-101], these qualities distinguish the glycocalyx as a vital element of a functional endothelium. Likewise, proteoglycans are proteins that contain specific sites where sulfated GAGs are covalently attached *en route* from the endoplasmic reticulum to the Golgi apparatus. These constituents provide a downstream signaling event upon interaction with the local fluid-shear environment [96, 102].

Caveolin-1 is also a membrane-associated element. Specifically, caveolin-1 is a protein that associates with cholesterol and sphingolipid-rich regions of the membrane and usually forms pits or caveolae. Similarly, glypicans, along with their heparin sulfate chains localize to these regions. Transmembrane syndecans are shown to cluster on the outer edge of caveolae and along with other molecules, are involved with eNOS signaling. Particularly, these molecules have been shown to inactivate eNOS [103-107]. On the other side of the plasma membrane, the cytoplasmic tails of the syndecans associate with the cytoskeleton and assist in its organization through molecules such as ezrin, tubulin, syntenin, syndesmos, dynamin and α-actinin [108-111]. Syndecans also directly associate

with proteins involved in signaling, such as protein kinase C-α (PKCα), phosphatidylinositol-4,5-biphosphate, and Calcium/Calmodulin-Dependent Serine Protein Kinase (CASK), a protein containing both a calcium/calmodulin-dependent and a guanylate kinase domain [108, 112-114]. Active participation in signaling stems from the phosphorylation of certain intracytoplasmic residues, which act as switches controlling the oligomerization state and thus altering the binding properties of syndecans. Ultimately, this enables them to orchestrate events on both sides of the membrane [108, 112-114]. Finally, it is also worth noting that the secondary structures of all syndecan ectodomains are predicted to contain almost exclusively solvent-accessible loops, implying that these molecules are flexible (models by PROFsec, and YASPIN) [115, 116].

Integrins are also membrane-associated mechanosensors. Integrins are hetero dimeric transmembrane proteins comprised of non-covalent interactions between α and β subunits that serve as major molecular links between ECs and the ECM. Extracellular domains of the α subunits participate in adhesion and ligand recognition, and upon activation, the short cytoplasmic domains of β subunits, which lack kinase function, physically connect to the cytoskeleton and recruit proteins for signaling [117-120]. The specificity of integrin signaling is made possible by α and β-subunits that form the hetero dimeric pair. The α-subunit generally confers ECM specificity [120, 121], whereas the β-subunit interacts with the cytoplasmic environment. Evidence for shear stress activation of integrins is provided by both direct assessment of integrin conformational changes in response to shear stress and blockade of the shear-induced responses by monoclonal antibodies or via the use of the integrin binding Arg-Gly-Asp (RGD) peptide. When cells are plated on ECM or treated with integrin-activating monoclonal antibodies, integrin activation is manifested by modulations of affinity and avidity [122, 123]. Tzima et al. have shown an increased immunostaining of integrins in sheared ECs, indicating a modulation of integrin affinity by shear stress [86]. Using multiple monoclonal antibodies to assess ligand-bound form of β_1 and β_3, Jalali et al. have demonstrated that shear stress leads to an

increase in integrin avidity in the endothelium [124]. Because integrins lack enzymatic activity, activation of signaling factors requires interaction with cellular proteins that have kinase activity. In ECs, the cytoplasmic tail of the β-subunit has been shown to directly bind to several cytoskeletal proteins that associate with signaling molecules [125]. In other cell types, β1 integrin has been shown to be important for coupling mechanical stretch to activation of the well-known mechanosensitive signaling pathway members mitogen activated protein kinases (MAPKs), as well as focal adhesion kinase (FAK) and Rho GTPases [126, 127]. EC motility is a critical function that is regulated by integrins in response to hemodynamic forces. The effect of shear stress on EC migration and the contribution of the integrins and integrin-dependent signaling pathways have been studied *in vitro* using scratch-wound assays. LS-induced endothelial migration was significantly reduced by integrin-receptor blocking with RGD peptides or with neutralizing antibodies against integrin subunits αv and β1, whereas antibodies against αvβ3 or α2β1 had no effect. Cell-surface levels of the integrin α5β1 were specifically upregulated in migrating ECs at the wound edges. Consistent with these previous results, blockade of the integrin-associated adapter protein Shc by overexpression of dominant negative construct inhibited shear stress-stimulated endothelial migration [128, 129]. Collectively, these studies imply that integrins are important endothelial mechanosensors and mechanotransducers.

Mechanical forces can also be directly sensed by the actin cortex and, in turn, be transmitted as signaling events. However, the mechanisms are poorly understood. Using an integrative approach of combining molecular and mechanical experimental perturbations with theoretical multiscale modeling, the process of cortical mechanosensing from molecular to cellular scales has been elucidated. Early evidence that the nucleus is under tension came from Ingber and coworkers in 1992, who showed that perturbing actomyosin forces altered cell and nuclear shape [130]. In a landmark paper in 1997, they showed that tugging on integrin receptors in the cell membrane causes nuclear distortion

and motion [131]. This established the concept that forces applied externally to the cell are propagated to the nuclear surface, which was consistent with mechanical models of the cell cytoskeleton that are 'hardwired' to the nuclear envelope [132-137]. These external forces have now been shown to induce clearly-detectable nuclear deformation [131, 138-145]. The F-actin cytoskeleton plays a major role in propagating the mechanical forces from the integrin receptors to the nuclear surface, although the molecules which connect the nucleus to the cytoskeleton have only recently been identified. In recent years, members of the so-called LINC complex (Linker of Nucleoskeleton to the Cytoskeleton) have been discovered in the nuclear envelope [146-151]. The LINC complex is comprised of two protein families that span the nuclear envelope, and physically connect the cytoskeleton to the nucleoskeleton. The SUN (Sad1p, UNC-84) domain proteins span the inner nuclear membrane and translumenally bind the KASH (Klarsicht/ANC-1/Syne Homology) domain proteins that span the outer nuclear membrane. In this way the KASH and SUN domain proteins create a mechanical tether that connects both membranes of the nuclear envelope. The KASH domain proteins bind to various cytoskeletal constituents, whereas the SUN domain proteins associate with the nuclear lamina [149-151]. Thus, the mechanical connections created by the LINC complex can integrate the forces of the cytoskeleton and the nucleus.

In the past decade, numerous studies have indicated that the nucleus itself may act as a cellular mechanosensor to directly modulate the expression of mechanosensitive genes [152]. The nucleus is tightly integrated into the structural network of the cell through LINC, which transmits forces between the nucleus and the cytoskeleton [150]. Lamins, which are type V nuclear intermediate filaments, contribute to the nuclear lamina as an extended part of the LINC complex. Through this interaction, lamins play a central role in the nuclear mechanosensory process. Lamins can be separated into A-type and B-type, with lamins A and C as the major A-type isoforms, and lamins B1 and B2 as the major B-type isoforms in somatic cells [153]. Lamins A and C provide structural support to the nucleus [140] and

play a major role in physically connecting the nucleus to the cytoskeleton, thereby enabling forces to be transmitted from the cytoskeleton and extracellular matrix to the nuclear interior. Lamins A and C are important contributors to the mechanical stiffness of nuclei, whereas lamin B1 contributes to nuclear integrity instead. Cells lacking lamins A and C have reduced nuclear stiffness and increased nuclear fragility, which leads to increased cell death under mechanical strain. Mutations in lamins A and C result in a variety of severe diseases, including dilated cardiomyopathy, which further indicates the critical role of these nuclear envelope proteins in maintaining normal cellular function. Recent studies have provided some insight into how the nuclear lamina responds to force-induced nuclear deformation and couples to biochemical responses in ECs in response to shear stress [138, 154-157]. However, it remains to be determined whether these changes reflect the role of lamins as mechanosensors or if transcriptional regulation of lamins is downstream of other mechanosensing pathways. Several other key questions remain to be addressed regarding the role of the nuclear envelope proteins in endothelial mechanotransduction. Issues that remain to be addressed include whether lamins are mechanosensors or merely serve as processing hubs, how the nuclear mechanosensing system is integrated with signaling originating from the plasma membrane, and the role of this system during adaptive and maladaptive stages of vessel remodeling.

Finally, G-protein coupled receptor (GPCRs), such as AT1R, can also serve as mechanosensors/transducers. One such, AT1R, binds angiotensin II (Ang II) in the canonical pathway. However, recently it was found that there are biased ligands of AT1R which can be activated by shear stress through an AngII-independent mechanism [158-162]. It is well established that AT1R, the first mechanosensitive GPCR discovered, mediates transformation of mechanical stimuli into biochemical information and gives rise to a variety of mechanosensor-induced cellular responses (such as inflammation, cell growth, and differentiation etc.) [162, 163]. Recent studies suggest that d-flow induces β-arrestin-based signaling downstream of AT1R in the absence of ligand or G protein

activation [164]. Mechanical stimulus triggered AT1R receptors mediate conformational changes in β-arrestin, similar to that induced by a β-arrestin-biased ligand, to selectively stimulate receptor signaling in the absence of detectable G protein activation [161, 162, 165]. Yatabe et al., demonstrated that mechanical stress caused an increase in the phosphorylation levels of ERK in rat mesangial cells through the AngII-independent AT1R activation [160].

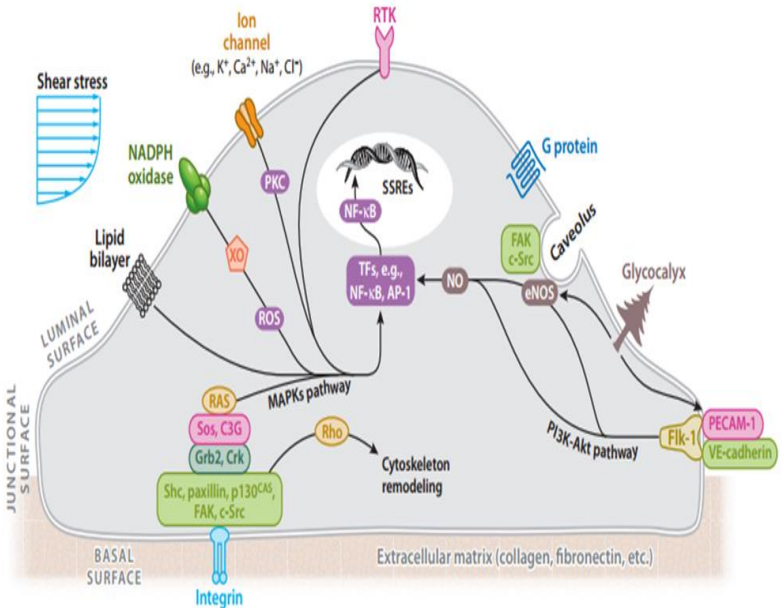

Figure 1.4 The endothelial cell senses shear stress through mechanosensors. These include surface mechanoreceptors (ion channels, receptor tyrosine kinases, G protein coupled receptors), cell-cell and cell-matrix adhesion complexes (PECAM1/VE-cadherin/VEGFR2 complex and focal adhesion kinases), the glycocalyx, and cytoskeletal elements. Adapted from Chatzizisis et al. (2007)

1.5.2 Mechanosensitive Signaling Pathways

Shear stress is translated from the cell surface through a variety of mechanosensors [166]. Once the shear stress stimulus is applied, various intracellular pathways are triggered. Interestingly, many of these pathways converge on common signaling pathways, such as the MAPK pathway and the PI3K /Akt pathway [104]. The MAPK pathway in particular can be activated through integrins (as previously discussed), among others. Briefly, integrins activated by mechanical stimuli phosphorylate and activate a complex of kinases,

adaptor proteins, and guanine nucleotide exchange factors, which ultimately lead to the activation of Ras. When Ras becomes activated, this leads to the activation of MAPKs. ERK1/2, members of the MAPK family, then activate transcription factors (such as c-myc, c-jun, and c-fos) and/or eNOS [167]. Furthermore, mechanosensitive membrane proteins activate the MAPK pathway through protein kinase C (PKC) [167], whereas NADPH oxidase activates the MAPK pathway through ROS [168]. An additional example of such is the activation of PECAM1, as discussed previously. Furthermore, the PI3K/Akt pathway can converge with the same integrins that the MAPKs interact with and can lead to activation of eNOS [169, 170].

These shear-responsive pathways often activate the MAPK and PI3K/Akt pathways differentially in response to LS vs. OS [171]. In LS, atheroprotective genes become upregulated [172-174]. Particularly, eNOS becomes phosphorylated and activated by Akt via a PI3K-dependent pathway [175] and leads to an anti-atherogenic phenotype in ECs [176]. Krüppel-Like Factor 2 (KLF2) is a mechanosensitive transcription factor which is intimately involved in the aforementioned mechanosensitive pathways. Klf2 is critical for vascular homeostasis and is a potent anti-atherogenic transcription factor [177]. Klf2 is a highly expressed in straight sections of the human aorta that experience LS, but is lower in the regions experiencing OS, such as the bifurcation in the iliac and carotid arteries [178]. Consequently, KLF2 downregulates a host of pro-inflammatory genes in ECs exposed to LS, such as vascular cell adhesion molecule (VCAM-1) and E-selectin, which mediate monocyte and T-cell adhesion to the endothelium [179]. Furthermore, KLF2 can inhibit the NFκB pathway by recruiting transcriptional coactivators to inhibit interleukin 1 (IL-1β) and tumor necrosis factor (TNFα)-mediated stimulation. KLF2 also inhibits thrombin-mediated induction of inflammatory factors, such as monocyte chemoattractant protein (MCP-1), IL-6, and IL-8, by inhibiting expression of its principal receptor protease-activated receptor 1 [180, 181]. Additionally, KLF2 prevents endothelial inflammation and thrombosis by preventing nuclear localization of phosphorylated activating transcription

factor 2 (ATF2), which mediates the expression of proinflammatory and procoagulant genes [182]. To further solidify the role of KLF2 as a potent anti-thrombotic agent, it was found that KLF2 overexpression strongly increases TM, which is a cell surface factor that inhibits coagulation, and KLF2 inhibits tissue factor and plasminogen activator inhibitor 1 production.

However, not only does KLF2 downregulate inflammation and prevent thrombosis, KLF2 is also responsible for the shear-induced alignment of ECs. Horrevoets et al first linked KLF2 expression to the morphological changes seen in endothelial cells exposed to shear. In this study, they found that Jun NH2-terminal kinase and MAPK signaling lead to inhibition of the phosphorylation of actin cytoskeleton-associated proteins [183]. KLF2 promotes vasodilation through the direct transcription of eNOS [184-187] and by inhibiting caveolin-1, which regulates eNOS by inducing arginosuccinate synthase, a limiting enzyme in eNOS substrate bioavailability [184-187]. In the long term, sustained expression of KLF2 inhibits expression of endothelin-1, adrenomedullin, and angiotensin converting enzyme, all ofwhich increase vascular contractile tone [188].

Furthermore, KLF2 inhibits angiogenesis and EC proliferation via inhibition of VEGF-A[189] and VEGFR2 expression by competing with its transcription factor Sp1 at the promoter. In addition to these mechanisms, KLF2 can inhibit angiogenesis through semaphorins, have been shown to inhibit EC migration. Klf2 can be upregulated by LS indirectly through the LS effect on the MAPK pathway (namely MEK5 and ERK5) [190]. KLF2 is regulated through a variety of mechanosensitive pathways. These include LS induction of MAPK pathway, which causes histone deacetylase 5 (HDAC5) dissociation from MEF2, thus allowing MEF2 transcription of KLF2 mRNA [191], PI3K inhibition by prolonged flow via Tie2, AMP-activated protein kinase activation by LS activating ERK5-MEF2. KLF2 mRNA is also stabilized via PI3K pathway [192]. Furthermore, OS causes prolonged suppression of KLF2 by the src signaling pathway [193]. Additionally, the OS sensitive gene regulator HuR plays a role in KLF2 regulation. Specifically, downregulation

of HuR leads to KLF2 mRNA stabilization [194]. Pro-inflammatory cytokines such as TNFα and IL1β repress KLF2 expression via HDAC4 and p65 (component of NFκB) cooperatively inhibiting MEF2 [195]. Finally, oxidative stress can also decrease KLF2. SUMOylation of ERK5 by hydrogen peroxide and advanced glycation end products inhibits KLF2 expression by decreasing MEF2 [196] and the Shc oxidative stress protein p66shc [197] reduces MEF2A expression as well.

Another transcription factor, nuclear factor (erythroid-derived 2)-like 2 (Nrf2) is a target of KLF2, is also mechanosensitive, and in conjunction with KLF2, controls 70% of the genes induced by LS [187]. Nrf2 becomes translocated to the nucleus in cultured endothelial cells exposed to LS [198]. Nrf2 which exerts its anti-atherogenic effects by modulating ROS and reactive nitrogen species (RNS) [174]. Shear stress plays a critical role in the production of ROS and RNS in ECs. Shear stress activates NADPH oxidase, resulting in production of superoxide (O^{2-}) [197, 199-201]. Xanthine oxidoreductase also contributes to superoxide production in response to OS [202]. In addition, NO is generated (via eNOS) [106, 203-206] Although NO plays an important role in vasodilation [207-209] and inflammation [161, 210]. NO may react with superoxide, thereby forming peroxynitrite ($ONOO^-$), which is highly reactive. Peroxynitrite can modify proteins and lipids and induce oxidative damage [211, 212]. Although both OS and LS induce superoxide and NO, the balance between the species determines the overall effect. In the case of LS, NO production is significantly higher than that of OS [213, 214]). Whereas in OS, superoxide production is much higher [202, 215-217] but eNOS is upregulated to a much lesser extent [218-220], which in turn leads to the reaction of NO with superoxide to form peroxynitrite, resulting in less bioavailable NO. In contrast, LS upregulates the expression of eNOS strongly, as well as dismutases that can convert superoxide into other species, thus preventing peroxynitrite formation. These include copper/zinc superoxide dismutase (CuZnSOD) and manganese (MnSOD) [221, 222]. Nrf2 is essential for upregulating cytoprotective genes under LS [174, 223, 224]. Nrf2 binds to the antioxidant response element (ARE) in its

target genes, which include phase II detoxification enzymes and antioxidant proteins, such as glutathione-S-transferase, HO-1, peroxiredoxin 1, NQO1, GCLM, and GCLC [212, 225, 226]. These enzymes are crucial for protecting cells from electrophile toxicity and oxidative stress.

Nrf2 is negatively regulated by Kelch-like ECH-associated protein 1 (Keap1), which facilitates the degradation of Nrf2 through the proteasome [193]. In response to oxidative stimuli, Nrf2 becomes activated by its dissociation from Keap1, which undergoes electrophilic attack that causes it to undergo the conformational change to dissociate from Nrf2 [30, 196, 227, 228]. In turn, Nrf2 upregulates its anti-oxidant target proteins [229, 230]. The upregulation of Nrf2 in LS is ROS dependent, as Nrf2 activation in LS was blocked by ROS scavengers [224, 231-235] and NADPH oxidase inhibitors. The subsequent ROS/RNS modifies Keap1 under LS conditions so that Nrf2 is no longer suppressed.

As opposed to LS, in OS , ECs express pro-inflammatory cytokines such as MCP-1 [169] and inflammatory cell adhesion molecules such as VCAM1 and ICAM1 [236]. The chemokine MCP-1, contains a phorbol ester (TPA)-responsive element (TRE) in its promoter region, which was also found to be shear-sensitive and regulated through MAPKs [169]. Similarly, VCAM1 and ICAM1 also contain these shear-responsive elements in their promoters [236]. Furthermore, ECs express other pro-inflammatory, shear-sensitive proteins such as NADPH oxidase [174], and bone morphogenetic protein (BMP4) [237]. Two of the main transcription factors that are responsible for the upregulation of many of these pro-inflammatory genes such as ICAM1, VCAM1, and E-selectin are the activator protein complex (AP-1) and nuclear factor (NFκB) complex [116, 183, 238-242].

NFκB is comprised of p65 (RelA) and p50, and its activity is regulated by its intracellular location. Under basal conditions, NFκB is located in the cytosol bound to IκBα. Under stimulation, IκBα becomes phosphorylated by IκB kinase, and thus NFκB becomes free to pass into the nucleus and bind to target genes for transcription. Whereas AP-1 is a heterodimer composed of different proteins from either the c-Fos, c-Jun, ATF, or JDP families depending on the target gene. ROS produced by NADPH oxidase or other oxidases can directly activate NFκB and AP-1 [243, 244] in MAPK, ERK, and c-Jun N-terminal kinase (JNK) dependent pathways [172, 245-249]. **Ultimately, these findings have demonstrated that LS upregulates "atheroprotective" genes and downregulates "pro-atherogenic" genes while OS results in the opposite phenomenon.**

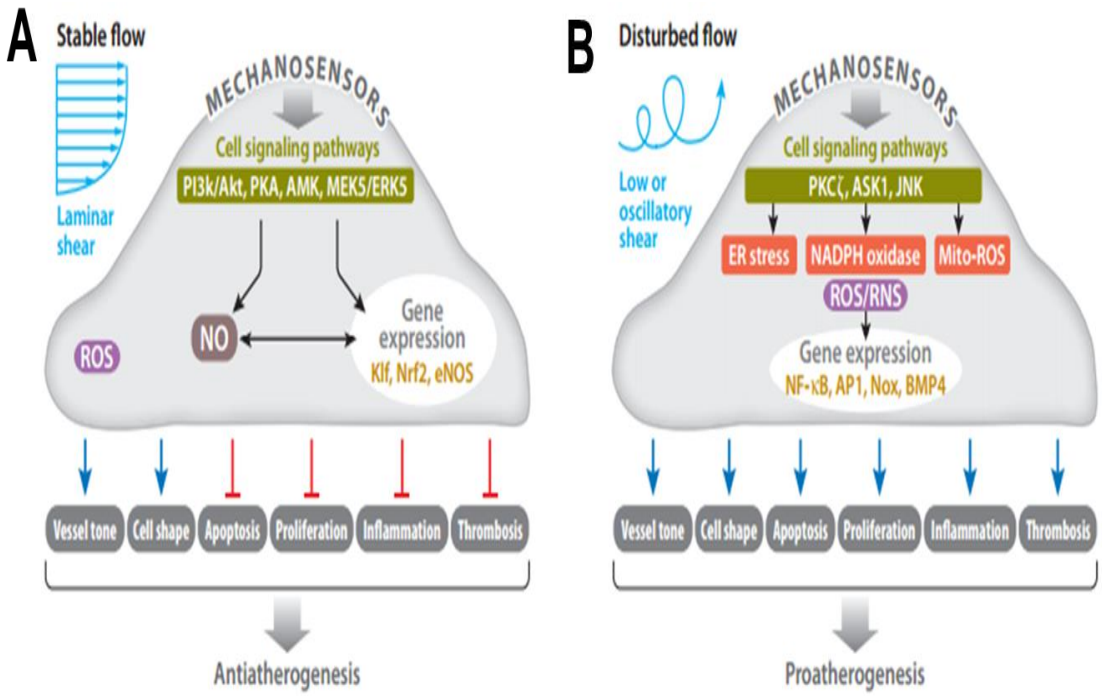

Figure 1.5 Shear stress leads to the activation of multiple intracellular pathways. (A) LS activates pathways that result in alignment in the direction of flow, increased NO production, and suppression of inflammatory cell adhesion molecules. (B) On the other hand, OS induces high expression of cell adhesion molecules, production of inflammatory cytokines, high oxidative stress, and a leaky cell barrier Adapted from Noguchi & Jo (2011).

1.6 MicroRNAs and Atherosclerosis

1.6.1 Biogenesis of miRNAs

microRNAs (miRNAs) are a large class of evolutionarily conserved, noncoding RNAs, typically 18 to 22 nucleotides in length. miRNAs primarily function as post-transcriptional regulators by interacting with the 3' untranslated region (3' UTR) of specific target mRNAs in a sequence-specific manner[250, 251]. . It is thought that a single miRNA can target hundreds of mRNAs. miRNAs are transcribed by RNA polymerase II and can be derived from individual miRNA genes, from introns of protein coding genes, or from polycistronic transcripts that often encode multiple, closely related miRNAs. Pri-miRNAs are processed in the nucleus by the RNase Drosha into 70–100 nucleotides, hairpin-shaped precursors, called pre-miRNAs. Following transport to the cytoplasm, the pre-miRNA is further processed by the RNA endonuclease Dicer to produce a double-stranded miRNA. The fully processed miRNA duplex is then incorporated into a multicomponent protein complex known as RNA induced silencing complex (RISC), of which argonaute (Ago2) is a member of. During this process, one strand of the miRNA duplex is selected as a mature miRNA while the other strand, known as miRNA*, is rapidly removed and degraded [252-255]. **As part of the RISC, miRNAs negatively regulate gene expression through translational repression or mRNA cleavage, depending on the degree of complementarity.**

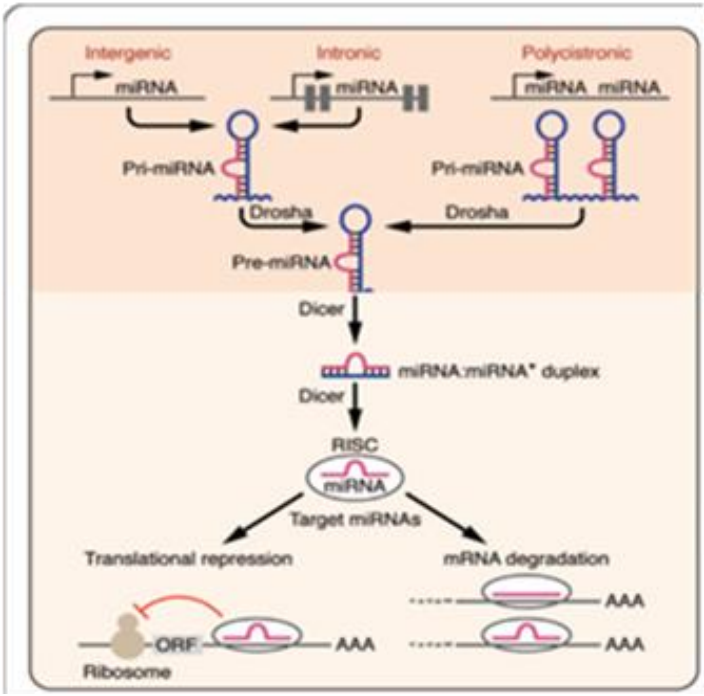

Figure 1.6 Biogenesis of miRNAs. Adapted from van Rooij (2008)

1.6.2 Mechanosensitive Endothelial-Derived miRNAs in Atherosclerosis

It has been previously demonstrated that LS and OS differentially regulate the expression of miRNAs in endothelial cells. The majority of flow sensitive miRNAs have been identified and characterized *in vitro* . However, a select few were subsequently validated *in vivo* . Therefore, only a limited number of direct links to atherosclerosis have been established. Current literature divides these shear-sensitive miRNAs into three classes according to their reported effects [256] (summarized in **Figure 1.7**): (A) anti atherogenic (B) dual role and (C) pro atherogenic. Anti atherogenic miRNAs include miR-10a, 19a, 23b, 101, 143 and 145, all of which are either upregulated by LS or are downregulated by d-flow/OS. Dual role miRNAs include miR 21, 155, and 126. Dual-role miRNAs have been implicated in both pro and anti-atherogenic events. Pro atherogenic miRNAs include miR-17~92, 92a, 663, 712, and 205, all of which are either upregulated by d-flow/OS or are downregulated by LS.

Anti-atherogenic miRNAs

miR-10a was one of the first to be identified as mechanosensitive. Its expression in the endothelium is decreased by d-flow in the athero-prone, lesser curvature region (LC) of the porcine aortic arch as compared to that of the athero-protected, thoracic aorta (TA)[257]. Mechanistically, miR-10a prevents inflammation by targeting MAP3K7 and βTRC, both of which promote IκB degradation (NFκB inhibitor) and p65(NFκB subunit) translocation[257]. Later studies using HUVECs found that following 12 hours of LS (12 dyn/cm^2), 35 miRs were upregulated and 26 miRs were downregulated as compared to static controls.[258]. Among these, LS increased expression of miR-19a, which targets cyclin D1, thus inhibiting proliferation[258]. Subsequent studies identified 8 upregulated and 13 downregulated miRNAs in response to 24 hours of pulsatile LS (12±4 dyn/cm^2) as compared to the static controls[259]. One of the upregulated miRNAs was miR-23b, which suppressed endothelial proliferation by reducing E2F1 expression and Rb phosphorylation[259]. Other anti-atherogenic miRNAs include miR-101, which is upregulated in response to LS and was reported to target the mTOR gene (inducing cell cycle arrest[260]) and miR-143/145, which increase by LS in an AMPKα2-dependent manner[261] and in a KLF2-dependent manner[262].

Dual Role miRNAs

Although miR-21 was upregulated by LS in HUVECs and was shown to prevent apoptosis (by targeting PTEN[263]), another study showed that OS upregulated miR-21 in a time-dependent manner. Furthermore, it was shown to inhibit PPARα, thus leading to the enhanced expression of VCAM1[264]. Interestingly, miR-21 was increased in arterial endothelium exposed to d-flow in the mouse PCL model[83, 265]. Whether miR-21 plays a pro or anti-atherogenic role still remains to be determined. Similarly, the effect of flow on the miR-126 and its role in atherosclerosis is also not well understood. Both miR-126-5p and 3p) are highly expressed in ECs and have been shown to regulate vascular

integrity, angiogenesis[266], and inflammation[267]. The secretion of miR-126-3p into conditioned media was decreased by LS in HUVECs[268]. Furthermore, knockout of miR-126 inhibited neointimal formation in a complete carotid ligation model, while local reintroduction of miR-126 in the knockout mice enhanced neointimal formation. However, a recent study showed that d-flow decreased expression of both miR-126-5p and 126-3p, treatment with the miR-126-5p mimic reduced atherosclerotic lesion formation, and miR-126-5p directly targets the Notch1 inhibitor, Dlk1, which promotes EC proliferation[269]. Another interesting report from the same group showed that miR-126-3p present in apoptotic bodies had an atheroprotective effect in a murine carotid cuff model of atherosclerosis[269]. Finally, the role of miR-155 in atherosclerosis is also unclear. Its expression is increased by LS in HUVECs and it is abundantly expressed in the intima of the athero-resistant TA[270]. However, other studies showed that miR-155 mediates pro-atherogenic responses[271, 272]. Specifically, miR-155 was shown to directly target eNOS mRNA in HUVECs and impair endothelium-dependent vascular relaxation in human arteries[273]. Furthermore, leukocyte-specific miR-155 deficiency reduced plaque size and lesional macrophage count in the PCL model of atherosclerosis[271]. Another study showed that genetic knockdown of miR-155 ameliorated atherogenesis in $ApoE^{-/-}$ mice by reducing inflammatory responses of macrophages and increasing macrophage cholesterol efflux[272]. **Ultimately, the role of miR-155 in atherosclerosis, as well as all miRNAs, may depend on the specific cell type and time-scale.**

Pro-atherogenic miRNAs

The miR-17~92a cluster comprises several miRs, including miR-17, 18a, 19a 19b, 20a and 92a. Of these, miR-17, miR-19b, miR-20a, miR-92a are mechanosensitive. Specifically, they were downregulated by 24 hours of pulsatile LS[191]. Subsequent studies showed that miR-92a was downregulated by LS and was upregulated by OS[274].

These *in vitro* findings are consistent with *in vivo* studies showing that ECs in the porcine aortic arch have increased miR-92a levels as compared to those of the thoracic aorta[274]. Further studies demonstrated that miR-92a induced endothelial inflammation by targeting KLF2 and KLF4 [275].

From our mouse model of d-flow-induced atherosclerosis, we identified miR-712 and miR-205 and established their function in two different animal models of atherosclerosis [36]. We found that d-flow induced expression of miR-712, and that it contributed to endothelial dysfunction, and thus atherosclerosis. Additionally, treatment with antimiR-712 prevented plaque development. The pro-inflammatory and pro-atherogenic effects of miR-712 were mediated by its target, tissue inhibitor of metalloproteinase-3 (TIMP3). Loss of TIMP3 by miR-712 resulted in activation of MMPs and a disintegrin and metalloproteinases (ADAMs), ultimately leading to endothelial inflammation, hyper-permeability, and atherosclerosis [36]. Interestingly, miR-712 is murine-specific, but miR-205 is a homolog which is conserved in humans and other vertebrates[36], also targets TIMP3, and is also mechanosensitive [36]. In addition to miR-712 and miR-205, our lab also identified a primate-specific miRNA, miR-663, as the most highly upregulated by OS in HUVECs using a miRNA array derived from 24 hours of OS vs. LS[276]. Furthermore, we found that inhibition of miR-663 in HUVECs correlate with decreased adhesion of monocytes even in OS conditions. Finally, we also found that increasing miR-663 in LS increases monocyte adhesion, thus implicating miR-663 in endothelial inflammation[276]. Consistent with this report, miR-663 was upregulated in HUVECs exposed to pro-atherogenic oxidized phospholipids, and was found to play a permissive role in the induction of VEGF and activation of ATF4 branch of unfolded protein response in ECs [277, 278]. **Although these initial studies indicate miR-663 may be pro-inflammatory in humans, the study of miR-663 and its human targets is limited in the physiologically relevant mouse model.**

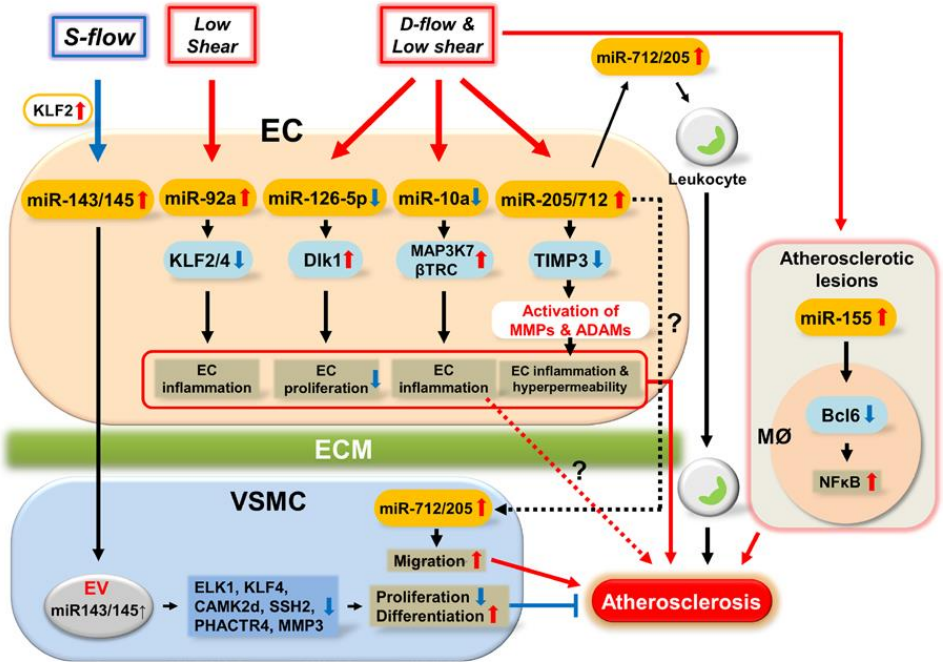

Figure 1.7 Role of mechanosensitive miRNAs in atherosclerosis. Adapted from Kumar (2014).

1.6.3 miRNA Animal Studies in Atherosclerosis

Many miRNAs have previously been identified as playing a role in atherosclerosis by their actions in the endothelium, smooth muscle cells, macrophages, or in cholesterol transport [256]. Some of the previously discussed mechano-miRs have been investigated as potential therapeutic targets for atherosclerosis through the use of antimiRs or knockout mice, including miR-712, 92a, 155, and 126, however, some non-mechanosensitive miRNAs have also been shown to be potential therapeutics in atherosclerosis. These include miR-1, 30c, 144, 146a, 181b, 195, 467b, 342, and 33. These studies were conducted using either antimiRs, mimics, adenoviral delivery, or knockout mice.

Anti-Atherogenic miRNAs Studies: Mimics and Viral Delivery

miR-1, 146a, 181b, and 195 have all been shown to reduce inflammation by their actions in the endothelium and in SMCs. Specifically, inhibition of miR-1 using antago-miR enhanced the endothelial hyper-permeability induced by hypercholesterolemia, whereas miR-1 mimic prevented endothelial barrier dysfunction[279]. Additionally, miR-146a mimics prevented endothelial activation by targeting HuR, thus repressing the NFκB and MAP kinase pathways, whereas deletion of miR-146a in mice aggravated endothelial inflammation [280]. Similarly, systemic delivery of miR-181b mimics reduced atherosclerosis through inhibition its target gene, importin-α3, which mediates NFκB nuclear translocation [281, 282]. Also, adenoviral delivery of miR-195 reduced neointimal formation in a balloon-injury carotid artery model by inhibiting VSMC proliferation, migration, and IL-1β, IL-6, and IL-8 synthesis [283].

Alternatively, miR-30c, 144, and 467b play an important role in the regulation of plasma cholesterol level, which is a critical risk factor of atherosclerosis. Overexpression of miR-30c via lentivirus in the liver reduced the hyperlipidemia seen in Western diet-fed mice by decreasing lipid synthesis and the secretion of triglyceride-rich ApoB-containing lipoproteins, which in turn prevented atherosclerosis in $ApoE^{-/-}$ mice[284]. Also, miR-467b mimic delivery reduced plasma cholesterol and atherosclerosis. Alternatively, miR-467b inhibition by using antago-miR-467 enhanced the progression of atherosclerosis by increasing lipid accumulation and inflammatory cytokine secretion [285]. Finally, miR-144 mimics decreased hepatic ABCA1 and HDL cholesterol, but its contribution to the development of atherosclerosis is unknown [286].

Pro-Atherogenic miRNAs Studies: AntimiRs

miR-342 and miR-33 are both pro-atherogenic miRs. Specifically, miR-342-5p is a macrophage-derived miRNA that increases atherosclerosis and inflammatory stimulation of macrophages through inhibition of Akt1 [287]. Suppression of Akt1 by miR-342-5p indirectly induces Nos2 and IL-6 in macrophages through miR-155.

Therefore, systemic miR-342-5p inhibition reduced atherosclerotic plaque development in the aorta of ApoE$^{-/-}$ mice.

Multiple studies show that silencing of miR-33 prevents inflammation and atherosclerosis [288-290]. AntimiR-33 treatment or genetic knockout of miR-33 in mice promotes reverse cholesterol transport and inhibition of atherosclerosis through regulation of ABCA1[288, 289, 291]. Also, antimiR-33 increased hepatic expression of ABCA1 and induces a sustained increase in plasma HDL in a non-human primate model[292]. However, a recent report showed that long-term silencing of miR-33 with antimiR-33 failed to demonstrate the anti-atherogenic effects in LDL receptor knockout mice [291]. The inconsistent responses reported in these studies may reflect a different target genes and roles of miR-33 in various cells and tissue types. While miR-33 may ABCA1 in hepatocytes, it may regulate other, unknown target genes in other cell types. **Thus, these observations raise an important concern regarding the off-target effects of systemically delivered miRNA mimics, antimiRs, or antago-miRs in animal studies and clinical use.**

1.6.4 miRNAs in the Clinic

Given the increasing number of *in vivo* studies using miRNAs both in the atherosclerosis field and beyond, some miRNA studies have moved into clinical trials. These include antimiR-122, both LNA modified and galactose conjugated, antimiR-103/107 (galactose modified), antimiR-155 (LNA), miR-29 mimic, miR-16 mimic, and miR-34 mimic [293].

Pro-atherogenic miRNAs Therapies: AntimiRs

The first of these was the LNA-modified antimiR-122, which is a 15-nucleotide antisense RNA oligo complementary to the 5′ end of miR-122. The antimiR is known as Miravirasen and is intended for the treatment of Hepatitis C Virus (HCV). Preclinical studies in rodents and in non-human primates indicate the antimiR passively accumulates in the liver and decreases cholesterol accumulation and reduced titers of HCV [294-296].

A Phase I clinical trial was initiated in 2009 and no adverse reactions were reported, thus prompting the launch of a Phase II trial. In the first Phase II Trial, 9 patients were enrolled in 4 groups, each of which received a dose of 3, 5, or 7 mg/kg Miravirsen or placebo once a week for 5 weeks. Patients experienced a significant dose-dependent reduction in HCV load and serum cholesterol levels. [297]. However, a more recent follow-up study showed mutations near the end of 5′ UTR of HCV viral RNA in both *in vitro* samples and in clinical samples [298].

Alternatively, RG-101 (Regulus Therapeutics), is a N-acetyl-D-galactosamine (GalNAc)-conjugated antimiR against miR-122. It has also undergone Phase I trials in HCV-infected patients at a single dose of 2–4 mg per kg. Furthermore, Phase II trials have combined RG-101 with direct-acting antivirals such as Harvoni (a combination of ledipasvir and sofosbuvir), but the (see Regulus Therapeutics, press release dated 7 June 2016). However, the trial was put on hold by the US FDA after a second case of jaundice was reported (see Regulus Therapeutics, press release dated 1st Nov 2016).

Furthermore, RG-125, a GalNAc-conjugated antimiR against miR-103/107, recently entered clinical trials for the treatment of non-alcoholic fatty liver disease. Furthermore, mir-103/107 expression is increased in the liver of obese mice and promotes diabetes progression by targeting caveolin 1, a protein involved in insulin signaling. Therefore, it is also being investigated at the pre-clinical stage in mice [299]. Finally, LNA-based antimiR-155 (MRG-106; miRagen Therapeutics) has recently entered clinical trials to treat patients with cutaneous T cell lymphoma.

Anti-Atherogenic miRNAs Therapies: Mimics

In addition to antimiRs, miRNA mimics have also entered clinical trials. One of the most advanced is MRX34, a miR-34 mimic by Mirna Therapeutics. It is encapsulated in a lipid carrier called NOV40, Preclinical studies of mice treated with MRX34 nanoparticles showed an accumulation of miR-34 in tumors with significant tumor regression [300-303]. MRX34 entered a multicentre phase I trial in 2013 in patients with

primary liver cancer, small cell lung cancer, lymphoma, melanoma, multiple myeloma or renal cell carcinoma. The trial included either a dosage a two times per week or five times per day schedule, via intravenous infusion. At the end of the trial, analysis of white blood cell samples showed significant reduction in the miR-34 target mRNAs FOXP1 and BCL2. However, the trial was terminated due to patient deaths (see Mirna Therapeutics Halts Phase 1 Clinical Study of MRX34) [304].

Finally, miR-16 mimics have been entered Phase I Trials in a collaboration between EnGeneIC and the Asbestos Diseases Research Institute of Australia, for patients with malignant pleural mesothelioma. miR-16 was delivered in an EDV nanocell with EGFR antibody surface conjugation, which facilitates targeting to the tumor site. Preliminary data reported manageable safety in response to infusion of 5 billion nanocells loaded with

1.5 μg miR-15/16 mimics as a first dose level in the first five patients that had been enrolled [305]. Finally, two Phase I clinical trials of the miR-29 miRNA mimic MRG-201 (miRagen Therapeutics) have been initiated in patients with scleroderma.

Although a considerable number of studies involving miRNA therapeutics have been conducted over the years, only a small number of miRNA therapeutics have moved into clinical development. One of the biggest challenges in developing miRNA-based therapeutics is maximize stability and minimize off-target effects.

1.6.5 TSB Studies

Given the wealth of targets for each individual miRNA, one of the pitfalls of targeting miRNAs is limiting targets to a single target. To address this, recent technology has been developed by Exiqon to specifically block the interaction between a miRNA and the 3'UTR of its target. Target site blockers (TSBs) are already in use now. TSB usage has been reported for miR-29b, 181a, 26, 155, and 103.

miR-29b is dysregulated in breast cancer. It was found that miR-29b was downregulated in human breast cancer tissue and that overexpression decreased cancer cell

growth, self-renewal, migration, invasiveness and paclitaxel resistance via SPIN1. Furthermore, they found that silencing SPIN1 mirrored the effects triggered by miR-29b overexpression, whereas SPIN1 rescue by TSBs reversed the molecular effects produced by the mimic, thus indicating the efficacy of TSBs [306].

miR-155 TSBs have been reported both *in vitro* [307] and a separate study *in vivo* [308]. In the *in vitro* study, miR-155 was found to induce cell migration in colon cancer cells by targeting RhoA in colon cancer cells. miR-155 binding to RhoA mRNA was verified using TSBs and functionally validated by RNA immunoprecipitation assays [307]. Whereas another study used TSBs for miR-155 against the Cebpb 3′ UTR. Furthermore, the same study used TSBs against 200b/200c/429-binding sites in the Zeb1 3′ UTR. These TSBs were used to modulate gonadotropin releasing hormone (GnRH) in a study of hypogonadotropic hypogonadism and infertility in mice [308]. Another study which utilized TSBs *in vivo* studied the effect of blocking the interaction between Smad1 and miR-26. They found that the TSBs inhibited key patterning functions in *Xenopus laevis* embryos [309].

Very few studies have utilized TSBs as therapeutics. One such study investigated miR-181a inhibition on stroke in mice [310]. In this studies, TSBs designed to block the interaction between 181a and estrogen receptor-α (ERα) were used in a mouse model of stroke. A miR-181a/ERα TSB, with/without miR-181a mimic, was used to confirm targeting of ERα by miR-181a in astrocytes. Individually, miR-181a inhibition decreased infarct volume and improved neurologic score in female mice. Treatment with ERα TSB was strongly protective in both sexes. Finally, a recent report has emerged directly investigating TSB treatment in atherosclerosis [311]. In this study, TSBs blocking the KLF4-miR-103 interaction blocked atherosclerosis in a HFD-induced model of atherosclerosis. **However, no TSB studies have been conducted in d-flow-induced atherosclerosis.**

1.7 MicroRNA miR-744 in Disease Development and Implications for Atherosclerosis

Fortunately, miR-744 is a broadly conserve miRNA that shares 7 out of the 8 nucleotides in the seed region with miR-663[312]. Unlike miR-663, miR-744 is derived from the intronic region of the MAP2K4 gene[313] and has not previously been described in the endothelium. Rather, miR-744 was first identified in human head and neck cancer tumor samples[314]. Following this original publication, other investigators have found that miR-744 is highly expressed in humans with gastric cancer[315], pancreatic cancer[316], and nasopharyngeal cancer[317], and interestingly, in patients with heart failure[318]. Furthermore, miR-744 has been reported as being highly expressed in mouse serum[319] and in murine models of disease such as diabetes[320, 321] and ischemic skeletal injury[322].

A variety of direct targets have been reported for miR-744. One of the first reports of miR-744, by Martin et al, demonstrated that TGFβ1 is a direct target of both miR-663 and miR-744 by qPCR, western blot, and luciferase assay in human proximal tubular epithelial cells[323]. Later, it was reported that eukaryotic elongation factor (eEF1A2) is a direct target of both miRNAs in a human breast cancer cell line MCF7 by qPCR, western blot, and luciferase assay[324]. Furthermore, secreted frizzled-related protein 1 (SFRP1), glycogen synthase kinase 3β (GSK3β), and transducin-like enhancer of split 3 (TLE3), which are important negative modulators of the Wnt/β-catenin signaling pathway, were identified as direct targets of miR-744 in a human pancreatic cell line by luciferase assay[325]. Recently, protein-tyrosine phosphatase 1B (PTP1B), which is a ubiquitously expressed phosphatase, was also identified as a direct target of miR-744 by luciferase assay in human renal mesangial cells[326]. **Given that miR-744 is upregulated in a variety of disease states in both humans and mice, miR-744 may be important in atherosclerosis as well. However, what role miR-744 may play is currently undefined.**

1.8 LIMS2/PINCH2

LIM Zinc Finger Domain Containing 2 (LIMS2) was first identified in 2002 by Zhang et al. [327]. They found that LIMS2, also known as PINCH2, forms a complex with the focal adhesion protein integrin-linked kinase (ILK) through interactions with the first LIM domain. PINCH2 localizes to both cell-ECM contact sites and the nucleus by interacting with ILK. Interestingly, two other LIM domain family members shuttle between the cytoplasm and nucleus. These are zyxin [328, 329] and HIC-5 [330, 331], which play a role in gene transcription in the nucleus. Furthermore, PINCH2 is co-expressed with the previously discovered isoform PINCH-1 in multiple cell types [332]. Finally, PINCH2-ILK and PINCH1-ILK interactions may be mutually exclusive in that overexpression of PINCH2 significantly inhibited the PINCH1-ILK complex in this study and a follow-up study [327, 333].

Later it was discovered that the structural basis for PINCH1 vs PINCH2 biased binding is that the LIM1 domains of PINCH1 and PINCH2 directly compete for the same binding site on the ankyrin repeat domain (ARD) of ILK. It was determined that the 1.9 Å crystal structure of the PINCH2 LIM1 domain complexed with the ARD of ILK, and disruption of this interface by point mutagenesis reduces binding *in vitro* and alters localization of PINCH2 in cells [334]. The direct competition of PINCH-1 and PINCH-2 for ILK binding may provide differential integrin signaling [335]. However, it has also been reported that PINCH2 can partially compensate for the loss of PINCH1 in preventing ILK degradation by the proteasome but not cell survival [336].

Pathologically, PINCH2 global knockout mice do not exhibit any diseased phenotype and appear to be viable and normal, albeit with significantly increased PINCH1 expression. Double knockout fibroblasts from the mice had increased ILK degradation, which was rescued by overexpression of alone [337]. Similarly, PINCH2 global knockout mice with hepatocyte-specific PINCH1 knockout were born normally but experienced abnormalities of the liver, where both PINCH1 and 2 were absent. Specifically, the mice

had enlarged, stiff livers due to reduced expression of Rsu1, which suppresses Ras signaling and cell migration [338]. Finally, it appears that inactivation of PINCH1 and PINCH2 independently leads to instability of ILK, loss of stretch-responsive VEGF expression, and progressive heart failure in zebrafish [339]. In agreement with these findings, Liang et al reported that deletion of cardiac-specific PINCH1 knockout or global PINCH2 knockout mice exhibit no basal cardiac phenotype, but mice that are doubly homozygous null for PINCH1 and PINCH2 in the myocardium developed dilated cardiomyopathy and died of heart failure within a few weeks and fibrosis and reduced expression/mislocalization of multiple cell adhesion proteins [340]

Despite the intertwined roles of PINCH1 and 2, PINCH2/LIMS2 alone has been found to be silenced by hypermethylation in gastric cancer cells, which ultimately promoted increased cell migration *in vitro* [341]. In human patients, it was discovered by sequencing that compound heterozygous missense mutations in LIMS2 lead a loss of LIMS2 in Limb Girdle Muscular Dystrophy and cardiomyopathy [342]. **Given the evidence that both PINCH1 and 2 play a role in cardiac pathology, LIMS2 alone is lost in cardiomyopathy, and LIMS2 alone can rescue ILK (an important mechanosensitive signaling component) from degradation, LIMS2 may play a key role in endothelial mechanosensing.**

1.9 ILK Signaling, Focal Adhesions, and Atherosclerosis

ILK is a widely expressed, mechanosensitive, serine/threonine kinase that binds to the C terminus of β1-integrin [343]. Many proteins associated with mechanosensing have been shown to bind to different domains of ILK including α-actinin via β-parvin/affixin and the aforementioned PINCH and thymosin β4 [335, 344]. It has also been shown to phosphorylate myosin light chain, GSK-3β (glycogen synthase kinase-3β), and AKT/PKB [345]. ILK has previously been implicated to play a role in cardiac physiology. In fact, it was identified as an essential regulator of cardiac growth, contractility, and repair [346] .

ILK gene knockouts in mice, flies, and worms result in early embryonic lethality because of cell adhesion defects and cytoskeletal disorganization. Although widely distributed in mammalian tissues, ILK expression is highest in the heart, and cardiac-specific ablation of ILK causes cardiomyopathy and sudden death in mice [347].

Bendig et al. a mutation in the ILK gene that causes progressive loss of contractility in zebrafish hearts. This mutation disrupted the interaction with β-parvin/affixin, suggesting that its presence is essential for normal cardiac function and potentially cardiac stress sensing [348]. Likewise, in another zebrafish study, a nonsense mutation (Y319X) led to a dysmorphic ventricle with reduced cardiac function combined with severe endothelial defects, similar to alterations observed in mice lacking the integrin-binding extracellular matrix protein laminin α4 [349].

ILK has recently been directly implicated in atherosclerosis. It was discovered that ILK is strongly expressed in the endothelial cell layer of non-atherosclerotic vessels but was absent from the endothelium of atherosclerotic arteries. Also, vasodilation was impaired in ILK knockout mice. Furthermore, these mice exhibited eNOS uncoupling, reflected in reduced tetrahydrobiopterin (BH4) levels, increased BH2 levels, decreased dihydrofolate reductase expression, and increased eNOS-dependent generation of superoxide accompanied by extensive vascular protein nitration. ILK re-expression prevented eNOS uncoupling in knockout cells, whereas superoxide formation was unaffected by ILK depletion in eNOS-KO cells, indicating eNOS as a primary source of superoxide anion. eNOS and ILK coimmunoprecipitated in aortic lysates from control animals, and eNOS-ILK–shock protein 90 interaction was detected in human normal mammary arteries but was absent from human atherosclerotic carotid arteries. eNOS- ILK interaction in endothelial cells was prevented by geldanamycin, suggesting heat shock protein 90 as a binding partner. Our results identify ILK as a regulatory partner of eNOS

in vivo that prevents eNOS uncoupling, and suggest ILK as a therapeutic target for prevention of endothelial dysfunction related to shear stress–induced atherosclerosis [350]

Furthermore, in a follow-up study, it was discovered that increased levels of inducible nitric oxide inversely correlated with decreased ILK levels in human atherosclerosis and in a mouse model of vascular remodeling (carotid artery ligation) comparing Furthermore, it was discovered that NO decreased ILK protein stability by promoting the dissociation of the complex ILK/heat shock protein 90/endothelial NO synthase, leading to endothelial NO synthase uncoupling. NO also destabilized ILK signaling platform and lead to decreased levels of paxillin and α-parvin. ILK phosphorylation of its downstream target GSK3-β was decreased by NO. Mechanistically, NO increased ILK ubiquitination mediated by the E3 ubiquitin ligase CHIP, but ILK ubiquitination was not followed by proteasome degradation. Alternatively, NO drove ILK to degradation through the lysosome [351]. **Given these results, preventing ILK degradation in atherosclerosis may be a key therapeutic strategy.**

A substantial portion of this chapter was published in:

Simmons, R., Kumar, S., Thabet, S., Sur, S., Jo, H. Omics-based approaches to understand mechanosensitive endothelial biology and atherosclerosis. WIREs Syst Biol Med. 8: 378-401. DOI:10.1002/wsbm.1344 (2016)

Simmons, R., Kumar S, Jo H. The role of endothelial mechanosensitive genes in atherosclerosis and omics approaches. Arch Biochem Biophys. 591:111-31. PMID: 26686737 (2016)

Kumar, S. Kim, C.W., Simmons, R., Jo, H. Role of Flow-Sensitive microRNAs in Endothelial Dysfunction and Atherosclerosis. ATVB. 34:1524-4636 DOI: 10.1161/atvbaha.114.303425 (2014)

CHAPTER 2 SPECIFIC AIMS AND HYPOTHESES

2.1 Significance and Impact

Cardiovascular disease (CVD) is the number one cause of death in the US. Atherosclerosis, an inflammatory disease characterized by plaque accumulation on the arterial walls, is the major cause of CVD. Atherosclerotic plaque rupture (thrombosis and embolism) blocks blood flow and oxygen delivery to tissues thereby causing a heart attack or stroke. While there are several known risk factors and behaviors that increase the likelihood of developing atherosclerosis, the underlying cause of the disease remains unknown.

MicroRNAs have emerged as key regulators of cell phenotypes and diseases. Furthermore, multiple miRNAs have emerged to play a role in atherosclerosis. In fact, multiple studies have been undertaken to study the role of mechanosensitive miRNAs in atherosclerosis **(Ch. 1.6.2).** However, prior to this project, there were no studies on miR-744 in ECs, its regulation by mechanical forces generated by blood flow, or the investigation of miR-744 as a potential therapeutic target for atherosclerosis. Only a few studies have used target site blocker technology **(Ch 1.6.5**), and this is the first to show the blockage of a specific miRNA-target interaction (744-LIMS2) by target site blockers is sufficient to reduce atherosclerotic plaques in a d-flow-induced model of atherosclerosis. Finally, this work may lead to a new therapy to help prevent CVD.

2.2 Rationale

Although miR-663 may be an important mediator of endothelial inflammation in humans, given that miR-663 is not broadly conserved, future studies of miR-663 as a therapeutic target are limited. Fortunately, we identified miR-744 as a homolog of miR-663 which is broadly conserved in mammalian species. In the literature, miR-744 plays a role in a variety of diseases in both humans and mice, however, the role of miR-744 in endothelial biology or cardiovascular disease is unknown. Preliminary results established

significant miR-744 upregulation in ECs under OS *in vitro* in both human ECs and mouse ECs. Furthermore, it was established that miR-744 plays a significant role in monocyte adhesion and endothelial inflammation in human cells *in vitro*, which is a key precipitating event in d-flow-induced atherosclerosis development. Therefore, the role of miR-744 in endothelial inflammation was investigated in Aim I.

The functional role of miR-744 is to bind to target mRNAs and thus suppress target translation. In Aim 2, the mRNA transcripts being loaded on the RISC complex under miR-744 overexpression *in vitro* were compared to mRNA transcripts which are depleted in d-flow *in vivo* from the partial carotid ligation microarray and a network of genes that change due to miR-744 was discovered. However, ultimately, LIMS2 was discovered to be the most consistent target of miR-744. To implicate miR-744 specifically in d-flow-induced suppression of LIMS2, the effect of miR-744 modulation on LIMS2 was tested *in vitro* and *in vivo* in Aim 3.

2.3 Innovation

The finding that miRNAs are induced by disturbed blood flow is relatively recent, and is supported by both *in vitro* studies in ECs and limited *in vivo* studies. However, the mechanisms by which miRNAs can lead to atherosclerosis are still not fully described. Although some miRNAs have already been implicated in atherosclerosis, there have been no previous studies of miR-744 in ECs and atherosclerosis. As a result of a lack of research surrounding miR-744 in ECs, investigation of gene change and functional changes with antimiR-744 or miR-744 mimics has not been previously attempted in this cell type. Modulation of miR-744 *in vitro* has provided important insight into the role miR-744 plays in EC inflammation. Results from *in vitro* studies indicate that there is a functional effect of miR-744 inhibition on EC inflammation. However, our *in vivo* model of acute d-flow-induced atherosclerosis has indicated that the interaction of miR-744 specifically with LIMS2 may be a novel therapeutic target for atherosclerosis.

Furthermore, although our lab has generated both miRNA arrays and mRNA microarrays from HUVECs subjected to LS or OS and from our mouse model of d-flow-induced atherosclerosis, these datasets have not yet been fully integrated with a specific focus on known mediators of EC processes. Additionally, with RNA sequencing information to inform us of the direct targets of miR-744 in HUVECs, the proposed study will be the first to identify a full network of targets of a miRNA. This work has identified a novel target of miR-744 and established its relevance to EC inflammation and atherosclerosis.

2.4 Project Objective

While we know that laminar, unidirectional flow upregulates "atheroprotective" genes and downregulates "pro-atherogenic" genes while disturbed, reversing, or stagnant flow results in the opposite phenomenon, the mechanism by which flow controls EC gene expression is unknown. The goal of this project was to determine how the miR-744 responds to flow, causes altered gene expression, and regulates atherosclerosis development.

2.5 Overall Hypothesis

Disturbed flow increases miR-744 expression in endothelial cells. This in turn causes a downregulation of key target genes such as LIMS2 in ECs, which ultimately initiates the pro-inflammatory, pro-atherosclerotic gene expression program for atherosclerosis development.

2.6 Specific Aim I: Demonstrate the Mechanosensitivity of miR-744 and Its Role in EC Inflammation

We initially discovered miR-744 through its homology with another miRNA miR-663. In Aim I, we validated that miR-744 is upregulated by OS in human endothelial cells like its sister miRNA. Furthermore, we found that miR-744 is also robustly expressed in mice and is upregulated by OS in mouse endothelial cells and in endothelial RNA derived from a murine model of d-flow-induced atherosclerosis (partial carotid ligation) and in the chronically flow disturbed lesser curvature (LC). Subsequently, in order to further investigate the role of miR-744 in OS-induced inflammation, its effect on monocyte adhesion and inflammatory marker expression (ICAM1, VCAM1, and MCP-1) were assessed under conditions of miRNA overexpression via miRNA mimics and inhibition via locked nucleic acid (LNA) complementary antimiRNAs respectively. We found that treatment with mimics increased monocyte adhesion and ICAM1/VCAM1/MCP-1 mRNA expression even in anti-inflammatory LS conditions. Furthermore, we found that p65 protein expression were increased by mimic treatment. Alternatively, we found that antimiR treatment under OS conditions drastically reduced monocyte adhesion and ICAM1/VCAM1 mRNA expression. These results established that miR-744 plays a role in endothelial inflammation.

2.7 Specific Aim II: Determine the Direct Targets of miR-744 and Their Role in EC Inflammation

The primary mechanism of action for miRNAs is to bind to the 3'UTR of target genes and initiate translational repression and/or mRNA degradation. Therefore, given the results described in Aim I, it was critical to identify direct targets of miR-744 which mediate its pro-inflammatory effects in the endothelium. Therefore, in Aim II, genes that are directly regulated by miR-744 and are suppressed by d-flow were determined by 1) sequencing of RNA derived from immunoprecipitation of the Ago2 complex under conditions of miR-744 overexpression 2) filtering out genes which do not have miR-744 binding sites in the human and mouse 3'UTR 3) filtering out genes which are not suppressed in the LCA 48 hours post ligation (from the gene array). Out of this criteria, 13 genes emerged. From this pool, validation was conducted *in vitro* and *in vivo* to arrive at LIMS2. The specific validation experiments were 1) significant suppression by OS in HUVECs at the mRNA level 2) significant rescue of mRNA levels by antimiR-744 in OS-treated HUVECs, and 3) significant suppression by mimic treatment in HUVECs. After LIMS2 emerged as the only gene that passed the validation experiments, 3'UTR luciferase assays were conducted on mimic and antimiR treated iMAECs in order to establish that LIMS2 is a conserved target in mice. After determining that LIMS2 is a valid target in both species, the effect of LIMS2 on endothelial inflammation was determined using siRNA against LIMS2 in human ECs and conducting monocyte binding assays and ICAM1/VCAM1 mRNA and protein expression. We found that siLIMS2 significantly increased monocyte adhesion and increased inflammatory marker expression. Therefore, these results strongly indicated that miR-744 exerts it pro-inflammatory effects on the endothelium through LIMS2.

2.8 Specific Aim III: Determine the Role of miR-744 in the Development of Atherosclerosis

Finally, we hypothesized that inhibition of the interaction between miR-744 and its target genes in ECs will inhibit atherosclerosis formation *in vivo*. Therefore, in Aim III, we tested the effect of global miR-744 inhibition (via antimiR-744) on the three week partial carotid ligation mouse model. The degree of atherosclerotic plaque formation was determined via gross plaque imaging and H/E staining. Furthermore, the expression of key targets, such as LIMS2, was determined in the liver, lung, kidney, and spleen. We found that global antimiR treatment did not significantly reduce plaque formation, although the antimiR-744 did significantly decrease miR-744 in the kidney and spleen. However, LIMS2 mRNA expression was only rescued in the spleen. Given that miRNAs have hundreds of targets and only LIMS2 emerged in human ECs as a major player, we then tested the effect of blocking the interaction between miR-744 and LIMS2 via target site blockers in the three week partial carotid ligation mouse model. Fortunately, we found that the plaque was significantly reduced in the LIMS2 TSB treated animals. Furthermore, LIMS2 mRNA expression was significantly rescued in the spleen and kidney. Given this exciting finding, LIMS2-744 TSBs may be a viable therapeutic for atherosclerosis and cardiovascular disease

CHAPTER 3 MATERIALS AND METHODS

3.1 Cell Culture and Shear Experiments

3.1.1 HUVECs

Human Umbilical Vein Endothelial Cells (HUVEC, Lonza CC-2519) were maintained in M199 (Corning 45000-378) base culture medium containing 20% Fetal Bovine Serum (Atlanta Biologicals S11150), 10% penicillin/streptomycin (Gibco 15070063), 10% glutamine (Gibco 25030081), 10% endothelial cell growth serum (cow brain extract), and 8,000U (USP) heparin (Sigma Aldrich H3393). Cells were cultured in 100 mm dishes (Falcon 353003) coated with 0.1% gelatin (Sigma Aldrich G9391) for 1 hr at 37°C. Cells were used at Passages 5-7 for experiments.

3.1.2 HAECs

Human Aortic Endothelial Cells (HAEC, Lonza CC-2535) were maintained in EGM™-2 BulletKit (CC-3162), which contains Hydrocortisone solution, GA-1000, Fetal Bovine Serum SDS attached, Human Fibroblast Growth Factor basic (hFGFb), Human Vascular Endothelial Growth Factor (hVEGF), Analog of Human Insulin-Like Growth Factor-1 (Long R3-IGF-1), Ascorbic Acid Solution, Human Epidermal Growth Factor (hEGF), and Heparin. Cells were cultured in 100 mm dishes (Falcon 353003) coated with 0.1% gelatin (Sigma Aldrich G9391) for 1 hr at 37°C. Cells were used at Passages 5-7 for experiments.

3.1.3 iMAECs

immortalized Mouse Aortic Endothelial Cells (iMAECs) were generated as described [352] and maintained in low glucose DMEM (Corning 45000-332) base culture medium containing 10% penicillin/streptomycin (Gibco 15070063), 10% endothelial cell growth serum (cow brain extract), and MEM Non-Essential Amino Acids (MNEAA) (Thermo Fisher 11140). Cells were cultured in 100 mm dishes (Falcon 353003) coated with 0.1% gelatin (Sigma Aldrich G9391) for 1 hr at 37°C. Cells were used within 3 passages of thawing for experiments.

3.1.4 Cone and Plate Viscometer

Briefly, cells were cultured to 100% confluency and then subjected to shear stress in the cone and plate viscometer for 24 Hr. Cells subjected to LS experienced a unidirectional shear stress of 15 dyn/cm^2, whereas cells subjected to OS experienced an oscillating shear stress of 5 dyn/cm^2. Alignment of ECs under LS was visually confirmed by microscopy. Cells were scraped in 600 µL HBSS (Corning 45000-462) and pelleted by centrifugation at 5000 rpm for 1 minute. One quarter was resuspended with Qiazol (Qiagen 79306) and the rest was resuspended in phosphate-buffered RIPA with glycerol (Boston Bioproducts BP-421) and protease inhibitor (Sigma Aldrich 11697498001).

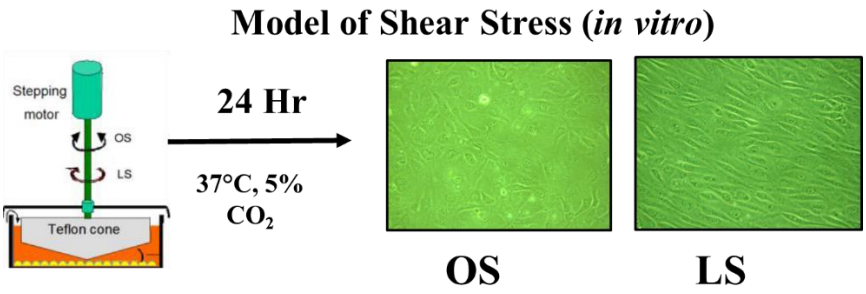

Figure 3.1 LS aligns endothelial cells

3.2 Partial Carotid Ligation and Lesser Curvature Endothelial RNA Isolation

3.2.1 Partial Carotid Ligation and Endothelial Flushing

8-week-old C57BL/6 mice (Jackson Laboratories) were used for all animal studies according to the approved Institutional Animal Care and Use Committee protocol by Emory University. Mice were partially ligated under 2% isoflurane anesthesia and the resultant disturbed flow conditions in the LCA were determined by ultrasound (Vevo770, Visualsonics) with a 30-MHz probe as described previously [83].

Briefly, 3 out of 4 caudal branches of the LCA (left external carotid, internal carotid, and occipital artery) were ligated with 6-0 silk suture, while the superior thyroid artery was left intact (**Figure 1.3E**). Mice were sacrificed by CO_2 inhalation and were subsequently perfused with saline containing heparin for 5 minutes. Total carotid intimal RNA was isolated 48 hours later by flushing the RCA and LCA with 150 µL Qiazol, by our method that we have demonstrated to be endothelial-enriched without any significant contamination of smooth muscle cells and leukocytes [36, 83, 353].

3.2.2 Lesser Curvature and Greater Curvature Endothelial RNA Isolation

8-week-old C57BL/6 mice (Jackson Laboratories) were used for all animal studies according to the approved Institutional Animal Care and Use Committee protocol by Emory University. Mice were sacrificed by CO_2 inhalation and were subsequently perfused with saline containing heparin for 5 minutes The lesser curvature (LC) of the aortic arch and the thoracic aorta (TA) were isolated 48 hours later in HBSS and opened *en face*. The endothelium was placed against a nitrocellulose-membrane soaked in isopropanol for 5 minutes, and the media and adventitia were peeled away leaving the endothelial monolayer adherent to the nitrocellulose membrane and RNA was extracted using Qiagen miREasy kit. For each experiment, the LC and TA regions from two to four mice were pooled.

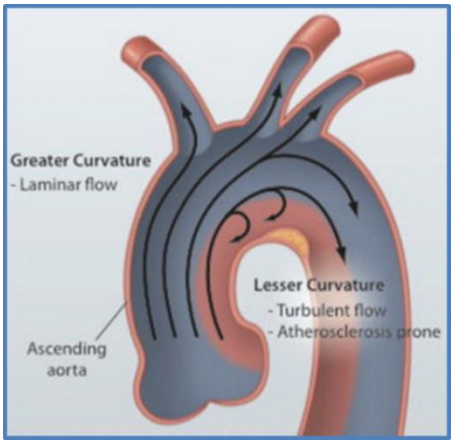

Figure 3.2 The Lesser Curvature is Chronically Flow-Disturbed

3.3 Quantitative real-time PCR (qPCR) Validation of miR-744

Total RNA was purified by the Qiagen miRNeasy Kit (217004), and reverse-transcribed into cDNA using the Qiagen miScript II Reverse Transcriptase Kit (218161). The resulting cDNA was subjected to qPCR using the Qiagen mature hsa-miR-744-5p (MIMAT0004945: 5'UGCGGGGCUAGGGCUAACAGC3' MS00010549) or RNU6b (218193) as the forward primer and Universal Primer (218193) as the reverse primer, SYBR Master Mix (ThermoFisher 4472903), and the ABI StepOne Plus qPCR machine. The PCR conditions were 95°C, 15 min, followed by 40 cycles of 94°C, 15 s; 55°C, 30 s, and 70°C, 30 s. RNU6B was used as a housekeeping control. Fold changes between samples were determined for all targets using the ΔΔCt method [354].

3.4 Transfection of Nucleic Acids

Briefly, HUVECs were plated in 100 mm dishes and 24 hr later, the cells were transfected with either antimiR-744 (Exiqon LNA Power Inhibitor 4100792) or miR-744 mimic (miRVana 4464066) for inhibition and overexpression respectively. 1 mL of oligonucleotide/Oligofectamine (Invitrogen 12252011) mixture in Opti-MEM media (Gibco 31985070) were added to 4 mL of OPTIMEM in the plate for final dosages of 100 nM for antimiR-744 or 40 nM miR-744 for mimic. Four hours after transfection, the media was replaced with standard HUVEC media. Cells treated with antimiR were immediately subjected to OS, but cells treated with miR-744 mimics were subject to LS 24 hr post-transfection to allow for processing into mature miRNA. A non-target "scrambled" double-stranded RNA (Ambion pre-miR-control) was used as a control in mimic experiments and a nontarget LNA oligonucleotide was used as a control in antimiR experiments.

3.5 Monocyte Adhesion Assay

Following shear, cells were washed and incubated with fluorescently labeled THP-1 human peripheral blood mononuclear leukocytes (ATCC TIB-202) in serum-free media at 37°C for 30 minutes. THP-1 cells were labeled with 5 μL of BCECF-AM (1mg/ml, Molecular Probes B1150) at 37°C for 30 minutes. 500,000 THP-1 cells were added per dish in a volume of 5 mL. Non-adherent THP-1 cells were be washed away with and bound cells will be fixed with 4% paraformaldehyde (Sigma Aldrich) and visualized by fluorescent microscopy at 5X magnification (Olympus).

3.6 qPCR for Inflammatory Markers

Total RNA was purified using the Qiagen miREasy kit and reverse transcribed for use in a two-step qRT-PCR using the High Capacity cDNA Reverse Transcription Kit (Applied Biosystems 4368814). The resulting cDNA was subjected to qPCR using the primers in **Table 3.1**, SYBR Master Mix (ThermoFisher 4472903), and the ABI StepOne Plus qPCR machine. The PCR conditions were 10 min at 95°C, followed by 40 cycles of 95°C for 5 s and 60°C for 30 s. 18S was used as a housekeeping control. Fold changes between samples were determined for all targets using the ΔΔCt method.

Table 3.1 Primer Sequences for qPCR of Inflammatory Markers

	FORWARD	REVERSE
18S (HUM/MS)	AGGAATTGACGGAAGGGCACCA	GTGCAGCCCCGGACATCTAAG
VCAM1 (HUMAN)	CATTGACTTGCAGCACCACA	AGATGTGGTCCCCTCATTCG
ICAM1 (HUMAN)	CACAAGCCACGCCTCCCTGAACCTA	TGTGGGCCTTTGTGTTTTGATGCTA
MCP-1 (HUMAN)	GCAGAAGTGGGTTCAGGATT	TGGGTTGTGGAGTGAGTGTT
VCAM1 (MOUSE)	GCTATGAGGATGGAAGACTCTGG	ACTTGTGCAGCCACCTGAGATC
ICAM1 (MOUSE)	CCCACGCTACCTCTGCTC	GATGGATACCTGAGCATCACC
MCP-1 (MOUSE)	CATCCACGTGTTGGCTCA	GATCATCTTGCTGGTGAATGAGT

3.7 BCA and Western Blotting for Inflammatory Markers

Cell lysate was centrifuged at 12,000g for 10 minutes at 4°C to remove cell debris. The protein-containing supernatant was collected in a separate tube and 2.5 µL was added to a 96 well plate. Bicinchoninic acid (BCA) was diluted 1:50 in Reagent A (Pierce 23225) and 97.5 µL of the reagent was added to each protein-containing well. Protein standards were prepared by diluting bovine serum albumin (2mg/mL, Pierce 23209) to concentrations of 0, 0.05, 0.1, 0.25, 0.5, and 0.75 mg/mL solutions. After a 30 minute incubation at 37°C, the absorbance was read by a microplate reader at 562 nm and a linear calibration curve was established.

Each protein sample was diluted in 1X RIPA and 6X reducing loading dye (Boston Bioproducts) to achieve a total protein amount of 15 µg, then subsequently boiled at 95°C for 5 minutes. Proteins were electrophoresed in 1X running buffer (Tris-Glycine pH 8.8) using a 10% polyacrylamide gel. Following electrophoresis, the proteins were transferred to a polyvinylidene fluoride (PVDF) membrane (BioRad) and blocked in 5% (w/v) nonfat milk in Tris-Buffered Saline with 0.1% Tween (TBST) for 1 hour at room temperature. Membranes were incubated with the primary antibody solution (1:1000) (**Table 3.2**) overnight at 4°C. Following primary antibody exposure, the membrane was washed and incubated with secondary antibody (1:5000) (goat anti-rabbit or goat anti-mouse HRP, Santa Cruz SC-2004 or SC-2005) for 1 hour at room temperature. After washing, the membrane was developed using Immobilon Western Chemiluminescent HRP (EMD Millipore, WBKLS0500) and Blue Lite Autorad Film (VWR, 490001-950).

Table 3.2 List of Inflammatory Marker Antibodies

ANTIBODY	SPECIES	CAT. NO.	
VCAM-1 ANTIBODY (H-276)	Rabbit	SC-8304	Santa Cruz
ICAM-1 ANTIBODY (15.2)	Mouse	SC-107	Santa Cruz
P65 NFKB ANTIBODY	Rabbit	8242S	Cell Signaling Technologies
PHOSPHOP65 NFKB ANTIBODY (SER536)	Rabbit	3033S	Cell Signaling Technologies

3.8 P65 Staining

Cells were seeded in 24-well plates (Corning) coated in 0.1% gelatin at a density of 50,000 cells/mL. 24 hours later, cells were transfected with either a mimic or inhibitor of miR-744 respectively. 24 hours after transfection, the cells were fixed in 4% paraformaldehyde and permeablized in 0.1% Triton X-100 (Sigma Aldrich) in PBS for 10 minutes, followed by blocking in 20% goat serum (Jackson ImmunoResearch, 005-000-121) in PBS for 1 hour. After blocking, cells were incubated with P65 (1:100 v/v) (**Table 3.2**) overnight at 4°C followed by incubation with secondary antibody (1:250 v/v) (Alexa Fluor 568 conjugated goat anti-rabbit, Life Technologies).

3.9 Ago2 Immunoprecipitation and RNA Sequencing

Static HUVECs were transfected with either 40 nM miR-744 mimic or control mimic and whole lysate was collected 24 hours later by scraping in ice cold HBSS and centrifugation at 500g for 2 minutes to pellet the cells. Next, the cells were lysed in RNA IP lysis buffer (Millipore MagnaRIP Kit). As per the manufacturer's protocol, RNase free magnetic Protein G beads were incubated with RIP grade Ago2 antibody (Millipore) for 30 minutes rotating at room temperature, washed, and then subsequently incubated with the lysate overnight at 4C while rotating. Following incubation, the beads were washed and directly added to Qiazol. RNAs bound to RISC were purified and sequenced by the Yerkes Sequencing Core. Briefly, RNA was extracted from Qiazol using the Qiacube. Next, the RNA was prepared for sequencing using the ClonTech Library Prep. Then, the resultant cDNA was sequenced using the Illumina Hiseq3000 and each sample was read at 30 million reads. After obtaining the total sequencing counts, the number of unique transcripts was mapped to annotated transcripts and normalized. Finally, the differential transcript counts for control mimics vs 744 mimics for each transcript was statistically calculated using the R package DESeq2.

3.10 Filtration Criteria

Following sequencing, mRNAs which were differentially enriched between the control-treated vs. mimic treated samples were determined based on a relaxed p value of 0.05. From this pool, the list of genes was compared to a list of conserved targets between human and mice generated from miRWalk. From this list, direct, EC-relevant targets were determined. Finally, this list was compared to genes which were significantly downregulated in the LCAs at the 48 hour time point in our partial carotid ligation microarray by more than 30%.

3.11 qPCR for Potential Targets

Total RNA was purified using the Qiagen miREasy kit and reverse transcribed for use in a two-step qRT-PCR using the High Capacity cDNA Reverse Transcription Kit (Applied Biosystems 4368814). The resulting cDNA was subjected to qPCR using the primers in **Table 3.3**, SYBR Master Mix (ThermoFisher 4472903), and the ABI StepOne Plus qPCR machine. The PCR conditions were 10 min at 95°C, followed by 40 cycles of 95°C for 5 s and 60°C for 30 s. 18S was used as a housekeeping control. Fold changes between samples were determined for all targets using the ΔΔCt method.

Table 3.3 List of Primers for qPCR of Potential Target Genes

	FORWARD	REVERSE
H-LIMS2	GCGCATTGTCAACAGCAA	TACTTCCGGCCTTCAAACTC
M-LIMS2	CTGCTGACCGGTGCTAGG	CCAAACACTCAGACATGTTGCT
H-CYB561	CCTCTGCATGGTCATAGGC	GAAGACACGGTAAACCAGCAG
H-CST3	CGAACCACGTGTACCAAGAC	TCTGGAAAGAGCAGAATGCTT
H-ADK	CATCACTGGTGACAACAGGTC	TCTCCAGATCAAGATGTTTTTCC
H-TCF7L2	GAATCGTCCCAGAGTGATGTCG	TGCACTCAGCTACGACCTTTGC
H-ANK3	AAAGGACTGCCTCAAACAGCGG	CTAAGGATGCGAAGCTCTGTCG
H-CALM1	CCAACAGAAGCTGAATTGCAGGA	CAAAGACTCGGAATGCCTCACG
H-EHD1	GCGTTTGGCAACGCTTTCCTCA	ATCCGCTGCTTCTCTCCAGACA
H-TRIB3	GCTTTGTCTTCGCTGACCGTGA	CTGAGTATCTCAGGTCCCACGT
H-PVRL3	ATTCCCGCTTGGAAATGCCCAG	GCTGCTACTGTTTCATTTCCTCC
H-KRAS	TGGACGAATATGATCCAACAAT	TCCCTCATTGCACTGTACTCC
H-DLGAP4	CCTCAGCAATAGTCGCACGCTT	ACTGCTCTGGACTGTGACTGAG
H-NDRG1	ATCACCCAGCACTTTGCCGTCT	GACTCCAGGAAGCATTTCAGCC
H-ZYX	CTCCTGTGGCTTCCAAGTTC	TGATTTGGTTGTGACCCAGA

3.12 3'UTR Luciferase Assay

3'UTR luciferase assays were conducted by co-transfecting iMAECs with a 500 ng of a plasmid encoding the 3'UTR of murine LIMS2 with secreted Gaussian luciferase (Genecopoeia) sequence:

AGGTCCTCGGCCGCCTGGCCTGCCTGCAGTACCTTAGCACTCATCCCCCTGCC
CCAGGTCCTGCTAGCCACCTCCCACTTCTGCTCCAGCCCAGCCCGTTCCTCCG
GTATGCCATCCTTTCTGCTTCCAGTCCACCTCGGGCTATGTAGCCCTTTCCTCT
GTGCTGAGGCCTGACCCACCTCACAGGCATTTCCTCCCGGGCCCACAACCTCC
AGGGACAGGAACAAACTGGAGCAGGATTATTTGTCACTTGCTTGA**CCCGCA**G
ATCCCAACCCGATGCCTCTCCTCTCCACTCTCCCAGGAGAGTTTCAGCCCTCG
TGTGACCCTTGGGCTTGGCTGAGAAGCTGTCCCAACCCCAGGGCCAGCACCA
CGCAGATAGAGGCTTCATGGAAGCACCCTTCTCAGTTATTCGAGCACAGTAG
GTCCTTGTGCTTACACTGTGTCAGCAAACCCACCTCTGGGGTGAAGCAGCCC
GAGAGCCCTACTGCCTTCACTACTCAGGAGACCTCATAGAAAGTGTCTCAGC
TGCCCACCAAGTGTGGGGGTCCCACTTCCCAGGGGCACATTGCCCTGGCCAT
CGAAGACCCACAAGTGGTCACATACTTACACAATGAAGGCTCATTCACATA

Alternatively, a plasmid or with the miR-744 binding site mutated was transfected with (provided by Oskar Laur of the Emory Genomics Core) 100 M mimic (miRVana) for 24 hours, followed by collection of the media. After addition of the luciferin substrate, the luciferase activity was measured immediately.

3.13 Immunofluorescence Staining

Frozen sections were permeabilized in 0.1% Triton-X in PBS for 10 minutes, followed by blocking in either 20% donkey serum or goat serum (Jackson ImmunoResearch,005-000-121 or 017-000-121) in PBS for 1 hour. Slides were incubated in the primary antibody (1:100) detailed in **Table 3.4** overnight at 4°C followed by incubation with secondary antibody (1:250 v/v) (Alexa Fluor 568 conjugated goat anti-rabbit, goat anti-rat, or donkey anti-goat, Life Technologies).

3.14 Human Plaque De-paraffinization and Immunostaining

Paraffin-embedded sections were provided by Giji Joseph (Dr. Robert Taylor) and graded according to H/E staining. Briefly, sections were deparaffinized by xylene and graded alcohol incubations. Following de-paraffinization, slides were either stained with hematoxylin and eosin for grading, or immunostained as above.

3.15 Partial Carotid Ligation and AntimiR-744 Injection

12-week-old ApoE$^{-/-}$ mice (Jackson Laboratories) were used according to the approved Institutional Animal Care and Use Committee protocol by Emory University. Mice were pretreated twice with either 5mg/kg antimiR-744 or saline subcutaneously (s.c.) on Days 1 and 2 pre-ligation. Then mice were partially ligated according to **Figure 1.3E**. and were fed a high fat diet for three weeks [83]. Throughout the three week period, mice were injected with either antimiR-744 or saline twice a week according to **Figure 3.3**. After 3 weeks, the aortic trees (including the carotids) were dissected and examined by bright field imaging. Gross lesion area was quantified using ImageJ software.

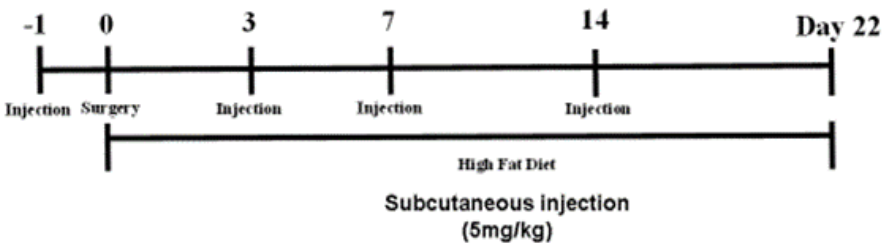

Figure 3.3 AntimiR-744 Injection Schedule

3.16 Oil Red O Staining

Frozen blocks containing the carotid arteries were prepared in TissueTek and stored at -80℃. Sections from the blocks were rinsed twice with distilled water for five minutes, incubated in 100% propanediol for ten minutes and incubation in 0.2% Oil Red-O solution for five minutes at room temperature. Slides were rinsed, mounted, and imaged on the Hamamatsu Nanozoomer. Oil Red O positive area (plaque area) was quantified using ImageJ software.

3.17 RNA Extraction from Organs and qPCR

Mice were sacrificed 3 weeks after the study and the liver, lung, kidney, and spleen was collected from each animal. Each organ was snap-frozen in liquid nitrogen and crushed by mortar and pestle. After crushing, part of the fragments were placed in Qiazol and disrupted by metal beads in a tissue lyser (Qiagen). Total RNA was purified and reverse-transcribed as previously described. The resulting cDNA was subjected to qPCR as previously described for miR-744. Alternatively, qPCR for LIMS2 was performed using mouse LIMS2 primers (Forward Primer: 5'CTGCTGACCGGTGCTAGG3') and (Reverse Primer:5'CCAAACACTCAGACATGTTGCT3'). The 18S primer in **Table 3.1** was used as a control.

3.18 Immunofluorescence Staining

Frozen sections were permeabilized in 0.1% Triton-X in PBS for 10 minutes, followed by blocking in either 20% donkey serum or goat serum (Jackson ImmunoResearch,005-000-121 or 017-000-121) in PBS for 1 hour. Slides were incubated in the primary antibody (1:100) detailed in **Table 3.4** overnight at 4°C followed by incubation with secondary antibody (1:250 v/v) (Alexa Fluor 568 conjugated goat anti-rabbit, goat anti-rat, or donkey anti-goat, Life Technologies).

Table 3.4 List of Antibodies for Immunostaining

ANTIBODY	SPECIES	CAT.NO.	
VCAM-1 ANTIBODY (C-19)	Goat	SC-1504	Santa Cruz
PECAM-1 ANTIBODY(MEC13.3)	Rat	550274	BD Biosciences
LIMS2 ANTIBODY HUMAN	Rabbit	bs-13650R	Bioss
LIMS2 ANTIBODY MOUSE	Rabbit	*Provided by Chuanyue Wu [327]*	

3.19 Hematoxylin and Eosin Staining

Frozen sections were stained using the American MasterTech kit. As per manufacturer's protocol, slides were rinsed in running tap water for 2 minutes, incubated in Harris Hematoxylin for five minutes, rinsed and incubated in Differentiating solution for 1 minute, rinsed and incubated with Bluing solution for 30 seconds, rinsed and incubated in 70% ethanol for 1 minute, followed by direct incubation in Eosin in 1 minute. Finally, the slides were dehydrated in 3 changes of 100% ethanol and xylene. Slides were mounted and imaged on the Hamamatsu Nanozoomer. Arterial diameter was quantified using ImageJ software.

3.20 TSB Design and Transfection

TSBs were custom-designed by Exiqon to be complementary to the 3'UTR of mouse LIMS2 (5'TGCGGGTCAAGCAAGT3')

or a scrambled TSB (5'TGACGAGCGATAGGCT3') was used as a control in all experiments. Briefly, iMAECs were seeded in 24 well plates and 24 hr later, the cells were transfected with either LIMS2 TSBs or scrambled TSBs. 50 µL of oligonucleotide/Oligofectamine (Invitrogen 12252011) mixture in Opti-MEM media (Gibco 31985070) were added to 200 µL of OPTIMEM in the plate for final dosages of 400 nM. Four hours after transfection, the media was replaced with standard media. Cells were lysed either 24 hours later for RNA extraction and qPCR analysis or cells were lysed after 72 hours for protein.

3.21 Partial Carotid Ligation and TSB Injection

12-week-old ApoE$^{-/-}$ mice (Jackson Laboratories) were used according to the approved Institutional Animal Care and Use Committee protocol by Emory University. Mice were pretreated twice with either 5mg/kg LIMS2 TSBs or scrambled TSBs subcutaneously (s.c.) on Days 1 and 2 pre-ligation. Then mice were partially ligated according to **Figure 1.3E**. and were fed a high fat diet for three weeks [83]. Throughout the three week period, mice were injected with LIMS2 TSBs or scrambled TSBs twice a week according to **Figure 3.4**. After 3 weeks, the aortic trees (including the carotids) were dissected and examined by bright field imaging. Gross lesion area was quantified using ImageJ software.

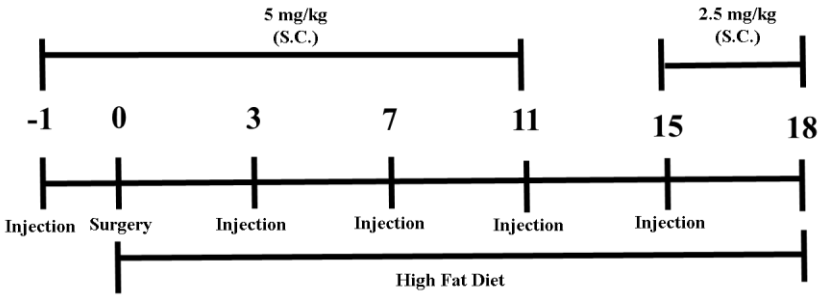

Figure 3.4 LIMS2 TSB Injection Schedule

3.22 Statistical Analysis

Statistical analyses were carried out with Graph-Pad Prism (GraphPad Software). All error bars reported are s.e.m. unless otherwise indicated. Pairwise comparisons were performed using one-way Student's t-tests. Multiple comparisons of means were performed using one-way analysis of variance followed by Tukey's multiple comparison tests. Differences between groups were considered significant at P-values below 0.05.

CHAPTER 4 AIM I: MIR-744 IS INDUCED BY DISTURBED FLOW AND INDUCES ENDOTHELIAL INFLAMMATION

4.1 Summary

We initially discovered miR-744 through its seed sequence homology with another miRNA, miR-663. Unlike its sister miRNA, miR-744 is conserved in multiple mammalian species, including mice. Therefore, we initially demonstrate that miR-744 is also induced by OS in human endothelial cells and then expand this work into mice with the ultimate goal of studying this miRNA in our mouse model of atherosclerosis. Specifically, we found that miR-744 is induced by OS in HUVECs, HAECs, iMAECs, endothelial enriched RNA from our model of d-flow-induced atherosclerosis (partial carotid ligation) and in the chronically flow disturbed lesser curvature (LC). Subsequently, in order to further investigate the role of miR-744 in OS-induced inflammation, its effect on monocyte adhesion and inflammatory marker expression (ICAM1, VCAM1, and MCP-1) were assessed under conditions of miRNA overexpression via miRNA mimics and inhibition via locked nucleic acid (LNA) complementary antimiRNAs respectively. We found that treatment with mimics increased monocyte adhesion and ICAM1/VCAM1/MCP-1 mRNA expression even in anti-inflammatory LS conditions. Furthermore, we found that ICAM1 and p65 protein expression were increased by mimic treatment. Alternatively, we found that antimiR treatment under OS conditions drastically reduced monocyte adhesion and ICAM1/VCAM1 mRNA expression. Additionally, we found that the effects of miR-744 on endothelial inflammation could also be replicated in iMAECs.

4.2 Results

4.2.1 miR-744 Shares a Seed Sequence with miR-663 and is Induced by OS in Human ECs

In previous studies by our group, the primate-specific miRNA, miR-663, was discovered to be the most highly upregulated by OS in human umbilical endothelial cells (HUVECs). Furthermore, we found that increased levels of miR-663 correlate with increased adhesion of monocytes, a marker of endothelial inflammation. Despite these findings, as it is not conserved in mice, animal studies could not be conducted. However, we found that another miRNA, miR-744, is conserved across many mammalian species (including mice) and shares a seed sequence with miR-663. Therefore, we initially assessed the expression of miR-744 in HUVECs and HAECs subjected to either OS or LS for 24 hours using miR-663 as a control. Interestingly, miR-744 is increased in OS conditions by more than four-fold in both cell types as compared to LS. Furthermore, miR-744 showed a greater magnitude of change in OS as compared to miR-663 in both cell types. These results indicate that miR-744 is a flow-sensitive miRNA in human ECs.

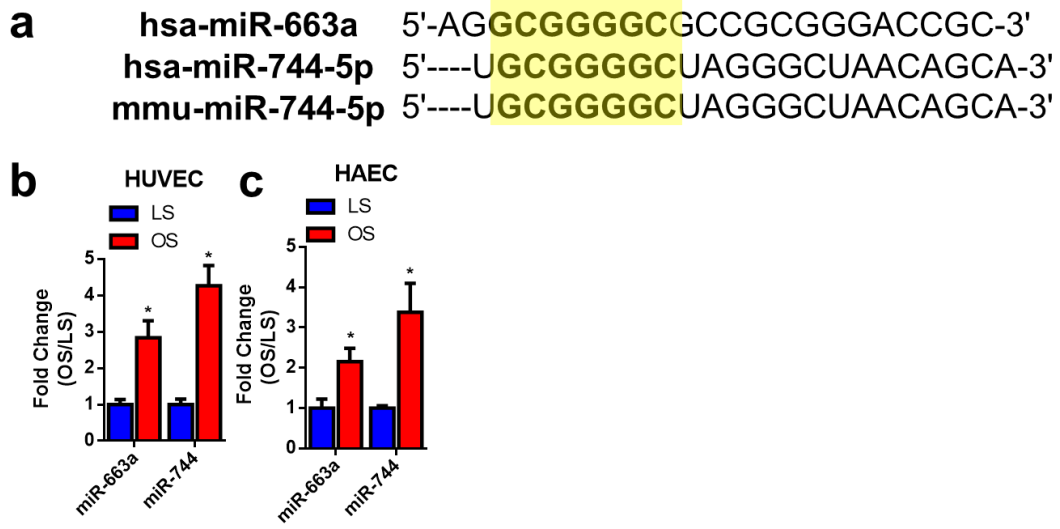

Figure 4.1 miR-744 shares a seed sequence with miR-663 and is induced by OS in human ECs.

A) Sequences of hsa-miR-663a, hsa-miR-744-5p, and mmu-miR-744-5p. Either (B) HUVECs or (C) HAECs were exposed to LS or OS for 24 hours. Following shear, RNA was collected for qPCR and miR-663a or miR-744 levels were measured and normalized to RNU6B. (n=4, *=p<0.05) Data are shown as the mean ± SEM

4.2.2 miR-744 is Induced by D-flow in Mouse ECs

After this initial result, we wanted to determine whether the mechanosensitivity of miR-744 could be replicated in mouse cells. Therefore, we subjected iMAECs to either LS or OS for 24 hours and discovered that miR-744 levels are increased by two-fold. These results indicate that miR-744 is a mechanosensitive miRNA both in human and mice ECs. Finally, to validate whether miR-744 is mechanosensitive *in vivo*, we tested miR-744 levels in endothelial RNA derived from our mouse model of acute d-flow-induced atherosclerosis (partial carotid ligation) and in the chronically flow disturbed LC. In ligated mice, miR-744 was increased by two-fold in the flow-disturbed LCAs as compared to the RCAs 48 hours post-ligation. Surprisingly, in the chronically flow-disturbed LC, miR-744 levels were more than 10 fold higher in the LC as compared to the GC. These results, taken together, show that miR-744 is mechanosensitive in both human and mouse endothelium and that miR-744 may increase over longer periods of exposure to d-flow.

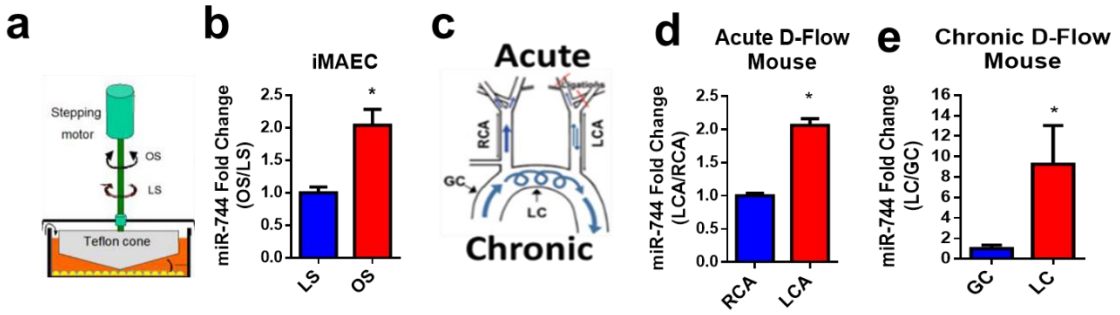

Figure 4.2 miR-744 is induced by D-flow in mice both *in vitro* and *in vivo*.

(A) Schematic diagram of the cone and plate viscometer (B) iMAECs were exposed to LS or OS for 24 hours. Following shear, RNA was collected for qPCR and miR-744 levels were measured and normalized to RNU6B. (n=6, *=p<0.05) (C) Schematic diagram of the partial carotid ligation model, in which 3 of the 4 caudal branches of the left common carotid artery (LCA) are ligated, while the contralateral right common carotid artery (RCA) remains untouched as an internal control. Also depicted are the naturally, chronically flow-disturbed lesser curvature (LC) and the unidirectional flow greater curvature (GC) (D) C57 Bl/6 mice were partially ligated for 48 hours and then sacrificed. Endothelial-enriched RNA was collected from the LCAs and RCAs of mice and miR-744 levels were measured by qPCR 48 hours post-ligation. (n=5, *=p<0.05) (E) Unligated animals were sacrificed and endothelial-enriched RNA was collected from the LC and GC. (n=4, 2 animals were pooled per sample, *=p<0.05) Data are shown as the mean ± SEM

4.2.3 miR-744 Modulates Endothelial Inflammation in human ECs

Given that our previous studies on miR-663 indicated that d-flow-induced miR-663 induces monocyte adhesion, we initially tested whether miR-744 also impacts monocyte adhesion. Therefore, we transfected HUVECs with a miR-744 mimic to artificially increase the levels of mature miR-744 and subjected the cells to LS for 24 hours. We discovered that the number of monocytes adhering to the normally quiescent LS-treated endothelium doubled, thus indicating that miR-744 may play a role in endothelial inflammation. To further test this hypothesis, HUVECs were treated with the miR-744 mimic, subjected to LS, and lysed for either RNA or protein to assess the expression of key d-flow-induced inflammatory markers which mediate monocyte adhesion to endothelium: VCAM1, ICAM1, and MCP1. We found that VCAM1 and ICAM1 were upregulated by two-fold at the mRNA level, whereas MCP1 was increased by more than four fold. Finally, as it has been well-established that the transcription factor NFkB mediates the increased transcription of these inflammatory markers, static cells were transfected with the mimic for 24 hours and then stained for the most common subunit of NFkB, p65. As NFkB remains in the cytosol unless activated by TNFα, the staining showed NFkB was mostly in the cytosol. However, treatment with miR-744 mimic increased total p65 levels by more than four-fold, which explains the upregulation of inflammatory markers downstream. Conversely, transfection of antimiR-744 before subjecting HUVECs to 24 hours of OS dramatically reduced d-flow-induced monocyte adhesion by more than eight-fold. Furthermore, VCAM1 and ICAM1 were decreased by 60% and MCP1 by 50%. Total p65 reduction (50%) was also observed. Overall, these results indicate that miR-744 modulates endothelial inflammation in human ECs

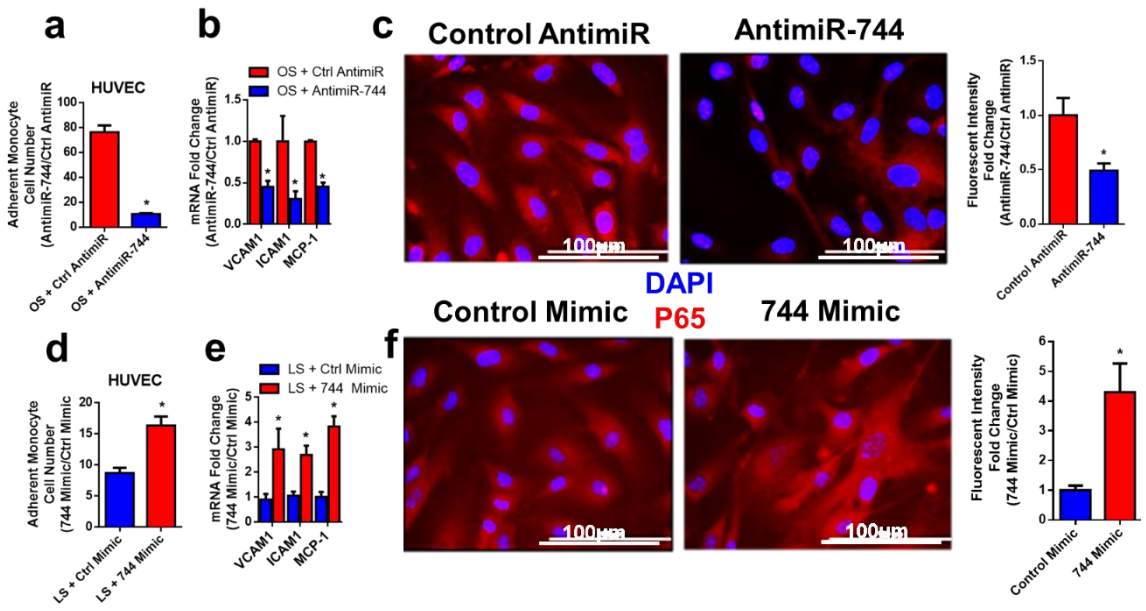

Figure 4.3 miR-744 modulates endothelial inflammation in human ECs.

HUVECs were transfected with (A-C) 100 nM of antimiR-744 and immediately subjected to OS or (D-F) 40 nM miR-744 for 24 Hr and subjected to LS. 24 Hr later, cells were (A,D) incubated with monocytes for 30 min, and the number of adherent monocytes was determined. (n=6,*=p<0.05). (B,E) Alternatively, the cells were lysed at 24 Hr and RNA was collected for determination of the inflammatory markers VCAM1, ICAM1, and MCP-1. (n=4,*=p<0.05 (C,F) Static HAECs were transfected for 24 Hr, fixed, and stained for DAPI and total P65. (n=12,*=p<0.05) Data are shown as the mean ± SEM

4.2.4 miR-744 Modulates Endothelial Inflammation in Mouse ECs

Given that ultimately we wanted to test the therapeutic potential of miR-744 in our mouse model of atherosclerosis, we next wanted to validate that miR-744 could modulate endothelial inflammation in mouse ECs. Therefore, we transfected static iMAECs with either a miR-744 mimic or antimiR-744 to modulate miR-744 levels. We discovered that miR-744 mimics increased VCAM1 mRNA levels by four-fold, ICAM1 by two-fold, and MCP1 by eight-fold. Furthermore, total p65 levels increased by two-fold. Interestingly, antimiR-744 treatment did not significantly reduce the levels of VCAM1 and ICAM1, but MCP1 levels were significantly reduced by more than 50% and total p65 levels by more than 70%. Overall, this data indicates that miR-744 is functionally active in both humans and mice.

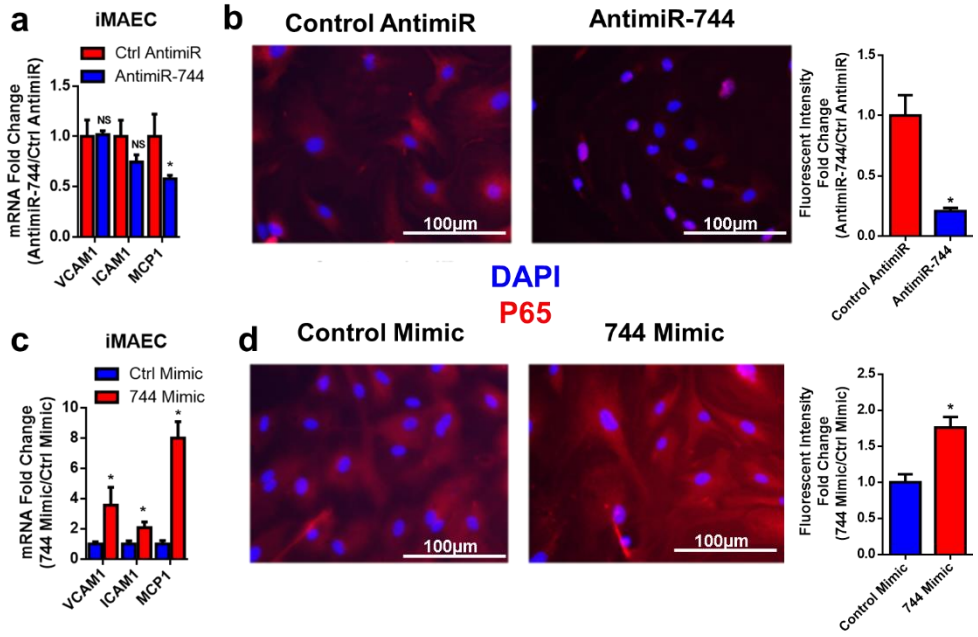

Figure 4.4 miR-744 modulates endothelial inflammation in iMAECs.

Static iMAECs were transfected with (A,B) 100 nM miR-744 for 24 Hr or (C,D) 400 nM of antimiR-744 for 24 Hr. Subsequently, cells were (A,C) lysed at 24 Hr and RNA was collected for determination of the inflammatory markers VCAM1, ICAM1, and MCP-1. (n=4,*=p<0.05) (B,D) Cells were transfected for 24 Hr, fixed, and stained for DAPI and total P65. (n=12,*=p<0.05) Data are shown as the mean ± SEM

4.3 Discussion

Prior to this work, there had been no investigation of the flow-dependent regulation of miR-744 and its role in endothelial biology. Through our *in vitro* and *in vivo* models of disturbed flow, we were able to study miR-744 modulation by flow. Furthermore, miRNA mimics and LNA-modified antisense antimiRs allowed us to discover the functional consequences of miR-744 in endothelial biology. Given what was previously published regarding miR-663, which shares a seed sequence with miR-744, we already had an indication that miR-744 may also be upregulated by disturbed flow and may induce endothelial inflammation. We showed that miR-744 is a mechanosensitive miRNA induced by d-flow *in vivo* and OS *in vitro* and that miR-744 increases endothelial inflammation and inhibition suppresses inflammation in both human and murine ECs. Given its dramatic flow-sensitivity and effect on endothelial inflammation, we expect that miR-744 may play a key role in atherosclerosis.

However, it would also be interesting to examine the interplay between miR-744 and miR-663. miR-663 is derived from the miR-663 gene on Chromosome 20 and from the RN45S region of ribosomal RNA, which is normally degraded by XRN1 under LS conditions [36], whereas miR-744 is derived from the miR-744 gene on Chromosome 17, overlaps with the MAP2K4 gene, and is not found in the RN45S region [313]. Given that miR-663 is derived from two locations, it is unsurprising that in HUVECs, miR-663 is expressed more than 20-fold higher than miR-744. In HAECs, miR-663 is only 5-fold higher in LS and three fold higher in OS. Surprisingly, both miRNAs are much higher expressed in HUVEC as opposed to HAEC. HUVEC expression of miR-663 is doubled under LS conditions, whereas miR-744 is more than 4 fold higher. However, although the expression of miR-744 in iMAECs is double that of HAECs, the OS levels are the same. This indicates that these pro-inflammatory miRNAs are basally higher in the less terminally differentiated HUVECs and are slightly less shear-responsive as in arterial cells

(HAEC and iMAEC). The difference in iMAEC versus HAEC may be explained by the immortalization process of the iMAECs possibly introducing basally higher levels of inflammation than seen in these early passage HAECs. Given that there is no difference in the copy numbers in OS conditions, it seems unlikely that miR-744 is more highly expressed in mice than human. However, future studies would be to more closely examine the miRNA profile in HUVEC versus HAEC, especially as HUVECs are widely used in vascular biology experiments to screen for miRNAs and look for phenotypic differences that will ultimately be observed in the arterial cells *in vivo*.

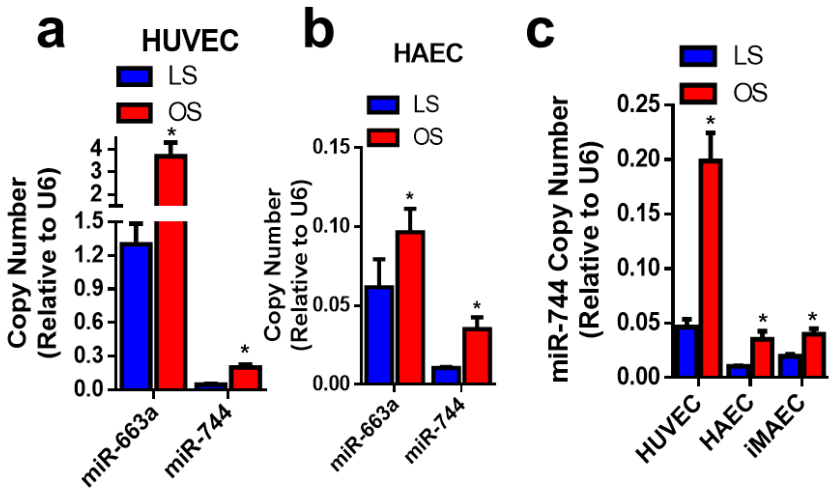

Figure 4.5 miR-663 and miR-744 copies vary in HUVECs, HAECs, and iMAECs.

HUVECs, HAECs, or iMAECs were exposed to LS or OS for 24 hours. Following shear, RNA was collected for qPCR and (A, B) miR-663 and/or (A-C) miR-744 levels were measured in (A) HUVECs or (B) HAECs or (C) iMAECs and normalized to RNU6B. (n=4, *=p<0.05) Data are shown as the mean ± SEM

Further examination of the copy number of miR-744 *in vivo* reveals that the RCA and LCA endothelial-enriched RNA has a similar copy number to iMAECs and HAECs. However, miR-744 copy numbers are significantly higher in the GC and LC and in fact are more than 50 fold higher than the levels seen in HUVECs. As the methodology for collecting endothelial enriched RNA from the GC and the LC involves directly incubating the areas with isopropanol-soaked nitrocellulose membranes and typically gives much lower yield than carotid flushings, the high copy numbers may be due to false inflation from the low yield.

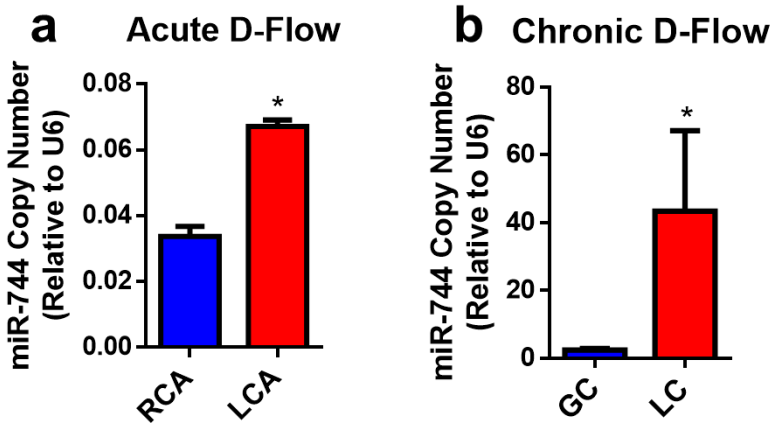

Figure 4.6 miR-744 copies vary in the carotids and in the aortic arches of mice.

(A) C57 Bl/6 mice were partially ligated for 48 hours and then sacrificed. Endothelial-enriched RNA was collected from the LCAs and RCAs of mice and miR-744 levels were measured by qPCR 48 hours post-ligation. (n=5, *=p<0.05) (B) Unligated animals were sacrificed and endothelial-enriched RNA was collected from the LC and GC. (n=4, 2 animals were pooled per sample, *=p<0.05) Data are shown as the mean ± SEM

Although the investigation of miR-744 in alternative cell types and among other endothelial cell types certainly merits further investigation, the results of this aim have also opened other potential avenues of investigation. Some potential future studies may be to investigate the role of miR-744 in other markers of EC dysfunction, such as proliferation [355-357] and migration. Several studies have found that physiologically relevant shear stress decreases endothelial turnover by decreasing proliferation and apoptosis. Specifically, apoptosis is triggered by lack of shear stress [358-360].

Furthermore, there is an increase in cell density before flow loading and endothelial cell proliferation increases dramatically within 48 hours after reduction of shear stress, whereas OS induces cell turnover. Alterations of shear stress in arteries revealed that EC apoptosis and cell turnover/proliferation increase significantly under low–shear stress conditions. It was first proposed that leaky junctions around cells in a state of apoptosis or mitosis provide the major pathway for transport of large molecules such as LDL across the endothelium [361] . More recent studies have shown a strong correlation between apoptosis and mitosis rates and LDL permeability of endothelial monolayers in culture [35]. Ultimately, chronic differences in shear stress affect LDL transport into the vessel wall and that low shear stress may be expected to increase LDL permeability, which is a factor in atherosclerosis. Furthermore, it has been found by our lab that LS inhibits EC migration and angiogenesis Angiogenesis also plays a role in atherosclerosis [38, 39]. Furthermore, miR-744 has previously been implicated in migration and proliferation (**Ch. 1.7**). Our preliminary studies reveal that in HUVECs, miR-744 mimic significantly increased proliferation and migration and antimiR-744 significantly inhibited these processes.

.

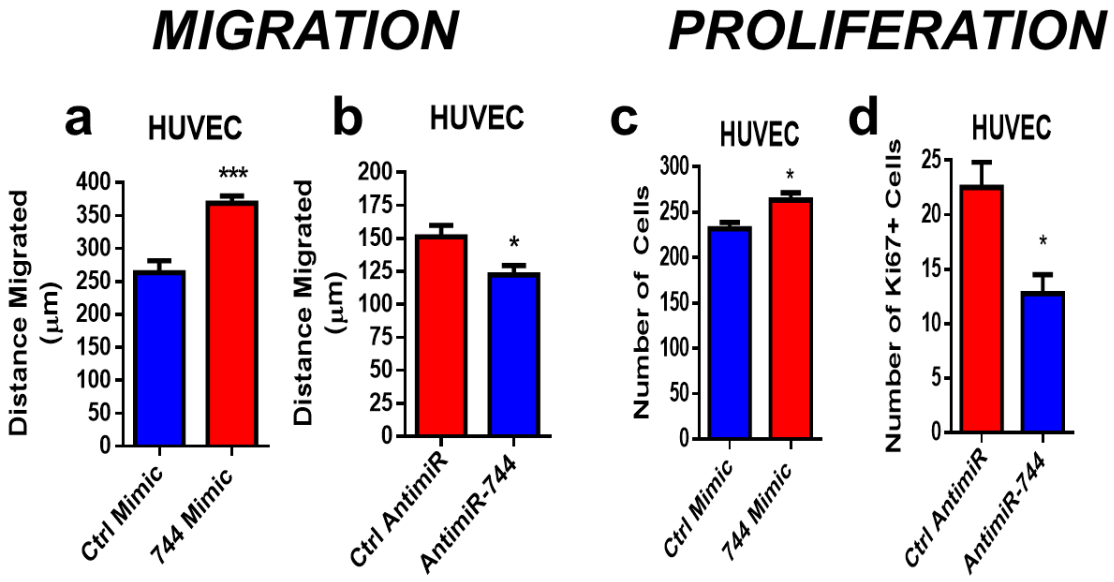

Figure 4.7 miR-744 modulates migration and proliferation in human ECs.

HUVECs were transfected with (A,C) 40 nM miR-744 for 24 Hr or (B,D) 100 nM of antimiR-744. 24 Hr later, cells were (A,B) scratched with a pipette tip and the wound was imaged in 6 places at 0, 6, and 16 hours. (n=3,*=p<0.05). (C,D) Alternatively, the cells were fixed at 24 Hr and stained with DAPI or Ki67. Data are shown as the mean ± SEM

CHAPTER 5 AIM II: MIR-744 MEDIATES ENDOTHELIAL INFLAMMATION VIA LIMS2

5.1 Summary

Next, we wanted to determine the mechanism by which miR-744 could induce endothelial inflammation and in the process, discovered multiple novel, flow-sensitive genes. To accomplish this goal, we treated HUVECs with a miR-744 mimic and sequenced the mRNAs derived from immunoprecipitating the RNA-Induced Silencing Complex in order to discover functional targets of miR-744 in human ECs. We found more than 300 mRNAs were differentially enriched in the RISC as a result of increased miR-744. From this pool of mRNAs, we specifically wanted to study direct targets of miR-744 that were conserved in humans and mice, so we filtered the pool down to 134 which are putative conserved direct targets. From this smaller pool, we compared this list to the genes which were lost in the flow-disturbed LCA at the 48 hour time point by more than 30% in our partial carotid ligation model and found 13 genes which were significantly downregulated. After arriving at this pool of genes, we subsequently screened out genes based on shear sensitivity and responsiveness to both anti-744 and mimic treatment in HUVECs. From the screening, LIMS2 emerged as a consistent target in HUVECs. Then, the shear sensitivity of LIMS2 was validated at the protein level in HAECs by LS/OS and at the mRNA level and protein level in partially ligated mice, as well as by 3'UTR luciferase assays in iMAECs. Furthermore, we discovered that LIMS2 expression is lost in advanced atherosclerotic lesions in human patients. Therefore, the functional consequences of the loss of LIMS2 was determined in HAECs. It was found that siLIMS2 profoundly induced EC inflammation by upregulating ICAM1/VCAM1/MCP-1 mRNA expression and monocyte adhesion.

5.2 Results

5.2.1 Sequencing of Ago2-Immunoprecipitated RNAs and Sequencing Reveals 13 Conserved Targets

Although there have been multiple published targets of miR-744, miRNAs can target hundreds of genes in a cell-type specific manner and thus it is crucial to identify targets of miR-744 which would be relevant to endothelial biology and atherosclerosis. Therefore, in order to discover these additional targets and gain a comprehensive picture of the miR-744 regulatory network in the context of EC dysfunction and atherosclerosis, genes directly regulated by miR-744 were determined by sequencing RNA derived from immunoprecipitation of Ago2 (RISC) under conditions of miR-744 elevation. To this end, static HUVECs were transfected with miR-744 mimic or control mimic for 24 hours. Following transfection, cell lysate was collected in RNA IP lysis buffer and was incubated with Ago2 antibody-conjugated beads overnight. Following incubation, the beads were washed and directly added to Qiazol and RNAs bound to RISC were purified and sequenced by the Yerkes Sequencing Core. Genes which were enriched in the sequencing were compared to predicted targets and our previously published mouse endothelial gene array data to reveal 13 potential targets. On first pass, more than 800 genes were differentially increased or decreased in the RISC in the mimic-treated vs. the control treated. After filtering out transcripts with less than 100 reads, more than 300 transcripts were enriched in the 744 treated, meaning they could be potential targets. This pool of genes was compared to a list of potential targets of miR-744, meaning they have a binding sequence for miR-744 in the 3'UTR in both the human and mouse isoforms. From these, more than 100 transcripts could be conserved targets of mIR-744 in ECs. Finally, to obtain potentially mechanosensitive targets of miR-744, this list was compared to genes which were decreased in the LCAs of partially ligated mice 48 hours post-ligation by at least 30%. Of these, 13 genes emerged which were decreased in the LCAs, potential conserved targets, and were enriched in the RISC.

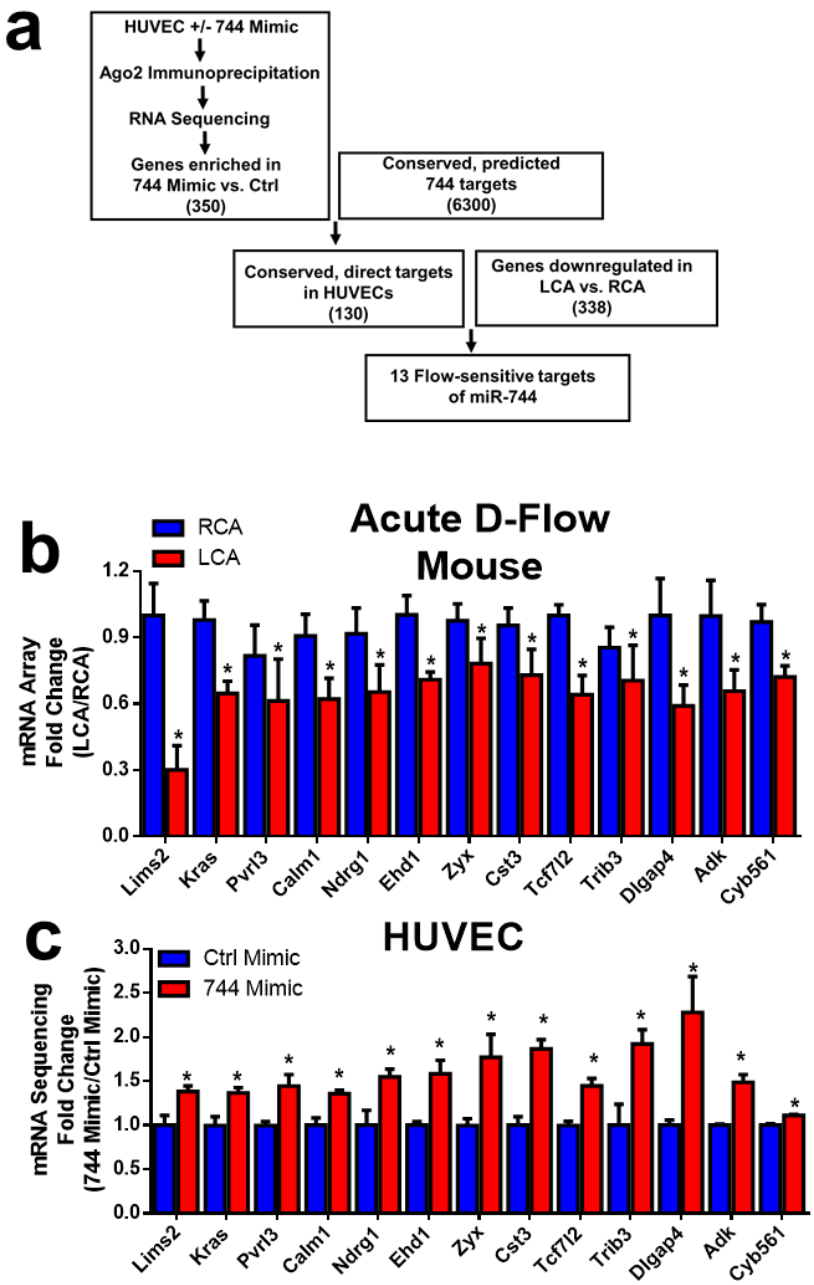

Figure 5.1 RNA Sequencing Reveals 13 Potential miR-744 Targets.

Static HUVECs were transfected with either 40 nM miR-744 or control mimic for 24 Hr, followed by Ago2 immunoprecipitation and sequencing of the resultant mRNAs. Genes which were enriched in the IP were compared to the miRWalk database of predicted targets in humans and mice, and the genes which were also downregulated at 48 Hr in the flow-disturbed LCAs of our previously-published mouse model (Ni et al Blood 2010) were selected for further analysis. (B) Fold change in the mRNA array (n=5) (C) Fold change in the RNA Seq data (n=3) *=p<0.05 Data are shown as the mean ± SEM

5.2.2 Target Screening Reveals LIMS2 is a mechanosensitive target of miR-744 in HUVECs

Initially, the mechanosensitivity of the 13 genes identified by RNA sequencing were validated in HUVECs were exposed to LS or OS for 24 hours. Following shear, RNA was collected for qPCR and potential targets were measured. Interesting, although all 13 genes change by more than 30 % in our partial carotid ligation microarray, only 9 genes were upregulated by LS *in vitro*. From the remaining genes, cells were either transfected with antimiR-744 for 4 hours, followed by 24 Hr of OS, or transfected with non-targeting antimiR and subjected to LS or OS in order to assess responsiveness to miR-744. Interestingly, only five of the original 9 genes were significantly upregulated by LS, and three were rescued by antimiR-744. Finally, in order to validate the effect of miR-744 on these remaining genes, static HUVECs were transfected with 40 nM 744 mimic and RNA was collected 24 Hr later. Although 5 genes were responsive to the mimic, only LIMS2 was consistently modulated by antimiR-744 and mimic

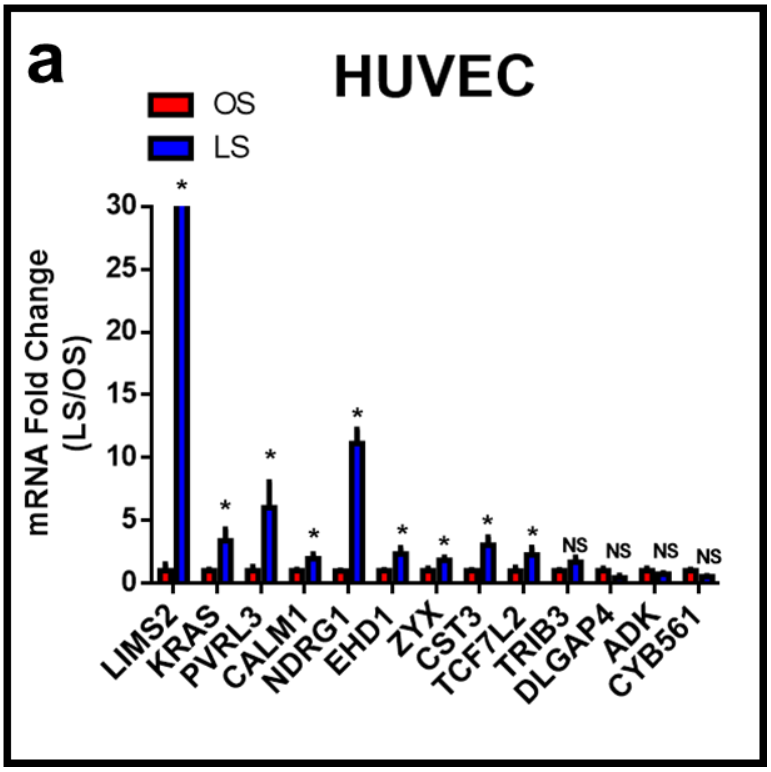
a
HUVEC
OS
LS
mRNA Fold Change
(LS/OS)
30
25
20
15
10
5
0
*
NS
LIMS2
KRAS
PVRL3
CALM1
NDRG1
EHD1
ZYX
CST3
TCF7L2
TRIB3
DLGAP4
ADK
CYB561

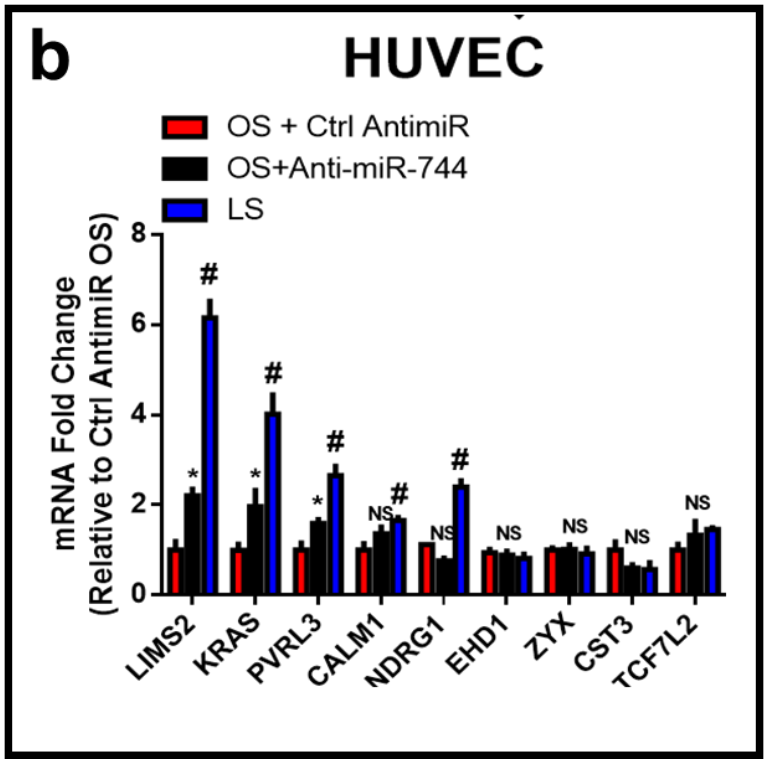
b
HUVEC
OS + Ctrl AntimiR
OS+Anti-miR-744
LS
mRNA Fold Change
(Relative to Ctrl AntimiR OS)
8
6
4
2
0
*
#
NS
LIMS2
KRAS
PVRL3
CALM1
NDRG1
EHD1
ZYX
CST3
TCF7L2

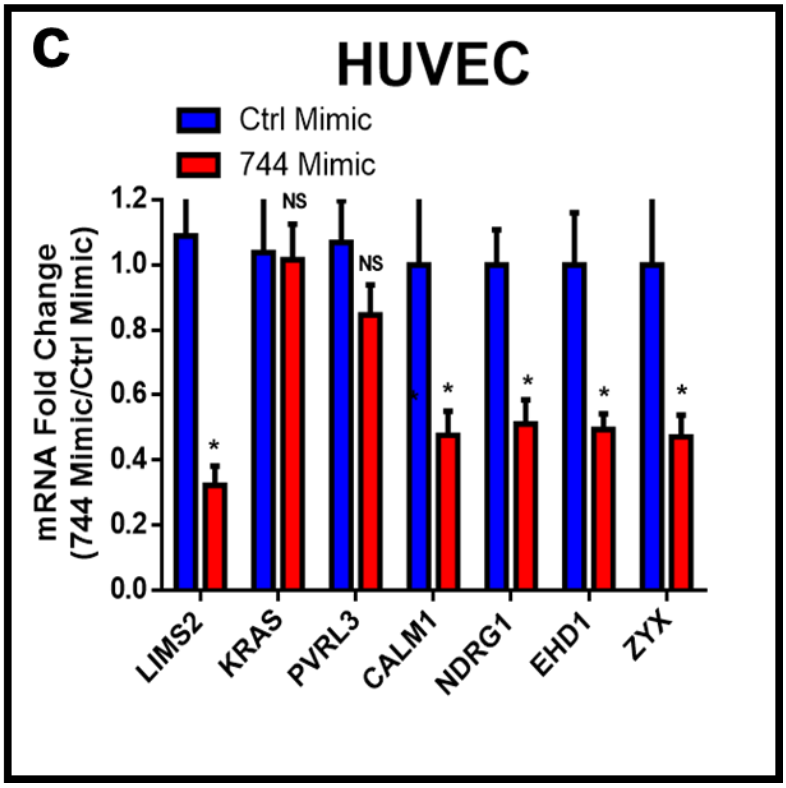

Figure 5.2 LIMS2 Emerges as a Consistent, Mechanosensitive Target of miR-744 in HUVECs. (A) HUVECs were exposed to LS and OS for 24 hours. Following shear, RNA was collected for qPCR and potential targets were measured. (n=3,*=p<0.05) (B) HUVECs were either transfected with antimiR-744 for 4 hours, followed by 24 Hr of OS, or transfected with non-targeting antimiR and subjected to LS or OS. (n=3,*=p<0.05) (C) Static HUVECs were transfected with 40 nM 744 mimic and RNA was collected 24 Hr later (n=4,*=p<0.05)

5.2.3 LIMS2 Identified as Conserved Target in Humans and Mice

After identifying LIMS2 as consistently modulated by both miR-744 mimic and antimiR, the mechanosensitivity of LIMS2 was validated in HAECs subjected to either 24 hours of LS or OS. LIMS2 was upregulated by more than 10 fold at the protein level, which is in agreement with the HUVEC qPCR data. Furthermore, LIMS2 sensitivity to antimiR-744 was validated at the protein level as well in HAECs, where antimiR was able to rescue LIMS2 expression by more than five fold. After establishing the mechanosensitivity of LIMS2 in HUVECs and HAECs, we assessed the expression of LIMS2 in our acute d-flow model of atherosclerosis. We found that LIMS2 expression is lost in the LCAs of mice under d-flow, but has robust expression in the endothelium of RCAs exposed to s-flow. This was quantified at the mRNA level by obtaining endothelial-enriched RNA from mice that had been partially ligated for 48 hours. At the mRNA level, LIMS2 expression was more than 70% reduced in the LCAs as opposed to the RCAs. Finally, as miR-744 has multiple binding sites in the 3'UTR of human LIMS2 and only one in the murine LIMS2, a construct containing the 3'UTR of murine LIMS2 fused to a luciferase reporter was transfected into iMAECs in conjunction with either the miR-744 mimic or control mimics in order to validate that LIMS2 is a bona fide target of miR-744. Furthermore, mutant plasmids containing a mutated binding sequence for miR-744 were transfected as controls. The mimic significantly reduced the luciferase activity of the wild-type plasmid, whereas the mutated plasmid was unaffected by mimic treatment, as miR-744 was unable to bind to it. Together, these results corroborate with the HUVEC data indicating that LIMS2 is a strongly mechanosensitive protein that is suppressed by miR-744 in d-flow.

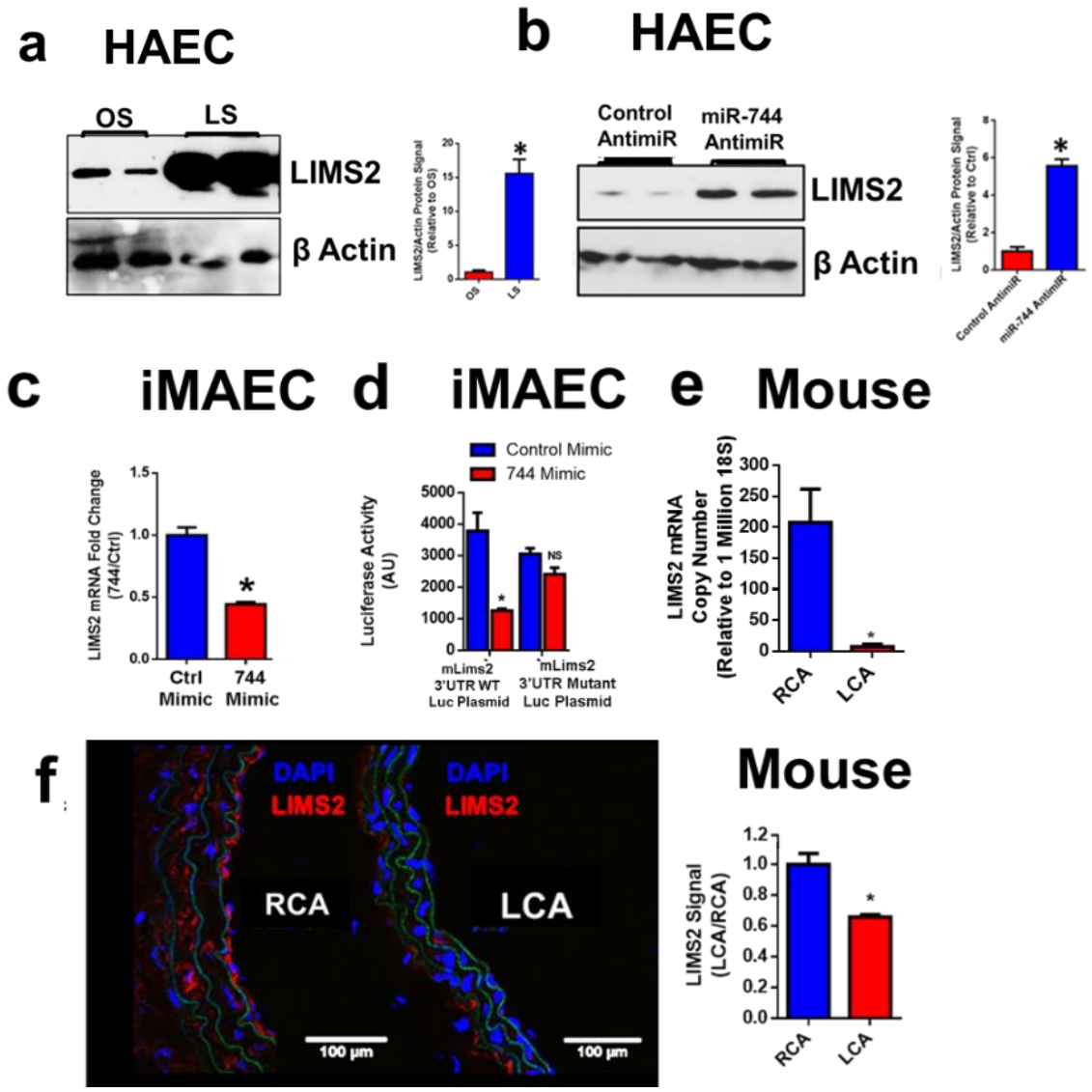

Figure 5.3 LIMS2 is a mechanosensitive, a conserved target of miR-744.

(A) HAECs were subjected to LS or OS and protein was collected 24 Hr later (n=5, *=p<0.05) (B) HAECs were transfected with 100 nM antimiR-744 and subjected to OS . Following shear, protein was collected (n=4, *=p<0.05). (C) Static iMAECs were transfected with 50 nM 744 mimic and RNA was collected 24 Hr later and LIMS2 levels were measured by qPCR. (n=6, *=p<0.05) (D) Static iMAECs were dual-transfected with 500 ng of the LIMS2 3'UTR luciferase plasmid (or mutants) and 50 nM 744 mimic. Media was collected 24 Hr later, incubated with luciferin, and read in a plate reader. (n=9, *=p<0.05) (E,F) C57 Bl/6 mice were partially ligated for 48 hours and then sacrificed. Endothelial-enriched RNA was collected and LIMS2 levels were measured by qPCR. LIMS2 decreased by 70% in the LCA. (F) Alternatively, frozen sections were generated of the LCA and RCA and stained with LIMS2. (n=5, *=p<0.05) Data are shown as the mean ± SEM

5.2.4 LIMS2 is Lost in Advanced Lesions in Human Patients

Given these results, we next wanted to ascertain whether LIMS2 also lost in human atherosclerotic patients. To this end, paraffin sections of right coronary arteries were obtained from Dr. Robert Taylor (Emory University) and stained for LIMS2. Initially, sections were stained with hematoxylin and eosin to assess the degree of severity. The sections were scored from Grades I to V. In agreement with our previous findings, LIMS2 was completely lost in Grades IV and V, which have advanced atherosclerotic lesions. However, more healthy arteries had strong, endothelial-specific staining of LIMS2. Taken with the previous results, this indicates that the loss of LIMS2 may be critical to atherosclerosis progression.

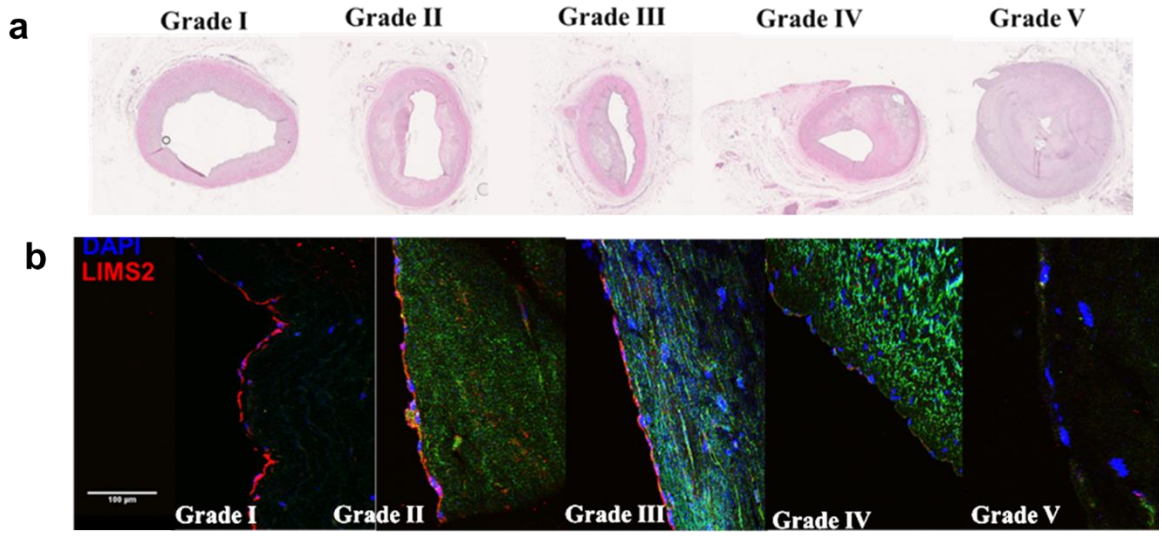

Figure 5.4 LIMS2 is lost in Atherosclerosis.

Right Coronary Artery sections were generated and stained for (A) Hematoxylin and Eosin for grading or (B) LIMS2.

5.2.5 LIMS2 Silencing Induces Endothelial Inflammation

The previous results indicate that the loss of LIMS2 may drive atherosclerosis progression. To test this hypothesis, HAECs were treated with siLIMS2 for 48 hours, subjected to LS, and either subjected to monocyte adhesion assay or lysed for RNA to determine the expression of VCAM1, ICAM1, and MCP1. Monocyte adhesion increased by more than four-fold in the siLIMS2-treated group, whereas we found that VCAM1 was upregulated by six-fold, ICAM1 was two-fold and MCP1 was increased by three-fold. As LIMS2 is lost by miR-744 mimics and in atherosclerosis, these results indicate that loss of LIMS2 can replicate the effects seen by miR-744 mimics. Furthermore, this indicates that rescuing LIMS2 in atherosclerotic plaques may blunt endothelial inflammation.

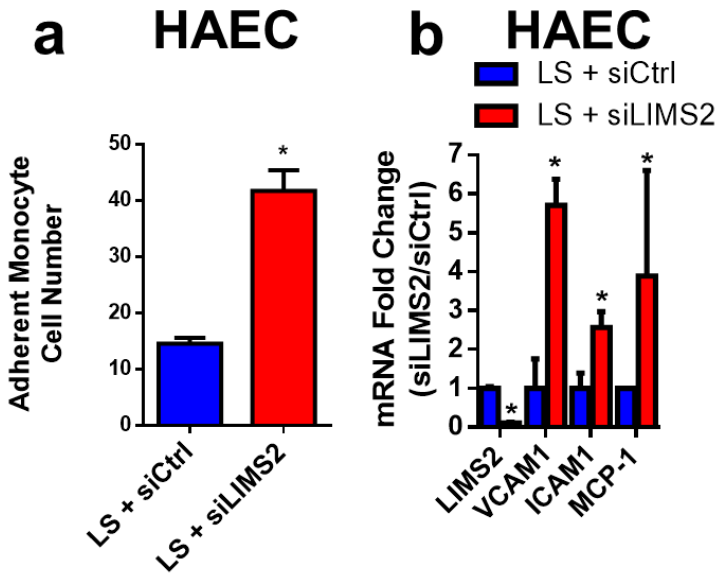

Figure 5.5 LIMS2 silencing induces endothelial inflammation in human ECs.

HAECs were transfected with 100 nM of siLIMS2 and and subjected to LS 24 hr later. 24 Hr post shear, cells were (A) incubated with monocytes for 30 min, and the number of adherent monocytes was determined. (n=6,*=p<0.05). (B) Alternatively, the cells were lysed at 24 Hr and RNA was collected for determination of the inflammatory markers VCAM1, ICAM1, and MCP-1. LIMS2 expression was also determined for knockdown efficiency. (n=3,*=p<0.05) Data are shown as the mean ± SEM

5.3 Discussion

The purpose of this aim was to identify the mechanism by which miR-744 mediates endothelial inflammation. In order to accomplish this, the scope of the study was limited to the identification of direct targets of miR-744 that are conserved in humans and mice, significantly expressed in ECs, and were previously implicated as being mechanosensitive. Thus, we used a combination of *in silico* analysis and single gene screening to identify a network of genes regulated by miR-744. Although more than 300 genes were significantly enriched in the RISC in miR-744 mimic-treated HUVECs (**Appendix A.1**), more than half of these genes were excluded from further study due to the lack of a 3'UTR miR-744 binding sequence (miRWalk). In some genes, there was no binding site in either the mouse or human 3'UTR, such as KLF2, whereas other genes did not have a binding site in either the human (SIRT1) or mouse (MAP1LC3B). Although these genes may be regulated by miR-744, we chose to focus on those that are canonically regulated by miRNA binding to the 3'UTR. However, in the future, studies could be conducted to study miR-744 binding and regulation in other areas of the transcript, such as the coding sequence region. Among the remaining 130 genes, 90% were eliminated upon comparison with genes which are downregulated in the LCAs of partially ligated mice by more than 30%. This stringent criteria was meant to ensure that all the genes selected for *in vitro* screening would be strongly mechanosensitive. Ultimately, less than half were consistently shear-sensitive *in vitro* (5 genes) and only one gene, LIMS2, was sensitive to both miR-744 mimic and antimiR-744.

LIMS2 is a novel mechanosensitive gene that had never been studied in the endothelium or in the context of atherosclerosis. Given the results of Aim I, we had an indication that the targets of miR-744 may be protective against endothelial inflammation. Thus, in agreement with this hypothesis, we found that LIMS2 is a conserved target of miR-744 in both humans and mice and that modulation of LIMS2 replicates the effects of

miR-744 on endothelial inflammation. Furthermore, we found that LIMS2 is lost in the flow-disturbed LCA in our PCL model, which validates our array data. Finally, we found that LIMS2 is lost in late stage atherosclerotic patients, which indicates the importance of this gene to atherosclerosis progression,

Interestingly, genes that were originally filtered out were later found to be connected to LIMS2, notably HIC-5. HIC-5, also known as TGFB1I1, is a LIM-domain containing protein family member which is also a cytoskeletal-associated protein localized to focal adhesion complexes with ILK and LIMS2. (**Ch.1.9**) HIC-5 was also the most differentially enriched on the RISC in our sequencing data. Also, ZYX, another cytoskeletal/focal adhesion protein which failed the validation studies, has been shown to localize to focal adhesions with ILK. (**Ch.1.9**). A preliminary investigation into this phenomenon reveals that in fact, there are multiple genes which are predicted targets of miR-744 and are cytoskeletal-associated proteins (**Appendix A.2**). Overall, the fact that miR-744 is associated with multiple members of the focal adhesion complex and many general cytoskeletal proteins, which may be direct mechanosensors (**Ch. 1.5**), indicates that miR-744 could be a master regulator of a distinct mechanosensitive pathway as yet to be discovered.

Overall, in this aim we found that LIMS2 is a functionally important mechanosensitive target of miR-744 that plays a key role in endothelial inflammation *in vitro* and is lost in advanced atherosclerotic patients. LIMS2 was validated as a bone fide target of miR-744 in both human and mouse ECs and d-flow-induced suppression was verified at the transcript and protein level *in vitro* and *in vivo*. Finally, silencing of LIMS2 was enough to replicate the effects of miR-744, thus indicating that LIMS2 is the key target of miR-744 and it has a key functional role in d-flow-induced EC dysfunction and atherosclerosis. However, one interesting question that arises is the differential expression of LIMS2 in HUVEC. In fact, HAECs, iMAECs, and the carotids have similar copies of LIMS2 (600, 400, and 200 copies under LS conditions), whereas HUVECs have a much lower copy number (50 copies in LS). This discrepancy mirrors the discrepancy observed in Aim I, where both miR-663 and miR-744 had much higher levels in HUVECs. This bolsters the hypothesis that miR-744 is a significant regulator of LIMS2 in ECs. This also further underscores the differences between venous and arterial cells.

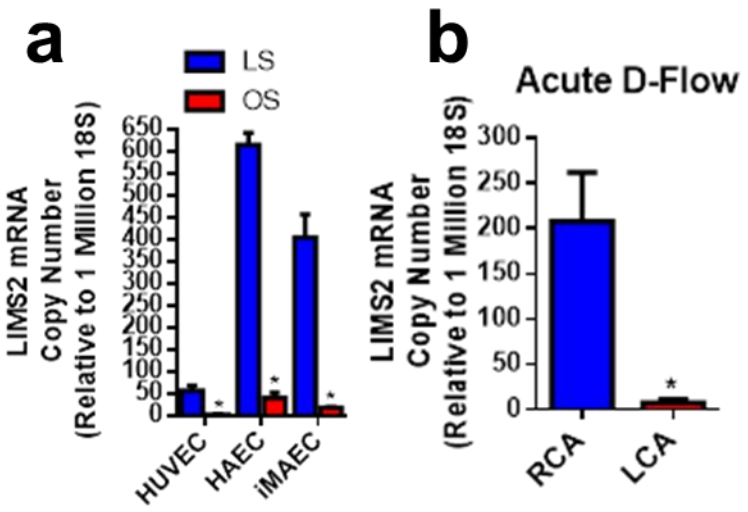

Figure 5.6 LIMS2 Copy Number is higher in arterial endothelium.

(A) HUVECs, HAECs, or iMAECs were exposed to LS or OS for 24 hours. Following shear, RNA was collected for qPCR and LIMS2 levels were measured and normalized to 18S. (n=4, *=p<0.05). (B) C57 Bl/6 mice were partially ligated for 48 hours and then sacrificed. Endothelial-enriched RNA was collected from the LCAs and RCAs of mice and LIMS2 levels were measured by qPCR 48 hours post-ligation. (n=5, *=p<0.05)

CHAPTER 6 AIM III: TARGETING THE LIMS2-744 AXIS INHIBITS ATHEROSCLEROSIS PROGRESSION

6.1 Summary

Finally, we wanted to determine the effect of miR-744 inhibition on a mouse model of acute disturbed flow induced atherosclerosis. Therefore, we initially treated partially ligated mice with antimiR-744 twice weekly for three weeks. After sacrificing, we found there was no significant difference between treated and non-treated animals. Given the multitude of targets of miRNAs, we subsequently decided to specifically test whether preventing the loss of LIMS2 due to miR-744 would prevent endothelial inflammation and atherosclerosis progression. Therefore we tested target site blockers, which specifically prevent miRNAs from binding to the 3'UTR of target genes, against the miR-744 binding site on the mouse LIMS2 3'UTR both *in vitro* and *in vivo*. In iMAECs, we found that the TSBs rescued LIMS2 expression both at the mRNA and protein levels, as well as rescued luciferase activity in 3'UTR luciferase assays. Furthermore, we found that TSB treatment decreased VCAM1 protein levels. Finally, we treated partially ligated mice with either LIMS2 TSBs or scrambled sequence TSBs twice weekly for three weeks. After sacrificing, we found that the overall plaque volume was substantially lower in LIMS2 TSB-treated animals, as well as the arterial diameter and structure of the artery was intact. In order to establish the mechanism by which LIMS2 rescue may prevent plaque progression, we discovered through the literature that LIMS2 can stabilize ILK, and can either compete with PINCH1 to bind to ILK or can compensate for PINCH1 loss. Interestingly, we found that loss of LIMS2 in LS could reduce ILK and PINCH1 mRNA levels, which would be consistent for ILK As not much is known about the PINCH1-LIMS2 interaction, this could be a novel finding. Furthermore, antimiR-744 rescued both PINCH1 and ILK, whereas mimic suppressed ILK at the protein levels. This is hypothesized to be due to the modulation of LIMS2.

6.2 Results

6.2.1 AntimiR-744 Treatment Does Not Reduce Plaque

In order to determine the role of miR-744 in the development of atherosclerosis, we used our murine model of acute d-flow-induced atherosclerosis, the partial carotid ligation model. As $ApoE^{-/-}$ mice develop atherosclerosis within three weeks of surgery (in conjunction with a high fat diet), we assessed atherosclerosis development in the LCAs of our mice while treating the mice either with saline or antimiR-744 at a dosage of 5 mg/kg for a period of three weeks. The LCAs of the mice rapidly developed atherosclerosis within the allotted time frame. However, upon gross examination, the degree of plaque was not significantly different between the treatment groups. After sectioning and staining with Oil Red O to clearly the lipid laden plaque area, quantification of the plaque revealed no significant differences between the treatment groups either.

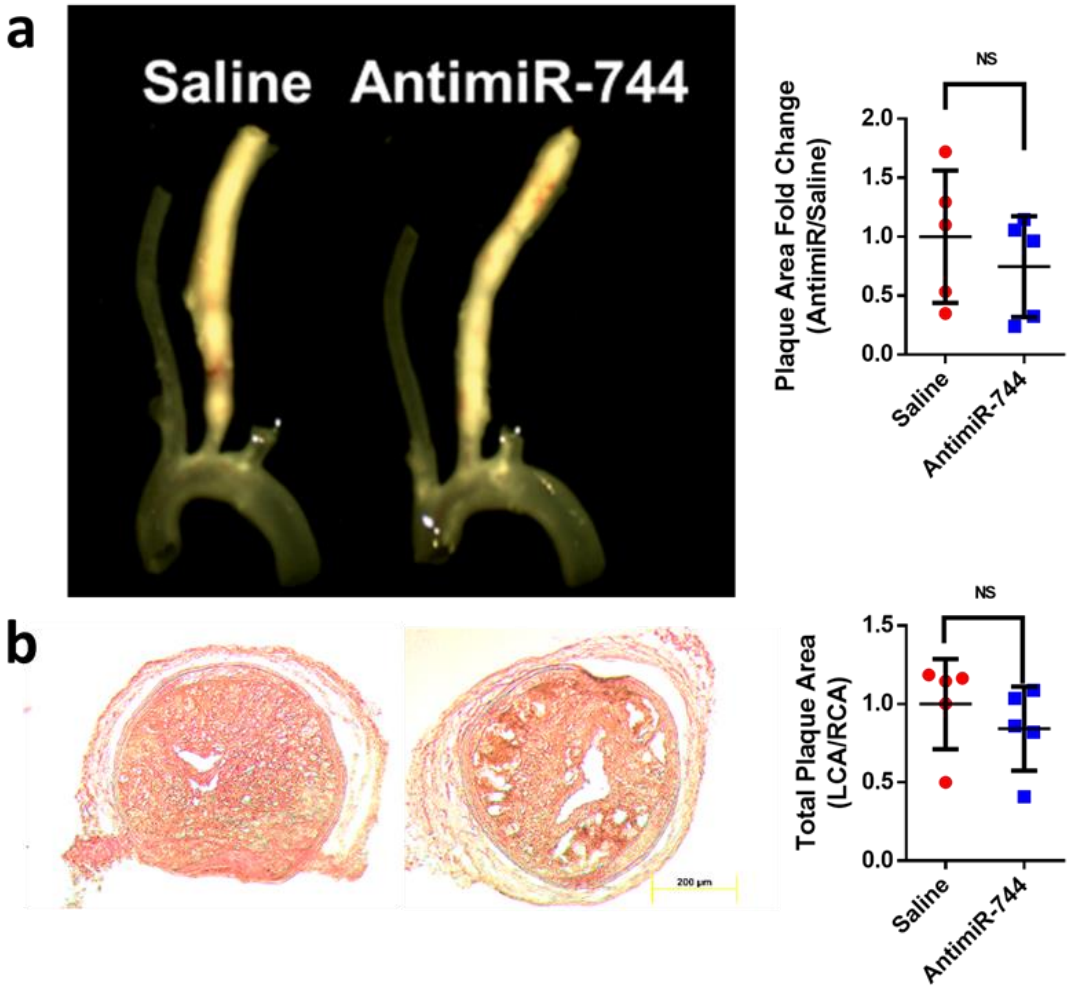

Figure 6.1 AntimiR-744 did not reduce plaque in the acute, partial carotid ligation model of atherosclerosis.

ApoE$^{-/-}$ mice were given 5mg/kg antimiR-744 twice before ligation and then twice a week for three weeks along with a high fat diet. Saline was used as a vehicle control. (A) Gross plaque was examined using light microscopy and quantified using ImageJ. (B) Frozen sections of the carotid arteries were examined by Oil Red O staining (scale bars: 200 µm) and plaque area quantification (mm2) was done using ImageJ (B) (n = 5 each, data are shown as the mean ± SEM. *P < 0.05).

6.2.2 AntimiR-744 Did not Rescue LIMS2 Expression in the Carotids

After the mice were sacrificed at the end of the study, the liver, lung, kidney, and spleen were collected in order to determine whether miR-744 was significantly inhibited at the given dosage. Surprisingly, miR-744 was not significantly suppressed in the liver or lung, but was significantly reduced by more than 40% in the kidney and spleen. However one of the key target genes, LIMS2 was increased by three fold in the spleen but in no other organ. Furthermore, on immunostaining of the carotids, LIMS2 was not significantly rescued in the endothelium of the treated group. Given the previous result indicating that the plaque burden was not reduced in these mice, miR-744 may not have sufficiently been suppressed in the carotid arteries.

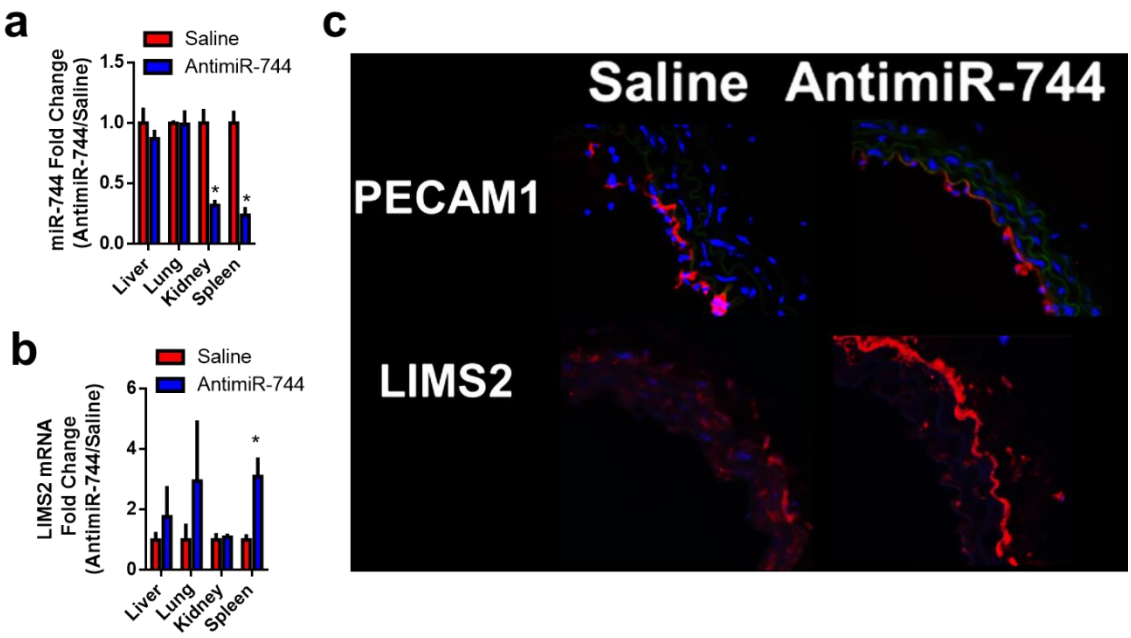

Figure 6.2 AntimiR-744 Rescued LIMS2 in the Spleen, but not in the Carotids.

(A,B) The liver, lung, kidney, and spleen were collected and crushed for RNA. RNA was collected for qPCR and (A) miR-744 levels were measured and normalized to RNU6B or (B) LIMS2 levels were measured and normalized to 18S (n=5, *=p<0.05) (C) LCAs were immunostained for PECAM1 (to denote the endothelium) or LIMS2 for either saline or antimiR-744 treated animals.

6.2.3 TSBs Rescue LIMS2 and Prevent VCAM1 Expression in iMAECs

iMAECs were transfected with either LIMS2 TSBs or scrambled TSBs in conjunction with either luciferase plasmids or mutant plasmids in order to demonstrate that the TSBs effectively and specifically target murine LIMS2. Luciferase assay results indicate that the luciferase activity is significantly rescued by the LIMS2 TSBs, but not the scrambled TSB. Furthermore, mutant plasmids which do not have a 744 targeting sequence do not experience a rescue in luciferase activity. Furthermore, we sought to demonstrate that the TSBs effect on inflammation would mirror that of siLIMS2 treatment. In fact, rescue of LIMS2 significantly increased LIMS2 protein but significantly decreased VCAM1 protein, indicating that TSBs may be a viable therapeutic option for endothelial inflammation.

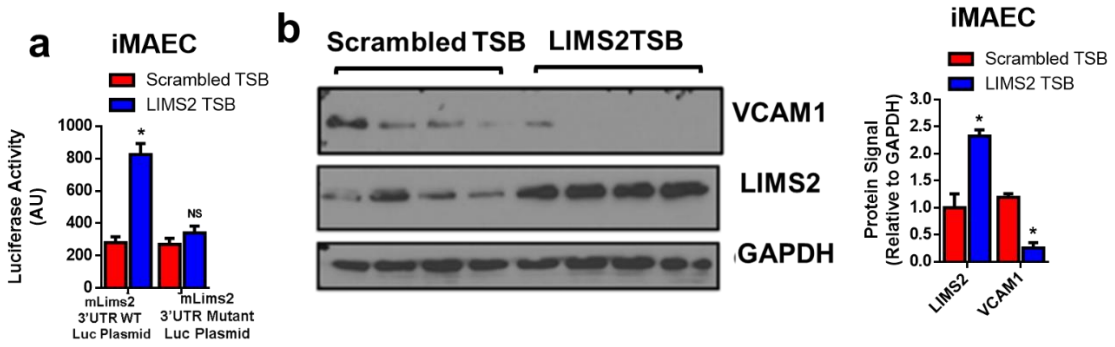

Figure 6.3 TSBs Rescue LIMS2 and Decrease VCAM1 Expression.

Static iMAECs were (A) dual-transfected with 500 ng of the LIMS2 3'UTR luciferase plasmid (or mutants) and 400 nM LIMS2 TSB or scrambled TSB. Media was collected 24 Hr later, incubated with luciferin, and read in a plate reader. (n=9, *=p<0.05) (B) Static iMAECs were transfected with TSBs for 72 hr and then protein was collected. Both LIMS2 and VCAM1 were immunoblotted for and GAPDH was used as a control (n=4, *=p<0.05)

6.2.4 LIMS2 TSBs Significantly Reduce Plaque Burden, Arterial Diameter, and VCAM1 Staining in Mice

Given that antimiR-744 did not significantly reduce the plaque burden in partially ligated mice and *in vitro* results indicate that LIMS2 TSBs can prevent endothelial inflammation, we next wanted to determine whether LIMS2 TSBs could rescue LIMS2 expression and prevent plaque development. Therefore, we assessed atherosclerosis development in the LCAs of partially ligated mice while treating with either LIMS2 TSBs or scrambled TSBs at a dosage of 5 mg/kg for a period of three weeks. Although the LCAs of the scrambled TSB-treated mice rapidly developed atherosclerosis within the allotted time frame, the LIMS2 TSB-treated mice had overall much lower volume of plaque (greater than 50%) by both gross examination and by H/E staining. The arterial diameters of the mice were 45% smaller and the elastic lamina structure was more conserved, indicating that the TSB-treated mice had much less outward remodeling as well. Furthermore, there was significantly less staining for the inflammatory marker VCAM1 in TSB-treated mice. Overall, this data indicates that LIMS2 TSBs can significantly reduce d-flow-induced plaque and may be a viable therapeutic option.

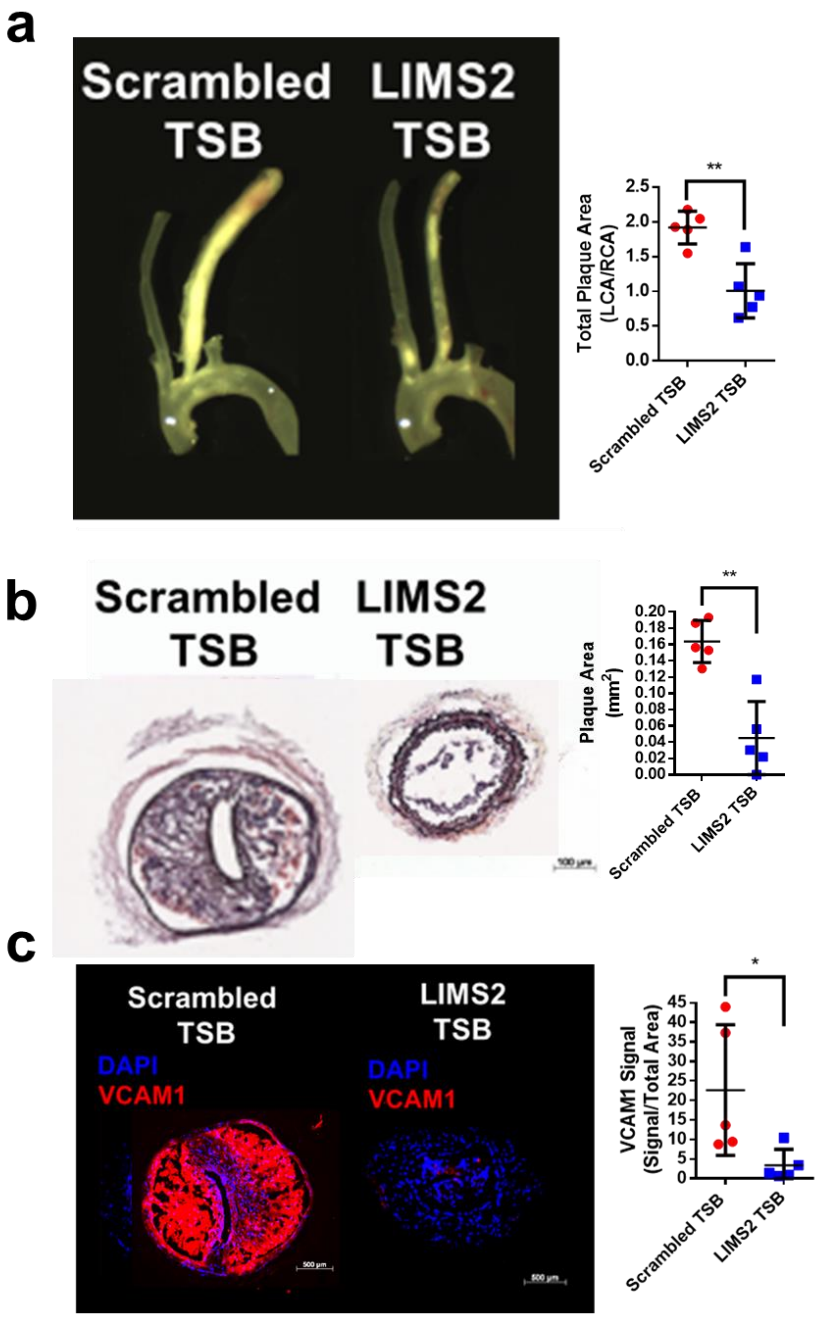

Figure 6.4 LIMS2 TSBs Significantly Reduce Plaque Burden and VCAM1 Expression.

ApoE–/– mice were given 5mg/kg LIMS2 TSBs twice a week for three weeks with a high fat diet. Scrambled TSBs were used as a control. (A) Gross plaque was examined using light microscopy and quantified using ImageJ. Frozen sections of the carotid arteries were examined by (B) hematoxylin and eosin and the plaque area was quantified using ImageJ (C) or stained for VCAM1 and fluorescent intensity was quantified. (n = 5 each, data are shown as the mean ± SEM. *P < 0.05).

6.2.5 LIMS2 TSBs Significantly Rescued LIMS2 Expression

After the mice were sacrificed at the end of the study, the liver, lung, kidney, and spleen were collected in order to determine whether LIMS2 TSBs could significantly rescue LIMS2 expression. Like the miR-744 study, the liver and lung did not have significantly increased expression of LIMS2, but LIMS2 was rescued in the spleen by more than four fold. In agreement with these findings, staining for LIMS2 in the LCAs revealed significantly more LIMS2 in the treated vs. the scrambled TSB-treated mice. Furthermore, there were no differences in the body weight, blood cholesterol, HDL, LDL, or triglycerides between the treated groups, indicating that the LIMS2 TSBs LIMS2 TSBs reduced atherosclerotic plaques directly be rescuing LIMS2 expression in the LCA.

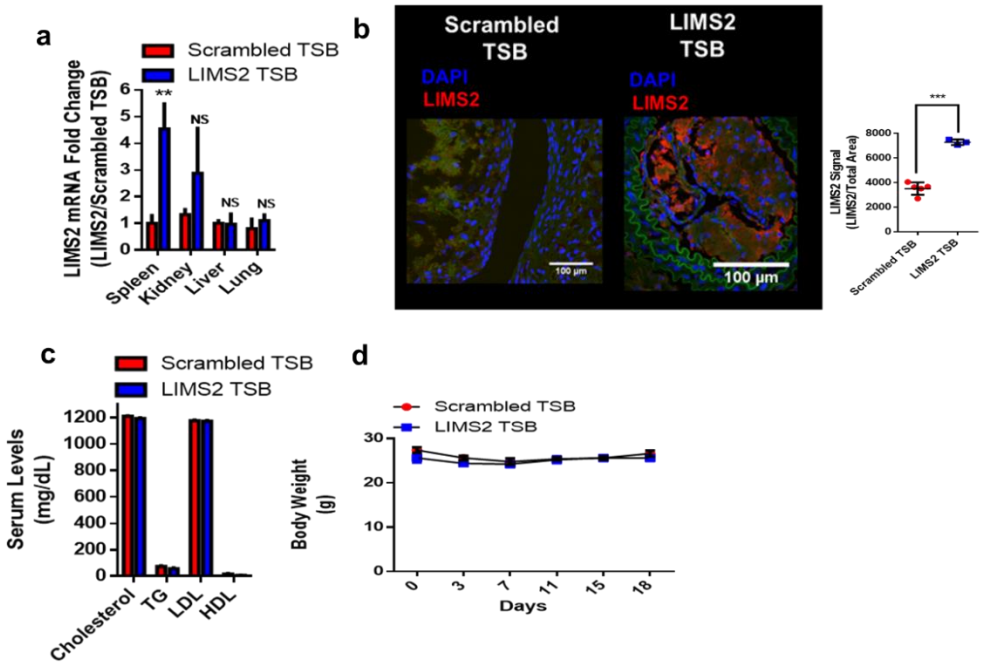

Figure 6.5 LIMS2 TSBs significantly rescued LIMS2

(A) The liver, lung, kidney, and spleen were collected and crushed for RNA. RNA was collected for qPCR and LIMS2 levels were measured and normalized to 18S (n=5, *=p<0.05) (B) LCAs were immunostained for LIMS2 in each animal. (C) Total blood serum cholesterol, triglycerides (TG), high density lipoprotein (HDL), and low density lipoprotein (LDL) was measured in blood collected immediately before sacrifice. (D) Mouse body weights were measured every three days over the course of the treatment

6.2.6 Binding Partners ILK and PINCH1 are Shear Sensitive and Regulated by siLIMS2 and Mimic

Finally, after discovering that LIMS2 is suppressed by d-flow both *in vitro* and *in vivo* and that rescue of LIMS2 in an acute d-flow model of atherosclerosis can significantly reduce plaque area, we sought to determine the mechanism by which the loss of LIMS2 may promote atherosclerosis development. In the literature, LIMS2 is known to bind and stabilize ILK, which is a well-known mechanosensitive protein recently shown to play an athero-protective role. Furthermore, LIMS2 has been reported to either compete with PINCH1 for binding or can act as PINCH1 when PINCH1 is lost. However, when LIMS2 would act antagonistic to PINCH1 is unknown and PINCH1 and LIMS2 have not been studied in the endothelium before. Therefore, we first silenced LIMS2 under LS conditions in order to determine what happens to PINCH1 and ILK. Both proteins are suppressed at the mRNA level with siRNA treatment (ILK by 50%, PINCH1 by 60%), and both are suppressed by OS (greater than 50%). For ILK, this aligns with previous literature. However, previous literature indicates that PINCH1 is increased when LIMS2 is silenced to compensate, thus, this is a novel finding. Lastly, we wanted to determine if miR-744 modulation could affect ILK and PINCH1 levels, which is when LIMS2 would be lost physiologically. Interestingly, antimiR-744 treatment increased PINCH1 (two fold) and ILK (1.7 fold) levels in OS conditions and in static mimic treatment, miR-744 was able to suppress ILK protein levels. Taken together, these results suggest that loss of LIMS2 does affect its binding partners ILK and PINCH1, which would promote endothelial inflammation through loss of ILK.

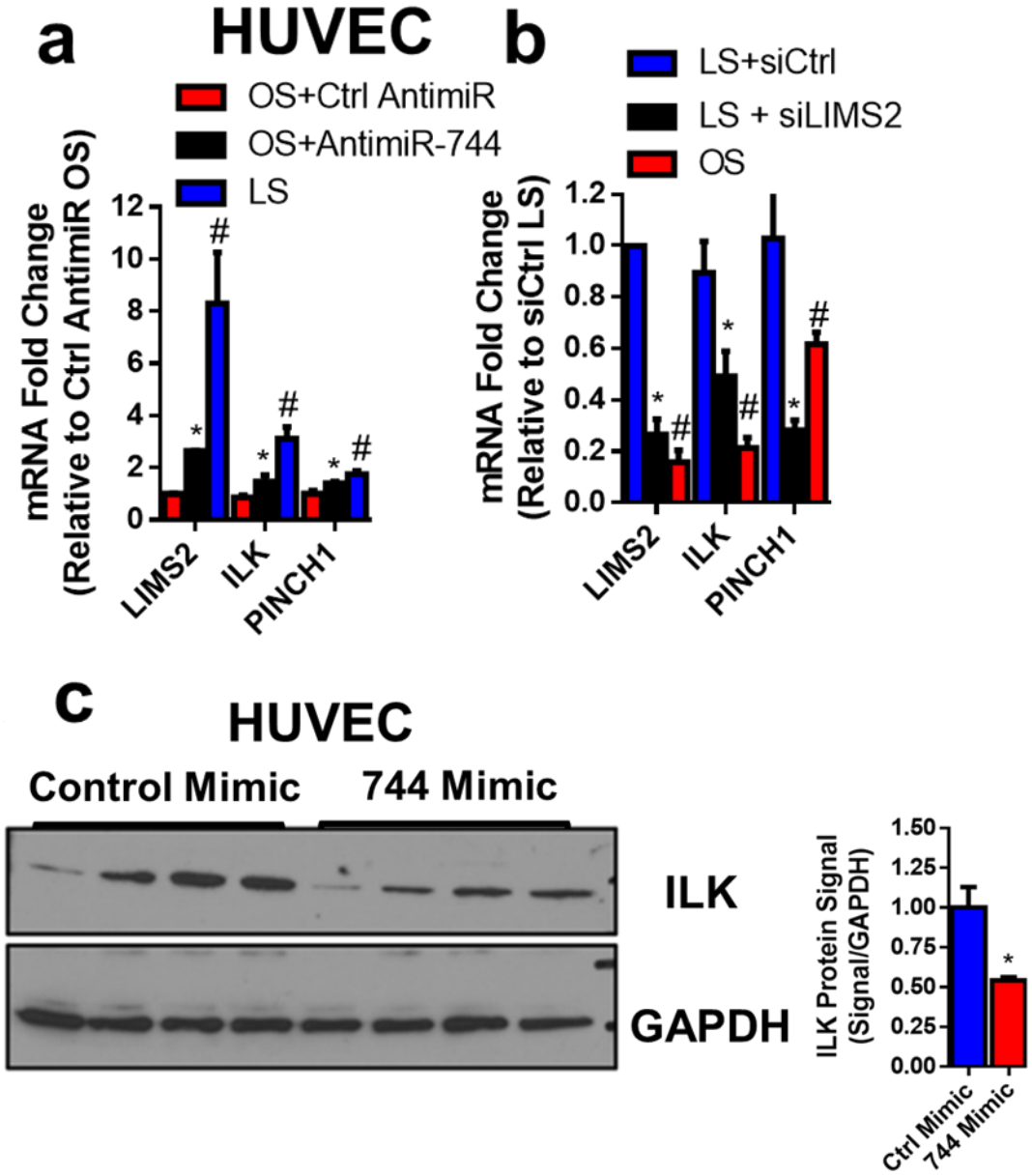

Figure 6.6 LIMS2 Modulates ILK and PINCH1 Expression.

HAECs were either transfected with (A) siLIMS2 for 24 hours, followed by 24 Hr of LS, or transfected with non-targeting siRNA and subjected to LS or OS. (B) antimiR-744 for 4 hours, followed by 24 hours of OS or non-targeting antimiR and subject to OS or LS. (C) Static HUVECs were transfected for 24 hours with 40 nM miR-744 mimic and protein was collected for ILK expression. *=P<0.05

6.3 Discussion

The goal of this aim was to evaluate the role of the miR-744-target axis in an animal model of d-flow induced atherosclerosis in order to discover a novel therapeutic agent for the treatment of atherosclerosis. Assessing the functional outcome of miRNA modulation in animal studies often involve multiple variables and multiple measurable outcomes. The animal studies described here used a dosage and dosage scheme of antimiR-744 or LIMS2 TSBs based upon previous studies in our group. The endpoints of the animal studies were based upon quantifiable measures of atherosclerosis, such as area of the gross plaque, lipid and VCAM1 staining in cross sections, diameters of the artery, and degree of preservation of the elastic laminae. Upon observing the degree of gross plaque and lipid area, a fair degree of variability among the mice was observed. This is not uncommon, as the size of lesions is never uniform among patients either. As the animals are allowed to eat freely, some animals may eat more or less. Furthermore, unknown genetic differences among the mice may make some of the mice more predisposed towards developing larger lesions. Due to the significant variability within the two treatment groups, there was no difference between the antimiR-744-treated and the saline-treated groups. The failure of antimiR-744 to reduce plaque burden may be due to miR-744 suppressing pro-inflammatory targets in other cell types which were not relevant targets in endothelial cells. This result underscores the importance of the miRNA-target interaction in individual cell types, as well as the need to develop cell type-specific delivery vehicles for atherosclerosis.

Examining the expression patterns of miR-744 and LIMS2 in the animal study perfectly illustrates this point. Although miR-744 has been reported as being highly expressed in many tissues throughout the body, particularly the heart, there is clearly differential expression among the organs. In our animal study, the copy number of miR-744 was 10 fold higher in the lungs than in any other organ. As this work was predominantly concerned with the expression of miR-744 in ECs, we have not measured the expression in other individual cell types. All four organs have endothelial populations, yet the lung is the most highly enriched in ECs. Despite the lung having the highest copies of miR-744, it also had the highest copies of LIMS2 as well. This may be due to the fact that LIMS2 could be highly expressed in other cell types where miR-744 is lower, or LIMS2 could not be the predominant target of miR-744 in those cell types.

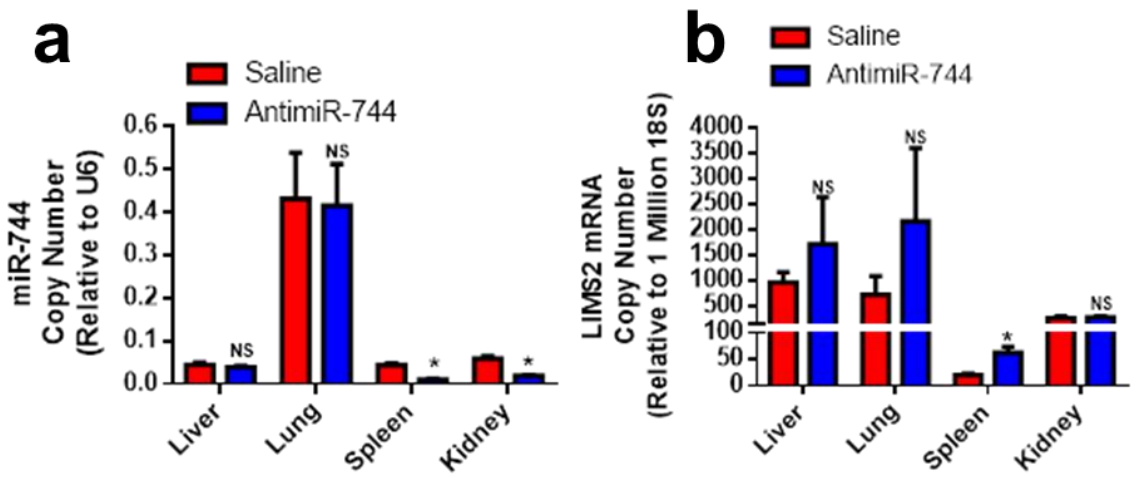

Figure 6.7 Differential expression of miR-744 and LIMS2 in organs.

(A,B) The liver, lung, kidney, and spleen were collected and crushed for RNA. RNA was collected for qPCR and (A) miR-744 levels were measured and normalized to RNU6B or (B) LIMS2 levels were measured and normalized to 18S (n=5, *=p<0.05

Although there was also variability in the degree of plaque developed among the LIMS2 TSB-treated mice, every marker of plaque was significantly lower in the treated animals. Although these results indicate that LIMS2 TSBs may be a novel therapeutic option for atherosclerosis, much work is still needed to translate these findings into a clinic. First of all, these studies must be repeated on a larger number of animals and additional dosages should be explored, such as 10 or 20 mg/kg. Alternatively, the route of administration and/or the frequency of dosages should be optimized. Furthermore, in the case of humans, patients have already developed atherosclerotic lesions at the time a drug would be administered. Therefore, treating mice that have already developed plaques and assessing the degree of regression would be beneficial for evaluating whether the TSBs would be appropriate for clinical use. Finally, one major limitation of this study is the fact that LIMS2 does not have a conserved binding site in humans. Therefore, the LIMS2 TSBs were easy to design in mice as there is only one binding site for miR-744. Before translating this therapy to the clinic, *in vitro* studies would need to be conducted in human ECs in order to determine the minimum number of binding sites that would need to be protected in order to rescue LIMS2 expression. Another confounding factor would be to determine whether the miR-663 binding sites also need to be protected in humans. As this study did not examine the effect of miR-663 on LIMS2, future studies examining this interplay are crucial for translation into humans. Finally, primate studies would need to be conducted in order to examine the therapeutic potential of these human LIMS2 TSBs.

CHAPTER 7 CONCLUSIONS AND FUTURE DIRECTIONS

Here, we demonstrate that disturbed blood flow regulates a conserved miRNA, miR-744, in endothelial cells and that this miRNA modulates endothelial inflammation and atherosclerosis by downregulating LIMS2. Not only have we identified a novel, flow-sensitive gene and miRNA, we are one of the first to use target site blockers as a potential therapeutic for atherosclerosis. Furthermore, our work advances the field of miRNA biology in that it underscores the importance of miRNA-target specific responses, as well as miRNAs targeting a family of related genes. Specifically, we found that OS induced expression of miR-744 in cultured human and mouse endothelial cells and that both acute and chronic d-flow induced miR-744 in mouse arterial endothelium. Furthermore, increasing the miRNA levels by miR-744 mimics increased endothelial inflammation and inhibition of the miRNA by antimiR-744 drastically reduced endothelial inflammation in both human and mouse cultured ECs.

In order to discover the underlying mechanism governing miR-744-induced endothelial inflammation, we merged our existing microarray of the endothelial transcriptome from our partial carotid ligation model with a dataset of sequenced RNA derived from immunoprecipitating the RISC under conditions of miR-744 elevation in HUVECs. Specifically, we identified genes which were downregulated in the partially-ligated left carotid artery (LCA exposed to d-flow) as opposed to the right contralateral control (RCA) after 48 hours and compared these genes which were predicted targets of miR-744 in both humans and mice and were enriched in the RISC after treatment with a miR-744 mimic in HUVECs.

Out of the hundreds of genes revealed in the RNA sequencing data, 13 genes were discovered to be significantly downregulated in the LCAs, significantly enriched in the

RISC post-mimic treatment, and predicted targets of miR-744. Of the 13 genes, only 5 genes were consistently downregulated by OS in HUVECs: LIMS2, KRAS, PVRL3, CALM1, and NDRG1. Of these genes, only LIMS2, KRAS, and PVRL3 responded to antimiR-744 treatment in OS, and only LIMS2 also responded to mimic treatment. The results of our screening studies identified LIMS2 as a major target of miR-744 in ECs, which we pursued for further study.

However, although the screening process revealed a novel target gene, it also uncovered phenomena which provide insight into miRNAs and endothelial biology. The first observation is that although all 13 genes were significantly downregulated in the LCAs of mice (decreased by greater than 30%), only 9 genes were significantly downregulated in the first shear-sensitivity screen, and this number decreased to 5 (less than half), in the second screen. It is a well-known phenomenon that endothelial cells lose the expression of some genes as they are cultured over time, and the genes that were unable to be validated a second time may have been lost due to the later passage number of the HUVECs. Alternatively, there are differences in venous cells versus arterial cells, especially umbilical vein cells, which are not as differentiated as arterial cells. The second observation is that only three genes responded to antimiR treatment, whereas 5 out of 7 genes tested were suppressed by mimic. In general, mimic treatment introduces supraphysiological levels of the miRNA on the order of several hundred fold greater than the control, thus in general we see more effects on target gene expression and phenotypic responses with mimic treatment than in inhibitor treatment. Given that the effect of inhibition is dose-respondent, future studies using much higher dosages of the antimiR may in fact rescue the genes which were sensitive to mimic treatment. Finally, we observed that although KRAS, PVRL3, and NDRG1 were strongly mechanosensitive and responsive to either antimiR-744 or mimic (respectively), lack of consistent response to miR-744 excluded these genes from further analysis. However, given the strong mechanosensitivity of these genes and preliminary studies conducted on NDRG1 silencing and endothelial inflammation, these genes may

play a role in endothelial inflammation either in a miR-744 dependent or independent manner and deserve further study.

After identifying LIMS2 as a highly mechanosensitive gene which is also responsive to miR-744 mimic and antimiR-744 in HUVECs, we also validated these findings at the protein level in an alternative cell type, HAECs. Upon studying LIMS2, we found that LIMS2 is actually much more highly expressed in HAECs versus HUVECs. In fact, although LIMS2 mRNA levels are easily detected in HUVECs, protein expression is almost completely undetected except for under LS. Alternatively, miR-744 is more highly expressed in HUVECs versus HAECs, indicating that LIMS2 may be critical to healthy arterial endothelium and thus miR-744 levels are lower. Whereas in the less differentiated umbilical vein cells, miR-744 (and miR-663) levels are higher. Upon discovering the differential expression of LIMS2 in different endothelial cells, we next wanted to measure the expression of LIMS2 in human coronary arteries. We received sections of right coronary arteries and graded the sections based upon degree of plaque severity. Patients that had slight to moderate plaque formation (Grades I through III) had a nice robust expression of LIMS2, whereas LIMS2 was lost in advanced plaques. Given that disturbed flow is a well-established initiating factor of plaque formation, the loss of LIMS2 was completely in line with our observations that LIMS2 is lost in HUVECs exposed to OS or when treated with OS-induced miR-744.

Although these experiments established the mechanosensitivity of LIMS2 in cultured ECs and its relevance in human atherosclerosis, it was necessary to directly implicate the loss of LIMS2 in a d-flow induced model of atherosclerosis. Thus, we carried out LIMS2 staining and qPCR on endothelial RNA flushings in C57 mice that had been ligated in the LCAs for 48 hours. As expected, we found significant loss of LIMS2 at both the mRNA and protein levels in the LCAs. Finally, in order to establish LIMS2 as a direct target of miR-744 in mice, a luciferase plasmid encoding either wild-type or a mutated 3’UTR of mouse LIMS2 was co-transfected with either miR-744 mimic or control in

iMAECs . This luciferase assay confirmed that LIMS2 is a viable target of miR-744 in mice. Although ultimately the main concern is the interaction of miR-744 and its targets, such as LIMS2, are in endothelial cells, given that we would be testing LIMS2 in our mouse model of atherosclerosis, it was necessary to ensure that LIMS2 would be a viable target in mice. Furthermore, one practical constraint was that although the human 3'UTR of LIMS2 contains multiple binding sites for miR-744, the murine 3'UTR only contains one binding site, thus necessitating the mutation of only one binding site for the luciferase assay. The fact that LIMS2 has multiple binding sites for miR-744 (and miR-663) in humans as opposed to just one site in mice may indicate that LIMS2 is strongly regulated by both miRNAs in human cells and is regulated in conjunction with other miRNAs in mice. In fact, other shear-sensitive miRNAs may be regulating LIMS2 as well in conjunction with miR-744 and thus one future direction may be to study other miRNAs which are interacting with miR-744. In any case, as LIMS2 is so strongly suppressed in both human and murine atherosclerosis, it is quite likely that other mechanosensitive miRNAs may be regulating the gene as well.

Following the identification of LIMS2, we wanted to establish that LIMS2 was a critical mediator of the inflammatory effects of miR-744. Therefore, we used both a silencing approach and rescue approach to study the effects of LIMS2 modulation on endothelial inflammation. Initially, we silenced LIMS2 in HAECs, where LIMS2 is highly expressed, and found significantly elevated endothelial inflammation. Silencing LIMS2 via siRNA exactly mirrored the same effects previously observed by miR-744 mimic treatment. However, to directly establish a causal effect between miR-744, LIMS2 silencing, and endothelial inflammation, we treated iMAECs with target site blockers designed specifically to block miR-744 from binding to the 3'UTR of LIMS2 and found significant blunting of endothelial inflammation. LIMS2 protection by the TSBs was confirmed by luciferase assay and by LIMS2 protein expression.

Upon establishing a direct link between miR-744, LIMS2, and endothelial inflammation, subsequent experiments were carried out to assess the role of miR-744 and LIMS2 directly in our model of d-flow-induced atherosclerosis. Initially, we tested the effect of global miR-744 inhibition on atherosclerosis by treating partially ligated mice with antimiR-744 twice weekly for a period of three weeks. We found that there was no significant reduction in plaque burden in the antimiR-744-treated group. Furthermore, we found that although miR-744 levels were significantly reduced in the spleen and kidney, LIMS2 levels were only significantly rescued in the spleen. Additionally, LIMS2 staining in the carotids did not reveal significant rescue of expression. Given these results, we next wanted to test the effect of specifically blocking the interaction between miR-744 and LIMS2. Therefore, after validating that our LIMS2 TSBs rescue LIMS2 expression and blunt endothelial inflammation *in vitro*, we treated partially ligated mice with either the LIMS2 TSBs or a scrambled sequence TSB twice weekly for three weeks. We found a significant reduction in gross plaque in the LIMS2 TSB-treated mice as opposed to scrambled TSB-treated mice. Upon internal examination, we discovered the LCAs of the LIMS2 TSB-treated mice to have significantly less plaque burden and the arteries maintained a similar size as the RCAs and retained their internal elastic laminae structure. Furthermore, LIMS2 was rescued in the spleen and in the carotids of the TSB-treated mice. Ultimately, these results indicate that preventing the loss of LIMS2 by d-flow-induced miR-744 blunts the process of plaque progression. In particular, protecting LIMS2 prevents degradation of the ECM which is a common hallmark of atherosclerosis.

The discrepancy between the antimiR-744 treatment and the LIMS2 TSB treatment may be explained by miRNA biology. As miRNAs target hundreds of genes, not all genes will act in concert. In fact, it is the balance of anti-inflammatory versus pro-inflammatory genes which will ultimately govern the response to a miRNA. Furthermore, this simplistic balance equation is further complicated by the fact that the miRNA may have preferential targets in certain cell types, so simply looking at a list of predicted targets and calculating

the balance will not be sufficient to predict the response. To even further complicate matters, specific target genes themselves may be pro-inflammatory in one cell type and anti-inflammatory in another. As an example, miR-744's sister miRNA, miR-663, has been indicated to be anti-inflammatory in smooth muscle cells by targeting the transcription factors JunB and JunD [362]. However, miR-663 was strongly pro-inflammatory in endothelial cells in previous studies carried out by our group. Upon further examination, we discovered that JunB and JunD were not consistently regulated by miR-663 in endothelial cells (unpublished results). Therefore, global inhibition of miR-663, which would affect not only the endothelium but SMCs and monocytes, could very well be anti-inflammatory. This stresses the need for more targeted delivery approaches in the future to specific cell types, such as the endothelium. Thus, the antimiR-744 may have allowed the rescue of an undesirable target gene in SMCs or in monocytes. However, in the case of the LIMS2 TSBs, the specific rescue of LIMS2 may be anti-atherosclerotic in both the endothelium and in other cell types. Our studies in Aim II have indicated that rescue of LIMS2 is strongly anti-inflammatory in cultured ECs. However, the previous literature indicates that LIMS2 is anti-migratory in SMCs [342], thus, LIMS2 TSBs may also be acting on the SMCs in the arterial wall as well and contributing to the anti-atherosclerotic effect.

Finally, although the work described here firmly establishes the link between disturbed flow, miR-744, LIMS2, and atherosclerosis and thus explains how LIMS2 is lost in atherosclerosis, preliminary studies have been conducted in order to further investigate how the loss of LIMS2 contributes to atherosclerosis. The only known literature regarding LIMS2 indicates that the biological function of LIMS2 is to compete with LIMS1/PINCH1 to bind and stabilize the focal adhesion protein ILK and prevent cell migration (**Ch.1.8**). Thus, as a first step in identifying the role of LIMS2 in endothelial biology, PINCH1 and ILK mRNA levels were measured under shear conditions in HAECs after silencing LIMS2. Both proteins were suppressed by OS and by LIMS2 silencing, which is consistent for ILK,

but seemingly contradictory for PINCH1. PINCH1 has previously been indicated to increase as a compensatory mechanism for the loss of LIMS2 (**Ch.1.8**). However, as PINCH1 and LIMS2 have never been studied under shear or in the endothelium, this is an interesting finding that merits further pursuit. Furthermore, PINCH1 and ILK mRNA levels were measured under shear with antimiR-744 treatment, which is a condition that rescues LIMS2. ILK and PINCH1 were rescued by antimiR-744 treatment, in agreement with the siRNA results. Furthermore, ILK protein expression was significantly reduced by miR-744 mimic treatment, which would mimic LIMS2 silencing. Previous reports have indicated that ILK is a strongly mechanosensitive protein which is degraded by ROS in atherosclerotic conditions and that under healthy conditions, ILK binds to eNOS in conjunction with Hsp90 and prevents ROS production (**Ch.1.9**). LIMS2 may be mediating its anti-inflammatory, anti-atherosclerotic effects via an ILK/eNOS-dependent pathway. However, future studies are needed to fully investigate the interaction of LIMS2, ILK, and eNOS under shear and directly implicate this mechanism is involved in preventing NFkB transcription of pro-inflammatory genes. These studies would most likely include more in depth assessment of eNOS activity and ROS production with miR-744 modulation and co-immunoprecipitation of these protein complexes. Furthermore, as both eNOS and ILK are predicted targets of miR-744 (miRWalk), this raises interesting questions as to the interconnectedness of miRNA target gene networks and the investigation of primary vs secondary targets in the network.

Throughout the course of these studies, a variety of robust experimental strategies were implemented, including an *in vitro* model of shear stress using different endothelial cell types, and an *in vivo* model of low shear-induced atherosclerosis. Furthermore, multiple methodologies of manipulating miRNA levels and gene levels were used in order to ensure that the observed phenomena could be replicated using different approaches. The findings by our group and others reveal that miRNAs are key regulatory elements in vascular biology, endothelial gene expression, and the pathology of atherosclerosis.

Although the scope of this project was limited to the in-depth study of one specific gene in the development of atherosclerosis, this project revealed that miRNAs may regulate a network of related genes, which has not previously been discussed (**Appendix A.2**). In fact, because the approaches used here are confined by the availabilities of technology, there were a variety of limitations throughout the study. One such limitation was cost constraints of sequencing RNA from multiple treatments, such as mimic treatment in iMAECs and mimic or antimiR treatment under shear conditions, or even endothelial-enriched RNA from antimiR-744 treated mice. Integration of these datasets would have provided a more complete, physiologically relevant picture of the miR-744 regulatory network. Furthermore, studying the interplay of the miR-744 regulatory network itself was limited due to the sheer number of genes which are potentially regulated by miR-744. In fact, our defined threshold for excluding genes was meant to provide a manageable set of genes for screening. Yet, relaxing the stringencies would result in more target genes for additional studies.

Additionally, the interplay between miR-744 and other miRNAs was not investigated due to the vast scope it would impose on the study. However, there are computational tools that can identify enriched miRNA seed motifs in lists of genes. Such tools could be used to find if the genes enriched in the RISC from miR-744 treatment also are targets of another group of common miRNAs, indicating they may act in concert with miR-744. Canonically, miRNAs bind to the 3'UTR of genes while on the RISC and facilitate their degradation (**Ch.1.6**). Given that this study was meant to uncover the molecular mechanisms of miR-744 in endothelial inflammation for the purposes of identifying therapeutic targets, this study did not closely examine the genes which were enriched on the RISC but were not predicted targets of miR-744 nor the genes which were depleted on the RISC with miR-744 mimic treatment.

Genes which were significantly depleted in the RISC may be pro-inflammatory genes which are the targets of anti-inflammatory miRNAs. As there were many genes which were enriched in the RISC but were not predicted targets of miR-744, such as KLF2, it would be interesting to investigate what are the miRNAs targeting these genes to the RISC under conditions of miR-744 elevation (**Appendix A.1**). An additional limitation in the RNA sequencing data was the fact that the library preparation was carried out using polyA enrichment, thus miRNAs loaded on the RISC were unable to be identified. In future studies, having both the miRNAs and mRNAs identified in the sample may provide a rich dataset to aid in these miRNA interactions.

One overarching limitation in this study is the inherent variability in biological samples and in animals. This ranges from batch-to-batch variation in cells, mimic/antimiR/siRNA reagents, and in the individual animals used in atherosclerosis studies. Even the microarray platforms experience variation, such as in the dye labeling, efficiency in RNA, amplification and reverse transcription, and hybridization. To address this to the best of our abilities, multiple biological replicates or animals are used in each study and quality control are performed as well.

The tools used in this study, such as the miR-744 mimic and antimiR-744, were specific to miR-744. Furthermore, the LIMS2 TSBs were specific to the interaction of miR-744 with LIMS2 in mice. Thus, the LIMS2 TSBs are the most specific in terms of future therapeutic strategies. Despite the fact there are multiple studies using miRNAs in animals and there are multiple miRNA clinical trials in use, no clinical trials using TSBs have been initiated. The LIMS2 TSBs may be a viable new therapeutic for CVD. However, one limitation of this study was that the dosage of the LIMS2 TSBs in the animal studies was not optimized due to the availability of the TSBs. Therefore, higher dosages of TSBs may have more significantly inhibited plaque progression. Furthermore, the dosing schedule was not optimized due to the availability of the TSBs. Future studies are needed to optimize the dosage, route of administration, and delivery vehicle for specific targeting of the

endothelium. Future studies are also needed to study the effect of miR-744 and LIMS2 in alternative cell types, including SMCs and monocytes.

because atherosclerosis is a systemic disease caused by multi-cell type dysfunctions.

7.1 Conclusions

The study presented here is the first to demonstrate that miR-744 and LIMS2 are regulated by flow, LIMS2 is lost in human and mouse atherosclerotic plaques, and that miR-744 targets LIMS2. We propose that d-flow induces miR-744 in endothelial cells, which in turn targets LIMS2 to the RISC, and the loss of LIMS2 facilitates the destabilization of ILK and eNOS, ultimately leading to activation of NFkB, which initiates endothelial inflammation and atherosclerosis. We further propose that the rescue of LIMS2 by blocking miR-744 from binding to its 3'UTR inhibits plaque progression. In conclusion, our study provides a novel insight into the mechanism by which flow regulates gene expression by a novel miRNA and uncovers novel genes, such as LIMS2, involved in the endothelial cell flow response.

7.2 Future Directions

The goal of this project was to determine the role of miR-744 in endothelial inflammation and atherosclerosis, as well as the key target genes involved in the response. We show that blood flow regulates miR-744 in human and mouse ECs. Despite the fact that several genes were identified that merit further study as potential therapeutic and diagnostic candidates, LIMS2 was the most flow-sensitive and the most consistent target of miR-744 in humans and mice. Also, LIMS2 silencing alone replicated the effects of miR-744 and LIMS2 rescue alone in our mouse model was sufficient to reduce atherosclerotic plaques. However, the upstream mechanism controlling miR-744 is unknown. Interestingly, miR-663 is derived from a chromosomal location and from the RN45S region, where it is degraded by XRN1 under LS conditions. However, miR-744 is not derived from the same RN45S region nor even from the same chromosome. It is

interesting that two completely unrelated miRs share a similar seed sequence and have similar phenotypic responses. Given what was known about miR-663, this study focused on endothelial inflammation. However, In order to determine whether there is a further functional role for the miR-744 and/or LIMS2 in atherosclerosis development, additional markers of EC dysfunction that increase in d-flow (including inflammation, apoptosis, proliferation, thrombosis and cell migration) could be examined in future studies. These functions could be independent of LIMS2 or may be mediated through LIMS2. Other functions of miR-744 and LIMS2 have already been reported in other cell types, such as proliferation and migration, yet these have not been studied extensively in ECs in our studies. We have undertaken preliminary studies showing that miR-744 induces proliferation and migration, however, nothing has yet been conducted with direct modulation of LIMS2. These studies will nevertheless form the backbone of future studies establishing the importance of miR-744 in CVD. Taking another cue from the literature, miR-744 may also serve as a biomarker for atherosclerosis and CVD in the future as well.

Our computational analyses merging our partial carotid ligation array with RNA sequencing data containing potential miR-744 targets were designed to ask very specific questions regarding mechanosensitive, conserved targets of miR-744. We addressed the difficulty of tackling the widely unknown disease mechanism of atherosclerosis by limiting the scope of our project to a specific hypothesis that the genes should be downregulated by d-flow, enriched in the IP, and responsive to standard doses of antimiR-744 or 744 mimic. The huge benefit of the data collected with our dual "omics" approach is the abundant potential for future analyses. For example, these datasets could be used to study other mechanosensitive, miR-744 sensitive genes that were screened out due to inconsistencies.

Functional studies of miRNA patterns are complicated by the various, and often conflicting, reports of the role of specific changes in gene expression control. We considered the functional consequences of specific direct targets by our computational analysis as described above and by performing validation studies at the single gene level

in vitro using qPCR, western blotting, luciferase assays, and EC inflammation assays we simplified the scope of the study to just one single target, LIMS2. Follow-up animal studies provided confirmation that the miR-744-LIMS2 axis is a crucial part of atherosclerotic plaque formation, but future studies will help draw more definitive links between LIMS2, ILK, eNOS, and the underlying mechanisms of gene expression control and ultimately disease development or prevention.

Although our current study focused on examining the role of miR-744 in vascular biology and disease, given what is known about miR-744 and LIMS2, our work may be extended to other diseases, such as cardiac hypertrophy. In fact, both LIMS2 and ILK mutations have been indicated to play a causal role in cardiac hypertrophy and heart failure (**Ch.1.8**). Therefore, it is crucial to understand the interplay between miR-744, LIMS2, and ILK not just in endothelial inflammation, but in other cell behaviors (such as migration) and in cell types (such as SMCs) as well. With the understanding that there is only one binding site on the mouse 3'UTR of LIMS2 and there are multiple binding sites in the human LIMS2, we foresee the major impact of this study as the identification of LIMS2 TSBs as a potential therapeutic for CVD with modifications to the sequence used in this study. The results of this body of work in conjunction with future studies on miR-744, other miR-744 target genes, and LIMS2 will elucidate novel mechanosensitive pathways in CVD.

APPENDIX

A.1. List of Genes Differentially Enriched in Ago2 Immunoprecipitation

Table A1. List of genes Differentially Enriched in Ago2 Immunoprecipitation

GENE NAME	CTRL MIMIC 1	CTRL MIMIC 2	CTRL MIMIC 3	744 MIMIC 1	744 MIMIC 2	744 MIMIC 3	744/ CTRL	P VALUE
CXCL1	783.7853382	716.6783723	464.4318065	4103.272188	3673.311523	4395.297687	6.194671062	0.000123931
MOB1B	252.9823568	222.4174259	204.6648639	508.9936874	512.1523251	555.3825736	2.318204003	0.000130519
CXCL2	1116.802113	1397.769957	601.2030377	4458.262657	4411.437 66	4366.417794	4.248098035	0.000136272
LINC00857	0	5.931131357	0.983965692	36.54313653	35.46304344	31.10142412	14.91050717	0.000205385
PTER	1.839871686	0	1.967931384	17.40149359	14.84499493	18.8830075	13.42755786	0.000297804
C15ORF61	50.59647136	59.31131357	51.16621598	88.7476173	87.42052 57	91.08274207	1.659180771	0.000299886
CCNI	1732.239192	1649.843039	1763.266 52	2425.768206	2545.091909	2357.043642	1.424180189	0.000352 55
LOC101926963	1.839871686	0	0	19.14164295	14.84499493	15.55071206	26.92435039	0.000408925
RNF26	1315.508255	1418.528916	1423.798356	1011.026777	962.4505046	973.0302689	0.708663806	0.000453838
GTF2H2C	0	0	0	0.870074679	0.824721941	1.110765147	#DIV/0!	0.000458967
CCDC173	0	0	0	2.610224038	2.474165822	3.332295442	#DIV/0!	0.000458967
SULF1	8020.920615	8028.774814	7557.840479	5841.681397	5313.683463	5601.588637	0.709813746	0.000469657
MAFF	916.2560996	792.7945581	787.1725535	1813.235632	1990.054043	2189.318105	2.400669841	0.000561344
RPP30	144.4299273	131.4734118	160.3864078	235.7902381	255.6638016	247.7006278	1.694182989	0.000576396
RHOJ	4557.362166	4765.664046	4365.855775	3373.279532	3133.943374	3264.538768	0.713846586	0.000631972
RAI14	4556.44223	4637.1562	4294.026279	5819.92953	5936.348528	6203.623347	1.331583714	0.000632769
GNPTG	413.0511935	401.3398885	395.5542081	341.939349	346.383215	352.1125517	0.859902612	0.000677123
MYEF2	413.9711293	474.4905086	443.768527	624.7136198	607.8200702	634.246899	1.401244799	0.000735467
GPR135	0	0	0	6.960597435	8.247219406	5.553825736	#DIV/0!	0.000881637
ZNF335	259.4219077	254.0501265	250.9112514	200.1171763	214.4277045	213.2669083	0.821331132	0.00095119
PDGFRB	30.35788282	29.65565679	30.50293645	3.480298718	9.071941346	12.21841662	0.273659092	0.001035502
ZNF658	47.83666383	52.39166032	48.2143189	36.54313653	33.81359956	35.54448471	0.713415085	0.001038057
C21ORF2	68.07525238	50.41461654	73.79742689	122.6805298	125.357735	123.2949313	1.93113744	0.001086612
PDS5B	840.8213605	878.7959628	865.8898088	573.3792137	508.8534373	625.3607779	0.660448 16	0.001180339

NET1	1709.240796	1704.211743	1623.543392	1121.526262	1046.572143	864.1752845	0.602000425	0.001194609
REPS2	31.27781866	35.58678814	19.67931384	68.73589967	66.80247719	71.08896942	2.387543166	0.001231335
SLC35B4	4691.672799	5291.557693	4646.285997	3138.359369	2781.787106	3025.724261	0.611494627	0.001245508
HGSNAT	1457.178375	1414.574829	1514.3232	1028.428271	1130.693781	1135.20198	0.751086787	0.001301133
HACL1	399.2521558	354.8793595	373.9069629	503.7732394	499.781496	535.3888009	1.364265108	0.001314554
FDFT1	707.4306632	802.679777	793.0763476	1155.459174	1051.520474	1114.097443	1.441948655	0.001367098
LAMA5	849.100783	825.4157806	849.1623921	660.3866816	718.3328102	665.3483232	0.809955565	0.001368454
BTF3	1113.12237	957.8777142	1102.041575	1506.969345	1442.438674	1472.874585	1.393704552	0.001455284
VPS33B	529.8830455	499.2035559	441.8005956	290.6049429	248.2413041	256.586749	0.540784499	0.001460945
MTCH1	12811.94648	12710.4145	11830.21951	9976.276274	9485.127038	9871.369863	0.785294424	0.001504888
SLC7A6	1723.039834	1650.831561	1737.683412	1218.104551	1268.422345	1060.780716	0.693978201	0.001559917
FRG1HP	56.11608642	51.40313843	51.16621598	27.84238974	19.79332657	14.43994691	0.391186885	0.001576979
PYCR1	801.2641192	847.1632622	821.6113527	1106.734992	1250.278462	1142.977336	1.416978099	0.001597866
FKBP1A	2860.080536	3777.142153	3057.181405	6287.159633	7341.674715	7716.485477	2.20181866	0.001604
VWA1	14.71897349	12.85078461	2.951897076	45.24388333	40.41137509	38.87678015	4.080120749	0.001609943
CAPN1	848.1808472	778.9552516	796.0282447	556.8477948	599.5728508	623.1392476	0.734395048	0.001658665
FBXL13	160.9887725	115.6570615	189.9053785	323.6677807	367.8259855	341.0049002	2.213044653	0.001686812
LINC00115	1.839871686	0	2.951897076	9.570821473	9.896663287	12.21841662	6.612568961	0.001706399
PFAS	701.9110482	740.4028978	582.5076896	260.1523291	206.1804851	307.6819458	0.382263181	0.00172067
SHH	9.199358429	8.896697036	11.8075883	2.610224038	0	0	0.087287825	0.002005116
IFNGR2	1216.155184	1146.685396	1000.693109	1711.436894	1839.954649	1639.489357	1.543281971	0.002136668
SFXN3	549.2016982	621.7802706	602.1870034	302.7859884	360.403488	392.100097	0.595143266	0.002138853
ZNF75A	207.9055005	278.7631738	246.9753887	468.1001775	517.9253787	585.3732326	2.141908956	0.002148758
TGOLN2	4100.154052	4319.840672	4186.774019	3503.790734	3232.910007	3115.696238	0.781516436	0.00221272
TPM1	3847.171695	3412.377574	4000.804503	5365.750548	5603.985586	6093.657597	1.515351478	0.00222444
HTATSF1	409.3714501	549.6181724	662.2089106	1058.880885	1078.736298	1031.900822	1.955046183	0.002265683
CYTH3	629.2361166	597.0672233	634.6578712	401.1044272	481.6376133	419.8692256	0.699966909	0.002324764
GARS	3889.488744	4140.918209	3970.301567	5555.426828	5210.593221	5964.80884	1.394153425	0.002379773
ZBTB17	555.6412491	495.2494683	495.9187087	318.4473327	311.7448935	368.7740289	0.645823744	0.002465348
RWDD3	182.1472969	229.3370792	226.3121091	329.7583035	348.0326589	317.6788321	1.56079536	0.002488268
CDRT4	0	0	0	4.350373397	3.298887762	5.553825736	#DIV/0!	0.002503281

WSCD1	1517.894141	1407.655175	1519.243028	1107.605067	1121.621839	1212.955541	0.774430 43	0.002523977
EIF3L	1585.049457	1665.659 39	1589.104592	2198.678715	2117.885943	2422.578786	1.392438682	0.002616446
MTCP1	21.15852439	15.81635029	18.69534814	31.32268846	36.28776538	37.76601 5	1.892869536	0.002633352
HSPA4	1067.125578	1026.085725	1129.592614	1596.587037	1433.366733	1433.997805	1.385114233	0.002634418
NDUFAF6	301.7389565	269.8664768	319.7888498	393.2737551	423.9070775	414.3153999	1.381539298	0.002727076
LPP-AS1	6.439550901	10.87374082	8.855691227	0.870074679	0	0	0.033248318	0.003031032
PPP1R15A	2035.818 02	1785.270539	1609.767872	2564.980155	2696.840746	2709.156194	1.467720091	0.003031693
FKBP4	1106.682819	1012.246418	1165.999345	1673.153608	1965.312384	2067.133939	1.736902276	0.003078909
IFRD1	815.9830927	685.0456718	953.4627554	2410.976937	1888.613244	2633.624164	2.824704949	0.003096489
PRMT1	1128.761279	1176.341053	1054.811222	1360.796799	1438.315064	1467.320759	1.269804283	0.003142438
NAA20	696.3914331	762.1503794	699.5996069	1117.175888	1231.309857	1394.010 26	1.734129178	0.003145338
BIK	2.759807529	0	0	25.23216 57	34.63832 15	21.10453 78	29.34082328	0.003160205
ADM2	15.63890933	33.60974436	20.66327953	195.7668029	122.8835691	166.6147721	6.941091767	0.003173657
C1GALT1C1	511.4843287	497.2265121	419.1693847	675.1779512	648.2314453	683.1205655	1.405250893	0.003227 53
POLR2L	448.9286914	445.8233737	388.6664483	558.5879442	592.1503533	558.7148 69	1.331953021	0.003248642
SPX	0.919935843	0	0	11.31097083	17.31916075	11.10765147	43.19625478	0.003282898
PCNT	725.8293801	709.7587191	670.0806361	551.6273467	555.8625879	489.8474299	0.758589107	0.003296343
ENTPD1	645.7949617	732.4947226	734.0384061	479.4111483	528.6467639	489.8474299	0.709125324	0.003346 39
OGFRL1	105.7926219	143.3356745	150.5467509	691.7093701	486.5859449	753.0987698	4.832410975	0.003352348
TTBK2	183.0672327	187.8191596	201.7129668	81.78701986	42.06081897	102.1903935	0.394758095	0.003365 4
PDCD2	446.1688838	445.8233737	664.1768 42	1022.337748	1185.125429	1269.604563	2.234376548	0.003376099
PIANP	0	0	0	4.350373397	6.597775525	7.775356 03	#DIV/0!	0.003416849
MLXIP	3837.052401	4046.020108	3592.458741	2515.385898	2869.207631	2851.334133	0.717694674	0.003459615
MRPS6	116.8318521	179.9109845	172.1939961	378.4824855	354.6304344	299.9065897	2.202896932	0.003552105
ZZZ3	594.2785545	459.6626802	550.0368217	796.9884063	856.0613743	915.2704813	1.601219076	0.003553571
CTSC	2829.722653	2989.290204	3126.059003	2441.429 55	2325.715872	2224.862 59	0.781660351	0.003569971
SFXN5	196.8662704	197.7043786	177.1138245	79.17679582	122.8835691	82.19662089	0.497227053	0.003577542
CYB561	1076.324936	1112.087 13	1126.640717	1198.962908	1237.082911	1237.392374	1.108108508	0.003701738
DENND6A	479.2865742	549.6181724	540.1971648	387.1832323	384.3204243	393.2108621	0.742280989	0.003714888
ZNF2	168.3482593	193.7502 91	147.5948538	92.22791601	86.59580376	83.30738604	0.514291736	0.003724157
SMG1P5	14.71897349	13.83930 65	15.74345107	6.960597435	2.474165822	6.664590883	0.363402372	0.003728752

DRG2	453.5283706	432.9725891	392.602311	323.6677807	310.9201716	303.2388852	0.733190868	0.003808706
ARHGAP39	9.199358429	10.87374082	10.82362261	42.63365929	69.27664301	58.8705528	5.527474917	0.003883382
CST3	762.6268138	574.3312198	586.4435523	1058.880885	1287.390949	1239.613904	1.864345836	0.003894545
KANK1	2661.374394	2777.746519	2548.471142	2027.274003	1674.185539	1977.161962	0.710930336	0.003922218
CIC	134.3106331	122.5767147	122.9957115	61.77530224	86.59580376	81.08585574	0.60401999	0.004042853
BEND7	128.791018	212.532207	194.825207	435.9074144	533.5950955	400.9862181	2.556174086	0.004136138
TBX3	0	4.942609464	0	72.21619839	43.71026285	77.7535603	39.18578292	0.004145153
FN1	31498.60326	28929.0932	32274.07469	22839.46033	24594.85771	21433.32428	0.742894569	0.004317489
NAA10	512.4042645	404.3054542	493.9507773	718.6816852	879.9783106	836.4061558	1.72618866	0.004323782
SLC39A1	2694.492084	2982.370551	2626.204432	2122.982218	2013.970979	1870.528508	0.723525615	0.004325447
FKBP1AP1	15.63890933	14.82782839	16.72741676	7.830672114	9.896663287	5.553825736	0.493306033	0.004339832
LCMT1	302.6588923	375.6383193	288.3019477	678.6582499	865.9580376	966.3656781	2.597748965	0.004354963
NBPF10	103.0328144	90.94401415	102.332432	40.02343525	64.32831136	52.20596192	0.528359148	0.004403427
TUB	413.9711293	430.0070234	506.7423313	174.8850106	270.5087965	211.045378	0.485991878	0.004417426
TGFB1I1	282.4203038	506.1232092	319.7888498	1166.770145	1515.838927	1792.774948	4.037944005	0.004425154
YWHAQ	3495.756203	3781.09624	3790.235845	6421.151134	5258.427093	6472.428513	1.640179085	0.004427627
PHLDA2	281.5003679	295.568046	330.6124725	896.1769198	959.9763388	1312.924404	3.491400679	0.004450673
HN1	2702.771507	2731.28599	2672.450819	2124.722367	2173.967035	2387.034301	0.824735317	0.004516133
ANKH	207.9055005	110.714452	203.6808982	353.2503198	425.5565213	414.3153999	2.284358219	0.004526008
S100A10	1425.900557	1698.280612	1837.063947	5288.313901	7650.120721	8476.248838	4.316392954	0.004692719
ICAM2	504.1248419	537.7559097	532.3254393	763.9255685	827.1961064	688.6743913	1.448219477	0.00472711
ZNF580	160.0688367	136.4160212	182.033653	381.0927096	426.3812433	547.6072176	2.83182602	0.004735508
CEND1	4.599679215	4.942609464	0.983965692	70.47604903	49.48331643	89.97197692	19.94359389	0.00482614
ELMOD2	673.393037	578.2853073	465.4157722	247.9712836	182.2635489	142.1779388	0.333361326	0.004840713
CDC42	1116.802113	1168.432877	951.494824	1468.686059	1672.536095	1587.283395	1.460889793	0.004866484
VEGFB	282.4203038	330.1663122	302.0774674	529.0054051	706.7867031	706.4466336	2.123444855	0.004885971
FAHD1	381.7733748	375.6383193	392.602311	541.1864506	531.9456517	468.7428921	1.340744537	0.004971561
GDF15	3212.415964	3561.64438	2263.121091	5712.910345	5067.091603	5533.831963	1.805190482	0.004990508
LSM4	2972.312709	2420.890116	2564.214593	1648.791517	1741.812738	1747.233577	0.645666497	0.005036947
PLEC	1165.558713	942.0613639	1044.971565	570.7689897	653.1797769	694.228217	0.60844448	0.005143872
MRPS2	135.2305689	167.0601999	153.4986479	463.7498041	457.720677	662.0160277	3.47416252	0.005161522

TM9SF1	1952.103859	2196.495646	2112.57434	1575.705244	1425.944235	1647.264713	0.74249882	0.00517201
ADK	212.5051797	220.4403821	217.4564179	324.5378554	352.9809906	287.6881731	1.484016115	0.00529038
AUTS2	100.2730069	86.00140468	74.78139258	148.7827702	186.3871586	154.3963555	1.875331927	0.00531709 8
LOC100128288	92.91352014	69.1965325	56.08604443	14.79126955	14.02027299	7.77535603	0.167678978	0.00532300 8
TXNL1	718.4698933	704.8161096	641.5456311	909.22804	881.6277545	1005.242458	1.354153146	0.00533156 4
BZW2	708.3505991	761.1618575	744.8620287	895.3068451	1013.583265	934.1534888	1.283903702	0.00535195
RAC1	3423.081272	4192.321348	3697.74307	5838.201099	6387.47143	7388.809759	1.733777928	0.00546461 4
HNRNPC	2719.330352	3375.802264	3024.710537	4264.236004	4229.998833	4744.077944	1.451594349	0.00551572 7
AFTPH	547.3618266	578.2853073	576.6038954	414.1555474	458.545399	366.5524986	0.728008633	0.00556096 6
FOSL1	1221.674799	2219.23165	1902.005682	6320.222471	7277.346404	9916.911234	4.401060607	0.00557084 4
KIF3C	287.9399188	307.4303087	277.4783251	371.5218881	394.2170876	433.1984074	1.373591535	0.00559697 9
PLPP3	2489.346391	2068.976322	2369.389386	1079.762677	1280.793174	1552.849676	0.564891478	0.00563324 9
RHOQ	591.518747	518.9739938	514.6140568	840.4921403	776.888068	716.4435199	1.436104834	0.00564275 6
KLF2	361.5347863	437.9151986	410.3136935	1303.37187	1820.986045	2164.881272	4.372125962	0.00565573 6
RUFY2	218.0247948	273.8205643	235.1678003	383.7029336	334.8371079	383.2139758	1.515452647	0.00568984 8
HMHA1	48.75659968	9.885218929	61.98983859	156.6134423	153.3982809	213.2669083	4.337821793	0.00577114 6
MT2A	5867.350806	5004.886344	4450.476824	7305.147008	8220.828304	8395.162982	1.561155441	0.00578310 8
HOXA2	9.199358429	0	5.903794151	31.32268846	53.60692614	51.09519677	9.006385299	0.00591124 7
RAP1GDS1	448.9286914	521.9395594	600.219072	848.3228124	865.1333157	1033.011587	1.748131803	0.00592825 4
KRIT1	711.1104066	682.0801061	692.7118471	325.4079301	404.9384728	506.5089071	0.592959351	0.00596171 4
MTFMT	174.7878102	172.0028094	181.0496873	152.2630689	160.8207784	152.1748252	0.881438318	0.00600750 2
ZNF778	292.5395981	312.3729182	421.1373161	544.6667493	607.8200702	573.1548159	1.68183024	0.00606055 1
NME2	5.519615058	5.931131357	8.855691227	17.40149359	26.3911021	21.1045378	3.19588963	0.00614555
ZBTB41	412.1312576	463.6167678	344.3879921	205.3376243	209.4793729	236.5929764	0.533883079	0.00616077 5
UBE2R2	1194.076724	1020.154593	1241.764703	1562.654124	1643.670828	1806.104129	1.450357307	0.00617401 7
BRI3	613.5972072	604.9753985	443.768527	929.2397576	1150.487107	968.5872083	1.833747606	0.00622495 1
DUSP10	11.95916596	21.74748164	21.64724522	40.02343525	37.93720927	34.43371956	2.030469012	0.00636704 4
THNSL1	17.47878102	28.66713489	37.39069629	120.0703058	133.6049544	193.2731356	5.350329442	0.00643487 6
NEK6	2543.622606	2365.53289	2557.326833	1827.156827	2048.6093	2060.469348	0.795051165	0.00645624 1
SHPK	544.602019	476.4675524	566.7642385	345.4196477	305.147118	219.9314991	0.548230085	0.00647279 4
NMT2	2521.544146	2539.512743	2270.008851	4099.791889	3689.805962	4810.723852	1.718757156	0.00658742 5

SRXN1	1057.926219	1240.594976	918.0399905	1573.09502	1529.034478	1626.160175	1.469982817	0.006663643
IFITM10	9.199358429	8.896697036	6.887759843	2.610224038	3.298887762	0	0.236517591	0.006834156
PLPPR3	0	0.988521893	0.983965692	4.350373397	3.298887762	5.553825736	6.693622306	0.006837049
KCTD18	315.5379941	211.5436851	274.526428	78.30672114	49.48331643	117.7411056	0.306298228	0.006843025
ST3GAL4	85.55403339	116.6455834	58.05397582	215.7785205	291.951567	329.8972487	3.218504413	0.006880271
DOT1L	218.9447306	183.8650721	180.0657216	111.369559	107.2138523	134.4025828	0.605594127	0.006921203
DACT3	22.07846023	21.74748164	6.887759843	72.21619839	50.30803837	77.7535603	3.949185137	0.006950192
SNORA3B	12.8791018	11.86226271	7.871725535	3.480298718	0	1.110765147	0.140773654	0.007109121
LGALS3	202.3858854	174.968375	235.1678003	366.30144	305.147118	323.2326578	1.623910842	0.007140387
FLT1	905.2168695	795.7601238	471.3195664	1593.976813	1569.445853	1339.582768	2.072923889	0.007160538
MPHOSPH8	557.4811208	511.0658186	565.7802728	252.321657	371.1248733	198.8269613	0.503126599	0.007271867
PLCG2	59.79582979	23.72452543	49.19828459	136.6017247	101.4407987	138.8456434	2.839753084	0.007306033
SENP6	984.331352	810.5879522	932.7994759	561.1981682	482.4623352	642.0222551	0.617982605	0.007353954
ZBTB1	391.8926691	308.4188306	212.5365894	1000.585881	670.4989377	888.6121177	2.804077663	0.007516699
RANBP3	85.55403339	95.88662361	86.58898088	113.979783	131.1307886	116.6303405	1.349630268	0.007550506
NFKBIA	2437.829984	3074.303087	2935.169659	5548.46623	8245.569962	8130.800877	2.595483762	0.007578402
SH3BGRL3	3401.002811	3551.759161	3300.22093	5686.808104	6162.322234	7754.251493	1.911968656	0.007750497
SMARCB1	231.8238324	288.6483927	223.360212	362.8211413	448.6487357	409.8723393	1.6419588	0.007787265
SEH1L	544.602019	451.7545051	490.9988802	729.992656	672.9731035	815.301618	1.491417163	0.007828518
LPP-AS2	8.279422587	12.85078461	21.64724522	54.8147048	40.41137509	39.9875453	3.160862033	0.007899493
LURAP1	62.55563732	54.36870411	46.24638752	29.5825391	24.74165822	32.21218927	0.530342587	0.007927054
ZBTB38	1161.87897	1002.361199	1116.80106	856.1534845	785.1352874	857.5106936	0.761587341	0.00801274
TMEM158	2.759807529	13.8393065	10.82362261	36.54313653	33.81359956	25.54759839	3.497256154	0.008149578
MEOX2	89.23377677	72.16209818	63.95776997	4.350373397	4.948331643	34.43371956	0.194061315	0.008171513
EMD	132.4707614	90.94401415	155.4665793	223.6091926	221.850202	213.2669083	1.738608391	0.008211313
SERPINE2	1217.07512	1372.068387	744.8620287	2327.449767	1965.312384	2198.204226	1.9468973	0.008254707
ZBTB42	97.51319935	84.0243609	105.284329	132.2513513	124.533013	138.8456434	1.379357791	0.008275582
PRKRA	247.4627418	208.5781194	217.4564179	334.9787516	287.0032353	319.9003624	1.398494661	0.008286994
AVL9	369.8142089	400.3513666	394.5702424	542.0565253	566.5839732	475.407483	1.360006241	0.008326026
CFLAR-AS1	7.359486744	8.896697036	4.919828459	1.740149359	0	1.110765147	0.134629432	0.008460949
NEU3	91.07364845	106.7603644	63.95776997	30.45261378	0.824721941	7.77535603	0.149174628	0.008462892

SLC24A5	0.919935843	0	3.935862767	14.79126955	18.14388269	9.996886325	8.841396032	0.008670086
PLXNB3	217.1048589	140.3701088	209.5846924	66.12567563	79.17330629	49.98443162	0.344378956	0.008673614
PRPF6	1608.047853	1575.703897	1850.839466	1083.242976	1277.494286	1190.740238	0.705415265	0.008772983
CBR3-AS1	1.839871686	3.954087572	21.64724522	36.54313653	42.88554091	43.31984074	4.473146151	0.008796387
EFNA2	0	0.988521893	0	3.480298718	6.597775525	6.664590883	16.93707064	0.008840648
RNF135	425.0103594	484.3757275	549.052856	277.5538227	275.4571281	331.0080139	0.606140537	0.00886031
TERF2	146.269799	177.9339407	126.9315742	317.577258	249.0660261	257.6975141	1.827258414	0.008952304
FAM87B	0	0	1.967931384	5.220448076	4.123609703	6.664590883	8.134759573	0.008984834
HAUS1	232.7437683	230.325601	231.2319376	187.0660561	196.2838219	211.045378	0.856105627	0.009007628
GPCPD1	999.0503254	905.4860539	1003.645006	696.9298182	673.7978254	486.5151345	0.638626871	0.009033656
MMP1	9585.731484	11780.2154	9470.669784	16962.10587	14075.52936	15781.75121	1.518304909	0.00907918
RPLP1	4475.487876	4653.961072	4134.623837	7758.455916	10860.76324	11653.03716	2.282274593	0.009090462
PMS2P5	15.63890933	8.896697036	16.72741676	42.63365929	42.06081897	28.87989383	2.752449129	0.009232201
AHCYL2	134.3106331	66.23096682	140.7070939	260.1523291	216.0771484	254.3652187	2.140945034	0.009237288
RSPH3	1.839871686	0.988521893	3.935862767	53.07455544	25.56638016	47.76290133	18.6870264	0.009251716
FEZ1	817.8229644	950.958061	744.8620287	1148.498577	1265.123457	1385.124139	1.511251236	0.009307672
TCF7L2	364.2945938	427.0414577	380.7947227	540.3163759	527.822042	630.9146036	1.4495422	0.00943947
LOXL4	91.07364845	50.41461654	95.44467211	176.6251599	146.8005054	152.1748252	2.007321128	0.009494308
THEM5	19.3186527	27.678613	21.64724522	6.960597435	8.247219406	12.21841662	0.399540081	0.009620134
AXL	10534.18534	11221.70053	9898.69486	8654.632836	7413.425524	8226.326068	0.767484025	0.009664701
TRAM2	8477.208793	8941.180521	9140.057311	7614.893594	6608.496091	6368.016589	0.775324227	0.009795238
GGCT	564.8406076	624.7458363	587.427518	718.6816852	670.4989377	720.8865805	1.187422974	0.009820195
UBXN7	633.8357958	565.4345227	587.427518	455.0490573	445.3498479	505.398142	0.786812979	0.009826105
CASP9	22.07846023	41.5179195	38.37466198	85.26731858	66.80247719	96.63656781	2.438990123	0.009848088
IGF2BP2	1112.202434	1173.375487	1043.003633	896.1769198	834.6186039	723.1081108	0.737222025	0.009885148
POLR1B	1196.836532	1290.02107	1069.570707	805.6891531	918.7402418	818.6339135	0.715061035	0.009921201
ACTR10	737.788546	1190.180359	826.5311811	1660.102488	1554.600858	1887.189985	1.852203003	0.00993995
OSMR	74.51480328	45.47200707	65.92570135	106.1491109	138.553286	117.7411056	1.94953798	0.010076262
EMC2	258.5019719	258.004214	266.6547025	466.3600281	441.2262382	614.2531264	1.943201474	0.010373543
INHBA	1437.859723	1342.412731	1222.085389	1070.191856	945.1313439	1001.910163	0.753863967	0.010402213
SNORD67	0	0	1.967931384	5.220448076	7.422497465	4.443060589	8.682216398	0.010414225

FKBP11	390.0527974	435.9381548	366.0352374	546.4068987	713.3844786	678.6775049	1.626196554	0.010525943
GNAS	3405.602491	2761.930169	2551.423039	4613.13595	6474.891955	6027.011689	1.962968982	0.010533 65
MIR6739	0	0	0	1.740149359	0.824721941	1.110765147	#DIV/0!	0.010566484
PPP1R35	366.1344655	222.4174259	270.5905653	462.0096548	555.8625879	529.8349752	1.801455866	0.010569965
PLVAP	78.19454665	79.08175143	65.92570135	160.9638157	163.2949442	235.4822112	2.507777585	0.010669221
OBFC1	261.2617794	273.8205643	330.6124725	398.4942032	381.0215365	426.5338165	1.393157882	0.010683219
HOXD-AS2	22.99839607	32.62122247	31.48690214	52.20448076	45.35970673	59.98131795	1.808653408	0.010709444
CTNNA1	3984.242136	3598.219 69	3875.840 86	4544.400 05	4369.376841	4333.094839	1.156093716	0.010733468
CCT6P1	189.5067836	166.0716 78	201.7129668	120.9403804	118.7599594	76.64279516	0.567643999	0.010742808
UNC119	287.9399188	207.5895975	181.0496873	466.3600281	430.5048 53	366.5524986	1.867360647	0.010773443
NLGN3	0	0	0	4.350373397	2.474165822	2.221530294	#DIV/0!	0.010900726
NPM1	7765.178 45	8550.714374	7301.025433	10447.85675	9492.549536	9836.936143	1.260847927	0.011074451
PARD3	437.8894612	300.5106554	493.9507773	646.4654868	716.6833664	763.0956561	1.725356406	0.011108315
GNAI1	520.6836871	466.5823334	438.8486986	662.9969057	597.0986 85	712.0004593	1.382845309	0.011396278
SLC3A2	3100.183791	3639.737 61	3054.229507	4393.007056	4029.591402	4496.377316	1.319050104	0.011453114
RELB	218.0247948	72.16209818	77.73328966	318.4473327	365.3518197	341.0049002	2.785397 76	0.011563087
FOSB	0	0	0.983965692	6.090522756	11.54610717	6.664590883	24.69722 37	0.011581494
FERMT2	972.3721 86	723.5980256	996.7572458	1444.323968	1306.359554	1629.492471	1.626668893	0.011737 1
HSPA9	3825.093235	3844.361641	4110.024695	5697.249001	5180.903231	4739.634883	1.325846954	0.011803518
FAM171B	7.359486744	5.931131357	52.15018167	112.2396336	89.89469152	87.75044663	4.429725383	0.011860947
LOC101928100	75.43473912	109.7259301	83.63708381	22.62194166	42.88554091	42.20907559	0.400734593	0.011976 35
SNORD116-21	26.67813945	40.52939761	37.39069629	7.830672114	14.84499493	16.66147721	0.376078477	0.012009792
EPM2A	191.3466553	95.88662361	152.5146822	268.8530759	260.6121332	282.1343474	1.845601636	0.012043759
RBPMS2	75.43473912	49.42609464	61.00587289	105.2790362	103.9149645	132.1810525	1.836665 96	0.012054092
MIR3654	11.95916596	9.885218929	11.80758 83	13.92119487	14.84499493	15.55071206	1.316918375	0.012165308
LOC102723582	7.359486744	7.908175143	9.839656918	4.350373397	0	1.110765147	0.217511817	0.012178688
GORAB	215.2649872	153.2208934	197.7771041	272.3333746	348.8573809	333.2295442	1.685471813	0.012189026
SQSTM1	12144.993	15009.71642	11575.37 24	20137.00838	18496.03896	23422.70466	1.602262352	0.012366 8
BATF3	89.23377677	79.08175143	70.84552981	46.11395801	37.93720927	56.64902251	0.588307273	0.012407977
PDLIM1	799.4242475	994.4530243	1119.752957	1747.109956	2393.343072	2745.811444	2.363465481	0.012501435
CHRFAM7A	12.8791018	9.885218929	16.72741676	29.5825391	42.06081897	28.87989383	2.545424898	0.012518898

IDUA	36.79743372	34.59826625	19.67931384	65.25560095	57.73053584	81.08585574	2.240702296	0.012521693
LAMA3	285.1801113	301.4991773	201.7129668	128.7710525	135.2543983	96.63656781	0.457465197	0.012609702
RABL2A	1.839871686	3.954087572	11.8075883	18.27156827	21.44277045	25.54759839	3.707738589	0.012614791
SLC6A9	2.759807529	38.55235382	10.82362261	79.17679582	75.87441853	58.8705528	4.103165828	0.012616503
FTH1	48108.04491	51647.30334	35442.44422	82986.85284	85451.08971	115429.6033	2.099646309	0.012664376
TTC1	214.3450514	286.6713489	196.7931384	385.443083	423.9070775	523.1703843	1.909576282	0.0128153
C2ORF76	37.71736956	60.29983547	40.34259337	84.3972439	81.64747212	105.522689	1.962762364	0.012866886
ATP6AP1L	2.759807529	29.65565679	13.77551969	74.82642243	57.73053584	99.96886325	5.034008834	0.012931816
P2RY2	81.87429002	87.97844847	56.08604443	24.36209102	28.86526792	37.766015	0.402734638	0.012961913
GPR155	57.03602226	70.1850544	89.54087796	156.6134423	117.9352375	131.0702874	1.871264576	0.013021684
CRTC1	34.03762619	36.57531004	35.42276491	26.10224038	30.5147118	24.43683324	0.76440009	0.013082877
CAMKK2	830.7020662	860.0140468	860.9699804	759.5751951	687.8180984	764.2064213	0.866720919	0.013115339
LOC727896	2.759807529	0	13.77551969	40.89350993	25.56638016	46.65213618	6.840628238	0.013129254
FOXP4	60.71576563	50.41461654	62.97380428	42.63365929	32.98887762	37.766015	0.651268383	0.013174527
MMP25-AS1	30.35788282	41.5179195	16.72741676	78.30672114	94.84302317	129.9595222	3.420973523	0.013178598
GSKIP	450.768563	423.0873702	383.7466198	772.6263153	594.6245191	831.9630952	1.748735262	0.013196079
MAP1LC3B	2758.887593	3736.612755	1884.2943	10471.34877	6973.024008	12458.34189	3.568430483	0.013216606
SHMT2	1032.168016	898.5664006	778.3168622	1206.79358	1428.418401	1468.431525	1.514789896	0.013217356
HUWE1	1452.578696	1430.391179	1663.885985	1115.435739	1171.929878	928.599663	0.70729431	0.013254295
C5ORF56	24.83826776	1.977043786	22.63121091	47.85410737	50.30803837	45.54137103	2.906241119	0.013259222
LOC102724467	0	0.988521893	0	2.610224038	1.649443881	2.221530294	6.556453894	0.013260022
SLC45A1	2.759807529	12.85078461	1.967931384	20.88179231	19.79332657	23.32606809	3.640873871	0.013336814
C17ORF58	822.4226436	768.0815108	636.6258026	976.2237903	1063.066581	977.4733295	1.354552163	0.013346879
ALAD	294.3794697	226.3715135	254.8471142	133.9915006	141.0274518	48.87366648	0.417603679	0.013349267
EGR1	148.1096707	93.90957982	90.52484365	236.6603128	200.4074316	284.3558777	2.16940741	0.013367363
ABCF2	1062.525899	1016.200506	1175.839002	801.3387797	644.1078356	475.407483	0.590202948	0.013490561
METTL1	126.0312105	130.4848899	101.3484663	169.6645625	221.850202	189.9408402	1.624792335	0.0135432
MCUR1	183.9871686	174.968375	260.7509083	327.1480794	423.0823555	447.6383543	1.932961623	0.013548125
COL5A2	10868.12205	13601.07272	12951.9404	8575.45604	7866.197869	9310.433464	0.688169593	0.013581093
ANK3	18.39871686	18.78191596	21.64724522	67.86582499	40.41137509	68.86743913	3.011236256	0.013640973
LACTB2	18.39871686	18.78191596	14.75948538	38.28328589	35.46304344	54.42749221	2.467722947	0.013657248

CITED2	34.95756203	55.357226	37.39069629	87.87754262	101.4407987	72.19973457	2.047821809	0.013690351
RNF121	1066.205642	910.4286634	904.2644708	736.0831788	703.4878153	751.9880046	0.760720584	0.013833771
LTBP4	912.5763562	641.5507085	741.9101316	433.2971903	432.9790188	439.8629983	0.568866745	0.014039715
CMC1	59.79582979	59.31131357	26.56707368	127.9009779	105.5644084	163.2824766	2.72352837	0.014058432
PPDPF	135.2305689	84.0243609	71.8294955	197.5069522	276.2818501	208.8238477	2.345067584	0.014089361
ME1	240.103255	250.0960389	102.332432	376.7423362	498.1320521	462.0783012	2.256339418	0.014215169
PIGG	1278.710822	1194.134447	1242.748669	1064.971408	883.2771983	829.7415649	0.747657095	0.014244824
CROT	413.9711293	280.7402176	383.7466198	212.2982218	132.7802324	139.9564085	0.449748509	0.014253223
ANXA5	5089.085083	5553.515994	5484.624766	8857.360236	8256.291347	11491.97621	1.773747579	0.014349058
KIAA1644	14.71897349	18.78191596	19.67931384	60.90522756	36.28776538	46.65213618	2.70486234	0.014359151
CEP104	258.5019719	327.2007465	198.7610698	490.7221192	400.8148631	457.6352406	1.719865523	0.014363723
MRPS11	247.4627418	247.1304732	206.6327953	287.9947189	288.6526792	295.4635292	1.243694493	0.014393224
SPINT2	321.0576092	316.3270057	280.4302222	185.3259067	236.6951969	152.1748252	0.625611949	0.014490946
MFI2	173.8678743	196.7158567	201.7129668	107.0191856	145.1510615	88.86121177	0.59589975	0.014507306
GPR4	150.8694782	194.7388129	158.4184764	699.5400422	503.0803837	964.1441478	4.298907743	0.01451786
SPAG5	547.3618266	602.0098328	572.6680326	379.3525602	482.4623352	440.9737634	0.756538113	0.014526819
FAM107A	82.79422587	61.28835736	45.26242182	15.66134423	21.44277045	15.55071206	0.278089336	0.014553021
IL15RA	103.9527503	148.2782839	145.6269224	220.1288939	204.5310413	267.6944005	1.740204825	0.014576922
TM7SF3	1486.616322	1770.44271	1740.635309	1326.863886	1191.723204	1265.161503	0.757098841	0.01458435
KIAA2026	900.6171902	1024.108681	1005.612937	669.9575031	818.948887	725.3296411	0.75562458	0.014703764
COL5A1	8566.44257	9744.84882	8012.432629	6871.849818	6496.334726	6430.219437	0.75211258	0.014711891
RALY-AS1	11.95916596	12.85078461	18.69534814	0.870074679	1.649443881	6.664590883	0.211103238	0.014767388
TBC1D5	412.1312576	542.6985192	410.3136935	231.4398647	236.6951969	297.6850594	0.560981419	0.014839968
ADRM1	860.1400132	940.0843201	1150.255894	1346.875604	1722.844134	1641.710888	1.59683518	0.014897108
ZNF546	34.95756203	69.1965325	41.32655906	3.480298718	0.824721941	8.886121177	0.090672825	0.014957365
ESD	422.2505519	330.1663122	365.0512717	795.248257	570.7075829	850.8461027	1.98377195	0.015055743
CACYBP	1075.405	1423.471526	1343.113169	1685.334654	1902.633517	1757.230463	1.391257931	0.01522136
TIMP1	665.1136145	674.171931	657.2890821	759.5751951	797.5061165	719.7758154	1.140381679	0.015244819
CNTNAP3	232.7437683	242.1878638	192.8572756	147.9126955	122.8835691	163.2824766	0.650023887	0.01527576
TMSB15A	12.8791018	4.942609464	5.903794151	23.49201634	23.09221434	35.54448471	3.46162132	0.015298494
GIN1	0.919935843	10.87374082	4.919828459	57.42492884	36.28776538	29.99065897	7.40140098	0.015362088

MIR34AHG	184.9071044	142.3471526	164.3222705	40.02343525	65.1530333	106.6334541	0.430878837	0.015376744
RNF10	1669.683555	1382.942128	1627.479254	2239.572225	2800.75571	3201.225154	1.760976132	0.015430559
NUMBL	271.3810737	278.7631738	232.2159033	411.5453233	423.0823555	333.2295442	1.492736078	0.015439907
DAZAP2	1461.778054	1394.804391	1141.400203	1689.685027	1753.358846	1779.445766	1.306281217	0.015660571
CORO1B	242.8630625	264.9238673	315.8529871	354.1203945	387.6193121	410.9831045	1.399547044	0.015680955
SEPT7P2	96.59326351	84.0243609	106.2682947	58.29500352	71.75080883	52.20596192	0.635276122	0.015699983
VAMP2	489.4058684	417.1562388	407.3617964	542.9265999	568.2334171	620.9177173	1.318248134	0.015749986
MPDU1	475.6068308	420.1218045	465.4157722	388.9233817	385.1451462	374.3278546	0.843699152	0.015754813
POLD4	332.0968393	331.1548341	297.1576389	388.053307	425.5565213	375.4386197	1.238064264	0.015804177
PODXL	4619.917803	5323.190393	4829.303616	3866.611875	4036.189177	4156.483181	0.816338211	0.015824151
MSX1	37.71736956	0.988521893	6.887759843	83.52716922	59.37997972	65.53514368	4.571739413	0.015839483
ZBTB47	367.9743372	318.3040495	426.0571446	241.0106862	218.5513143	255.4759839	0.642825806	0.015855965
DNAJA2	505.0447778	759.1848137	527.4056108	1104.124768	1137.291556	893.0551783	1.74950319	0.015976673
YJEFN3	4.599679215	2.965565679	0.983965692	6.960597435	9.896663287	11.10765147	3.271051978	0.016035815
CYTL1	11.95916596	0	0	25.2321657	52.7822042	41.09831045	9.959948776	0.016093858
NDUFS8	224.4643457	162.1175904	269.6065996	328.8882288	409.0620825	403.2077484	1.739070401	0.016189365
LIPT2	87.39390508	120.5996709	112.1720889	17.40149359	58.55525778	51.09519677	0.396831897	0.016190808
LTN1	514.2441362	546.6526068	679.9202931	404.5847259	324.9404446	329.8972487	0.608577695	0.016207748
DOK4	429.6100387	361.7990128	350.2917863	141.8221727	225.9738117	259.9190444	0.549806927	0.016276637
ARFGEF1	1178.437815	1335.493077	1215.197629	918.7988614	975.6460557	707.5573988	0.697750775	0.01636938
PTGS1	18341.68084	18948.97616	16312.18324	14828.68276	14327.06955	13079.25961	0.787924889	0.016389901
DIAPH3	397.4122842	304.464743	280.4302222	199.2471016	172.3668856	171.0578327	0.552446111	0.016420395
IGFBP3	137.0704406	164.0946342	165.3062362	109.6294096	48.65859449	64.42437854	0.477440686	0.016533422
DGKA	537.2425323	418.1447607	446.7204241	248.8413583	324.1157226	183.2762493	0.539354659	0.016570119
DIS3L2	96.59326351	100.8292331	66.90966704	155.7433676	212.7782607	155.5071206	1.982463056	0.016617099
PET117	265.8614586	297.5450898	273.5424623	227.0894913	218.5513143	177.7224235	0.744804308	0.016667385
OGFR-AS1	35.87749787	26.69009111	16.72741676	6.960597435	0.824721941	2.221530294	0.126197729	0.016684 74
PDK1	83.71416171	129.496368	117.0919173	209.6879977	297.7246205	208.8238477	2.168426157	0.016710174
CDK5RAP2	537.2425323	468.5593772	550.0368217	393.2737551	381.8462585	289.9097034	0.684537347	0.016734 93
GRAMD1A	411.2113218	561.4804352	468.3676693	712.5911624	635.0358942	749.7664744	1.455452491	0.016746871
ZNF697	461.8077932	270.8549987	410.3136935	691.7093701	586.3772997	632.0253687	1.671173522	0.016769229

TMEM42	580.4795169	503.1576435	467.3837036	388.9233817	342.2596053	283.2451125	0.654038977	0.016794466
HHIP	7170.899896	6813.881408	7780.216725	8877.371954	10290.05565	11164.30049	1.393601234	0.016863141
ZNF555	118.6717237	127.5193242	110.2041575	328.0181541	307.6212838	198.8269613	2.341407479	0.016908942
EIF4EBP1	1119.561921	1276.181764	1218.149526	1477.386806	1702.226085	1862.753152	1.395272563	0.016911906
NAMPT	474.686895	455.7085926	493.9507773	703.8904156	707.611425	568.7117554	1.390261374	0.016935186
PRIMPOL	0.919935843	41.5179195	13.77551969	66.99575031	89.06996958	66.64590883	3.961897477	0.016973811
DPYSL2	2194.046985	1988.906049	1960.059658	1705.346372	1288.215671	1487.314532	0.729426553	0.017189456
SLBP	792.9846966	876.818919	977.077932	1133.707307	1347.595651	1463.988464	1.490543249	0.017238446
ATP6V0C	507.8045853	544.675563	421.1373161	657.7764576	633.3864504	728.6619366	1.37065751	0.017246896
PAPLN	35.87749787	51.40313843	27.55103937	86.13739326	80.82275018	63.31361339	2.005315654	0.017255753
UBTD1	589.6788753	522.9280813	587.427518	687.3589967	712.5597567	645.3545505	1.203077546	0.017291534
HIST1H3F	0	0	0	5.220448076	8.247219406	3.332295442	#DIV/0!	0.017362941
RARA	102.1128786	81.05879522	104.3003633	198.3770269	177.3152172	276.5805216	2.268995525	0.017380068
ZNF585B	86.47396924	45.47200707	90.52484365	145.3024715	138.553286	188.830075	2.124709356	0.017411099
CALM1	6625.377941	8784.994062	8347.96493	10163.34233	10907.77239	11143.19596	1.355916063	0.017510047
LOC100506258	0	0	0	1.740149359	0.824721941	2.221530294	#DIV/0!	0.017621861
RHNO1	148.1096707	270.8549987	234.1838347	423.7263689	351.3315467	475.407483	1.914519272	0.017672291
ZNF701	60.71576563	31.63270057	13.77551969	274.073524	174.0163295	143.288704	5.572524934	0.017978139
ZNF350	294.3794697	204.6240318	249.9272857	136.6017247	59.37997972	133.2918177	0.439658147	0.017998125
RNFT1	222.624474	241.1993419	192.8572756	139.2119487	165.7691101	114.4088102	0.638650746	0.018021955
MKI67	1154.519483	1098.247823	1494.643886	833.5315428	607.8200702	675.3452095	0.564842424	0.018110165
TSPO	1083.684423	1116.041217	1060.715016	2074.258036	3015.183415	3731.060129	2.705309653	0.018131224
DYNLL1	1934.625078	1652.808605	1639.286843	2075.998185	2162.420928	2143.776734	1.221070807	0.018150994
CRIM1	13710.7238	13324.28659	12429.45462	11746.00817	11073.5415	10430.08473	0.842520845	0.018176178
PTPN13	236.4235116	354.8793595	262.7188397	47.85410737	22.2674924	155.5071206	0.264195532	0.018264577
LSS	419.4907444	382.5579726	430.976973	462.8797294	470.0915061	486.5151345	1.151222056	0.018492208
ZNF816	23.91833192	29.65565679	64.94173566	108.7593349	190.5107683	213.2669083	4.32463299	0.018497539
NR2F1	149.9495424	146.3012401	118.075883	207.9478484	295.2504547	232.1499158	1.774803024	0.018540561
KAT6A	628.3161807	671.2063653	609.0747632	527.2652557	414.8351361	358.7771425	0.681588268	0.018549529
UBE2D1	270.4611378	497.2265121	488.0469832	1670.543384	1244.505408	2439.240263	4.263869861	0.018729292
CDC42EP1	524.3634305	439.8922423	549.052856	665.6071297	879.1535886	894.1659435	1.611651963	0.018857133

SKP2	436.9695254	507.1117311	462.4638752	197.5069522	106.3891303	328.7864836	0.4498132	0.018959097
SEC14L2	115.9119162	47.44905086	140.7070939	254.9318811	254.0143577	192.1623705	2.305762095	0.019005883
KXD1	807.7036701	771.0470765	547.0849247	1070.191856	1010.284377	1004.131693	1.451009581	0.019127322
C16ORF74	115.9119162	128.5078461	117.0919173	248.8413583	352.1562686	219.9314991	2.270823247	0.019157331
CRBN	752.5075195	873.8533533	889.5049854	565.5485416	459.3701209	662.0160277	0.670518535	0.01917371
HOXB5	43.23698462	47.44905086	56.08604443	36.54313653	31.33943374	28.87989383	0.659270238	0.019365347
CDK7	194.1064629	259.9812578	286.3340163	341.939349	408.2373606	437.641468	1.604245416	0.019369247
AKAP8	1022.048722	908.4516196	850.1463577	726.5123573	661.4269963	534.2780358	0.691284294	0.019455637
UBE2N	675.2329087	1800.098367	1657.982191	3199.264596	2936.83483	4355.310142	2.538256451	0.01949304
TERF2IP	845.4210397	940.0843201	1010.532766	1123.266411	1276.669564	1367.351896	1.347366417	0.019550875
YAE1D1	425.9302953	468.5593772	587.427518	1148.498577	939.3582903	764.2064213	1.924576695	0.019599389
CACNB1	126.0312105	123.5652366	105.284329	141.8221727	162.4702223	168.8363024	1.33320464	0.019600394
SLC41A1	649.4747051	614.8606174	456.560081	314.9670339	378.5473707	276.5805216	0.563715217	0.019630247
NUDT13	59.79582979	86.98992657	61.00587289	29.5825391	35.46304344	9.996886325	0.361142887	0.019644309
MYO9B	1053.32654	1263.330979	933.7834416	729.1225813	736.4766929	628.6930733	0.644310225	0.019716287
DSTN	1492.135937	1755.614882	1795.737388	2490.153732	2196.234528	2900.207799	1.504235907	0.019718394
PKD1	607.1576563	564.4460008	551.0207874	396.7540538	473.3903939	485.4043693	0.78690908	0.019724805
FRMD3	351.415492	436.9266767	360.1314432	180.1054586	164.1196662	283.2451125	0.546351462	0.019749292
NBEAL1	217.1048589	152.2323715	267.6386682	42.63365929	87.4205257	91.08274207	0.347166867	0.019754604
IKBKE	434.2097179	564.4460008	551.0207874	361.9510666	319.9921129	369.884794	0.6787403 5	0.019808284
TLL1	32.1977545	9.885218929	18.69534814	42.63365929	45.35970673	51.09519677	2.288456792	0.019855246
LINC01530	20.23858854	12.85078461	14.75948538	8.700746794	3.298887762	2.221530294	0.297210117	0.019893905
FIBP	365.2145296	358.8334471	366.0352374	505.5133887	532.7703736	686.452861	1.582206387	0.019895333
LTBP2	6561.902368	6060.627725	5202.226613	4429.550193	4475.765971	3764.383084	0.710792268	0.020015759
INPP5D	314.6180583	294.5795241	278.4622908	337.5889756	383.4957024	394.3216273	1.25656948	0.020100892
DNAAF2	393.7325408	362.7875347	342.4200608	682.1385486	649.8808892	482.0720739	1.650764634	0.020167823
TTC31	132.4707614	47.44905086	105.284329	219.2588192	225.9738117	174.3901281	2.172558772	0.020205325
TFCP2	856.4602698	1063.649557	835.3868724	504.643314	560.8109196	683.1205655	0.634576989	0.020228046
CEBPD	45.99679215	92.92105793	60.0219072	144.4323968	210.3040948	265.4728702	3.117573733	0.020300902
GPS2	397.4122842	235.2682105	331.5964381	628.1939185	897.2974713	1122.983564	2.746591631	0.020322335
ACP2	380.853439	344.0056187	323.7247126	250.5815077	247.4165822	295.4635292	0.7566983 6	0.020329618

LOC100288162	1.839871686	1.977043786	1.967931384	0.870074679	0	1.110765147	0.342418715	0.020358825
WIPF1	145.3498632	121.5881928	86.58898088	187.9361307	183.9129927	227.7068552	1.695926806	0.020512676
ZMYM3	337.6164544	289.6369146	349.3078206	210.5580724	261.4368552	187.7193099	0.675548286	0.020553973
SLC35E2B	1072.645193	1027.074247	895.4087796	680.3983993	776.888068	523.1703843	0.661226067	0.020570921
MINK1	388.2129257	336.0974436	434.9128358	151.3929942	188.8613244	282.1343474	0.53690149	0.020640148
CDC40	174.7878102	119.611149	159.4024421	266.2428519	318.3426691	223.2637946	1.780182506	0.021118662
SH3RF2	1.839871686	0	8.855691227	18.27156827	19.79332657	33.32295442	6.674529414	0.021137095
ARPC5L	6007.181054	6251.412451	6843.481387	4933.323432	5433.268144	5433.8631	0.827159079	0.021208561
GTF2A2	795.7445041	719.643938	695.6637441	838.7519909	861.009706	901.9412995	1.176680954	0.021216701
SUMF2	938.3345598	1212.916363	1027.260182	782.1971368	762.867795	697.5605124	0.705558474	0.021262028
CEBPG	1668.763619	2601.789622	1859.695158	3301.933408	2933.535943	3365.618396	1.566182497	0.021301309
ABLIM1	2835.242268	2577.076575	2833.821192	2380.524323	2426.331949	2178.210454	0.847071078	0.021540132
RPL29	2234.524163	2425.832725	2015.161737	1671.413459	1859.747976	1642.821653	0.775068332	0.021590085
EHD1	832.5419379	959.854758	890.4889511	1168.510294	1430.067845	1642.821653	1.580909644	0.021616247
RPUSD3	306.3386357	387.500582	429.0090416	245.3610596	239.9940847	242.1468021	0.647907623	0.021679062
ZNF781	0.919935843	0	0	13.05112019	15.66971687	5.553825736	37.25766646	0.021786992
ADSS	2306.279158	2305.233054	2097.814855	2674.609564	2490.660261	2811.346588	1.188884717	0.021881455
PEAR1	2708.291122	2153.000683	2433.347156	1911.554071	1793.770221	1646.153948	0.733617972	0.021882603
FBXO42	1067.125578	801.6912551	819.6434213	604.7019022	535.2445394	393.2108621	0.570273375	0.022013341
ORMDL2	237.3434475	188.8076815	255.8310799	350.6400958	343.0843273	289.9097034	1.442316403	0.022034472
STXBP5	870.2593074	760.1733356	826.5311811	510.7338368	625.139231	678.6775049	0.738533695	0.022134484
MAP7D3	232.7437683	228.3485573	265.6707368	120.9403804	192.9849341	119.9626359	0.597014313	0.022162507
C17ORF62	513.3242004	405.2939761	379.810757	910.0981146	615.2425677	857.5106936	1.835180436	0.022170847
YBX2	0	0	0	5.220448076	6.597775525	2.221530294	#DIV/0!	0.022307472
RBPMS	213.4251156	209.5666413	328.6445411	564.6784669	676.2719913	1004.131693	2.9869262	0.022371165
CCDC85A	399.2521558	621.7802706	725.1827149	943.1609524	896.4727494	997.4671022	1.624714353	0.022386294
TCTN1	210.665308	102.8062769	160.3864078	56.55485416	39.58665315	14.43994691	0.233364122	0.022410065
PEA15	1716.600283	1795.155757	1549.745965	2012.482733	1957.065165	2192.650401	1.21746436	0.022428007
DNAJA4	1113.12237	927.2335355	1070.554673	693.4495195	809.8769456	835.2953907	0.751748338	0.022436862
SNORA71D	14.71897349	20.75895975	10.82362261	6.090522756	2.474165822	4.443060589	0.280935466	0.022539566
PLEKHJ1	5094.604698	6473.829877	5760.13516	3369.799233	4361.954344	4170.923128	0.686881658	0.022549353

EDNRB	29.43794697	44.48348518	33.45483352	6.960597435	21.44277045	5.553825736	0.316244874	0.022603078
DNAJA3	663.2737428	873.8533533	684.8401215	399.3642778	494.0084424	234.3714461	0.507543116	0.022630763
UBE2D2	1151.759675	932.176145	1219.133492	1419.091802	1763.255509	1874.971568	1.531096808	0.022677551
SERPINB8	494.0055477	505.1346873	458.5280124	936.200355	638.334782	849.7353376	1.663115376	0.022823881
GATA3-AS1	14.71897349	12.85078461	19.67931384	23.49201634	22.26749 24	24.43683324	1.485666048	0.023009891
APBB1	234.58364	154.2094153	336.5162666	428.0767423	447.8240137	553.1610433	1.970279102	0.023134835
ZNF32	305.4186999	197.7043786	291.2538448	125.2907538	159.9960565	96.63656781	0.480783576	0.023234064
SRM	1176.597943	1561.864591	1637.318911	2336.150514	2879.929016	3709.955592	2.039872245	0.023252342
PARVA	798.5043117	831.3469119	1166.983311	1522.630689	1321.204549	1721.685978	1.632388745	0.023313809
TSKU	298.0592131	296.5565679	251.8952171	329.7583035	382.6709804	380.9924455	1.291680477	0.023331127
PTP4A1	2329.277554	2167.828511	2026.969325	5042.952842	3858.873 96	6790.107345	2.405234 95	0.023360136
ABCA6	258.5019719	276.7861 3	261.734874	158.3535916	224.3243678	199.9377265	0.730989825	0.023549043
PIGH	111.312237	174.968375	171.2100304	214.0383711	256.4885235	245.4790975	1.565072432	0.023655125
YBEY	167.4283234	157.174981	171.2100304	90.48776666	138.553286	91.08274207	0.645653863	0.023659 26
NBEAL2	767.226493	862.9796125	865.8898088	620.3632464	644.9325575	430.9768771	0.679570313	0.023663133
METAP1	1218.914992	1137.788699	1067.602776	1533.941 66	1614.805 56	1320.699 76	1.305212318	0.023702951
RPL10	5475.458137	3922.454871	3560.971839	6057.459918	7397.755807	7142.219896	1.589445069	0.023743215
ETV6	770.9062364	1081.442951	966.2543094	1457.375088	1397.078967	1894.965341	1.685025724	0.023749711
VDAC1	2631.936447	2923.059237	3191.984704	3814.407394	3475.378258	4146.486294	1.307453708	0.023751535
MYL5	29.43794697	19.77043786	9.839656918	38.28328589	42.88554091	52.20596192	2.258750413	0.023856605
RNF220	648.5547693	657.3670588	573.6519983	490.7221192	545.1412027	515.3950283	0.825324512	0.023898459
PP7080	240.103255	276.7861 3	292.2378105	127.0309032	159.1713345	212.1561431	0.615920938	0.023953185
FANCE	129.7109539	161.1290685	176.1298588	218.3887445	211.9535387	264.362105	1.487685644	0.023973243
DNAJC13	767.226493	759.1848137	759.6215141	1088.463424	875.0299789	977.4733295	1.286493661	0.024031783
ABCG1	122.3514671	90.94401415	169.242099	261.8924785	495.6578863	509.8412026	3.313116496	0.024222596
NUPR1	113.1521087	95.88662361	109.2201918	164.4441144	283.7043476	262.1405747	2.231796135	0.024319272
AIMP1	618.1968865	564.4460008	548.0688904	693.4495195	676.2719913	786.4217242	1.245813002	0.024360096
LINC00539	16.55884517	10.87374082	10.82362261	5.220448076	5.773053584	6.664590883	0.461574557	0.024402313
CIT	321.0576092	171.0142875	307.9812615	110.4994843	97.31718899	53.31672706	0.326395062	0.024402886
RBMS2	1552.851703	1224.778625	1221.101424	944.9011018	903.0705249	970.8087386	0.704918594	0.024446086
USP27X	3.679743372	11.86226271	0.983965692	26.97231506	23.91693628	15.55071206	4.020336249	0.024468319

INO80C	102.1128786	200.6699443	207.616761	346.2897224	296.0751767	282.1343474	1.811324452	0.024513669
PSMC5	7382.48514	6972.044911	7202.628864	5525.844289	6598.600246	5874.836863	0.834956103	0.024585834
ZNF655	485.7261251	350.925272	431.9609387	233.1800141	172.3668856	298.7958246	0.555207217	0.024617976
ZBED5-AS1	229.9839607	184.853594	237.1357317	84.3972439	68.4519207	158.839416	0.478069558	0.024650225
CENPF	1030.328144	902.5204882	1288.011091	650.8158602	620.1908993	718.6650502	0.617745565	0.024752051
ESM1	1778.235984	2224.174259	1741.619275	3652.573504	2577.256064	3165.680669	1.635700201	0.02482024
FLJ42393	105.7926219	50.41461654	111.1881232	28.71246442	17.31916075	1.110765147	0.176302199	0.025012818
NAT1	125.1112746	71.17357629	108.2362261	3.480298718	54.43164808	12.21841662	0.23029724	0.025126924
DCXR	287.019983	243.1763857	213.5205551	340.1991996	377.7226488	316.5680669	1.39097267	0.025200483
CEP97	222.624474	256.0271703	328.6445411	177.4952346	102.2655206	126.6272268	0.503393908	0.025240501
ATP5D	413.9711293	313.36144	341.4360951	449.8286092	566.5839732	528.7242101	1.44571678	0.025336162
ICAM1	1315.508255	1154.593571	658.2730478	3412.432893	1919.127956	2755.80833	2.585166262	0.025392411
FRG1DP	0	0	0	2.610224038	0.824721941	2.221530294	#DIV/0!	0.025398779
CSF2	0	0	0	43.50373397	23.09221434	67.75667398	#DIV/0!	0.025604242
SMAD3	1587.809265	1685.429827	1767.202383	2169.096176	2143.452324	2704.713133	1.392191868	0.025699748
EBP	287.019983	266.9009111	267.6386682	297.5655403	332.362942	316.5680669	1.152072951	0.025734657
SNHG20	113.1521087	109.7259301	92.49277503	207.0777737	148.4499493	236.5929764	1.877538039	0.025874199
ESCO1	68.07525238	119.611149	110.2041575	194.0266535	157.5218906	155.5071206	1.702154196	0.025989106
FBLL1	4.599679215	14.82782839	2.951897076	29.5825391	53.60692614	29.99065897	5.057334	0.025996669
DAP	1348.625946	1299.906289	1250.620394	2177.796922	2413.136398	3486.691797	2.071636041	0.026078868
ARMCX3	1221.674799	1270.250632	1547.778033	2029.014152	1760.781343	1712.799857	1.362128532	0.026096685
UBE2I	1535.372922	2002.745355	1645.190637	2240.442299	2556.638016	2224.86259	1.354722055	0.026097486
ZKSCAN2	126.0312105	64.25392304	244.0234916	348.8999464	364.5270977	301.0173549	2.335768485	0.026108006
MYL6B	463.6476648	305.4532649	441.8005956	614.2727236	994.6146603	864.1752845	2.042331781	0.026136648
CROCCP3	41.39711293	95.88662361	92.49277503	6.090522756	21.44277045	14.43994691	0.182669847	0.026188498
PPP3CB-AS1	104.8726861	84.0243609	62.97380428	22.62194166	26.3911021	49.98443162	0.39304856	0.026325565
RAB11FIP3	272.3010095	288.6483927	298.1416046	361.9510666	357.1046003	314.3465367	1.202901899	0.026356221
ARSA	113.1521087	85.01288279	142.6750253	23.49201634	45.35970673	63.31361339	0.387763555	0.026378489
COTL1	1124.1616	1031.028334	1470.044744	1664.452862	2171.492 87	2387.034301	1.716573018	0.026518447
PHLDA1	1648.525031	2761.930169	1564.505 45	4175.488386	3667.538 47	5772.646 47	2.278788786	0.026520692
CEP19	16.55884517	47.44905086	20.66327953	61.77530224	62.67886748	83.30738604	2.453745969	0.026581687

SELPLG	9.199358429	6.91965325	14.75948538	17.40149359	27.21582404	25.54759839	2.272290516	0.026640701
ZCCHC8	253.9022927	181.8880283	255.8310799	161.8338904	91.5441354	102.1903935	0.514108469	0.0266892
NAV3	287.019983	402.3284104	444.7524927	174.0149359	205.3557632	236.5929764	0.543129525	0.026728556
VPS8	543.6820832	485.3642494	464.4318065	977.9639396	748.847522	693.1174518	1.620330991	0.026806663
DDTL	0	0	0.983965692	12.18104551	5.773053584	5.553825736	23.8910005	0.026885536
TMEM120A	338.5363902	285.682827	323.7247126	368.9116641	454.4217893	433.1984074	1.325533949	0.026966812
LDB1	206.0656288	221.428904	219.4243493	372.3919628	358.7540441	550.939513	1.981833512	0.027045125
SAFB2	621.8766298	516.99695	584.475621	435.9074144	446.1745698	318.7895972	0.696824289	0.02707128
NAT8L	2.759807529	20.75895975	25.58310799	40.02343525	78.34858435	66.64590883	3.768042003	0.027098613
WDR92	224.4643457	159.1520248	181.0496873	125.2907538	125.357735	114.4088102	0.646501227	0.027122328
GLB1	1296.189603	1054.75286	1092.201918	1532.20151	1391.305914	1691.695319	1.34040349	0.027126573
ICOSLG	2.759807529	39.54087572	7.871725535	100.0585881	60.20470166	64.42437854	4.478311363	0.027185888
NDST2	642.1152184	710.747241	722.2308178	453.308908	446.1745698	600.9239446	0.723055411	0.027210154
DAAM1	2123.211926	2342.796886	1914.797236	1717.527417	1282.442618	1568.400388	0.715955067	0.027263922
RUBCN	1823.312841	1874.237509	1561.553553	1303.37187	1380.584529	977.4733295	0.696207908	0.027464456
EIF5	4996.171563	4822.009794	4083.457621	7332.989398	6367.678103	5730.437394	1.397756403	0.02748038
TUBGCP4	377.1736956	448.7889394	348.3238549	295.825391	145.9757835	164.3932418	0.516223614	0.027497427
TTYH3	2681.612982	3352.077739	2541.583382	2104.710649	1665.113598	1946.060538	0.666554179	0.02754422
HOOK2	165.5884517	156.1864591	111.1881232	79.17679582	91.5441354	87.75044663	0.596982554	0.027649239
LOC100506603	97.51319935	59.31131357	61.00587289	38.28328589	17.31916075	13.32918177	0.31644634	0.027694324
ZNF841	118.6717237	127.5193242	83.63708381	55.68477948	68.45192107	32.21218927	0.474031396	0.027703761
SMYD5	282.4203038	358.8334471	294.2057419	240.1406115	138.553286	166.6147721	0.582931355	0.027818477
PCNXL3	603.477913	444.8348518	605.1389005	383.7029336	375.248483	325.4541881	0.655843547	0.027880134
RNF170	482.0463817	590.1475701	627.7701114	696.0597435	803.2791701	743.1018835	1.319110707	0.027911085
GDF6	3089.144561	3606.127865	3407.473191	2714.633	2567.359401	2941.30611	0.8139667	0.027967606
PIGW	420.4106802	418.1447607	336.5162666	579.4697365	491.5342766	500.9550814	1.337755887	0.027969092
BCAT1	4042.198094	4886.263717	5108.749872	6870.979743	6177.992057	5712.665152	1.336564367	0.02812445
FIGNL1	167.4283234	92.92105793	178.0977902	454.1789826	370.3001513	255.4759839	2.46313624	0.02813475
SF1	489.4058684	648.4703617	763.5573769	913.5784133	933.5852367	875.282936	1.431786298	0.028141 9
FLJ37453	84.63409755	64.25392304	87.57294657	120.9403804	98.96663287	119.9626359	1.437318189	0.028258892
PDIA5	1139.800509	1552.967894	1332.289547	916.1886374	982.2438312	894.1659435	0.693803281	0.028300703

CHST2	223.5444098	229.3370792	268.6226339	394.1438298	353.8057125	295.4635292	1.446163699	0.028353059
PLEKHO2	627.3962449	898.5664006	839.3227351	1128.486859	1110.075732	1020.79317	1.377996832	0.028383946
WHSC1	3341.206982	3054.532649	2686.226339	2516.255973	2097.267895	2100.456893	0.739265131	0.028389912
BET1	797.5843758	933.1646669	531.3414736	1486.087552	1128.219615	1241.835435	1.704680946	0.028424163
MT1M	2.759807529	0	1.967931384	11.31097083	16.49443881	6.664590883	7.291011869	0.02844241
TDP2	597.9582979	706.7931534	562.8283757	853.5432605	770.2902925	765.3171864	1.279276369	0.02862767
ZFC3H1	788.3850174	669.2293215	852.1142891	515.0842102	612.7684018	573.1548159	0.736453368	0.028672974
FBXO32	165.5884517	141.3586307	132.8353684	336.7189009	295.2504547	525.3919146	2.631667699	0.028689647
SRPK2	745.1480328	839.2550871	569.7161356	997.1055826	1510.065873	1415.114798	1.820830599	0.028727787
PLS3	2148.970129	2013.619096	2277.880577	3053.962125	2661.377702	3623.31591	1.449996044	0.028910389
EPOR	324.7373526	272.8320424	251.8952171	184.455832	191.3354902	224.3745597	0.706522524	0.028950643
KMT2D	230.9038966	176.9454188	239.1036631	142.6922474	138.553286	159.9501812	0.681959477	0.028984061
SAMHD1	51.5164072	81.05879522	82.65311811	41.76358461	12.37082911	28.87989383	0.385703458	0.029026305
SPTAN1	3780.936315	3109.889875	3624.929609	2879.947189	2837.868197	2710.266959	0.801471859	0.029144263
LAMP3	34.03762619	19.77043786	33.45483352	126.1608285	59.37997972	102.1903935	3.297291401	0.029167405
CMSS1	186.7469761	221.428904	274.526428	306.2662871	371.1248733	324.343423	1.467308037	0.029332179
ARL8A	136.1505048	243.1763857	167.2741676	272.3333746	336.4865518	377.66015	1.804753324	0.029352384
NCAPH	187.666912	130.4848899	235.1678003	95.70821473	74.22497465	73.31049971	0.439607938	0.029386087
ZC3H10	178.4675535	179.9109845	152.5146822	370.6518134	307.6212838	234.3714461	1.786370433	0.029456863
IFNGR1	361.5347863	218.4633383	191.8733099	597.7413047	414.0104142	502.0658465	1.961230197	0.029717065
POLDIP3	1861.03021	2122.356504	2033.857085	1792.35384	1603.259452	1522.859017	0.817396215	0.029748781
MPRIP	1447.979017	1810.972108	1746.539103	1328.604035	1235.433467	1299.595222	0.771878987	0.029785932
HOXA-AS2	26.67813945	15.81635029	17.71138245	4.350373397	5.773053584	11.10765147	0.352641324	0.029790344
KIAA1143	160.0688367	115.6570615	138.7391625	101.7987375	88.24524764	91.08274207	0.678288121	0.029954789
SAMD9	59.79582979	91.93253604	108.2362261	37.41321121	45.35970673	27.76912868	0.425219626	0.030048118
FAM83G	77.27461081	19.77043786	59.03794151	100.0585881	133.6049544	115.5195753	2.237163175	0.030100264
DUS2	503.2049061	727.5521132	561.84441	354.1203945	403.2890289	351.0017865	0.618325519	0.030159067
FAIM	49.67653552	116.6455834	81.66915242	155.7433676	209.4793729	149.9532949	2.07739584	0.030235528
GLCCI1	228.1440891	333.1318779	283.3821192	180.1054586	136.0791202	188.830075	0.597892404	0.030283056
DIAPH2	165.5884517	166.071678	228.2800405	108.7593349	80.82275018	126.6272268	0.56471982	0.030307917
CRIP2	1815.033418	2306.221576	2413.667842	2956.513761	4155.773859	4610.786126	1.793911579	0.03039892

GTF2H2B	1.839871686	1.977043786	2.951897076	0.870074679	0	1.110765147	0.292642146	0.030421179
TMEM101	1126.921408	775.001164	1043.003633	528.1353304	645.7572795	653.1299065	0.620396706	0.030481691
ARHGEF10	1070.805321	1119.006783	994.7893144	957.952222	930.286349	887.5013526	0.871612977	0.030522521
GTF2I	206.0656288	192.7617691	197.7771041	211.4281471	220.2007581	229.9283855	1.108870765	0.030524612
PERP	1126.921408	1022.131637	750.7658229	1417.351653	1298.937056	1619.495585	1.495191421	0.030553214
AHCY	1467.297669	1158.547658	1304.738507	999.7158066	1039.149645	1007.463988	0.775032303	0.030625575
MNAT1	330.2569676	354.8793595	332.5804038	272.3333746	296.0751767	312.1250064	0.865204954	0.030702981
LOC101926935	3.679743372	0.988521893	3.935862767	34.80298718	32.16415568	12.21841662	9.203205622	0.030741819
CCDC122	7.35948674	13.8393065	4.91982845	18.2715682	32.1641556	23.3260680	2.82410737	0.03074494
GNG11	3635.586451	3893.787736	3765.636703	4362.554442	4898.848327	5589.370221	1.314808205	0.030883089
RNF144B	1976.942126	2523.696393	2381.196974	1359.056649	1283.26734	1858.310091	0.653987455	0.031138389
CALM3	4463.52871	4782.468918	4228.100578	3348.917441	3909.181998	3862.130417	0.825304201	0.031139138
LINC01006	1.839871686	0	0	17.40149359	16.49443881	5.553825736	21.44158119	0.031343756
SNX2	187.666912	354.8793595	374.8909286	469.8403269	570.7075829	520.948854	1.702020327	0.031456189
COL3A1	2115.852439	3131.637357	3171.321425	1224.195074	1815.212991	1618.384819	0.553260165	0.031599826
SIRT1	333.0167751	370.6957098	413.2655906	617.7530224	470.9162281	686.452861	1.589218401	0.031605813
AK5	14.71897349	23.72452543	10.82362261	75.69649711	50.30803837	37.766015	3.324134746	0.031778901
RARRES3	12.8791018	15.81635029	17.71138245	10.44089615	2.474165822	0	0.27830086	0.031780015
MBD1	1280.550693	1106.155998	1178.790899	632.5442919	987.1921629	544.2749221	0.606931101	0.03187854
WDTC1	76.35467496	52.39166032	95.44467211	40.89350993	27.21582404	27.76912868	0.427664177	0.031908209
DLEU2L	64.39550901	63.26540115	54.11811305	12.18104551	6.597775525	44.43060589	0.347726739	0.031939656
EXOC6	867.4994999	1077.488863	1190.598487	1642.700995	1303.060666	1518.415956	1.423713592	0.031987175
S100A16	3010.950014	3837.441988	3610.170123	4773.229691	5517.389782	7031.143382	1.656227945	0.032015684
TRAP1	1551.931767	1156.570615	1555.649759	800.468705	1005.336046	1011.907049	0.660790635	0.032126184
TBC1D22B	694.5515614	596.0787014	747.8139258	554.2375708	357.9293222	349.8910214	0.61912802	0.032129717
FURIN	1736.838871	1592.508769	1436.58991	1220.714775	1110.075732	1354.022714	0.773156002	0.032138974
AMN1	42.31704878	13.8393065	49.19828459	108.7593349	74.22497465	144.3994691	3.107445283	0.03221208
PIK3R4	527.123238	316.3270057	438.8486986	632.5442919	649.8808892	604.2562401	1.471327285	0.032253534
COMMD4	480.20651	391.4546696	554.9566502	346.2897224	303.4976741	257.6975141	0.636109329	0.032271093
RALA	3401.922747	4378.163464	3855.177581	5190.865537	4798.23225	5988.134908	1.373173224	0.032295451
DCAF8	1620.926955	1409.632219	1340.161272	1179.821265	1157.084883	945.2611403	0.750944227	0.032310031

FAM96B	409.3714501	338.0744874	306.0133302	476.8009243	447.8240137	554.2718084	1.403848057	0.032356053
FBXL3	482.9663175	423.0873702	535.2773364	964.0427448	625.9639529	908.6058904	1.733545276	0.032404277
GNB2L1	5253.753599	4160.688647	4519.354423	5488.431078	6534.271935	6219.174059	1.309182092	0.032415815
PRR13	455.3682423	534.7903441	495.9187087	561.1981682	649.8808892	675.3452095	1.269398485	0.032423107
HSPD1	6376.075327	8090.063171	7773.328966	10596.63952	9466.158434	12749.36236	1.475402249	0.032555543
BIN3	245.6228701	311.3843963	349.3078206	384.5730083	424.7317994	409.8723393	1.345202308	0.032557853
DUS1L	2562.941258	2499.971867	2855.468438	1531.331436	2173.142313	2049.361697	0.726642863	0.032704791
PAXIP1-AS2	1.839871686	3.954087572	13.77551969	21.75186698	25.56638016	42.20907559	4.574844481	0.032771631
RNF114	605.3177847	450.7659832	393.5862767	660.3866816	710.0855908	795.3078454	1.493981424	0.032782423
TRIOBP	4609.798509	5552.527472	5569.245816	4024.965467	4157.423302	4360.863968	0.797329911	0.032797011
TRIB3	1284.230437	2351.693583	1164.031413	2908.659653	2720.757682	3582.2176	1.91910843	0.03282448
CCDC18-AS1	125.1112746	36.57531004	122.9957115	3.480298718	0.824721941	0	0.015122193	0.032827714
KIDINS220	1469.137541	1622.164426	1278.171434	1062.361184	959.9763388	1192.961768	0.735855101	0.032873533
RAB33A	0	0	10.82362261	16.53141891	16.49443881	27.76912868	5.616879726	0.032899331
UBE3A	1419.461006	1412.597785	1227.989183	1050.180138	1115.848786	1185.186412	0.825412743	0.032901901
FERMT3	94.75339182	87.97844847	162.3543392	189.6762801	192.1602122	191.0516053	1.660130517	0.033006604
PCBP1	1399.222417	780.9322954	757.6535827	1536.551884	2319.118097	2080.463121	2.020599203	0.033009186
GTF2F2	170.1881309	208.5781194	131.8514027	242.7508355	385.9698682	337.6726047	1.892596746	0.033039887
ANP32A	468.2473441	479.4331181	477.2233605	270.5932253	308.4460058	418.7584605	0.700256169	0.033092959
PVRL3	397.4122842	431.9840672	460.4959438	702.1502663	650.7056111	510.9519677	1.444932924	0.033205511
HEPH	55.19615058	158.1635029	151.5307165	13.92119487	18.96860463	13.32918177	0.126665391	0.033280701
PXDC1	1813.193546	1570.761288	1449.381464	1911.554071	1968.611272	2080.463121	1.233232719	0.033297887
SNORD116-20	27.59807529	23.72452543	23.6151766	6.090522756	18.96860463	12.21841662	0.49744662	0.033414365
ZNF329	52.43634305	39.54087572	23.6151766	13.92119487	8.247219406	12.21841662	0.297483505	0.033427108
C2CD4B	204.2257571	157.174981	97.41260349	254.9318811	381.8462585	456.5244755	2.382891943	0.033469648
COX5A	877.6187942	746.3340291	871.793603	1017.987375	1366.564256	1461.766934	1.541149583	0.033502022
KRAS	490.3258043	675.1604528	669.0966704	897.0469944	771.9397364	838.6276861	1.366858036	0.033583176
MAP1LC3B2	4.599679215	5.931131357	3.935862767	33.06283782	18.96860463	51.09519677	7.128566243	0.033780847
DNM1L	1078.164808	954.9121485	831.4510096	677.7881752	710.9103128	760.8741258	0.750410762	0.033889927
GLRX2	183.0672327	157.174981	198.7610698	252.321657	359.5787661	266.5836353	1.629830625	0.03400227
PLEKHM1P1	24.83826776	33.60974436	23.6151766	81.78701986	46.18442867	94.41503751	2.709942052	0.034022771

MAP3K14	111.312237	147.289762	105.284329	224.4792673	192.1602122	161.0609463	1.587584862	0.034027099
POLG	1099.323332	775.9896859	926.8956817	671.6976525	417.3093019	579.8194068	0.59553964	0.03404942
EFNA1	4475.487876	7398.097846	4950.331396	8623.310147	8361.031033	10462.29692	1.631405927	0.034238384
PTPRE	1841.711558	2345.762452	1859.695158	1332.954409	1273.370676	1603.944873	0.696238164	0.034268806
GABARAPL2	785.6252099	733.4832445	811.7716958	881.3856502	1134.81739	1055.22689	1.317712509	0.034407717
HEG1	4985.132333	4712.283863	3766.620668	3518.582003	3100.129775	2695.827012	0.691808771	0.034490242
NDUFA11	540.0023398	384.5350163	415.233522	602.9617528	635.0358942	577.5978765	1.355153746	0.034531719
DYRK1B	117.7517879	104.7833206	139.7231282	158.3535916	179.789383	219.9314991	1.540543229	0.034552808
SLC25A5	2354.115822	1905.87021	2282.800405	2540.618064	3063.017287	3120.139298	1.333342412	0.034586137
BRIP1	98.4331352	48.43757275	51.16621598	23.49201634	4.948331643	6.664590883	0.177264614	0.034712444
NR4A3	0	0	0	5.220448076	11.54610717	4.443060589	#DIV/0!	0.034744316
ENG	5232.595075	5373.60501	5767.02292	6063.550441	7490.124664	7116.672298	1.262448291	0.034823493
LOC100652768	22.99839607	30.64417868	14.75948538	8.700746794	7.422497465	8.886121177	0.365622985	0.03492002
LINC00346	105.7926219	160.1405466	147.5948538	75.69649711	92.36885734	84.41815119	0.610559604	0.034996383
GAR1	264.0215869	239.2222981	284.3660849	223.6091926	190.5107683	217.7099688	0.802211696	0.035001618
ANKRD17	1837.111878	1817.891761	2156.852797	1590.496514	1625.526945	1527.302077	0.816146371	0.035021556
SNRNP27	468.2473441	475.4790305	479.1912919	390.663531	323.2910007	425.4230514	0.800733317	0.035029168
NFATC2	253.9022927	240.21082	395.5542081	616.012873	603.6964605	1010.796284	2.507123242	0.035054527
SELE	118.6717237	196.7158567	38.37466198	522.0448076	391.7429218	263.2513399	3.327203778	0.03507241
GYG1	584.1592603	443.8463299	456.560081	850.9330364	655.6539428	996.356337	1.685976825	0.035128128
TGFB1	692.7116897	679.1145404	585.4595866	812.6497505	867.6074815	741.9911183	1.237554745	0.035326386
CDR2	1762.597075	1545.059719	1895.117922	1429.532698	1416.872294	1397.342555	0.815670057	0.035537219
HACD3	1240.073516	815.5305616	929.8475788	1779.302719	1558.724468	1335.139707	1.565313203	0.035549591
LHPP	49.67653552	37.56383193	33.45483352	17.40149359	28.04054598	12.21841662	0.477736113	0.035577821
DLGAP4	418.5708085	365.7531004	450.6562869	611.6624996	1037.500201	1162.971109	2.27706794	0.035630741
ST13	1193.156788	1468.943533	1558.601656	2031.624376	1684.906925	2130.447552	1.385309573	0.035797323
COL12A1	3443.31986	3211.70763	3019.790708	2814.691588	2898.897621	2701.380838	0.86978069	0.035969114
ACYP1	322.8974809	257.0156922	324.7086783	214.9084458	207.829929	246.5898627	0.739898375	0.036033189
FXYD5	704.6708557	859.0255249	756.669617	902.2674425	985.542719	917.4920116	1.208991244	0.036067776
CENPQ	49.67653552	51.40313843	75.76535827	33.9329125	26.3911021	34.43371956	0.535823557	0.036088479
ZNF232	105.7926219	189.7962034	179.0817559	254.9318811	229.2726995	245.4790975	1.537242262	0.036297249

LOC100289561	0.919935843	0	0.983965692	2.610224038	5.773053584	7.77535603	8.487116249	0.036505959
NOP14	191.3466553	124.5537585	263.7028054	336.7189009	319.167391	305.4604155	1.658628999	0.036587177
CCNH	396.4923483	360.8104909	383.7466198	276.683748	135.2543983	278.8020519	0.605355178	0.036702618
NRXN3	68.99518822	145.3127183	156.450545	30.45261378	35.46304344	46.65213618	0.303614909	0.036755554
KIAA0430	482.0463817	421.1103264	503.7904342	637.76474	627.6133968	530.9457404	1.276752923	0.036785272
C3ORF58	880.3786017	884.7270941	900.328608	818.7402733	616.8920115	654.2406717	0.784064703	0.036944959
ITPR3	1040.447438	706.7931534	1117.785026	600.3515288	565.7592512	507.6196723	0.584193887	0.036967236
NGEF	0	1.977043786	0.983965692	3.480298718	2.474165822	4.443060589	3.511479854	0.037025053
SEPT8	1212.475441	975.6711083	1061.698981	853.5432605	798.3308385	901.9412995	0.785826703	0.037039529
TEAD2	763.5467496	688.9997593	621.8663172	590.7807073	512.1523251	537.6103312	0.790847098	0.037082594
LRRC28	61.63570148	105.7718425	163.3383048	209.6879977	432.9790188	344.3371956	2.984177173	0.037330256
RPL23A	2366.074988	1990.883092	2173.580213	2493.634031	3173.530027	2964.632178	1.321758766	0.037411917
ZRSR2	22.99839607	38.55235382	62.97380428	121.8104551	70.92608689	106.6334541	2.404104139	0.03766887
OSBPL1A	162.8286442	103.7947988	202.6969325	251.4515823	273.8076843	231.0391506	1.611475778	0.037693552
METTL18	80.95435418	72.16209818	46.24638752	101.7987375	96.49246705	97.74733295	1.484923357	0.037755283
CDK2AP1	2267.641853	2754.021994	2018.113634	4222.472419	2960.751767	4294.218059	1.630370033	0.037783557
HPS5	529.8830455	489.318337	357.1795461	696.0597435	583.9031339	746.4341789	1.472264701	0.03779449
CRTC3	267.7013303	372.6727536	347.3398892	594.261006	419.7834677	519.8380889	1.552962299	0.037906099
ZBTB3	11.95916596	0.988521893	24.5991423	64.38552627	40.41137509	35.54448471	3.737769221	0.037929288
BAG3	321.0576092	446.8118956	439.8326643	864.8542313	835.4433258	1486.203767	2.638482737	0.037930689
TMEFF2	78.19454665	115.6570615	98.39656918	8.700746794	4.948331643	67.75667398	0.278550077	0.03801941
GEMIN8	171.1080668	96.8751455	149.5627852	224.4792673	204.5310413	201.0484916	1.508956628	0.038029358
RNF126	222.624474	169.0372437	179.0817559	232.3099394	283.7043476	307.6819458	1.443198689	0.03806601
ALPK3	579.5595811	722.6095037	595.2992436	332.3685275	404.1137509	517.6165586	0.660932685	0.038202876
TOP2A	1493.055873	1014.223462	1436.58991	945.7711765	764.5172389	688.6743913	0.608276456	0.038296669
ZNF17	115.9119162	40.52939761	31.48690214	298.435615	376.0732049	154.3963555	4.41075424	0.038334023
F2RL2	1793.874894	2793.562869	1911.845339	1042.349466	754.6205756	1382.902608	0.489265139	0.03839458
CAMK2N1	601.6380413	340.0515312	324.7086783	670.8275778	748.0228001	693.1174518	1.667696421	0.038435794
CD81	1444.299273	1464.989445	1433.638013	1741.019433	2374.374467	2623.627278	1.551723433	0.038462206
LIMS2	91.99358429	68.20801061	66.90966704	109.6294096	94.84302317	108.8549844	1.379620784	0.038529132
TIMM50	216.1849231	184.853594	180.0657216	267.9830012	389.2687559	284.3558777	1.62037647	0.038745231

ACAA2	1390.942995	1510.461452	1457.25319	1296.411272	1025.129372	1230.727783	0.814991386	0.038795195
CBX8	0	0.988521893	0	9.570821473	32.16415568	18.8830075	61.32184334	0.038850393
YARS	1389.103123	1896.973512	1709.148407	2048.155795	2150.050099	2210.422643	1.282950915	0.038887768
TRAFD1	428.6901028	444.8348518	442.7845613	476.8009243	505.5545496	460.9675361	1.096492119	0.039020703
KIAA1656	45.9967921595	41.5179195	28.5350050657	25.2321657	20.6180485177	13.3291817647	0.509948	0.039195895
CYFIP2	153.6292858	128.5078461	204.6648639	228.8296407	254.8390796	318.7895972	1.64842857	0.039282651
KDM4B	387.2929899	358.8334471	247.9593543	476.8009243	565.7592512	449.8598846	1.501299056	0.039303569
NFKB1	544.602019	657.3670588	624.8182143	689.0991461	765.3419608	806.4154969	1.237613494	0.039382248
ZNF185	460.8878573	314.3499619	475.2554292	701.2801916	534.4198175	673.1236792	1.526456613	0.039410925
ZNF737	208.8254363	339.0630093	285.3500506	129.6411272	136.0791202	187.7193099	0.5441894	0.039443375
DNMT1	1194.076724	689.9882812	856.0501519	387.1832323	534.4198175	418.7584605	0.489162474	0.039480296
STAT2	952.1335974	543.6870411	639.5776997	426.3365929	216.9018704	169.9470675	0.380812102	0.039489007
PEX10	132.4707614	129.496368	171.2100304	276.683748	280.4054598	184.3870144	1.711715878	0.039606089
PCK2	262.1817152	209.5666413	207.616761	316.7071833	272.1582404	349.8910214	1.381814316	0.039648449
TOB1	293.4595339	528.8592127	267.6386682	659.516607	565.7592512	738.6588229	1.801845333	0.039775893
MAPK8IP2	0	0	0	23.49201634	5.773053584	17.77224235	#DIV/0!	0.039820557
NUP205	815.0631569	645.5047961	1227.989183	379.3525602	320.8168349	412.0938696	0.41370267	0.039858505
TMEM60	474.686895	401.3398885	375.8748943	341.939349	320.8168349	308.7927109	0.776058465	0.039993892
KIF18B	160.0688367	187.8191596	193.8412413	147.0426208	88.24524764	62.20284824	0.549150195	0.040048708
CDH20	0	0	0.983965692	2.610224038	2.474165822	1.110765147	6.296108755	0.040209871
MMRN2	3929.045985	4283.265362	3997.852606	3387.200727	3797.844536	3582.2176	0.881827869	0.040218261
GCHFR	59.79582979	42.50644139	63.95776997	40.0234352524	22.2674924	28.87989383	0.548362799	0.040253564
AAED1	135.2305689	162.1175904	79.70122104	247.1012089	181.4388269	267.6944005	1.8465338	0.040293798
DDIT3	819.6628361	797.7371676	500.8385371	1189.392087	935.2346806	1176.300291	1.558335851	0.040384199
ATAD1	518.8438154	500.1920778	526.4216451	992.7552092	695.2405959	717.5542851	1.556529397	0.040463884
EIF1	7436.761354	9587.673839	6813.962416	11863.46825	10638.91303	14869.81303	1.567730974	0.040585641
CNDP2	1867.469761	1610.302164	1561.553553	1899.373025	2131.906216	2053.804757	1.207519543	0.040694828
TJAP1	123.271403	126.5308023	130.867437	155.7433676	227.6232556	247.7006278	1.657781922	0.040706276
BIRC5	2918.95643	2527.65048	2549.455108	2354.422082	2018.919311	2194.871931	0.821431013	0.040731947
RAPGEF2	1260.312105	1296.940723	1155.175722	878.7754262	776.0633461	1106.322087	0.743761347	0.04076578
ZNF517	55.19615058	69.1965325	60.0219072	48.72418205	18.14388269	15.55071206	0.446921128	0.040812848

SREK1IP1	313.6981224	315.3384838	346.3559235	239.2705368	257.3132455	297.6850594	0.814306874	0.040825256
CTNNB1	6814.884725	7409.960109	7269.538531	6334.143666	6751.998527	6461.320861	0.909421904	0.040889175
TARS2	250.2225493	369.7071879	232.2159033	171.4047118	144.3263396	143.288704	0.538663503	0.041123874
TMEM107	138.9103123	162.1175904	122.0117458	107.0191856	88.24524764	108.8549844	0.718891051	0.041271416
SLC25A20	294.3794697	290.6254365	249.9272857	235.7902381	236.6951969	204.3807871	0.810684063	0.041284375
DENR	1455.338504	1733.8674	1541.874239	2398.795891	1812.738825	2238.191772	1.363267223	0.041368598
SASH1	1178.437815	1760.557491	1641.254774	2089.91938	2095.618451	1998.2665	1.350101899	0.041371309
SNORA80A	0	0	5.903794151	8.700746794	14.02027299	7.77535603	5.16555541	0.041468837
VEPH1	1403.822096	1359.217603	1317.530061	1106.734992	795.0319507	1154.084988	0.748878738	0.041503681
KGFLP2	61.635701483	27.678613	38.37466198	13.92119487	12.37082911	12.21841662	0.301595656	0.041504425
CISD1	487.5659968	382.5579726	464.4318065	526.395181	684.5192107	619.8069521	1.371783313	0.041539842
SPCS1	943.8541749	1378.988041	1318.514027	1957.668029	2416.435286	3497.799448	2.161805173	0.041550591
GIT2	401.0920275	456.6971145	664.176842	707.3707143	762.0430731	831.9630952	1.512107962	0.041592071
ATPIF1	991.6908387	991.4874586	909.1842993	1031.90857	1058.942972	1057.44842	1.088487303	0.041611817
MEGF8	994.4506462	1169.421399	1219.133492	965.7828941	892.3491397	848.6245724	0.800104102	0.041676497
CLCN2	44.15692046	51.40313843	34.43879921	59.1650782	75.87441853	59.98131795	1.50017329	0.041687945
ARFGEF2	685.352203	877.8074409	1105.977438	1242.466642	1240.381799	1267.383033	1.40503517	0.041688976
TRIM47	240.103255	437.9151986	382.7626541	548.147048	535.2445394	719.7758154	1.699848715	0.041743904
TRDMT1	109.4723653	101.817755	62.97380428	127.9009779	164.9443881	194.3839008	1.77649783	0.041763758
TMEM69	59.79582979	115.6570615	84.6210495	274.9435987	163.2949442	369.884794	3.107283008	0.041818341
PDSS2	77.27461081	79.08175143	56.08604443	145.3024715	171.5421636	97.74733295	1.95154995	0.041872936
PCSK7	1027.568337	1136.800177	750.7658229	421.1161448	546.7906466	702.003573	0.57284165	0.041969918
LINC01116	69.91512406	50.41461654	85.60501519	102.6688122	194.634378	164.3932418	2.241954886	0.042024703
LINC01186	0	4.942609464	0.983965692	7.830672114	9.896663287	5.553825736	3.92826557	0.042115028
SARM1	14.71897349	11.86226271	17.71138245	33.06283782	28.04054598	19.99377265	1.83094066	0.042126622
SELM	316.45793	282.7172614	193.8412413	346.2897224	450.2981796	418.7584605	1.532561385	0.042187722
STC2	1060.686027	1306.825942	946.5749955	1757.550852	1369.863143	1550.628145	1.41156288	0.042204487
PSMD4	2849.041306	2682.848417	3191.984704	2048.155795	2579.73023	2113.786075	0.772784175	0.042340773
IFT172	539.082404	370.6957098	305.0293645	191.4164295	226.7985337	155.5071206	0.47227408	0.042372
PALD1	184.9071044	240.21082	135.7872655	253.1917317	312.5696155	323.2326578	1.584927401	0.042423744
RHBDL3	12.8791018	31.63270057	13.77551969	3.480298718	0	0	0.05970936	0.042439872

ACSS2	293.4595339	312.3729182	204.6648639	147.9126955	156.6971687	191.0516053	0.611552265	0.042460403
FLJ10038	286.1000472	273.8205643	323.7247126	216.6485952	261.4368552	206.6023174	0.774844555	0.042466364
ACTB	39180.06755	55869.28034	63408.71711	85022.82759	98767.87488	144080.6795	2.069136601	0.042496196
EXD2	185.8270403	399.3628447	338.484198	465.4899535	523.6984323	516.5057934	1.630114135	0.042602568
TMOD2	3.679743372	17.79339407	0.983965692	25.2321657	19.79332657	27.76912868	3.241496488	0.042638126
RBKS	26.67813945	9.885218929	17.71138245	6.960597435	0	0	0.128247456	0.042697046
CXCL5	0	0	0.983965692	11.31097083	35.46304344	17.77224235	65.5980764	0.042730426
ANO5	4.599679215	1.977043786	4.919828459	6.090522756	9.896663287	11.10765147	2.356779562	0.042905499
BORCS8	101.1929427	71.17357629	78.71725535	105.2790362	122.0588472	137.7348783	1.453987868	0.043162373
IFI27L2	92.91352014	57.33426979	38.37466198	108.7593349	108.0385742	112.1872799	1.744146498	0.043352418
PPP1R16A	241.9431267	285.682827	277.4783251	198.3770269	230.9221434	158.839416	0.7305123	0.043355403
GPX4	1697.28163	1413.586307	1384.439728	1740.149359	2254.789786	2088.238477	1.353228316	0.043408368
ERCC3	1098.403396	1047.833206	955.4306868	857.8936339	925.3380173	910.8274207	0.868584158	0.043447983
A1BG	19.3186527	14.82782839	14.75948538	33.06283782	21.44277045	36.65524986	1.864002794	0.043469213
NUAK2	206.0656288	155.1979372	122.0117458	240.1406115	231.7468653	304.3496503	1.606200665	0.043514206
PRDM8	26.67813945	29.65565679	16.72741676	14.79126955	11.54610717	11.10765147	0.5125153	0.043617924
PLIN4	0	0	0	4.350373397	4.948331643	1.110765147	#DIV/0!	0.043647599
TP73	11.03923012	8.896697036	8.855691227	13.05112019	18.14388269	13.32918177	1.546428689	0.043783704
HSPB1	969.6123785	1094.293735	853.0982548	1339.915006	1858.098532	2361.486703	1.905893697	0.043817879
AGTPBP1	165.5884517	242.1878638	279.4462565	365.4313653	409.8868045	305.4604155	1.572676203	0.043879601
CGNL1	886.8181526	765.1159451	1171.903139	597.7413047	589.6761875	585.3732326	0.627794939	0.043894977
SPTLC3	0.919935843	0	0	7.830672114	31.33943374	21.1045378	65.52048615	0.043926248
TIPARP	539.082404	667.2522777	626.7861457	390.663531	503.0803837	488.7366648	0.754167733	0.044017707
MYO5C	65.31544485	91.93253604	52.15018167	168.7944878	117.9352375	111.0765147	1.899759937	0.044024797
SNORA71C	0	0	0	3.480298718	1.649443881	1.110765147	#DIV/0!	0.044087152
APOL1	83.71416171	63.26540115	68.87759843	87.00746794	110.51274	97.74733295	1.367883925	0.044157518
ANGPT2	128.791018	107.7488863	95.44467211	54.8147048	58.55525778	89.97197692	0.612504176	0.044242554
MCM7	1910.706746	1467.955011	1969.899315	1408.650906	1260.175125	1098.546731	0.704371271	0.044252485
MTSS1L	16.55884517	14.82782839	22.63121091	26.97231506	43.71026285	53.31672706	2.295523162	0.044259686
WDR4	1145.320124	1073.534776	1186.662624	810.9096012	1039.149645	914.1597161	0.811688368	0.044270994
WASH7P	2.759807529	0	1.967931384	5.220448076	4.948331643	3.332295442	2.855715049	0.044336545

NBPF11	6.439550901	4.942609464	9.839656918	2.610224038	3.298887762	0	0.278445136	0.04433759
KIF14	300.8190206	286.6713489	245.991423	129.6411272	194.634378	225.4853249	0.659595488	0.044385409
MCC	815.9830927	691.965325	820.627387	687.3589967	586.3772997	589.8162932	0.800297154	0.044434349
HIVEP1	588.7589395	562.4689571	604.1549348	852.6731858	674.6225474	961.9226175	1.418048705	0.044508562
SDK1	10.11929427	4.942609464	0	12.18104551	23.91693628	17.77224235	3.576587999	0.044514327
SRP14	1560.21119	1898.950556	1909.877408	2056.856542	2470.866934	2635.845694	1.334236716	0.044549221
LRRC75B	57.03602226	45.47200707	56.08604443	91.35784133	79.99802824	134.4025828	1.927931133	0.044599719
PNRC1	1599.768431	2086.769716	1710.132372	2331.800141	2226.74924	2774.691338	1.358845364	0.044605
SORT1	52.43634305	113.6800177	43.29449044	180.1054586	193.809656	116.6303405	2.342502561	0.044685431
STARD7	9049.408887	11297.81671	9773.731217	7513.094856	6326.442006	8451.812005	0.740061114	0.044693986
SNORD45B	12.8791018	16.80487218	17.71138245	12.18104551	10.72138523	11.10765147	0.717582581	0.044733651
FASN	257.582036	204.6240318	215.4884865	138.341874	191.3354902	127.7379919	0.674957993	0.044788553
NDFIP2	87.39390508	301.4991773	153.4986479	412.415398	320.8168349	456.5244755	2.1935377	0.044894316
PDP2	68.07525238	56.34574789	51.16621598	154.0032183	80.82275018	135.513348	2.109147376	0.044963934
NRSN2	229.0640249	258.004214	211.5526237	381.0927096	347.207937	272.1374611	1.432018654	0.044988877
RNPS1	1650.364902	1689.383915	1451.349395	1944.616908	1908.40657	1752.787402	1.170047165	0.045040731
CORO7	80.95435418	79.08175143	74.78139258	82.65709454	93.19357928	93.30427236	1.146230363	0.045057745
LOC101929231	5.519615058	2.965565679	6.887759843	2.610224038	0.824721941	0	0.22344105	0.045194805
MIR4458HG	310.0183791	289.6369146	390.6343797	218.3887445	249.0660261	244.3683324	0.718802914	0.045205346
C1QL1	2.759807529	2.965565679	0	4.350373397	9.071941346	6.664590883	3.508401094	0.045228699
WDR11	1835.272007	1610.302164	1997.450354	1575.705244	1304.71011	1360.687305	0.779181251	0.04525022
METTL5	373.4939522	281.7287395	431.9609387	478.5410737	651.530333	763.0956561	1.74134986	0.045477311
CUL9	257.582036	225.3829916	238.1196974	118.3301564	192.9849341	53.31672706	0.505671255	0.045541042
DTX3L	104.8726861	185.8421159	183.0176187	294.9553163	215.2524265	267.6944005	1.642070733	0.045620695
POLR3C	315.5379941	510.0772967	368.9871344	759.5751951	541.842315	630.9146036	1.617552478	0.045645663
TCEB1	519.7637513	602.9983547	724.1987492	740.4335522	859.3602621	885.2798223	1.345493398	0.045693328
FAM76A	90.15371261	170.0257656	141.6910596	255.8019557	205.3557632	196.6054311	1.63675385	0.045736172
NQO1	2509.58498	2800.482523	2935.169659	3170.552132	3923.202271	4391.965392	1.393012665	0.045785314
TM9SF4	545.5219549	614.8606174	457.5440467	311.4867352	404.1137509	417.6476953	0.700432373	0.045803417
NHLRC3	372.5740164	569.3886103	510.6781941	313.2268846	275.4571281	338.7833699	0.638469861	0.045838819
GTF3A	417.6508727	431.9840672	314.8690214	553.3674961	763.692517	1000.799398	1.990426386	0.045905406

MYL12A	2485.666648	2473.281776	2625.220466	2915.620251	2780.962384	3308.969373	1.187414487	0.045979048
ANGPTL2	251.1424851	225.3829916	241.0715945	204.4675497	155.8724468	204.3807871	0.786960825	0.046058947
C22ORF29	1772.716369	1500.576233	1623.543392	2785.979123	2760.344335	1909.405288	1.522560436	0.046075683
DLD	1694.521823	1379.976562	1617.639597	2213.469984	1826.759098	1931.620591	1.272735307	0.046076476
ING5	348.6556845	357.8449252	374.8909286	400.2343525	527.822042	536.4995661	1.354325338	0.046091264
YWHAG	902.4570619	785.8749049	986.9175889	1031.038495	1077.086854	1155.195753	1.219819323	0.046102725
STOML1	525.2833663	561.4804352	499.8545715	430.6869663	462.6690087	337.6726047	0.775881964	0.046221817
ATG4A	380.853439	296.5565679	360.1314432	272.3333746	268.8593526	199.9377265	0.714314068	0.046231813
LRRC16A	76.35467496	158.1635029	93.47674072	21.75186698	50.30803837	31.10142412	0.314521121	0.04636921
AMBRA1	160.0688367	125.5422804	211.5526237	358.4707679	222.674924	360.9986728	1.895038369	0.046485516
MKNK1	275.060817	343.0170968	389.650414	164.4441144	268.0346307	177.7224235	0.6055215	0.046526321
CDC42SE1	217.1048589	162.1175904	292.2378105	370.6518134	385.9698682	303.2388852	1.578441242	0.046537042
NDRG1	83.71416171	131.4734118	154.4826136	174.8850106	211.9535387	184.3870144	1.545230272	0.046662167
LOC100506302	17.47878102	2.965565679	38.37466198	54.8147048	43.71026285	71.08896942	2.883658547	0.046754961
SOX18	426.8502311	415.179195	737.9742689	949.2514752	1757.482455	2271.514726	3.15078292	0.046948638
CORO1C	4513.205245	4788.400049	5381.308369	3982.331808	4337.212685	3776.6015	0.823824635	0.047037851
KIAA1549	599.7981696	578.2853073	518.5499196	354.9904692	315.8685032	502.0658465	0.691324844	0.047317343
ANKRD33	1.839871686	0	0	7.830672114	8.247219406	19.99377265	19.60553252	0.047400308
SKAP2	294.3794697	387.500582	355.2116148	471.5804762	572.3570268	768.6494819	1.747759666	0.047422039
SPATA2L	156.3890933	103.7947988	100.3645006	76.56657179	60.20470166	64.42437854	0.558026762	0.047434665
HEXDC	134.3106331	103.7947988	148.5788195	95.70821473	57.73053584	85.52891633	0.617991723	0.047470933
TSPYL2	418.5708085	220.4403821	318.8048842	179.235384	154.2230029	112.1872799	0.465272695	0.047620865
MFSD9	286.1000472	306.4417868	319.7888498	364.5612907	401.6395851	500.9550814	1.38892178	0.047622301
PIK3CD	76.35467496	64.25392304	40.34259337	113.979783	303.4976741	247.7006278	3.67600832	0.047778011
TFE3	218.0247948	159.1520248	149.5627852	225.349342	307.6212838	264.362105	1.513713273	0.047799479
DNAJC16	836.2216812	982.5907615	812.7556615	700.4101169	583.078412	743.1018835	0.77010753	0.047804433
BBX	721.2297009	742.3799416	859.9860147	910.9681893	1050.695752	905.273595	1.233836674	0.047817783
ZYX	1082.764487	1134.823133	1385.423694	1749.72018	1872.943527	2744.700679	1.76723408	0.047842284
HIST1H4E	8.279422587	3.954087572	16.72741676	18.27156827	22.2674924	27.76912868	2.358632703	0.04788191
SLC9A5	48.75659968	26.69009111	50.18225028	84.3972439	91.5441354	57.75978765	1.860249438	0.047955975
SALL2	36.79743372	77.10470765	55.10207874	4.350373397	32.98887762	4.443060589	0.24722644	0.047968105

IFT88	34.03762619	66.23096682	112.1720889	128.7710525	161.6455004	222.1530294	2.412765661	0.048009465
BRCA2	89.23377677	92.92105793	154.4826136	65.25560095	40.41137509	37.766015	0.426075565	0.048214347
NHP2	1136.120766	980.6137178	1026.276217	1138.927755	1292.339281	1296.262927	1.185974315	0.048395616
GHDC	103.9527503	58.32279168	107.2522604	31.32268846	56.9058139	23.32606809	0.413888918	0.048449584
DYNC1LI2	3764.377469	3112.855441	3880.760689	2913.010027	2998.688976	2694.716247	0.800001894	0.048466971
PCDH10	5991.542145	7090.667538	4805.688439	4401.707803	3880.31673	3848.801235	0.678158255	0.048473334
C2CD5	543.6820832	574.3312198	415.233522	376.7423362	181.4388269	331.0080139	0.579938704	0.048507255
DDX47	1298.94941	1388.87326	1442.493704	760.4452698	1183.475985	1067.445306	0.729088595	0.048557199
GRWD1	636.5956033	605.9639203	658.2730478	457.6592814	584.7278559	419.8692256	0.769271521	0.04856843
ATHL1	566.6804793	276.78613	507.726297	151.3929942	256.4885235	129.9595222	0.398049041	0.048646982
NUDT16L1	400.1720917	552.5837381	490.9988802	339.329125	376.0732049	344.3371956	0.734016324	0.048875604
DOK3	76.35467496	30.64417868	57.07001013	21.75186698	18.14388269	3.332295442	0.263475008	0.048927971
ST7L	154.5492216	120.5996709	214.5045208	247.1012089	230.0974214	247.7006278	1.480433381	0.049044447
BCDIN3D	63.47557316	71.17357629	68.87759843	36.54313653	32.16415568	59.98131795	0.632293355	0.049166076
PPIL3	26.67813945	55.357226	46.24638752	82.65709454	61.0294236	96.63656781	1.873400389	0.049183697
ARMCX2	1022.968657	756.2192481	1155.175722	542.0565253	681.2203229	663.1267929	0.642866352	0.049307587
MAGOH	57.95595811	89.95549225	115.1239859	125.2907538	149.2746712	179.9439538	1.727939723	0.049376384
UROD	2837.08214	2153.989205	2813.157913	1540.032183	2034.589027	1958.278954	0.708961767	0.049392898
CHMP1A	1041.367374	1009.280853	1070.554673	637.76474	954.2032852	729.7727017	0.743860877	0.049477632
CCDC80	850.0207189	759.1848137	1018.404491	1081.502826	1150.487107	1066.334541	1.255256467	0.04948579
EARS2	143.5099915	196.7158567	198.7610698	234.9201634	221.850202	239.9252718	1.292602128	0.049530136
SNAI2	0	0	10.82362261	67.86582499	46.18442867	18.8830075	12.28177164	0.049641
UBL5	1093.803717	729.529157	645.4814938	1169.380369	1385.53286	1195.183298	1.518986837	0.04974
FAM195B	264.9415228	164.0946342	185.9695158	288.8647936	282.8796256	304.3496503	1.424530063	0.049742479
STARD13	489.4058684	732.4947226	648.4333909	418.5059208	447.8240137	396.5431575	0.675212611	0.049763398
CDIPT	745.1480328	790.8175143	759.6215141	828.3110948	795.8566726	808.6370272	1.059774572	0.049810779
LOC102723703	13.79903764	30.64417868	36.4067306	9.570821473	9.071941346	0	0.230584726	0.049874456
UBOX5	11.95916596	42.50644139	40.34259337	57.42492884	90.71941346	64.42437854	2.242092132	0.049890715
ITGAE	201.4659496	179.9109845	166.2902019	203.597475	245.7671383	254.3652187	1.28495903	0.049977774
PXMP2	102.1128786	108.7374082	177.1138245	179.235384	214.4277045	223.2637946	1.590164825	0.049990088
ZMIZ2	526.2033022	455.7085926	674.0164989	346.2897224	380.1968146	384.3247409	0.670808763	0.049994519

A.2. miR-744 Targets Which are Cytoskeletal-Associated Proteins

A list of known cytoskeletal-associated proteins was obtained from Pantherdb.org and compared to a list of predicted miR-744 targets from miRWalk.

Table A2. List of predicted miR-744 Targets which are cytoskeletal-associated proteins

ABLIM1	ABLIM2	ABLIM3	ABTB2	ACTB
ACTG1	ACTR1A	ACTR2	ACTR3B	ADD1
ADD2	ARHGAP36	ARHGAP6	ARPC4	ARPC5
BFSP2	BTBD1	BTBD11	BTBD2	BTBD3
BTBD9	CALD1	CAP2	CAPG	CAPZA1
CCDC67	CFL2	CGN	CGNL1	CKAP5
CLIP1	CLIP2	CLIP4	CNN3	CORO1C
CORO2A	CORO2B	CORO6	COTL1	CRIP2
CRIP3	CSRP1	CTNNA3	CTNNB1	CTNND2
CTTN	DAAM1	DAAM2	DBNL	DCTN5
DMTN	DNAL4	DNALI1	DNM1	DNM1L
DNM2	DNM3	DSTN	DYNC1I1	DYNC1LI2
EMP2	ERMN	ESPNL	EVPL	FBLIM1
FCHO2	FHDC1	FHL1	FHOD3	FIGNL1
FMNL1	FMNL3	FNBP4	FRMD4A	FRMD4B
FSCN1	GAS7	GFAP	GSG1L	GSN
HCLS1	HIP1	IFT57	JUP	KIF11
KIF13A	KIF14	KIF17	KIF1A	KIF1B
KIF1C	KIF21A	KIF21B	KIF24	KIF26A
KIF3B	KIF3C	KIF5C	KLHL11	KPRP
KRT1	KRT2	KRT20	KRT25	KRT6B
KRT71	KRT73	KRT76	KRT80	KRT81
KRT9	LCP1	LDB3	LHX2	LHX3
LHX5	LHX6	LIMA1	LIMCH1	LIMD2
LIMS1	LIMS2	LMNA	LMNB1	LMNB2
LMO1	LMO7	LMOD1	LMX1B	LPP
MAP1A	MAP1B	MAP1S	MAP7D2	MAPKAPK3
MAPRE1	MAPRE2	MESDC1	MKNK1	MKNK2
MLLT4	MLPH	MOBP	MPRIP	MSN
MTSS1	MTSS1L	MYH10	MYH11	MYH9
MYL6B	MYO10	MYO16	MYO18A	MYO1C
MYO1D	MYO1E	MYO1H	MYO5A	MYO5B
MYO5C	MYO6	MYO9A	MYO9B	MYRIP
NES	NF2	NFE2L1	NUDC	NUDCD3

ODF4	OPA1	PACSIN1	PACSIN2	PARVB
PARVG	PDE4DIP	PDLIM5	PDZD7	PKP1
PKP4	PLEK	PLS3	PMP22	PPL
PRC1	PRICKLE1	PRICKLE2	PRICKLE3	PXN
RCSD1	RDX	SDC1	SDC4	SGCD
SGIP1	SHROOM3	SNCG	SPAG16	SPAST
SPOP	SPOPL	SPTB	SPTBN1	SPTBN4
STOML1	SUN1	SUN2	SYN2	SYN3
SYNM	SYNPO	TBCEL	TEX9	TGFB1I1/HIC5
TLN2	TMOD1	TMOD2	TMOD3	TNNI1
TNNT2	TPM1	TPM3	TPM4	TPPP
TPPP3	TRIOBP	TTL	TTLL10	TTLL11
TTLL12	TTLL4	TTLL5	TTLL6	TUBB2A
TUBE1	TUBG2	TUBGCP4	TUBGCP5	TWF2
VCL	VPS4A	WASF2	WASF3	WASL
WDR1	WDR78	WIPF1	XIRP1	XIRP2
ZBTB10	ZBTB43	ZBTB8B	ZBTB9	ZFHX2
ZFHX3	ZW10	ZYX		

REFERENCES

1. Domanski, M., et al., *Can we dramatically reduce the incidence of coronary heart disease?* Nat Rev Cardiol, 2011. **8**(12): p. 721-5.
2. Glaser, R., et al., *Clinical progression of incidental, asymptomatic lesions discovered during culprit vessel coronary intervention.* Circulation, 2005. **111**(2): p. 143-9.
3. Finn, A.V., et al., *Concept of vulnerable/unstable plaque.* Arterioscler Thromb Vasc Biol, 2010. **30**(7): p. 1282-92.
4. Finn, A.V. and R.K. Jain, *Coronary plaque neovascularization and hemorrhage: a potential target for plaque stabilization?* JACC Cardiovasc Imaging, 2010. **3**(1): p. 41-4.
5. Maldonado, N., et al., *A mechanistic analysis of the role of microcalcifications in atherosclerotic plaque stability: potential implications for plaque rupture.* Am J Physiol Heart Circ Physiol, 2012. **303**(5): p. H619-28.
6. Spain, D.M., *Atherosclerosis.* Sci Am, 1966. **215**(2): p. 48-56.
7. Suo, J., J.N. Oshinski, and D.P. Giddens, *Blood flow patterns in the proximal human coronary arteries: relationship to atherosclerotic plaque occurrence.* Mol Cell Biomech, 2008. **5**(1): p. 9-18.
8. Steinman, D.A. and C.A. Taylor, *Flow imaging and computing: large artery hemodynamics.* Ann Biomed Eng, 2005. **33**(12): p. 1704-9.

9. Davies, P.F., et al., *A spatial approach to transcriptional profiling: mechanotransduction and the focal origin of atherosclerosis.* Trends Biotechnol, 1999. **17**(9): p. 347-51.

10. Libby, P., *Coronary artery injury and the biology of atherosclerosis: inflammation, thrombosis, and stabilization.* Am J Cardiol, 2000. **86**(8B): p. 3J-8J; discussion 8J-9J.

11. Caro, C.G., J.M. Fitz-Gerald, and R.C. Schroter, *Arterial wall shear and distribution of early atheroma in man.* Nature, 1969. **223**(5211): p. 1159-60.

12. Caro, C.G., *Discovery of the role of wall shear in atherosclerosis.* Arterioscler Thromb Vasc Biol, 2009. **29**(2): p. 158-61.

13. Caro, C.G. and R.M. Nerem, *Transport of 14 C-4-cholesterol between serum and wall in the perfused dog common carotid artery.* Circ Res, 1973. **32**(2): p. 187-205.

14. Friedman, M.H., et al., *Correlation of human arterial morphology with hemodynamic measurements in arterial casts.* J Biomech Eng, 1981. **103**(3): p. 204-7.

15. Friedman, M.H., et al., *Correlation between intimal thickness and fluid shear in human arteries.* Atherosclerosis, 1981. **39**(3): p. 425-36.

16. Zarins, C.K., et al., *Carotid bifurcation atherosclerosis. Quantitative correlation of plaque localization with flow velocity profiles and wall shear stress.* Circ Res, 1983. **53**(4): p. 502-14.

17. Ku, D.N., et al., *Pulsatile flow and atherosclerosis in the human carotid bifurcation. Positive correlation between plaque location and low oscillating shear stress.* Arteriosclerosis, 1985. **5**(3): p. 293-302.

18. Tada, S. and J.M. Tarbell, *A computational study of flow in a compliant carotid bifurcation-stress phase angle correlation with shear stress.* Ann Biomed Eng, 2005. **33**(9): p. 1202-12.

19. Davies, P.F., *Hemodynamic shear stress and the endothelium in cardiovascular pathophysiology.* Nat Clin Pract Cardiovasc Med, 2009. **6**(1): p. 16-26.

20. Janiczek, R.L., et al., *Three-dimensional phase contrast angiography of the mouse aortic arch using spiral MRI.* Magn Reson Med, 2011. **66**(5): p. 1382-90.

21. Nerem, R.M., M.J. Levesque, and J.F. Cornhill, *Vascular endothelial morphology as an indicator of the pattern of blood flow.* J Biomech Eng, 1981. **103**(3): p. 172-6.

22. Dewey, C.F., Jr., et al., *The dynamic response of vascular endothelial cells to fluid shear stress.* J Biomech Eng, 1981. **103**(3): p. 177-85.

23. Frangos, J.A., et al., *Flow effects on prostacyclin production by cultured human endothelial cells.* Science, 1985. **227**(4693): p. 1477-9.

24. Grabowski, E.F., E.A. Jaffe, and B.B. Weksler, *Prostacyclin production by cultured endothelial cell monolayers exposed to step increases in shear stress.* J Lab Clin Med, 1985. **105**(1): p. 36-43.

25. Bell, R.M. and D.J. Burns, *Lipid activation of protein kinase C.* J Biol Chem, 1991. **266**(8): p. 4661-4.

26. Shen, J., *[Effects of verapamil on prostacyclin, thromboxane and pancreatic blood flow of rats with experimental acute pancreatitis]*. Zhonghua Yi Xue Za Zhi, 1991. **71**(9): p. 488-91, 34.

27. Kuchan, M.J. and J.A. Frangos, *Role of calcium and calmodulin in flow-induced nitric oxide production in endothelial cells.* Am J Physiol, 1994. **266**(3 Pt 1): p. C628-36.

28. Kuchan, M.J., H. Jo, and J.A. Frangos, *Role of G proteins in shear stress-mediated nitric oxide production by endothelial cells.* Am J Physiol, 1994. **267**(3 Pt 1): p. C753-8.

29. Korenaga, R., et al., *Laminar flow stimulates ATP- and shear stress-dependent nitric oxide production in cultured bovine endothelial cells.* Biochem Biophys Res Commun, 1994. **198**(1): p. 213-9.

30. Meadows, S.M., M.C. Salanga, and P.A. Krieg, *Kruppel-like factor 2 cooperates with the ETS family protein ERG to activate Flk1 expression during vascular development.* Development, 2009. **136**(7): p. 1115-25.

31. Warboys, C.M., et al., *Acute and chronic exposure to shear stress have opposite effects on endothelial permeability to macromolecules*. Vol. 298. 2010. H1850-H1856.

32. Kurose, I., et al., *Mechanisms of endothelin-induced macromolecular leakage in microvascular beds of rat mesentery.* Eur J Pharmacol, 1993. **250**(1): p. 85-94.

33. Baldwin, A.L., G. Thurston, and H. al Naemi, *Inhibition of nitric oxide synthesis increases venular permeability and alters endothelial actin cytoskeleton.* Am J Physiol, 1998. **274**(5 Pt 2): p. H1776-84.

34. Hillsley, M.V. and J.M. Tarbell, *Oscillatory shear alters endothelial hydraulic conductivity and nitric oxide levels.* Biochem Biophys Res Commun, 2002. **293**(5): p. 1466-71.

35. Tarbell, J.M., *Shear stress and the endothelial transport barrier.* Cardiovasc Res, 2010. **87**(2): p. 320-30.

36. Son, D.J., et al., *The atypical mechanosensitive microRNA-712 derived from pre-ribosomal RNA induces endothelial inflammation and atherosclerosis.* Nat Commun, 2013. **4**: p. 3000.

37. Huynh, J., et al., *Age-related intimal stiffening enhances endothelial permeability and leukocyte transmigration.* Sci Transl Med, 2011. **3**(112): p. 112ra122.

38. Kim, C.W., et al., *Prevention of abdominal aortic aneurysm by anti-microRNA-712 or anti-microRNA-205 in angiotensin II-infused mice.* Arterioscler Thromb Vasc Biol, 2014. **34**(7): p. 1412-21.

39. Tressel, S.L., et al., *Laminar shear inhibits tubule formation and migration of endothelial cells by an angiopoietin-2 dependent mechanism.* Arterioscler Thromb Vasc Biol, 2007. **27**(10): p. 2150-6.

40. Harrison, M., et al., *The role of platelet-endothelial cell adhesion molecule-1 in atheroma formation varies depending on the site-specific hemodynamic environment.* Arterioscler Thromb Vasc Biol, 2013. **33**(4): p. 694-701.

41. Chien, S., J.J. Chiu, and Y.S. Li, *Focal adhesion kinase phosphorylation in flow-activation of endothelial NF-kappaB. Focus on "Focal adhesion kinase modulates activation of NF-kappaB by flow in endothelial cells".* Am J Physiol Cell Physiol, 2009. **297**(4): p. C800-1.

42. Chiu, J.J., S. Usami, and S. Chien, *Vascular endothelial responses to altered shear stress: pathologic implications for atherosclerosis.* Ann Med, 2009. **41**(1): p. 19-28.

43. Hajra, L., et al., *The NF-kappa B signal transduction pathway in aortic endothelial cells is primed for activation in regions predisposed to atherosclerotic lesion formation.* Proc Natl Acad Sci U S A, 2000. **97**(16): p. 9052-7.

44. Passerini, A.G., et al., *Coexisting proinflammatory and antioxidative endothelial transcription profiles in a disturbed flow region of the adult porcine aorta.* Proc Natl Acad Sci U S A, 2004. **101**(8): p. 2482-7.

45. Bussolari, S.R., C.F. Dewey, Jr., and M.A. Gimbrone, Jr., *Apparatus for subjecting living cells to fluid shear stress.* Rev Sci Instrum, 1982. **53**(12): p. 1851-4.

46. Franke, R.P., et al., *Induction of human vascular endothelial stress fibres by fluid shear stress.* Nature, 1984. **307**(5952): p. 648-9.

47. Go, Y.M., et al., *Protein kinase B/Akt activates c-Jun NH(2)-terminal kinase by increasing NO production in response to shear stress.* J Appl Physiol (1985), 2001. **91**(4): p. 1574-81.

48. Jo, H., H. Song, and A. Mowbray, *Role of NADPH oxidases in disturbed flow- and BMP4- induced inflammation and atherosclerosis.* Antioxid Redox Signal, 2006. **8**(9-10): p. 1609-19.

49. Frangos, J.A., L.V. McIntire, and S.G. Eskin, *Shear stress induced stimulation of mammalian cell metabolism.* Biotechnol Bioeng, 1988. **32**(8): p. 1053-60.

50. Schaff, U.Y., et al., *Vascular mimetics based on microfluidics for imaging the leukocyte--endothelial inflammatory response.* Lab Chip, 2007. **7**(4): p. 448-56.

51. Ashpole, N.E., et al., *Shear stress-triggered nitric oxide release from Schlemm's canal cells.* Invest Ophthalmol Vis Sci, 2014. **55**(12): p. 8067-76.

52. Ganguly, A., et al., *Isolation of human umbilical vein endothelial cells and their use in the study of neutrophil transmigration under flow conditions.* J Vis Exp, 2012(66): p. e4032.

53. Rezvan, A., et al., *Animal, in vitro, and ex vivo models of flow-dependent atherosclerosis: role of oxidative stress.* Antioxid Redox Signal, 2011. **15**(5): p. 1433-48.

54. Paigen, B., et al., *Comparison of atherosclerotic lesions and HDL-lipid levels in male, female, and testosterone-treated female mice from strains C57BL/6, BALB/c, and C3H.* Atherosclerosis, 1987. **64**(2-3): p. 215-21.

55. Paigen, B., et al., *Quantitative assessment of atherosclerotic lesions in mice.* Atherosclerosis, 1987. **68**(3): p. 231-40.

56. Paigen, B., et al., *Variation in susceptibility to atherosclerosis among inbred strains of mice.* Atherosclerosis, 1985. **57**(1): p. 65-73.

57. Paigen, B., M.B. Havens, and A. Morrow, *Effect of 3-methylcholanthrene on the development of aortic lesions in mice.* Cancer Res, 1985. **45**(8): p. 3850-5.

58. Piedrahita, J.A., et al., *Generation of mice carrying a mutant apolipoprotein E gene inactivated by gene targeting in embryonic stem cells.* Proc Natl Acad Sci U S A, 1992. **89**(10): p. 4471-5.

59. Plump, A.S., et al., *Severe hypercholesterolemia and atherosclerosis in apolipoprotein E-deficient mice created by homologous recombination in ES cells.* Cell, 1992. **71**(2): p. 343-53.

60. Zhang, S.H., et al., *Spontaneous hypercholesterolemia and arterial lesions in mice lacking apolipoprotein E.* Science, 1992. **258**(5081): p. 468-71.

61. Ishibashi, S., et al., *The two-receptor model of lipoprotein clearance: tests of the hypothesis in "knockout" mice lacking the low density lipoprotein receptor, apolipoprotein E, or both proteins.* Proc Natl Acad Sci U S A, 1994. **91**(10): p. 4431-5.

62. Lichtman, A.H., et al., *Hyperlipidemia and atherosclerotic lesion development in LDL receptor-deficient mice fed defined semipurified diets with and without cholate.* Arterioscler Thromb Vasc Biol, 1999. **19**(8): p. 1938-44.

63. Hardin, N.J., C.R. Minick, and G.E. Murphy, *Experimental induction of atheroarteriosclerosis by the synergy of allergic injury to arteries and lipid-rich diet. 3. The role of earlier acquired fibromuscular intimal thickening in the pathogenesis of later developing atherosclerosis.* Am J Pathol, 1973. **73**(2): p. 301-26.

64. Melkumyants, A.M., S.A. Balashov, and V.M. Khayutin, *Endothelium dependent control of arterial diameter by blood viscosity.* Cardiovasc Res, 1989. **23**(9): p. 741-7.

65. Clowes, A.W., et al., *Absence of enhanced intimal thickening in the response of the carotid arterial wall to endothelial injury in hypercholesterolemic rats.* Lab Invest, 1976. **35**(1): p. 6-17.

66. Lindner, V., J. Fingerle, and M.A. Reidy, *Mouse model of arterial injury.* Circ Res, 1993. **73**(5): p. 792-6.

67. Feuerstein, G.Z. and R.R. Ruffolo, Jr., *Carvedilol, a novel vasodilating beta-blocker with the potential for cardiovascular organ protection.* Eur Heart J, 1996. **17 Suppl B**: p. 24-9.

68. Morishita, T., et al., *Vasculoprotective roles of neuronal nitric oxide synthase.* FASEB J, 2002. **16**(14): p. 1994-6.

69. Hollestelle, S.C., et al., *Toll-like receptor 4 is involved in outward arterial remodeling.* Circulation, 2004. **109**(3): p. 393-8.

70. Lardenoye, J.H., et al., *Accelerated atherosclerosis by placement of a perivascular cuff and a cholesterol-rich diet in ApoE*3Leiden transgenic mice.* Circ Res, 2000. **87**(3): p. 248-53.

71. Sasaguri, Y., et al., *Role of histamine produced by bone marrow-derived vascular cells in pathogenesis of atherosclerosis.* Circ Res, 2005. **96**(9): p. 974-81.

72. da Cunha, V., et al., *Angiotensin II induces histomorphologic features of unstable plaque in a murine model of accelerated atherosclerosis.* J Vasc Surg, 2006. **44**(2): p. 364-71.

73. Ivan, E., et al., *Expansive arterial remodeling is associated with increased neointimal macrophage foam cell content: the murine model of macrophage-rich carotid artery lesions.* Circulation, 2002. **105**(22): p. 2686-91.

74. Jonsson-Rylander, A.C., et al., *Role of ADAMTS-1 in atherosclerosis: remodeling of carotid artery, immunohistochemistry, and proteolysis of versican.* Arterioscler Thromb Vasc Biol, 2005. **25**(1): p. 180-5.

75. Leidenfrost, J.E., et al., *A model of primary atherosclerosis and post-angioplasty restenosis in mice.* Am J Pathol, 2003. **163**(2): p. 773-8.

76. Liu, S.L., et al., *Dextromethorphan reduces oxidative stress and inhibits atherosclerosis and neointima formation in mice.* Cardiovasc Res, 2009. **82**(1): p. 161-9.

77. Nakamura, K., et al., *Statin prevents plaque disruption in apoE-knockout mouse model through pleiotropic effect on acute inflammation.* Atherosclerosis, 2009. **206**(2): p. 355-61.

78. Rekhter, M., et al., *Genetic ablation of IRAK4 kinase activity inhibits vascular lesion formation.* Biochem Biophys Res Commun, 2008. **367**(3): p. 642-8.

79. Tsutsui, M., *Neuronal nitric oxide synthase as a novel anti-atherogenic factor.* J Atheroscler Thromb, 2004. **11**(2): p. 41-8.

80. Yamada, S., et al., *Matrix metalloproteinase 12 accelerates the initiation of atherosclerosis and stimulates the progression of fatty streaks to fibrous plaques in transgenic rabbits.* Am J Pathol, 2008. **172**(5): p. 1419-29.

81. Zhang, L.N., et al., *Endothelial NO synthase deficiency promotes smooth muscle progenitor cells in association with upregulation of stromal cell-derived factor-1alpha in a mouse model of carotid artery ligation.* Arterioscler Thromb Vasc Biol, 2006. **26**(4): p. 765-72.

82. Sawchuk, A.P., et al., *A prospective, in vivo study of the relationship between blood flow hemodynamics and atherosclerosis in a hyperlipidemic swine model.* J Vasc Surg, 1994. **19**(1): p. 58-63; discussion 63-4.

83. Nam, D., et al., *Partial carotid ligation is a model of acutely induced disturbed flow, leading to rapid endothelial dysfunction and atherosclerosis.* American journal of physiology. Heart and circulatory physiology, 2009. **297**(4): p. H1535-43.

84. Osawa, M., et al., *Tyrosine phosphorylation of platelet endothelial cell adhesion molecule-1 (PECAM-1, CD31) in mechanically stimulated vascular endothelial cells.* Eur J Cell Biol, 1997. **72**(3): p. 229-37.

85. Osawa, M., et al., *Evidence for a role of platelet endothelial cell adhesion molecule-1 in endothelial cell mechanosignal transduction: is it a mechanoresponsive molecule?* J Cell Biol, 2002. **158**(4): p. 773-85.

86. Tzima, E., et al., *Activation of integrins in endothelial cells by fluid shear stress mediates Rho-dependent cytoskeletal alignment*. Vol. 20. 2001. 4639-4647.

87. Tzima, E., et al., *A mechanosensory complex that mediates the endothelial cell response to fluid shear stress.* Nature, 2005. **437**(7057): p. 426-31.

88. Pries, A.R., T.W. Secomb, and P. Gaehtgens, *The endothelial surface layer.* Pflugers Arch, 2000. **440**(5): p. 653-66.

89. Adamson, R.H. and G. Clough, *Plasma proteins modify the endothelial cell glycocalyx of frog mesenteric microvessels.* J Physiol, 1992. **445**: p. 473-86.

90. Koo, A., C.F. Dewey, Jr., and G. Garcia-Cardena, *Hemodynamic shear stress characteristic of atherosclerosis-resistant regions promotes glycocalyx formation in cultured endothelial cells.* Am J Physiol Cell Physiol, 2013. **304**(2): p. C137-46.

91. Ihrcke, N.S. and J.L. Platt, *Shedding of heparan sulfate proteoglycan by stimulated endothelial cells: evidence for proteolysis of cell-surface molecules.* J Cell Physiol, 1996. **168**(3): p. 625-37.

92. Fuster, M.M. and L. Wang, *Endothelial heparan sulfate in angiogenesis.* Prog Mol Biol Transl Sci, 2010. **93**: p. 179-212.

93. Coombe, D.R. and W.C. Kett, *Heparan sulfate-protein interactions: therapeutic potential through structure-function insights.* Cell Mol Life Sci, 2005. **62**(4): p. 410-24.

94. Hileman, R.E., et al., *Glycosaminoglycan-protein interactions: definition of consensus sites in glycosaminoglycan binding proteins.* Bioessays, 1998. **20**(2): p. 156-67.

95. Munoz, E.M. and R.J. Linhardt, *Heparin-binding domains in vascular biology.* Arterioscler Thromb Vasc Biol, 2004. **24**(9): p. 1549-57.

96. Jackson, R.L., S.J. Busch, and A.D. Cardin, *Glycosaminoglycans: molecular properties, protein interactions, and role in physiological processes.* Physiol Rev, 1991. **71**(2): p. 481-539.

97. Florian, J.A., et al., *Heparan sulfate proteoglycan is a mechanosensor on endothelial cells.* Circ Res, 2003. **93**(10): p. e136-42.

98. Hecker, M., et al., *Vasoconstriction and increased flow: two principal mechanisms of shear stress-dependent endothelial autacoid release.* Am J Physiol, 1993. **265**(3 Pt 2): p. H828-33.

99. Mochizuki, S., et al., *Role of hyaluronic acid glycosaminoglycans in shear-induced endothelium-derived nitric oxide release.* Am J Physiol Heart Circ Physiol, 2003. **285**(2): p. H722-6.

100. Moon, J.J., et al., *Role of cell surface heparan sulfate proteoglycans in endothelial cell migration and mechanotransduction.* J Cell Physiol, 2005. **203**(1): p. 166-76.

101. Thi, M.M., et al., *The role of the glycocalyx in reorganization of the actin cytoskeleton under fluid shear stress: a "bumper-car" model.* Proc Natl Acad Sci U S A, 2004. **101**(47): p. 16483-8.

102. Bernfield, M., et al., *Functions of cell surface heparan sulfate proteoglycans.* Annu Rev Biochem, 1999. **68**: p. 729-77.

103. Rizzo, V., et al., *Recruitment of endothelial caveolae into mechanotransduction pathways by flow conditioning in vitro.* Am J Physiol Heart Circ Physiol, 2003. **285**(4): p. H1720-9.

104. Gambillara, V., et al., *Plaque-prone hemodynamics impair endothelial function in pig carotid arteries.* Am J Physiol Heart Circ Physiol, 2006. **290**(6): p. H2320-8.

105. Balligand, J.L., O. Feron, and C. Dessy, *eNOS activation by physical forces: from short-term regulation of contraction to chronic remodeling of cardiovascular tissues.* Physiol Rev, 2009. **89**(2): p. 481-534.

106. Arnal, J.F., et al., *Endothelium-derived nitric oxide and vascular physiology and pathology*. Cell Mol Life Sci, 1999. **55**(8-9): p. 1078-87.

107. Yang, B. and V. Rizzo, *Shear Stress Activates eNOS at the Endothelial Apical Surface Through 1 Containing Integrins and Caveolae.* Cell Mol Bioeng, 2013. **6**(3): p. 346-354.

108. Tkachenko, E., J.M. Rhodes, and M. Simons, *Syndecans: new kids on the signaling block.* Circ Res, 2005. **96**(5): p. 488-500.

109. Yoneda, A. and J.R. Couchman, *Regulation of cytoskeletal organization by syndecan transmembrane proteoglycans.* Matrix Biol, 2003. **22**(1): p. 25-33.

110. Yoo, J., et al., *Dynamin II interacts with syndecan-4, a regulator of focal adhesion and stress-fiber formation.* Biochem Biophys Res Commun, 2005. **328**(2): p. 424-31.

111. Essner, J.J., E. Chen, and S.C. Ekker, *Syndecan-2.* Int J Biochem Cell Biol, 2006. **38**(2): p. 152-6.

112. Simons, M. and A. Horowitz, *Syndecan-4-mediated signalling.* Cell Signal, 2001. **13**(12): p. 855-62.

113. Zimmermann, P. and G. David, *The syndecans, tuners of transmembrane signaling.* FASEB J, 1999. **13 Suppl**: p. S91-S100.

114. Park, P.W., O. Reizes, and M. Bernfield, *Cell surface heparan sulfate proteoglycans: selective regulators of ligand-receptor encounters.* J Biol Chem, 2000. **275**(39): p. 29923-6.

115. Rost, B., *Review: protein secondary structure prediction continues to rise.* J Struct Biol, 2001. **134**(2-3): p. 204-18.

116. Lin, S.J., et al., *Superoxide dismutase inhibits the expression of vascular cell adhesion molecule-1 and intracellular cell adhesion molecule-1 induced by tumor*

necrosis factor-alpha in human endothelial cells through the JNK/p38 pathways. Arterioscler Thromb Vasc Biol, 2005. **25**(2): p. 334-40.

117. Juliano, R.L. and S. Haskill, *Signal transduction from the extracellular matrix.* J Cell Biol, 1993. **120**(3): p. 577-85.

118. Schwartz, M.A., M.D. Schaller, and M.H. Ginsberg, *Integrins: emerging paradigms of signal transduction.* Annu Rev Cell Dev Biol, 1995. **11**: p. 549-99.

119. Hynes, R.O., *Integrins: versatility, modulation, and signaling in cell adhesion.* Cell, 1992. **69**(1): p. 11-25.

120. Hynes, R.O., *Integrins: bidirectional, allosteric signaling machines.* Cell, 2002. **110**(6): p. 673-87.

121. Hynes, R.O., *A reevaluation of integrins as regulators of angiogenesis.* Nat Med, 2002. **8**(9): p. 918-21.

122. Loftus, J.C. and R.C. Liddington, *Cell adhesion in vascular biology. New insights into integrin-ligand interaction.* J Clin Invest, 1997. **99**(10): p. 2302-6.

123. Humphries, M.J. and P. Newham, *The structure of cell-adhesion molecules.* Trends Cell Biol, 1998. **8**(2): p. 78-83.

124. Jalali, S., et al., *Integrin-mediated mechanotransduction requires its dynamic interaction with specific extracellular matrix (ECM) ligands.* Proceedings of the National Academy of Sciences, 2001. **98**(3): p. 1042-1046.

125. Liu, S., D.A. Calderwood, and M.H. Ginsberg, *Integrin cytoplasmic domain-binding proteins.* J Cell Sci, 2000. **113 (Pt 20)**: p. 3563-71.

126. Verma, S.K., et al., *Rac1 and RhoA differentially regulate angiotensinogen gene expression in stretched cardiac fibroblasts.* Cardiovasc Res, 2011. **90**(1): p. 88-96.

127. Lal, H., et al., *Stretch-induced MAP kinase activation in cardiac myocytes: differential regulation through beta1-integrin and focal adhesion kinase.* J Mol Cell Cardiol, 2007. **43**(2): p. 137-47.

128. Urbich, C., et al., *Shear stress-induced endothelial cell migration involves integrin signaling via the fibronectin receptor subunits alpha(5) and beta(1).* Arterioscler Thromb Vasc Biol, 2002. **22**(1): p. 69-75.

129. Chavakis, E., et al., *Role of beta2-integrins for homing and neovascularization capacity of endothelial progenitor cells.* J Exp Med, 2005. **201**(1): p. 63-72.

130. Sims, J.R., S. Karp, and D.E. Ingber, *Altering the cellular mechanical force balance results in integrated changes in cell, cytoskeletal and nuclear shape.* J Cell Sci, 1992. **103 (Pt 4)**: p. 1215-22.

131. Maniotis, A.J., C.S. Chen, and D.E. Ingber, *Demonstration of mechanical connections between integrins, cytoskeletal filaments, and nucleoplasm that stabilize nuclear structure.* Proc Natl Acad Sci U S A, 1997. **94**(3): p. 849-54.

132. Wang, N., et al., *Cell prestress. I. Stiffness and prestress are closely associated in adherent contractile cells.* Am J Physiol Cell Physiol, 2002. **282**(3): p. C606-16.

133. Stamenovic, D., et al., *Cell prestress. II. Contribution of microtubules.* Am J Physiol Cell Physiol, 2002. **282**(3): p. C617-24.

134. Wang, N., et al., *Mechanical behavior in living cells consistent with the tensegrity model.* Proc Natl Acad Sci U S A, 2001. **98**(14): p. 7765-70.

135. Ingber, D.E., *Tensegrity I. Cell structure and hierarchical systems biology.* J Cell Sci, 2003. **116**(Pt 7): p. 1157-73.

136. Chen, C.S. and D.E. Ingber, *Tensegrity and mechanoregulation: from skeleton to cytoskeleton.* Osteoarthritis Cartilage, 1999. **7**(1): p. 81-94.

137. Ingber, D.E., *Tensegrity: the architectural basis of cellular mechanotransduction.* Annu Rev Physiol, 1997. **59**: p. 575-99.

138. Poh, Y.C., et al., *Dynamic force-induced direct dissociation of protein complexes in a nuclear body in living cells.* Nat Commun, 2012. **3**: p. 866.

139. Pajerowski, J.D., et al., *Physical plasticity of the nucleus in stem cell differentiation.* Proc Natl Acad Sci U S A, 2007. **104**(40): p. 15619-24.

140. Lammerding, J., et al., *Lamin A/C deficiency causes defective nuclear mechanics and mechanotransduction.* J Clin Invest, 2004. **113**(3): p. 370-8.

141. Lammerding, J., et al., *Lamins A and C but not lamin B1 regulate nuclear mechanics.* J Biol Chem, 2006. **281**(35): p. 25768-80.

142. Lammerding, J. and R.T. Lee, *Mechanical properties of interphase nuclei probed by cellular strain application.* Methods Mol Biol, 2009. **464**: p. 13-26.

143. Lombardi, M.L., et al., *The interaction between nesprins and sun proteins at the nuclear envelope is critical for force transmission between the nucleus and cytoskeleton.* J Biol Chem, 2011. **286**(30): p. 26743-53.

144. Guilak, F., *Compression-induced changes in the shape and volume of the chondrocyte nucleus.* J Biomech, 1995. **28**(12): p. 1529-41.

145. Guilak, F., J.R. Tedrow, and R. Burgkart, *Viscoelastic properties of the cell nucleus.* Biochem Biophys Res Commun, 2000. **269**(3): p. 781-6.

146. Horn, H.F., et al., *The LINC complex is essential for hearing.* J Clin Invest, 2013. **123**(2): p. 740-50.

147. Wang, W., et al., *Structural insights into SUN-KASH complexes across the nuclear envelope.* Cell Res, 2012. **22**(10): p. 1440-52.

148. Simon, D.N. and K.L. Wilson, *The nucleoskeleton as a genome-associated dynamic 'network of networks'.* Nat Rev Mol Cell Biol, 2011. **12**(11): p. 695-708.

149. Starr, D.A. and H.N. Fridolfsson, *Interactions between nuclei and the cytoskeleton are mediated by SUN-KASH nuclear-envelope bridges.* Annu Rev Cell Dev Biol, 2010. **26**: p. 421-44.

150. Crisp, M., et al., *Coupling of the nucleus and cytoplasm: role of the LINC complex.* J Cell Biol, 2006. **172**(1): p. 41-53.

151. Burke, B. and K.J. Roux, *Nuclei take a position: managing nuclear location.* Dev Cell, 2009. **17**(5): p. 587-97.

152. Wang, N., J.D. Tytell, and D.E. Ingber, *Mechanotransduction at a distance: mechanically coupling the extracellular matrix with the nucleus.* Nat Rev Mol Cell Biol, 2009. **10**(1): p. 75-82.

153. Ho, C.Y. and J. Lammerding, *Lamins at a glance.* J Cell Sci, 2012. **125**(Pt 9): p. 2087-93.

154. Tkachenko, E., et al., *The nucleus of endothelial cell as a sensor of blood flow direction.* Biol Open, 2013. **2**(10): p. 1007-12.

155. Morgan, J.T., et al., *Integration of basal topographic cues and apical shear stress in vascular endothelial cells.* Biomaterials, 2012. **33**(16): p. 4126-35.

156. Dragt, B.S., et al., *Effect of laminar shear stress on the distribution of Weibel-Palade bodies in endothelial cells.* Thromb Res, 2012. **130**(5): p. 741-5.

157. Fedorchak, G.R., A. Kaminski, and J. Lammerding, *Cellular mechanosensing: getting to the nucleus of it all.* Prog Biophys Mol Biol, 2014. **115**(2-3): p. 76-92.

158. Zimmerman, B., et al., *Differential beta-arrestin-dependent conformational signaling and cellular responses revealed by angiotensin analogs.* Sci Signal, 2012. **5**(221): p. ra33.

159. Mehta, P.K. and K.K. Griendling, *Angiotensin II cell signaling: physiological and pathological effects in the cardiovascular system.* Am J Physiol Cell Physiol, 2007. **292**(1): p. C82-97.

160. Yatabe, J., et al., *Angiotensin II type 1 receptor blocker attenuates the activation of ERK and NADPH oxidase by mechanical strain in mesangial cells in the absence of angiotensin II.* Am J Physiol Renal Physiol, 2009. **296**(5): p. F1052-60.

161. Zou, Y., et al., *Mechanical stress activates angiotensin II type 1 receptor without the involvement of angiotensin II.* Nat Cell Biol, 2004. **6**(6): p. 499-506.

162. Yasuda, N., et al., *A novel mechanism of mechanical stress-induced angiotensin II type 1-receptor activation without the involvement of angiotensin II.* Naunyn Schmiedebergs Arch Pharmacol, 2008. **377**(4-6): p. 393-9.

163. Storch, U., M. Mederos y Schnitzler, and T. Gudermann, *G protein-mediated stretch reception.* Am J Physiol Heart Circ Physiol, 2012. **302**(6): p. H1241-9.

164. Rakesh, K., et al., *beta-Arrestin-biased agonism of the angiotensin receptor induced by mechanical stress.* Sci Signal, 2010. **3**(125): p. ra46.

165. Mederos y Schnitzler, M., U. Storch, and T. Gudermann, *AT1 receptors as mechanosensors.* Curr Opin Pharmacol, 2011. **11**(2): p. 112-6.

166. Chatzizisis, Y.S., et al., *Role of endothelial shear stress in the natural history of coronary atherosclerosis and vascular remodeling: molecular, cellular, and vascular behavior.* Journal of the American College of Cardiology, 2007. **49**(25): p. 2379-93.

167. Traub, O., et al., *Characterization of the gap junction protein connexin37 in murine endothelium, respiratory epithelium, and after transfection in human HeLa cells.* Eur J Cell Biol, 1998. **77**(4): p. 313-22.

168. Hwang, J., et al., *Oscillatory shear stress stimulates endothelial production of O2- from p47phox-dependent NAD(P)H oxidases, leading to monocyte adhesion.* J Biol Chem, 2003. **278**(47): p. 47291-8.

169. Shyy, J.Y. and S. Chien, *Role of integrins in endothelial mechanosensing of shear stress.* Circ Res, 2002. **91**(9): p. 769-75.

170. Liu, Y., et al., *Shear stress activation of SREBP1 in endothelial cells is mediated by integrins.* Arterioscler Thromb Vasc Biol, 2002. **22**(1): p. 76-81.

171. Chien, S., *Mechanotransduction and endothelial cell homeostasis: the wisdom of the cell.* Am J Physiol Heart Circ Physiol, 2007. **292**(3): p. H1209-24.

172. Topper, J.N., et al., *Identification of vascular endothelial genes differentially responsive to fluid mechanical stimuli: cyclooxygenase-2, manganese superoxide dismutase, and endothelial cell nitric oxide synthase are selectively up-regulated by steady laminar shear stress.* Proc Natl Acad Sci U S A, 1996. **93**(19): p. 10417-22.

173. Wang, N., et al., *Shear stress regulation of Kruppel-like factor 2 expression is flow pattern-specific.* Biochem Biophys Res Commun, 2006. **341**(4): p. 1244-51.

174. Takabe, W., E. Warabi, and N. Noguchi, *Anti-atherogenic effect of laminar shear stress via Nrf2 activation.* Antioxid Redox Signal, 2011. **15**(5): p. 1415-26.

175. Dimmeler, S. and A.M. Zeiher, *Nitric oxide-an endothelial cell survival factor.* Cell Death Differ, 1999. **6**(10): p. 964-8.

176. Hecker, M., I. Fleming, and R. Busse, *Kinin-mediated activation of endothelial no formation: possible role during myocardial ischemia.* Agents Actions Suppl, 1995. **45**: p. 119-27.

177. Nayak, L., Z. Lin, and M.K. Jain, *"Go with the flow": how Kruppel-like factor 2 regulates the vasoprotective effects of shear stress.* Antioxid Redox Signal, 2011. **15**(5): p. 1449-61.

178. Dekker, R.J., et al., *Prolonged fluid shear stress induces a distinct set of endothelial cell genes, most specifically lung Krüppel-like factor (KLF2).* Vol. 100. 2002. 1689-1698.

179. Das, H., et al., *Kruppel-like factor 2 (KLF2) regulates proinflammatory activation of monocytes.* Proc Natl Acad Sci U S A, 2006. **103**(17): p. 6653-8.

180. Lin, Z., et al., *Kruppel-like factor 2 inhibits protease activated receptor-1 expression and thrombin-mediated endothelial activation.* Arterioscler Thromb Vasc Biol, 2006. **26**(5): p. 1185-9.

181. SenBanerjee, S., et al., *KLF2 Is a novel transcriptional regulator of endothelial proinflammatory activation.* J Exp Med, 2004. **199**(10): p. 1305-15.

182. Fledderus, J.O., et al., *KLF2 primes the antioxidant transcription factor Nrf2 for activation in endothelial cells.* Arterioscler Thromb Vasc Biol, 2008. **28**(7): p. 1339-46.

183. Boon, R.A., et al., *KLF2-induced actin shear fibers control both alignment to flow and JNK signaling in vascular endothelium.* Blood, 2010. **115**(12): p. 2533-42.

184. Razani, B., et al., *Caveolin-1 null mice are viable but show evidence of hyperproliferative and vascular abnormalities.* J Biol Chem, 2001. **276**(41): p. 38121-38.

185. Goodwin, B.L., L.P. Solomonson, and D.C. Eichler, *Argininosuccinate synthase expression is required to maintain nitric oxide production and cell viability in aortic endothelial cells.* J Biol Chem, 2004. **279**(18): p. 18353-60.

186. Dekker, R.J., et al., *Endothelial KLF2 links local arterial shear stress levels to the expression of vascular tone-regulating genes.* Am J Pathol, 2005. **167**(2): p. 609-18.

187. Dekker, R.J., et al., *KLF2 provokes a gene expression pattern that establishes functional quiescent differentiation of the endothelium.* Blood, 2006. **107**(11): p. 4354-63.

188. Boon, R.A., et al., *KLF2 suppresses TGF-beta signaling in endothelium through induction of Smad7 and inhibition of AP-1.* Arterioscler Thromb Vasc Biol, 2007. **27**(3): p. 532-9.

189. Bhattacharya, R., et al., *Inhibition of vascular permeability factor/vascular endothelial growth factor-mediated angiogenesis by the Kruppel-like factor KLF2.* J Biol Chem, 2005. **280**(32): p. 28848-51.

190. Parmar, K.M., et al., *Integration of flow-dependent endothelial phenotypes by Kruppel-like factor 2.* J Clin Invest, 2006. **116**(1): p. 49-58.

191. Wang, W., et al., *Fluid shear stress stimulates phosphorylation-dependent nuclear export of HDAC5 and mediates expression of KLF2 and eNOS.* Blood, 2010. **115**(14): p. 2971-9.

192. van Thienen, J.V., et al., *Shear stress sustains atheroprotective endothelial KLF2 expression more potently than statins through mRNA stabilization.* Cardiovascular Research, 2006. **72**(2): p. 231-240.

193. Zhang, Y., et al., *Negative regulation of the Nrf1 transcription factor by its N-terminal domain is independent of Keap1: Nrf1, but not Nrf2, is targeted to the endoplasmic reticulum.* Biochem J, 2006. **399**(3): p. 373-85.

194. Rhee, W.J., et al., *HuR regulates the expression of stress-sensitive genes and mediates inflammatory response in human umbilical vein endothelial cells.* Proc Natl Acad Sci U S A, 2010. **107**(15): p. 6858-63.

195. Kumar, A., et al., *Tumor necrosis factor alpha-mediated reduction of KLF2 is due to inhibition of MEF2 by NF-kappaB and histone deacetylases.* Mol Cell Biol, 2005. **25**(14): p. 5893-903.

196. Woo, C.H., et al., *Extracellular signal-regulated kinase 5 SUMOylation antagonizes shear stress-induced antiinflammatory response and endothelial nitric oxide synthase expression in endothelial cells.* Circ Res, 2008. **102**(5): p. 538-45.

197. Kumar, S., et al., *Shear stress stimulates nitric oxide signaling in pulmonary arterial endothelial cells via a reduction in catalase activity: role of protein kinase C delta.* Am J Physiol Lung Cell Mol Physiol, 2010. **298**(1): p. L105-16.

198. Yoshida, T., K.H. Kaestner, and G.K. Owens, *Conditional deletion of Kruppel-like factor 4 delays downregulation of smooth muscle cell differentiation markers but accelerates neointimal formation following vascular injury.* Circ Res, 2008. **102**(12): p. 1548-57.

199. Duerrschmidt, N., et al., *NO-mediated regulation of NAD(P)H oxidase by laminar shear stress in human endothelial cells.* J Physiol, 2006. **576**(Pt 2): p. 557-67.

200. Doehner, W., et al., *Effects of xanthine oxidase inhibition with allopurinol on endothelial function and peripheral blood flow in hyperuricemic patients with chronic heart failure: results from 2 placebo-controlled studies.* Circulation, 2002. **105**(22): p. 2619-24.

201. Kang-Decker, N., et al., *Nitric oxide promotes endothelial cell survival signaling through S-nitrosylation and activation of dynamin-2.* J Cell Sci, 2007. **120**(Pt 3): p. 492-501.

202. McNally, J.S., et al., *Role of xanthine oxidoreductase and NAD(P)H oxidase in endothelial superoxide production in response to oscillatory shear stress.* Am J Physiol Heart Circ Physiol, 2003. **285**(6): p. H2290-7.

203. Ziegler, T., et al., *Nitric oxide synthase expression in endothelial cells exposed to mechanical forces.* Hypertension, 1998. **32**(2): p. 351-5.

204. Xiao, Z., et al., *Shear stress induction of the endothelial nitric oxide synthase gene is calcium-dependent but not calcium-activated.* J Cell Physiol, 1997. **171**(2): p. 205-11.

205. Redmond, E.M., P.A. Cahill, and J.V. Sitzmann, *Flow-mediated regulation of G-protein expression in cocultured vascular smooth muscle and endothelial cells.* Arterioscler Thromb Vasc Biol, 1998. **18**(1): p. 75-83.

206. Hori, N., R. Wiest, and R.J. Groszmann, *Enhanced release of nitric oxide in response to changes in flow and shear stress in the superior mesenteric arteries of portal hypertensive rats.* Hepatology, 1998. **28**(6): p. 1467-73.

207. Villa, L.M., et al., *Peroxynitrite induces both vasodilatation and impaired vascular relaxation in the isolated perfused rat heart.* Proc Natl Acad Sci U S A, 1994. **91**(26): p. 12383-7.

208. Hartsfield, C.L., et al., *Regulation of heme oxygenase-1 gene expression in vascular smooth muscle cells by nitric oxide.* Am J Physiol, 1997. **273**(5 Pt 1): p. L980-8.

209. Bouloumie, A., et al., *Endothelial dysfunction coincides with an enhanced nitric oxide synthase expression and superoxide anion production.* Hypertension, 1997. **30**(4): p. 934-41.

210. Zingarelli, B., et al., *Effects of a novel guanylyl cyclase inhibitor on the vascular actions of nitric oxide and peroxynitrite in immunostimulated smooth muscle cells and in endotoxic shock.* Crit Care Med, 1999. **27**(9): p. 1701-7.

211. Kalyanaraman, B., et al., *Measuring reactive oxygen and nitrogen species with fluorescent probes: challenges and limitations.* Free Radic Biol Med, 2012. **52**(1): p. 1-6.

212. Alfieri, A., et al., *Sulforaphane preconditioning of the Nrf2/HO-1 defense pathway protects the cerebral vasculature against blood-brain barrier disruption and neurological deficits in stroke.* Free Radic Biol Med, 2013. **65**: p. 1012-22.

213. Tsao, P.S., et al., *Exposure to shear stress alters endothelial adhesiveness. Role of nitric oxide.* Circulation, 1995. **92**(12): p. 3513-9.

214. Noris, M., et al., *Nitric oxide synthesis by cultured endothelial cells is modulated by flow conditions.* Circ Res, 1995. **76**(4): p. 536-43.

215. Sorescu, G.P., et al., *Bone morphogenic protein 4 produced in endothelial cells by oscillatory shear stress stimulates an inflammatory response.* J Biol Chem, 2003. **278**(33): p. 31128-35.

216. Dickhout, J.G., et al., *Peroxynitrite causes endoplasmic reticulum stress and apoptosis in human vascular endothelium: implications in atherogenesis.* Arterioscler Thromb Vasc Biol, 2005. **25**(12): p. 2623-9.

217. Chappell, D.C., et al., *Oscillatory shear stress stimulates adhesion molecule expression in cultured human endothelium.* Circ Res, 1998. **82**(5): p. 532-9.

218. Brooks, A.R., P.I. Lelkes, and G.M. Rubanyi, *Gene expression profiling of human aortic endothelial cells exposed to disturbed flow and steady laminar flow.* Physiol Genomics, 2002. **9**(1): p. 27-41.

219. Silacci, P., et al., *Unidirectional and oscillatory shear stress differentially modulate NOS III gene expression.* Nitric Oxide, 2000. **4**(1): p. 47-56.

220. Hsiai, T.K., et al., *Hemodynamics influences vascular peroxynitrite formation: Implication for low-density lipoprotein apo-B-100 nitration.* Free Radic Biol Med, 2007. **42**(4): p. 519-29.

221. Ai, L., et al., *Shear stress influences spatial variations in vascular Mn-SOD expression: implication for LDL nitration.* Am J Physiol Cell Physiol, 2008. **294**(6): p. C1576-85.

222. Cunningham, K.S. and A.I. Gotlieb, *The role of shear stress in the pathogenesis of atherosclerosis.* Lab Invest, 2005. **85**(1): p. 9-23.

223. Warabi, E., et al., *Shear stress stabilizes NF-E2-related factor 2 and induces antioxidant genes in endothelial cells: role of reactive oxygen/nitrogen species.* Free Radic Biol Med, 2007. **42**(2): p. 260-9.

224. Hsieh, C.Y., et al., *Regulation of shear-induced nuclear translocation of the Nrf2 transcription factor in endothelial cells.* J Biomed Sci, 2009. **16**: p. 12.

225. Okouchi, M., et al., *NRF2-dependent glutamate-L-cysteine ligase catalytic subunit expression mediates insulin protection against hyperglycemia- induced brain endothelial cell apoptosis.* Curr Neurovasc Res, 2006. **3**(4): p. 249-61.

226. Acar, N., et al., *Expression of nuclear factor erythroid 2-related factor 2 (Nrf2) and peroxiredoxin 6 (Prdx6) proteins in healthy and pathologic placentas of human and rat.* Acta Histochem, 2014. **116**(8): p. 1289-300.

227. Kumar, A., et al., *Transcriptional repression of Kruppel like factor-2 by the adaptor protein p66shc.* Faseb j, 2009. **23**(12): p. 4344-52.

228. Wu, J., et al., *KLF2 transcription factor modulates blood vessel maturation through smooth muscle cell migration.* J Biol Chem, 2008. **283**(7): p. 3942-50.

229. Knorr-Wittmann, C., et al., *Characterization of Nrf2 activation and heme oxygenase-1 expression in NIH3T3 cells exposed to aqueous extracts of cigarette smoke.* Free Radic Biol Med, 2005. **39**(11): p. 1438-48.

230. Kataoka, K., H. Handa, and M. Nishizawa, *Induction of cellular antioxidative stress genes through heterodimeric transcription factor Nrf2/small Maf by antirheumatic gold(I) compounds.* J Biol Chem, 2001. **276**(36): p. 34074-81.

231. Chen, X.L., et al., *Laminar flow induction of antioxidant response element-mediated genes in endothelial cells. A novel anti-inflammatory mechanism.* J Biol Chem, 2003. **278**(2): p. 703-11.

232. Dai, G., et al., *Biomechanical forces in atherosclerosis-resistant vascular regions regulate endothelial redox balance via phosphoinositol 3-kinase/Akt-dependent activation of Nrf2.* Circ Res, 2007. **101**(7): p. 723-33.

233. Han, Z., et al., *Shear-induced reactive nitrogen species inhibit mitochondrial respiratory complex activities in cultured vascular endothelial cells.* Am J Physiol Cell Physiol, 2007. **292**(3): p. C1103-12.

234. Hosoya, T., et al., *Differential responses of the Nrf2-Keap1 system to laminar and oscillatory shear stresses in endothelial cells.* J Biol Chem, 2005. **280**(29): p. 27244-50.

235. Jones, C.I., 3rd, et al., *Regulation of antioxidants and phase 2 enzymes by shear-induced reactive oxygen species in endothelial cells.* Ann Biomed Eng, 2007. **35**(5): p. 683-93.

236. Nagel, T., et al., *Shear stress selectively upregulates intercellular adhesion molecule-1 expression in cultured human vascular endothelial cells.* J Clin Invest, 1994. **94**(2): p. 885-91.

237. Rhee, W.J., et al., *Target accessibility and signal specificity in live-cell detection of BMP-4 mRNA using molecular beacons.* Nucleic Acids Res, 2008. **36**(5): p. e30.

238. Zhou, Z., et al., *Protocatechuic aldehyde suppresses TNF-alpha-induced ICAM-1 and VCAM-1 expression in human umbilical vein endothelial cells.* Eur J Pharmacol, 2005. **513**(1-2): p. 1-8.

239. Ueno, H., et al., *Nicotine enhances human vascular endothelial cell expression of ICAM-1 and VCAM-1 via protein kinase C, p38 mitogen-activated protein kinase, NF-kappaB, and AP-1.* Cardiovasc Toxicol, 2006. **6**(1): p. 39-50.

240. Ishii, H. and K. Takada, *Bleomycin induces E-selectin expression in cultured umbilical vein endothelial cells by increasing its mRNA levels through activation of NF-kappaB/Rel.* Toxicol Appl Pharmacol, 2002. **184**(2): p. 88-97.

241. Hubbard, A.K. and R. Rothlein, *Intercellular adhesion molecule-1 (ICAM-1) expression and cell signaling cascades.* Free Radic Biol Med, 2000. **28**(9): p. 1379-86.

242. Fan, H., et al., *Oxygen radicals trigger activation of NF-kappaB and AP-1 and upregulation of ICAM-1 in reperfused canine heart.* Am J Physiol Heart Circ Physiol, 2002. **282**(5): p. H1778-86.

243. Suzuki, Y., et al., *Effect of NADPH oxidase inhibition on endothelial cell ELAM-1 mRNA expression.* Biochem Biophys Res Commun, 1992. **184**(3): p. 1339-43.

244. Weber, C., et al., *Antioxidants inhibit monocyte adhesion by suppressing nuclear factor-kappa B mobilization and induction of vascular cell adhesion molecule-1 in endothelial cells stimulated to generate radicals.* Arterioscler Thromb, 1994. **14**(10): p. 1665-73.

245. Holland, J.A., et al., *Low-density lipoprotein stimulated peroxide production and endocytosis in cultured human endothelial cells: mechanisms of action.* Endothelium, 1997. **5**(3): p. 191-207.

246. Khachigian, L.M., et al., *Nuclear factor-kappa B interacts functionally with the platelet-derived growth factor B-chain shear-stress response element in vascular endothelial cells exposed to fluid shear stress.* J Clin Invest, 1995. **96**(2): p. 1169-75.

247. Lan, Q., K.O. Mercurius, and P.F. Davies, *Stimulation of transcription factors NF kappa B and AP1 in endothelial cells subjected to shear stress.* Biochem Biophys Res Commun, 1994. **201**(2): p. 950-6.

248. Sorescu, D., et al., *Superoxide production and expression of nox family proteins in human atherosclerosis.* Circulation, 2002. **105**(12): p. 1429-35.

249. Woodman, C.R., et al., *Flow regulation of ecNOS and Cu/Zn SOD mRNA expression in porcine coronary arterioles.* Am J Physiol, 1999. **276**(3 Pt 2): p. H1058-63.

250. Bartel, D.P., *MicroRNAs: genomics, biogenesis, mechanism, and function.* Cell, 2004. **116**(2): p. 281-97.

251. Bartel, D.P., *MicroRNAs: Target Recognition and Regulatory Functions.* Cell, 2009. **136**(2): p. 215-233.

252. van Rooij, E., *The art of microRNA research.* Circ Res, 2011. **108**(2): p. 219-34.

253. van Rooij, E., W.S. Marshall, and E.N. Olson, *Toward microRNA-based therapeutics for heart disease: the sense in antisense.* Circ Res, 2008. **103**(9): p. 919-28.

254. van Rooij, E., A.L. Purcell, and A.A. Levin, *Developing microRNA therapeutics.* Circ Res, 2012. **110**(3): p. 496-507.

255. van Rooij, E., et al., *Control of stress-dependent cardiac growth and gene expression by a microRNA.* Science, 2007. **316**(5824): p. 575-9.

256. Kumar, S., et al., *Role of flow-sensitive microRNAs in endothelial dysfunction and atherosclerosis: mechanosensitive athero-miRs.* Arterioscler Thromb Vasc Biol, 2014. **34**(10): p. 2206-16.

257. Fang, Y., et al., *MicroRNA-10a regulation of proinflammatory phenotype in athero-susceptible endothelium in vivo and in vitro.* Proc Natl Acad Sci U S A, 2010. **107**(30): p. 13450-5.

258. Qin, X., et al., *MicroRNA-19a mediates the suppressive effect of laminar flow on cyclin D1 expression in human umbilical vein endothelial cells.* Proc Natl Acad Sci U S A, 2010. **107**(7): p. 3240-4.

259. Wang, K.C., et al., *Role of microRNA-23b in flow-regulation of Rb phosphorylation and endothelial cell growth.* Proc Natl Acad Sci U S A, 2010. **107**(7): p. 3234-9.

260. Chen, K., et al., *MicroRNA-101 mediates the suppressive effect of laminar shear stress on mTOR expression in vascular endothelial cells.* Biochem Biophys Res Commun, 2012. **427**(1): p. 138-42.

261. Kohlstedt, K., et al., *AMP-activated protein kinase regulates endothelial cell angiotensin-converting enzyme expression via p53 and the post-transcriptional regulation of microRNA-143/145.* Circ Res, 2013. **112**(8): p. 1150-8.

262. Hergenreider, E., et al., *Atheroprotective communication between endothelial cells and smooth muscle cells through miRNAs.* Nat Cell Biol, 2012. **14**(3): p. 249-56.

263. Weber, M., et al., *MiR-21 is induced in endothelial cells by shear stress and modulates apoptosis and eNOS activity.* Biochem Biophys Res Commun, 2010. **393**(4): p. 643-8.

264. Zhou, J., et al., *MicroRNA-21 targets peroxisome proliferators-activated receptor-alpha in an autoregulatory loop to modulate flow-induced endothelial inflammation.* Proc Natl Acad Sci U S A, 2011. **108**(25): p. 10355-60.

265. Nam, D., et al., *A model of disturbed flow-induced atherosclerosis in mouse carotid artery by partial ligation and a simple method of RNA isolation from carotid endothelium.* J Vis Exp, 2010(40).

266. Wang, S., et al., *The endothelial-specific microRNA miR-126 governs vascular integrity and angiogenesis.* Dev Cell, 2008. **15**(2): p. 261-71.

267. Harris, T.A., et al., *MicroRNA-126 regulates endothelial expression of vascular cell adhesion molecule 1.* Proc Natl Acad Sci U S A, 2008. **105**(5): p. 1516-21.

268. Zhou, J., et al., *Regulation of vascular smooth muscle cell turnover by endothelial cell-secreted microRNA-126: role of shear stress.* Circ Res, 2013. **113**(1): p. 40-51.

269. Zernecke, A., et al., *Delivery of microRNA-126 by apoptotic bodies induces CXCL12-dependent vascular protection.* Sci Signal, 2009. **2**(100): p. ra81.

270. Weber, M., et al., *MiRNA-155 Targets Myosin Light Chain Kinase and Modulates Actin Cytoskeleton Organization in Endothelial Cells.* Am J Physiol Heart Circ Physiol, 2014.

271. Nazari-Jahantigh, M., et al., *MicroRNA-155 promotes atherosclerosis by repressing Bcl6 in macrophages.* J Clin Invest, 2012. **122**(11): p. 4190-202.

272. Du, F., et al., *MicroRNA-155 Deficiency Results in Decreased Macrophage Inflammation and Attenuated Atherogenesis in Apolipoprotein E-Deficient Mice.* Arterioscler Thromb Vasc Biol, 2014. **34**(4): p. 759-67.

273. Sun, H.X., et al., *Essential role of microRNA-155 in regulating endothelium-dependent vasorelaxation by targeting endothelial nitric oxide synthase.* Hypertension, 2012. **60**(6): p. 1407-14.

274. Wu, W., et al., *Flow-Dependent Regulation of Kruppel-Like Factor 2 Is Mediated by MicroRNA-92a.* Circulation, 2011. **124**(5): p. 633-41.

275. Fang, Y. and P.F. Davies, *Site-specific microRNA-92a regulation of Kruppel-like factors 4 and 2 in atherosusceptible endothelium.* Arterioscler Thromb Vasc Biol, 2012. **32**(4): p. 979-87.

276. Ni, C.W., H. Qiu, and H. Jo, *MicroRNA-663 upregulated by oscillatory shear stress plays a role in inflammatory response of endothelial cells.* Am J Physiol Heart Circ Physiol, 2011. **300**(5): p. H1762-9.

277. Afonyushkin, T., O.V. Oskolkova, and V.N. Bochkov, *Permissive role of miR-663 in induction of VEGF and activation of the ATF4 branch of unfolded protein*

response in endothelial cells by oxidized phospholipids. Atherosclerosis, 2012. **225**(1): p. 50-5.

278. Liu, Z.Y., et al., *MicroRNA-663 targets TGFB1 and regulates lung cancer proliferation.* Asian Pac J Cancer Prev, 2011. **12**(11): p. 2819-23.

279. Zhang, X.Y., et al., *Induction of thoracic aortic remodeling by endothelial-specific deletion of microRNA-21 in mice.* PLoS One, 2013. **8**(3): p. e59002.

280. Cheng, H.S., et al., *MicroRNA-146 represses endothelial activation by inhibiting pro-inflammatory pathways.* EMBO Mol Med, 2013. **5**(7): p. 949-66.

281. Sun, X., et al., *Systemic Delivery of MicroRNA-181b Inhibits Nuclear Factor-kappaB Activation, Vascular Inflammation, and Atherosclerosis in Apolipoprotein E-Deficient Mice.* Circ Res, 2014. **114**(1): p. 32-40.

282. Wang, D., et al., *Gut microbiota metabolism of anthocyanin promotes reverse cholesterol transport in mice via repressing miRNA-10b.* Circ Res, 2012. **111**(8): p. 967-81.

283. Wang, Y.S., et al., *MicroRNA-195 regulates vascular smooth muscle cell phenotype and prevents neointimal formation.* Cardiovasc Res, 2012. **95**(4): p. 517-26.

284. Soh, J., et al., *MicroRNA-30c reduces hyperlipidemia and atherosclerosis in mice by decreasing lipid synthesis and lipoprotein secretion.* Nat Med, 2013. **19**(7): p. 892-900.

285. Tian, G.P., et al., *The effects of miR-467b on lipoprotein lipase (LPL) expression, pro-inflammatory cytokine, lipid levels and atherosclerotic lesions in*

apolipoprotein E knockout mice. Biochem Biophys Res Commun, 2014. **443**(2): p. 428-34.

286. de Aguiar Vallim, T.Q., et al., *MicroRNA-144 regulates hepatic ATP binding cassette transporter A1 and plasma high-density lipoprotein after activation of the nuclear receptor farnesoid X receptor.* Circ Res, 2013. **112**(12): p. 1602-12.

287. Wei, Y., et al., *The microRNA-342-5p fosters inflammatory macrophage activation through an Akt1- and microRNA-155-dependent pathway during atherosclerosis.* Circulation, 2013. **127**(15): p. 1609-19.

288. Rayner, K.J., et al., *Antagonism of miR-33 in mice promotes reverse cholesterol transport and regression of atherosclerosis.* J Clin Invest, 2011. **121**(7): p. 2921-31.

289. Horie, T., et al., *MicroRNA-33 deficiency reduces the progression of atherosclerotic plaque in ApoE-/- mice.* J Am Heart Assoc, 2012. **1**(6): p. e003376.

290. Rotllan, N., et al., *Therapeutic silencing of microRNA-33 inhibits the progression of atherosclerosis in Ldlr-/- mice--brief report.* Arterioscler Thromb Vasc Biol, 2013. **33**(8): p. 1973-7.

291. Marquart, T.J., et al., *Anti-miR-33 therapy does not alter the progression of atherosclerosis in low-density lipoprotein receptor-deficient mice.* Arterioscler Thromb Vasc Biol, 2013. **33**(3): p. 455-8.

292. Rayner, K.J., et al., *Inhibition of miR-33a/b in non-human primates raises plasma HDL and lowers VLDL triglycerides.* Nature, 2011. **478**(7369): p. 404-7.

293. Rupaimoole, R. and F.J. Slack, *MicroRNA therapeutics: towards a new era for the management of cancer and other diseases.* Nat Rev Drug Discov, 2017. **16**(3): p. 203-222.

294. van Rooij, E. and S. Kauppinen, *Development of microRNA therapeutics is coming of age.* EMBO Mol Med, 2014. **6**(7): p. 851-64.

295. Elmen, J., et al., *LNA-mediated microRNA silencing in non-human primates.* Nature, 2008. **452**(7189): p. 896-9.

296. Elmen, J., et al., *Antagonism of microRNA-122 in mice by systemically administered LNA-antimiR leads to up-regulation of a large set of predicted target mRNAs in the liver.* Nucleic Acids Res, 2008. **36**(4): p. 1153-62.

297. Janssen, H.L., et al., *Treatment of HCV infection by targeting microRNA.* N Engl J Med, 2013. **368**(18): p. 1685-94.

298. Ottosen, S., et al., *In vitro antiviral activity and preclinical and clinical resistance profile of miravirsen, a novel anti-hepatitis C virus therapeutic targeting the human factor miR-122.* Antimicrob Agents Chemother, 2015. **59**(1): p. 599-608.

299. Trajkovski, M., et al., *MicroRNAs 103 and 107 regulate insulin sensitivity.* Nature, 2011. **474**(7353): p. 649-53.

300. Bader, A.G., *miR-34 - a microRNA replacement therapy is headed to the clinic.* Front Genet, 2012. **3**: p. 120.

301. Misso, G., et al., *Mir-34: a new weapon against cancer?* Mol Ther Nucleic Acids, 2014. **3**: p. e194.

302. Cortez, M.A., et al., *PDL1 Regulation by p53 via miR-34.* J Natl Cancer Inst, 2016. **108**(1).

303. Stahlhut, C. and F.J. Slack, *Combinatorial Action of MicroRNAs let-7 and miR-34 Effectively Synergizes with Erlotinib to Suppress Non-small Cell Lung Cancer Cell Proliferation.* Cell Cycle, 2015. **14**(13): p. 2171-80.

304. Reid, G., et al., *Clinical development of TargomiRs, a miRNA mimic-based treatment for patients with recurrent thoracic cancer.* Epigenomics, 2016. **8**(8): p. 1079-85.

305. van Zandwijk, N. and K.M. Fong, *Update in lung cancer: prologue to a modern review series.* Respirology, 2015. **20**(2): p. 183-4.

306. Drago-Ferrante, R., et al., *Suppressive role exerted by microRNA-29b-1-5p in triple negative breast cancer through SPIN1 regulation.* Oncotarget, 2017. **8**(17): p. 28939-28958.

307. Al-Haidari, A.A., I. Syk, and H. Thorlacius, *MiR-155-5p positively regulates CCL17-induced colon cancer cell migration by targeting RhoA.* Oncotarget, 2017. **8**(9): p. 14887-14896.

308. Messina, A., et al., *A microRNA switch regulates the rise in hypothalamic GnRH production before puberty.* Nat Neurosci, 2016. **19**(6): p. 835-44.

309. Liu, C., et al., *Identification of microRNAs and microRNA targets in Xenopus gastrulae: The role of miR-26 in the regulation of Smad1.* Dev Biol, 2016. **409**(1): p. 26-38.

310. Stary, C.M., et al., *Inhibition of miR-181a protects female mice from transient focal cerebral ischemia by targeting astrocyte estrogen receptor-alpha.* Mol Cell Neurosci, 2017. **82**: p. 118-125.

311. Hartmann, P., et al., *Endothelial Dicer promotes atherosclerosis and vascular inflammation by miRNA-103-mediated suppression of KLF4.* Nat Commun, 2016. **7**: p. 10521.

312. Jacobsen, A., et al., *miRMaid: a unified programming interface for microRNA data resources.* BMC Bioinformatics, 2010. **11**: p. 29.

313. Kozomara, A. and S. Griffiths-Jones, *miRBase: annotating high confidence microRNAs using deep sequencing data.* Nucleic Acids Res, 2014. **42**(Database issue): p. D68-73.

314. Nurul-Syakima, A.M., et al., *Differential microRNA expression and identification of putative miRNA targets and pathways in head and neck cancers.* Int J Mol Med, 2011. **28**(3): p. 327-36.

315. Song, M.Y., et al., *Identification of serum microRNAs as novel non-invasive biomarkers for early detection of gastric cancer.* PLoS One, 2012. **7**(3): p. e33608.

316. Miyamae, M., et al., *Plasma microRNA profiles: identification of miR-744 as a novel diagnostic and prognostic biomarker in pancreatic cancer.* Br J Cancer, 2015. **113**(10): p. 1467-76.

317. Yu, Q., et al., *Up-regulation of serum miR-744 predicts poor prognosis in patients with nasopharyngeal carcinoma.* Int J Clin Exp Med, 2015. **8**(8): p. 13296-302.

318. Cakmak, H.A., et al., *The prognostic value of circulating microRNAs in heart failure: preliminary results from a genome-wide expression study.* J Cardiovasc Med (Hagerstown), 2015. **16**(6): p. 431-7.

319. Mi, Q.S., et al., *Identification of mouse serum miRNA endogenous references by global gene expression profiles.* PLoS One, 2012. **7**(2): p. e31278.

320. Chavali, V., S.C. Tyagi, and P.K. Mishra, *Differential expression of dicer, miRNAs, and inflammatory markers in diabetic Ins2+/- Akita hearts.* Cell Biochem Biophys, 2014. **68**(1): p. 25-35.

321. Chen, Y.Q., et al., *Abated microRNA-195 expression protected mesangial cells from apoptosis in early diabetic renal injury in mice.* J Nephrol, 2012. **25**(4): p. 566-76.

322. Yang, J.C., et al., *TLR4/NF-kappaB-responsive microRNAs and their potential target genes: a mouse model of skeletal muscle ischemia-reperfusion injury*. Biomed Res Int, 2015. **2015**: p. 410721.

323. Martin, J., et al., *Post-transcriptional regulation of Transforming Growth Factor Beta-1 by microRNA-744.* PLoS One, 2011. **6**(10): p. e25044.

324. Vislovukh, A., et al., *Proto-oncogenic isoform A2 of eukaryotic translation elongation factor eEF1 is a target of miR-663 and miR-744.* Br J Cancer, 2013. **108**(11): p. 2304-11.

325. Zhou, W., et al., *MiR-744 increases tumorigenicity of pancreatic cancer by activating Wnt/beta-catenin pathway.* Oncotarget, 2015. **6**(35): p. 37557-69.

326. Zhang, X., et al., *miR-744 enhances type I interferon signaling pathway by targeting PTP1B in primary human renal mesangial cells.* Sci Rep, 2015. **5**: p. 12987.

327. Zhang, Y., et al., *Characterization of PINCH-2, a new focal adhesion protein that regulates the PINCH-1-ILK interaction, cell spreading, and migration.* J Biol Chem, 2002. **277**(41): p. 38328-38.

328. Nix, D.A. and M.C. Beckerle, *Nuclear-cytoplasmic shuttling of the focal contact protein, zyxin: a potential mechanism for communication between sites of cell adhesion and the nucleus.* J Cell Biol, 1997. **138**(5): p. 1139-47.

329. Nix, D.A., et al., *Targeting of zyxin to sites of actin membrane interaction and to the nucleus.* J Biol Chem, 2001. **276**(37): p. 34759-67.

330. Thomas, S.M., M. Hagel, and C.E. Turner, *Characterization of a focal adhesion protein, Hic-5, that shares extensive homology with paxillin.* J Cell Sci, 1999. **112 (Pt 2)**: p. 181-90.

331. Heitzer, M.D. and D.B. DeFranco, *Hic-5, an adaptor-like nuclear receptor coactivator.* Nucl Recept Signal, 2006. **4**: p. e019.

332. Braun, A., et al., *PINCH2 is a new five LIM domain protein, homologous to PINCHand localized to focal adhesions.* Exp Cell Res, 2003. **284**(2): p. 239-50.

333. Shi, X., et al., *Roles of PINCH-2 in regulation of glomerular cell shape change and fibronectin matrix deposition.* Am J Physiol Renal Physiol, 2008. **295**(1): p. F253-63.

334. Chiswell, B.P., et al., *Structural basis of competition between PINCH1 and PINCH2 for binding to the ankyrin repeat domain of integrin-linked kinase.* J Struct Biol, 2010. **170**(1): p. 157-63.

335. Legate, K.R., et al., *ILK, PINCH and parvin: the tIPP of integrin signalling.* Nat Rev Mol Cell Biol, 2006. **7**(1): p. 20-31.

336. Fukuda, T., et al., *PINCH-1 is an obligate partner of integrin-linked kinase (ILK) functioning in cell shape modulation, motility, and survival.* J Biol Chem, 2003. **278**(51): p. 51324-33.

337. Stanchi, F., et al., *Consequences of loss of PINCH2 expression in mice.* J Cell Sci, 2005. **118**(Pt 24): p. 5899-910.

338. Donthamsetty, S., et al., *Role of PINCH and its partner tumor suppressor Rsu-1 in regulating liver size and tumorigenesis.* PLoS One, 2013. **8**(9): p. e74625.

339. Meder, B., et al., *PINCH proteins regulate cardiac contractility by modulating integrin-linked kinase-protein kinase B signaling.* Mol Cell Biol, 2011. **31**(16): p. 3424-35.

340. Liang, X., et al., *Targeted ablation of PINCH1 and PINCH2 from murine myocardium results in dilated cardiomyopathy and early postnatal lethality.* Circulation, 2009. **120**(7): p. 568-76.

341. Kim, S.K., et al., *The epigenetic silencing of LIMS2 in gastric cancer and its inhibitory effect on cell migration.* Biochem Biophys Res Commun, 2006. **349**(3): p. 1032-40.

342. Chardon, J.W., et al., *LIMS2 mutations are associated with a novel muscular dystrophy, severe cardiomyopathy and triangular tongues.* Clin Genet, 2015. **88**(6): p. 558-64.

343. Hannigan, G.E., et al., *Regulation of cell adhesion and anchorage-dependent growth by a new beta 1-integrin-linked protein kinase.* Nature, 1996. **379**(6560): p. 91-6.

344. Hannigan, G.E., J.G. Coles, and S. Dedhar, *Integrin-linked kinase at the heart of cardiac contractility, repair, and disease.* Circ Res, 2007. **100**(10): p. 1408-14.

345. Delcommenne, M., et al., *Phosphoinositide-3-OH kinase-dependent regulation of glycogen synthase kinase 3 and protein kinase B/AKT by the integrin-linked kinase.* Proc Natl Acad Sci U S A, 1998. **95**(19): p. 11211-6.

346. Dostal, D.E., et al., *Mechanosensing and Regulation of Cardiac Function.* J Clin Exp Cardiolog, 2014. **5**(6): p. 314.

347. White, D.E., et al., *Targeted ablation of ILK from the murine heart results in dilated cardiomyopathy and spontaneous heart failure.* Genes Dev, 2006. **20**(17): p. 2355-60.

348. Bendig, G., et al., *Integrin-linked kinase, a novel component of the cardiac mechanical stretch sensor, controls contractility in the zebrafish heart.* Genes Dev, 2006. **20**(17): p. 2361-72.

349. Knoll, R., et al., *Laminin-alpha4 and integrin-linked kinase mutations cause human cardiomyopathy via simultaneous defects in cardiomyocytes and endothelial cells.* Circulation, 2007. **116**(5): p. 515-25.

350. Herranz, B., et al., *Integrin-linked kinase regulates vasomotor function by preventing endothelial nitric oxide synthase uncoupling: role in atherosclerosis.* Circ Res, 2012. **110**(3): p. 439-49.

351. Reventun, P., et al., *iNOS-Derived Nitric Oxide Induces Integrin-Linked Kinase Endocytic Lysosome-Mediated Degradation in the Vascular Endothelium.* Arterioscler Thromb Vasc Biol, 2017. **37**(7): p. 1272-1281.

352. Ni, C.W., et al., *Development of immortalized mouse aortic endothelial cell lines.* Vasc Cell, 2014. **6**(1): p. 7.

353. Ni, C.W., et al., *Discovery of novel mechanosensitive genes in vivo using mouse carotid artery endothelium exposed to disturbed flow.* Blood, 2010. **116**(15): p. e66-73.

354. Schmittgen, T.D., *Regulation of microRNA processing in development, differentiation and cancer.* J Cell Mol Med, 2008. **12**(5B): p. 1811-9.

355. Cho, A., et al., *Effects of changes in blood flow rate on cell death and cell proliferation in carotid arteries of immature rabbits.* Circ Res, 1997. **81**(3): p. 328-37.

356. Levesque, M.J., R.M. Nerem, and E.A. Sprague, *Vascular endothelial cell proliferation in culture and the influence of flow.* Biomaterials, 1990. **11**(9): p. 702-7.

357. DePaola, N., et al., *Vascular endothelium responds to fluid shear stress gradients.* Arterioscler Thromb, 1992. **12**(11): p. 1254-7.

358. Dimmeler, S., et al., *Shear stress inhibits apoptosis of human endothelial cells.* FEBS Lett, 1996. **399**(1-2): p. 71-4.

359. Chiu, J.J., et al., *Effects of disturbed flow on endothelial cells.* J Biomech Eng, 1998. **120**(1): p. 2-8.

360. Malek, A.M. and S. Izumo, *Molecular aspects of signal transduction of shear stress in the endothelial cell.* J Hypertens, 1994. **12**(9): p. 989-99.

361. Weinbaum, S., et al., *Effect of cell turnover and leaky junctions on arterial macromolecular transport.* Am J Physiol, 1985. **248**(6 Pt 2): p. H945-60.

362. Li, P., et al., *MicroRNA-663 regulates human vascular smooth muscle cell phenotypic switch and vascular neointimal formation.* Circ Res, 2013. **113**(10): p. 1117-27.